Electrophysiological signals for closed-loop deep brain stimulation in Parkinson's disease

Doctoral Thesis



Anders Christian Meidahl

University of Oxford

October 2019

St. Peter's College

Nuffield Department of Clinical Neuroscience

Brain Network Dynamics Unit

I. Declaration

I, Anders Christian Meidahl, confirm that the work presented in this thesis is my own. Where information has been derived from other sources, I confirm that this has been indicated in the thesis.

Signed:……

Date:……..…….

II. Abstract

Continuous high-frequency deep brain stimulation (DBS) in the subthalamic nucleus (STN) is an established treatment for Parkinson's disease (PD). Current developments focus on trying to widen the therapeutic window of such treatments. Closed-loop DBS, where stimulation is dynamically controlled by feedback from biomarkers of pathological brain circuit activity, is one such development. Numerous electrophysiological signals extracted from local field potentials (LFPs) or electrocorticography (ECoG) in the basal ganglia-thalamo-cortical circuit relate to symptom severity and have consequently been proposed as real-time biomarkers. These signals include phase-amplitude coupling, beta-oscillatory bursts, single neuronal firing patterns, and features of waveform morphology. The neuronal basis and interdependency of these signals, however, are poorly understood. To address this a two-fold approach was taken. First, subthalamic macro- and micro electrode recordings of LFPs and single unit activity were studied in human PD patients undergoing DBS-surgery. Simultaneously recorded ECoGs were analysed in order to relate previously proposed cortical biomarkers to subthalamic neuronal activity. Second, selective optogenetic stimulation of basal-ganglia or cerebellar receiving thalamus was deployed in rodents to investigate if cortical electrophysiological signals observed in PD could be generated from driving inputs to motor thalamus.

In human PD patients, phase-amplitude coupling in the STN was found to reflect the locking of spiking activity to network beta oscillations and this coupling increased progressively with beta-burst duration, suggesting subthalamic beta bursts to capture higher levels of input-output synchronisation. Furthermore, cortical beta bursts were associated with several other cortical and subthalamic biomarkers and cortical waveform sharpness was linked to subthalamic neuronal synchronisation. In rodents, cortical phase-amplitude coupling in the ECoG could be produced by driving basal-ganglia, but not cerebellar, recipient thalamus. Thus, providing experimental evidence to a theory of a basal-ganglia-thalamic origin of cortical phase-amplitude coupling in PD. Overall, this thesis gives novel insights into the neuronal basis of electrophysiological biomarkers in PD with direct implications for future closed-loop DBS trials.

III. Contents

I. Declaration

II. Abstract

III. Contents

IV. List of figures

V. List of tables

VI. Acknowledgements

VII. Abbreviations

VIII. Publications incorporated into the thesis

1. General introduction 1

1.1 Basal ganglia networks 2

1.1.1 Overview of the dual direct/indirect pathway model

1.1.2 The subthalamic nucleus 5

1.1.3 Basal ganglia functions 6

1.2 Neuronal oscillations and electrophysiological biomarkers in Parkinson's disease 8

1.2.1 Parkinson's disease 8

1.2.2 Oscillations and neuronal synchronisations 9

1.2.3 Communication through coherence 10

1.2.4 Neurophysiological signals in Parkinson's disease 11

1.2.5 Beta-oscillations 12

1.2.6 Phase-amplitude coupling 16

1.3 Biomarker guided closed-loop deep brain stimulation in movement disorders 19

1.3.1 Overview 19

1.3.2 Applications and supporting evidence 22

1.3.3 Limitations and roadblocks 29

1.3.4 Conclusion 38

1.4 Main aims and findings 40

2. General methods 43
2.1 Overview 44
2.2 Ethics 44
2.3 Electrophysiological recording techniques 44
2.4 Principles behind optogenetic stimulation 46
2.5 General data analysis 49
2.5.1 Phase-amplitude coupling 49
2.5.2 Time-frequency decompositions 52
2.5.3 Beta bursts analysis 53
2.5.4 Waveform asymmetries 54
2.6 Statistical analysis 55
3. Synchronised spiking activity, beta bursts and phase-amplitude coupling in the subthalamic nucleus of Parkinson's disease patients 57
3.1 Introduction 58
3.2 Methods 60
3.2.1 Surgical procedure and recordings 60
3.2.2 Data selection and processing 63
3.2.3 Phase amplitude coupling by general linear model 63
3.2.4 Spike-amplitude coupling 66
3.2.5 Spike triggered averages 66
3.2.6 Comparison of firing rates and HFO amplitude coupling 67
3.2.7 Unit power spectral densities 67
3.2.8 Spike-phase locking 67
3.2.9 PAC during beta bursts 68
3.3 Results 72
3.3.1 Defining the presence of STN LFP phase-amplitude coupling 72
3.3.2 STN firing predicts HFO amplitude only in the presence of PAC 73
3.3.3 Specific features of PAC are associated with the presence of synchronised beta-oscillations in STN neurons 79
3.3.4 Increased PAC is captured by the duration of beta bursts 83
3.4 Discussion 88
3.4.1 Physiological basis of PAC in the STN 89
3.4.2 PAC during episodes of transient input synchronisation 92
3.4.3 Subthalamic PAC as a biomarker of pathophysiology 93

4. Cortical beta burst duration modulates other candidate electrophysiological biomarkers for closed-loop deep brain stimulation in Parkinson's disease 95
4.1 Introduction 96
4.2 Methods 98
4.2.1 Surgical procedure and micro recordings 100
4.2.2 Beta-bursts identification 102
4.2.3 Non-sinusoidal features 102
4.2.4 PAC within and between areas 104
4.2.5 Spike-triggered averages 105
4.2.6 Power spectral densities 105
4.2.7 Spike-phase locking 105
4.3 Results 106
4.3.1 Cortical beta bursts capture higher levels of non-sinusoidal sharpness 106
4.3.2 Cortico-subthalamic PAC predicts the locking of single units to HFO amplitude at beta frequencies 111
4.3.3 PAC and sharpness 116
4.3.4 Cortico-subthalamic PAC increases with cortical beta burst duration 119
4.4 Discussion 121
5. Cortical phase-amplitude coupling and signal asymmetries during selective optogenetic stimulation of basal ganglia and cerebellar inputs to motor thalamus 125
5.1 Introduction 126
5.2 Materials and methods 130
5.2.1 Animals 130
5.2.2 Viral Constructs 131
5.2.3 Surgical procedures 131
5.2.4 In vivo electrophysiology and optogenetic stimulation of BZ neurons 132
5.2.5 Data analysis 134
5.3 Results 136
5.3.1 Cortical power spectral changes in ECoG signals during motor thalamic stimulation 136

5.3.2 Selective stimulation of basal ganglia receiving thalamus generates PAC in ipsilateral ECoG signals 143
5.3.3 Laminar-specific changes in PAC and oscillations in motor cortex during motor thalamic stimulation 147
5.3.4 BZ thalamic stimulation induces cortical waveform asymmetries 153
5.3.5 Basal ganglia thalamic projections to cortex give rise to ECoG asymmetries and PAC 158
5.3.6 Laminar PAC throughout motor cortex is not explained by waveform asymmetries 159
5.4 Discussion 162
5.4.1 Cortical PAC and asymmetries as biomarkers of basal ganglia-thalamo-cortical network activity 162
5.4.2 Origins of cortical beta oscillations 163
5.4.3 Theories of PAC generation 164
5.4.4 Implications for Parkinson's disease and closed-loop modulations 166
6. General discussion 168
6.1 General summary of results 169
6.2 Implications for basal ganglia network models 170
6.3 Biomarkers in PD: One to rule them all? 172
6.3.1 Overview 172
6.3.2 PAC-responsive DBS 172
6.3.3 Implications for beta-responsive DBS 178
6.3.4 Waveform asymmetry responsive DBS 179
6.3.5 Spatial and multimodal considerations 182
6.3.6 Conclusion 184
6.4 Symptom versus signal attenuation 184
6.5 Limitations 184
6.6 Open questions 185
6.7 AI, machine learning and future technologies 186
6.8 Final remarks 188
7. References 189

Appendix – supplementary figures

IV. List of Figures

1.1 Schematic of basal ganglia thalamo-cortical networks

1.2 Schematic of proposed electrophysiological biomarkers in PD

1.3 Schematic summary displaying different forms of DBS

1.4 Improvements in motor scores after aDBS from existing studies

1.5 Potential combined beta-tremor control loops

2.1 Transsynaptic gene activation by WGA-Cre

3.1 Schematic of micro- and macro-electrode recordings during DBS surgery

3.2 Examples of significant and non-significant PAC-clustering

3.3 Example of HFOs, spiking and beta bursts in single recordings

3.4 Spike triggered HFO amplitude

3.5 PAC and spike-amplitude coupling

3.6 Firing rate and HFO amplitude in the presence of PAC

3.7 Firing rate and PAC clustering

3.8 Phase-locked spiking and phase-locked HFOs

3.9 The power spectral density features of single unit activity predict PAC

3.10 PAC during beta-oscillation bursts

3.11 PAC and burst progression

3.12 HFOs during beta-bursts

4.1 Schematic of cortico-subthalamic recordings

4.2 Non-sinusoidal features of cortical beta-oscillations

4.3 Peak sharpness and STN unit phase locking during cortical beta-burst progression

4.4 Determination of cortico-subthalamic PAC

4.5 Cortico-subthalamic spike-HFO synchronisation

4.6 Cortico-subthalamic phase-spike locking

4.7 Cortical PAC and nonsinusoidal features

4.8 Cortico-subthalamic PAC and nonsinusoidal features

4.9 Cortico-subthalamic PAC increases with beta bursts duration

5.1 Induction of ChR2 in basal ganglia and cerebellar recipient thalamus for optogenetic control

5.2 Example of ECoG time-resolved spectral changes during 25 Hz BZ-stimulation

5.3 ECoGs changes during 25 Hz opto-stimulation of motor thalamus

5.4 ECoGs changes during 10 Hz opto-stimulation of motor thalamus

5.5 10 Hz opto-stimulation and changes in HFO amplitude

5.6 25 Hz opto-stimulation of motor thalamus and PAC in ECoGs

5.7 10 Hz opto-stimulation of motor thalamus and PAC in ECoGs

5.8 Time-resolved laminar-specific power spectral changes in motor cortex during opto-stimulation

5.9 Statistics across subjects for laminar-specific time-resolved power spectral opto-stimulation induced changes

5.10 Individual time-resolved laminar-specific power spectral changes in motor cortex during opto-stimulation

5.11 Laminar PAC changes in motor cortex during motor thalamic opto-stimulation

5.12 Cortical beta waveform asymmetries during basal-ganglia recipient thalamic opto-stimulation

5.13 Waveform asymmetries and PAC in ECoGs during opto-stimulation of motor t halamus

5.14 Laminar PAC and waveform asymmetries during BZ-stimulation

5.15 Laminar PAC and waveform asymmetries during CZ-stimulation

V. List of Tables

2.1 Frequency band definitions

3.1 Patient details

3.2 Associations between measures of PAC, spiking activity and beta bursts.

4.1 Patient details

VI. Acknowledgements

I would like to express my deepest gratitude for the supervision and guidance I have received from my two supervisors, Andrew Sharott and Peter Brown, during my DPhil studies at the University of Oxford. Both have been extraordinarily supportive, continually accessible and always allowed time for meaningful discussions. I am very grateful for the scientific training they have given me and for being taught never to settle with the immediate result and constantly challenge any conclusion. I am also very grateful for having been accepted into both the Sharott and Brown research groups with such open arms and could not have asked for a more welcoming and scientifically stimulating environment. I am especially thankful for all the wonderful colleagues and friends I have gained in both labs, the broader Oxford neuroscience community and St. Peter's college throughout the years.

Additionally, I would like to thank Bernadette van Wijk for assisting me with advanced data analysis when I started out, and Rahul Shah for patiently teaching me optogenetics and various recording techniques. I would also like to thank Alek Pogosyan for teaching me the practical aspects of performing DBS LFP recordings in Parkinson's patients during my first year. I would also like to acknowledge the Rosetrees Trust for their financial support.

Finally, I would like to thank all my friends, parents and partner, who have supported me unconditionally throughout the whole journey.

VII. Abbreviations

aDBS	Adaptive deep brain stimulation
ANOVA	Analysis of variance
BCI	Brain computer interface
BTC	Basal ganglia-thalamo-cortical
BZ	Basal ganglia-recipient zone
cDBS	Conventional deep brain stimulation
CFC	Cross-frequency coupling
ChR2	Channel-rhodopsin 2
CTC	Cerebello-thalamo-cortical
CTX	Cortex
CTX-STN	Cortico-subthalamic
CZ	Cerebellar-recipient zone
DBS	Deep brain stimulation
DCN	Deep cerebellar nuclei
ECoG	Electrocorticography
EEG	Electroencephalography
EMG	Electromyography
GLM	General linear model
GLM	General linear model
GPe	Globus pallidus pars externa
GPi	Globus pallidus pars interna
HFO	High-frequency oscillation
IPG	Implanted pulse generator
ISI	Inter spike interval
ITAE	Integral Time-weighted Absolute error
L-DOPA	Levodopa
LFP	Local field potential
MEG	Magnetoencephalograms
MFR	Mean firing rate
MSN	Medium spiny neuron

MTPT	methyl-phenyl-tetrahydropyridine
NpHR	Halo-rhopdopsin
PAC	Phase-amplitude coupling
PD	Parkinson’s disease
PID	Proportional-Integral-Derivative
PLV	phased locking value
RDR	Rise-decay ratio
SNc	Substantia nigra pars compacta
SNr	Substantia nigra pars reticulata
SR	Steepness ratio
STA	Spike-triggered average
STN	Subthalamic nucleus
tACS	Transcranial alternating current
UPDRS	Unified Parkinson’s Disease Rating Scale
VA	Ventral anterior
VL	Ventrolateral
VM	Ventromedial
WGA	Wheat germ agglutinin

VIII. Publications incorporated into this thesis

Publications incorporated into this thesis by the time of submission (28.11.2019):

Meidahl AC, Moll CKE, van Wijk BCM, Gulberti A, Tinkhauser G, Westphal M, Engel AK, Hamel W, Brown P, Sharott A (2019) Synchronised spiking activity underlies phase amplitude coupling in the subthalamic nucleus of Parkinson's disease patients. Neurobiol Dis 127:101–113. doi: 10.1016/j.nbd.2019.02.005

Meidahl AC, Tinkhauser G, Herz DM, Cagnan H, Debarros J, Brown P (2017) Adaptive Deep Brain Stimulation for Movement Disorders: The Long Road to Clinical Therapy. Mov Disord 32:810–819 doi: 10.1002/mds.27022

1

General introduction

Contents

1.1 Basal ganglia networks
- 1.1.1 Overview of the dual direct/indirect pathway model
- 1.1.2 The subthalamic nucleus
- 1.1.3 Basal ganglia functions

1.2 Neuronal oscillations and electrophysiological biomarkers in Parkinson's disease
- 1.2.1 Parkinson's disease
- 1.2.2 Oscillations and neuronal synchronisations
- 1.2.3 Communication through coherence
- 1.2.4 Neurophysiological signals in Parkinson's disease
- 1.2.5 Beta-oscillations
- 1.2.6 Phase-amplitude coupling

1.3 Biomarker guided closed-loop deep brain stimulation in movement disorders
- 1.3.1 Overview
- 1.3.2 Applications and supporting evidence
- 1.3.3 Limitations and roadblocks
- 1.3.4 Conclusion

1.4 Main aims and findings

1.1 Basal ganglia networks

1.1.1 Overview of the dual direct/indirect pathway model

The basal ganglia refer to a group of subcortical nuclei in vertebrates involved in numerous aspects of motor, cognitive and affective control (Smith et al., 1998; Nelson and Kreitzer, 2014). The structures traditionally comprise striatum (nucleus caudatus and putamen), globus pallidus pars interna (GPi) and pars externa (GPe), the subthalamic nucleus (STN) and substantia nigra (Smith et al., 1998). Together with cortex and thalamus these highly interconnected nuclei form the basal ganglia-thalamic-cortical (BTC) network (Fig. 1.1). This network encompasses at least four functional circuits: the motor, oculomotor, associative, and limbic loops (Nambu et al., 2000; Nambu, 2008; Volkmann et al., 2010). Much knowledge of basal ganglia function has been inferred from clinical studies of movements disorders like Parkinson's disease and Huntington's disease or from animal models of dopamine depletion (Albin et al., 1989; Smith et al., 1998; Redgrave et al., 2010). Several models of basal ganglia function have been brought forward to account for the physiological and pathophysiological changes observed in health and disease (Alexander and DeLong, 1985; Mink, 1996; Bar-Gad et al., 2003; Nelson and Kreitzer, 2014), of which the most influential has been the famous rate model (Albin et al., 1989).

The classical rate model as first outlined by Albin and Delong describes a duality of pathways within the BTC network: A direct and an indirect pathways with opposing effects with regards to locomotion and reinforcement behaviour (Albin et al., 1989; DeLong, 1990).

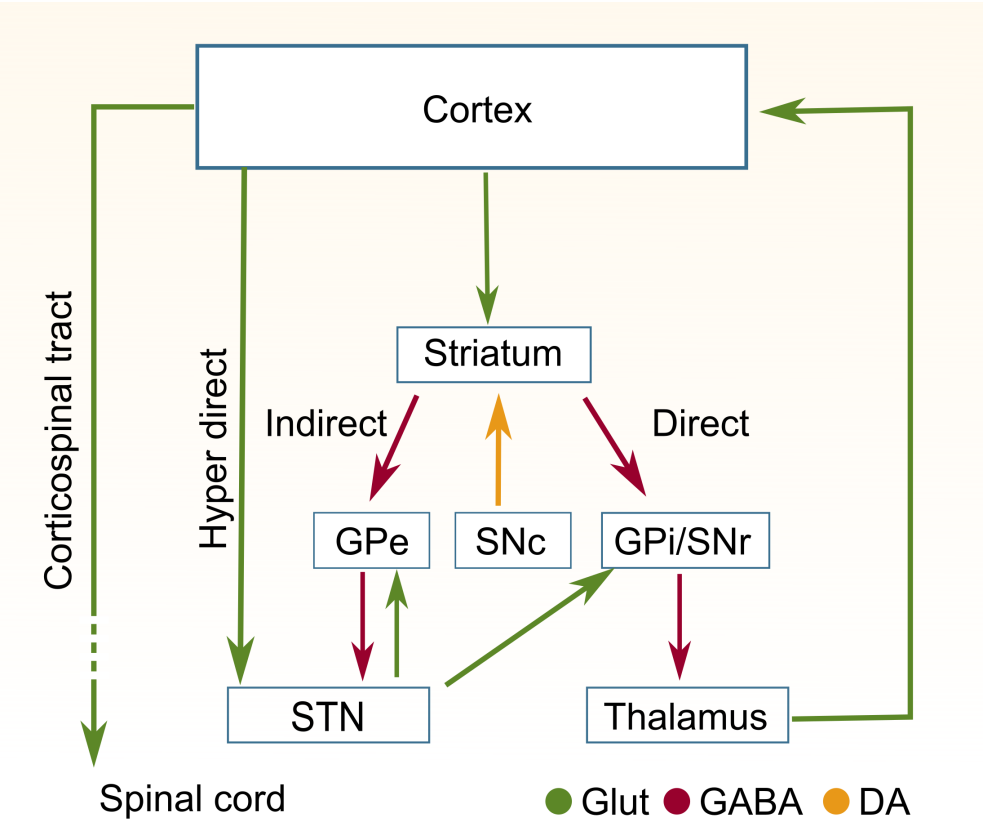


Figure 1.1 - Classical cortical basal ganglia thalamic network. Green arrows mark glutamatergic, yellow dopaminergic, and red GABAergic projections. Inspired by Bolam et al. 2009.

In accordance with the classical direct/indirect pathway model, cortical glutamatergic neurons project to GABAergic medium spiny neurons (MSNs) in the striatum, whose projections in turn initiate the so-called direct and indirect pathways (Fig 1.1). In the direct pathway, striatal MSNs project to the GPi and substantia nigra pars reticulata (SNr) and, via GABAergic projections neurons, these nuclei (directly) inhibit thalamic glutamatergic projection neurons to cortex (Smith et al., 1998). Consequently, increases in the direct pathway activity will lead to disinhibition of thalamic glutamatergic cortical outputs (Bolam et al., 2009).

In the indirect pathway MSNs inhibit neurons in GPe, which in turn send GABAergic projections to the STN. The STN, the only glutamatergic structure within the basal ganglia structures, activates GPi and SNr neurons, which inhibit thalamic glutamatergic neurons that project to cortex. Accordingly, activation of the indirect pathway would manifest in decreased activity of glutamatergic thalamo-cortical projections (DeLong, 1990; Smith et al., 1998; McIntyre and Hahn, 2010).

Dopaminergic neurons in substantia nigra pars compacta (SNc) project to striatal MSNs integrated in both pathways. The effect of dopamine on membrane potentials is critically dependent on the receptor to which it binds (Sibley and Monsma, 1992). Through differences in G-protein mediated signal cascades, dopamine can either have an excitatory or inhibitory effect on neuronal membrane potentials (Mink, 1996). MSNs in the direct pathway predominantly express D1-receptors, whereas MSNs in the indirect pathway mainly express D2-receptors (Sibley and Monsma, 1992; Smith et al., 1998; Cui et al., 2013). Consequently, activity in SNc dopaminergic projections to striatum should have an excitatory effect on the direct pathway and an inhibitory effect of the indirect pathway. According to this model, striatal dopamine release, ultimately, results in increases in basal ganglia receiving thalamo-cortical excitatory output. Since the first descriptions of the classical model, a hyper direct pathway (Fig. 1.1) with direct glutamatergic cortical-STN projections has been established to exist and added to the network models (Monakow et al., 1978; Kitai and Deniau, 1981; Nambu et al., 1996, 2000; Bolam et al., 2009; Steiner et al., 2019).

The rate model has proven very useful as a foundation for the understanding of basal ganglia physiology and pathophysiology but the somewhat reductionistic, functional dichotomy has been criticised for failing to account for recent experimental paradoxes

(Calabresi et al., 2014). These will be addressed further down (Chapter 1.1.3) and discussed in relation to Parkinsonian pathophysiology (Chapter 1.2.4).

1.1.2 The subthalamic nucleus

The STN is a grey lens-shaped basal ganglia structure situated in close proximity to thalamus (as its name suggests), zona incerta, substantia nigra and the internal capsule (Yelnik and Percheron, 1979). Historically, it was considered a so-called relay nucleus within the indirect pathway, but has since additionally been shown to receive direct projections from cortex, thalamus and brain stem nuclei, highlighting it as a perhaps equally important structure for basal ganglia input (Nambu et al., 2002; Volkmann et al., 2010). It has also received widespread attention for being the only glutamatergic nucleus in the basal ganglia (Smith et al., 1998) and for being the most established therapeutic target for deep brain stimulation (DBS) in Parkinson's disease. Subthalamic neurons have been shown to fire at tonic rates between 5-30 Hz (Fujimoto and Kita, 1993; Wichmann et al., 1994; Bevan et al., 2007) and display hypersensitivities to the synaptic inputs (Wilson, 2015). Based on these properties the STN has been proposed as a pacemaker within the BTC network for the generation of synchronised oscillatory activity (Plenz and Kital, 1999; Humphries and Gurney, 2001).

The STN receives GABAergic inputs as part of the indirect pathway from the GPe (with reciprocal connections) (Shink et al., 1996) and glutamatergic from cortex (hyper direct) (Nambu et al., 2000). These inputs all modulate the tonic firing properties of STN neurons. Furthermore, the intralaminar nuclei of thalamus, the dorsal raphe, SNc and the mesopontine tegmentum have all been demonstrated to project to the STN (Smith et al.,

1998) adding to a proposed role of the STN as a dual basal ganglia relay and input structure. The STN glutamatergic output goes to GPi and SNr.

The STN can be functionally divided in relation to the basal ganglia loops with a large dorsolateral motor area, a smaller medial limbic area and a ventral associative part (Hamani et al., 2004). As with other basal ganglia structures a distinct somatotopic organisation within the STN has been described (Alexander and DeLong, 1985; Iwamuro et al., 2017).

1.1.3 Basal ganglia function

Several models and theories regarding the role of the BTC-networks in both health and disease have been proposed and these are constantly undergoing modifications to encompass evidence from the latest experimental studies (Calabresi et al., 2014; Nelson and Kreitzer, 2014). Overall, experimental and clinical observations state, that the basal ganglia are involved in functions as diverse as facilitation and inhibition of movements (Alexander and Crutcher, 1990), emotional processing (Groenewegen et al., 1999), reinforcement learning (Bar-Gad et al., 2003), cognition (Volkmann et al., 2010), planning and action selection (Cui et al., 2013), impulsivity (Frank, 2007) decision making (Herz et al., 2018) and control of movement vigour (Panigrahi et al., 2015).

Many of the motor functions, but also limbic and associative functions, attributed to the basal ganglia in humans, have been inferred from the dopaminergic depleted state in Parkinson's disease (Smith et al., 1998; Poewe et al., 2017). In the classical rate model, as outlined above, activity in the direct and indirect pathways have opposing behavioural effects. According to the model, hyperactivity in the indirect and hypoactivity in direct pathway are thought to result from dopamine depletion and manifest in cortical under-facilitation resulting in slowness of movement. The model has been used to infer that the

opposite occurs in Huntington's chorea and levo-dopa induced dyskinesias, where cortical over-facilitation is thought to manifest in choreiform movements (DeLong, 1990). This theory was recently supported by an experiment in which optogenetic activation of MSNs in the direct pathway led to increased locomotion and reduced freezing, whereas indirect pathway activation resulted in slowness of movement and freezing (Kravitz et al., 2013). Lately, however, the classical rate model of basal ganglia function has been challenged in both the experimental setting and literature reviews (Cui et al., 2013; Calabresi et al., 2014; Nelson and Kreitzer, 2014). It has been argued the model's relatively simplistic duality fails to explain certain paradoxical findings (Calabresi et al., 2014). First, if an opposing duality exists why do more than half of striatal MSNs from the direct pathway project collaterally to GPe in the indirect pathway (Fujiyama et al., 2011). Second, a non-selective dopamine receptor antagonist attenuated Parkinsonian symptoms without resulting in firing rate changes in the STN (Levy et al., 2001). Third, the descending pyramidal tract have been found to project to both direct and indirect striatal MSNs (Kress et al., 2013). Fourth, and perhaps most strikingly, a calcium imaging study showed concurrent activation of both the direct and indirect pathways in mice performing an operant task (Cui et al., 2013). How do any of these findings align with the antagonistic view of the pathway duality?

One explanation could be that it is not the dichotomous pathway activation per se, but rather the manner (see Chapter 1.2.3) in which the neuronal pathway populations within the basal ganglia pathways are active, that determines behavioural outcomes (Cui et al., 2013; Sharott et al., 2017). If so physiological assessments of neural network dynamics must complement studies of structural properties to further pioneer the understanding of basal ganglia function.

1.2 Neuronal oscillations and electrophysiological biomarkers in Parkinson's disease

The classical rate model has failed to explain several basal ganglia paradoxes (Cui et al., 2013; Calabresi et al., 2014; Nelson and Kreitzer, 2014) and it has been proposed that timing, frequency and coherence is of vital importance for effective neuronal information transmission and computations throughout dynamic brain networks (Fries, 2005).

The study of Parkinson's has proven of vital importance in the understanding of basal ganglia function, and vice versa. This chapter will begin with a brief introduction to Parkinson's disease and neuronal oscillations followed by a discussion of neurophysiological BTC network changes resulting from basal ganglia dopamine depletion in Parkinson's disease.

1.2.1 Parkinson's disease

Parkinson's disease is a neurogenerative disease and movement disorder that affects around 2-3 % of people above 65 years of age worldwide (Twelves et al., 2003; Pringsheim et al., 2014). Pathologically it is characterised by neuronal degeneration in substantia nigra pars compacta, resulting in striatal dopamine deficiencies, and intracellular alpha-synuclein aggregates, including so-called Lewy-bodies in neurons (Poewe et al., 2017). The diagnostic criteria are based on clinical assessments of motor function like bradykinesia, resting tremor, muscle rigidity, postural instability and dopaminergic replacement therapy responsiveness as outlined in the MDS diagnostic criteria (Postuma et al., 2015). Non-motor symptoms like hyposmia, sleep disorders, dementia, depression and constipation are also prominent but often over-looked (Schapira et al., 2017). Complex contributions of mitochondria dysfunction, oxidative stress, disruption in calcium homeostasis, alpha-synuclein proteostasis and inflammatory

processes have all been demonstrated as part of the cytological pathogenesis of substantia nigra and other brain areas (Poewe et al., 2017). Recently, a lot of attention has been given to the Braak hypothesis that proposes a gut-to-brain propagation of alpha-synuclein via the vagus nerve in idiopathic PD (Braak et al., 2003; Knudsen et al., 2018; Kim et al., 2019).

Treatment options are currently symptomatic and range from pharmacological interventions like dopamine-replacement therapy to DBS surgical interventions, where electric current is applied to the STN or globus pallidus at frequencies above 100 Hz (see Chapter 1.3). In the last decades numerous studies have paved our understanding of the neurophysiological changes that underpin symptom manifestations in Parkinson's disease and lead to motor impairments (Oswal et al., 2013). Several electrophysiological brain signals, or biomarkers, have been linked to symptom severity and proposed for more sophisticated closed-loop deep brain stimulation devices. In the following we will discuss some of the general theories behind these pathophysiological changes in neuronal network activity.

1.2.2 Oscillations and neuronal synchronisations

Rate provides only one level of information. But the basal ganglia can be approached on other information levels, one of which are electrophysiological oscillations. These have been studied in the brain systematically for almost a century, since Hans Berger's initial electroencephalography (EEG) experiments (Berger, 1929). Since then, neuronal oscillations, also sometimes referred to as brain waves, have been explored across species in cortical and subcortical structures in both health and disease through an expanding repertoire of increasingly refined recording techniques, such as the electrocorticography (ECoG), local field potentials (LFPs) and magnetoencephalograms (MEGs) (Buzsáki et

al., 2012; Akam and Kullmann, 2014). These so-called macro signals capture summations of extracellular potentials generated by cellular transmembrane currents as described in biophysics under the volume conductor theories (Buzsáki et al., 2012; Einevoll et al., 2013).

Numerous components of these signals such as alpha, beta and gamma oscillations, cross-frequency coupling and signal morphology have been studied across various neuroscientific fields and been implied in functions as diverse as memory formation (Lundqvist et al., 2016), visual processing (Ray and Maunsell, 2010), sleep (Steriade et al., 1993; Muller et al., 2016), motor control (Torrecillos et al., 2018), sensory processing (Mirzaei et al., 2017) and decision making (Herz et al., 2018) to name a few. But to what extent signal oscillations are causally important or represent mere epiphenomena remains an active topic of debate (Fries, 2015; Jones, 2016). In this chapter, meanwhile, focus will remain on signals with proven statistical significance to Parkinson's disease and motor control and briefly touch on general computational theories in the healthy state.

1.2.3 Communication through coherence

One prominent theory of rhythmic function proposed by Pascal Fries is 'Communication Through Coherence' (Fries, 2005). This theory argues that effective communication between brain areas is achieved through pre and post synaptic rhythmic synchronisations in order to optimise the potential for effective information transfer (Fries, 2015). The theory has received some experimental, evidential support from visual processing experiments in primates (Brunet et al., 2015). By the logic of this theory communication disruption in BTC-networks could result in either non-preferred scenarios with disrupted rhythm modulations resulting in what might be referred to as *miscommunication through incoherence* or states of sustained maladaptive oscillatory dominance. For instance, the

degeneration of substantia nigra pars compacta's dopaminergic effects on cortical excitation through oscillatory modulations of the direct and indirect pathway could theoretically result in the dominance and sustainment of inexpedient rhythms . Alternatively, a disruption in the effective communication by temporal disturbances or changes could manifest in miscommunications trough decreased likelihood of successful information transfer as deducted by the theories outlined by Fries (Engel and Fries, 2010; Fries, 2015).

The communication trough coherence theory has been challenged from different sides. It has been pointed out that brain rhythms are not always rhythmic and that raw signal features are often lost and neglected in heavy band pass filtering and signal averaging (Jones, 2016). This has lately been shown to have significant consequences for interpretation of electrophysiological signals in cortex in Parkinson's disease (de Hemptinne et al., 2015; Cole and Voytek, 2016; van Wijk, 2017). Modifications to the original CTC theory to incorporate nonsinusoidal and nonlinear excitability have recently been made (Fries, 2015), but challenges to the theory remain (Jones, 2016).

1.2.4 Neurophysiological signals in Parkinson's disease

Several electrophysiological signals across BTC-structures have been linked to symptom severity in Parkinson's disease and consequently been proposed as feedback signal for closed-loop applications of DBS (Fig. 1.2), where stimulation in real-time is focused on the activity of electrophysiological feedback signals. The most established of these is the beta-oscillation (13-35 Hz), but gamma (50-150 Hz), high frequency oscillations (HFOs, 100-300 Hz), spiking activity, phase-amplitude coupling and raw waveform morphology have been brought forward as biomarkers for PD movement impairment (Brown et al., 2001; Lopez-Azcarate et al., 2010; Sharott et al., 2014; de Hemptinne et al., 2015; Cole

et al., 2017). In the following the implications and basis of these biomarkers will be discussed with particular emphasis on the beta oscillation and phase-amplitude coupling followed by a discussion of the biomarkers immediate relevance for closed-loop DBS applications in Chapter 1.3.

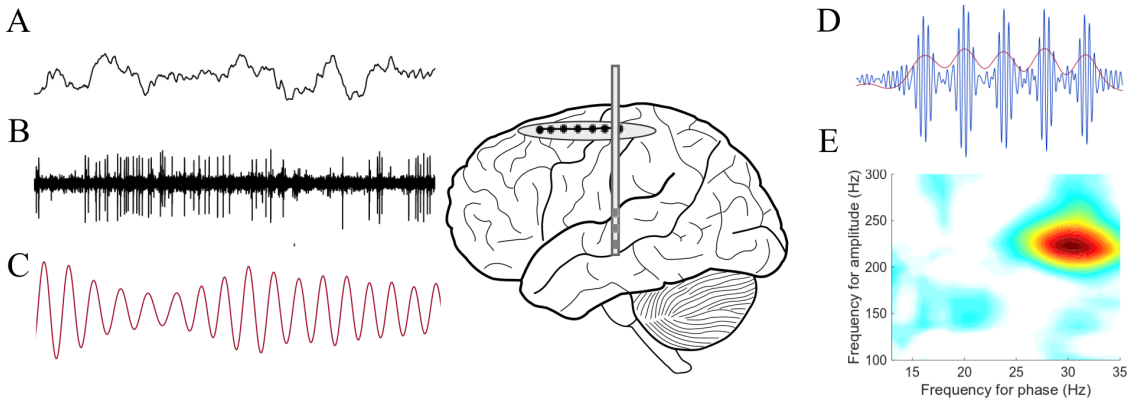


Figure 1.2 - Schematic of proposed electrophysiological biomarkers in PD extracted from local field potentials and/or ECoG recordings. **A**) Raw macro signal extracted from local field potential in the STN. **B**) Neuronal single unit activity extracted from subthalamic microelectrode. **C**) Band pass filtered beta-signal. **D**) HFO bandpass filtered signal (blue) with amplitude curve (red) oscillation at beta frequencies indicative of PAC. **E**) Phase amplitude coupling comodulogram from the STN.

1.2.5 Beta-oscillations

Beta oscillations (13-35 Hz) across BTC-networks have been implicated in human motor control (Sanes and Donoghue, 1993; Baker et al., 1997; Kühn et al., 2004; Anzak et al., 2012; Tan et al., 2014; Fischer et al., 2018, 2019; Torrecillos et al., 2018). It has been widely established in both cortical and subthalamic signals in humans that a significant reduction of mean beta power occurs before and during voluntary movement, and is

followed by beta-resynchronisation (Kühn et al., 2004; Fischer et al., 2018; Torrecillos et al., 2018; Wessel, 2019). This has led to the theory that beta-oscillations and beta bursts (transient beta-synchronisation events) hold anti-kinetic properties. This has been demonstrated for both upper (Fischer et al., 2019) and lower (Fischer et al., 2018) contralateral limp movements. Whether these oscillations are causally important or represent mere epiphenomena of what mechanistically is at play is an active topic for debate. Regardless of such interpretations, the signals provide biomarkers of behavioural and cognitive states (Buzsáki and Wang, 2012; Buzsáki et al., 2012; Einevoll et al., 2013). One of the hallmarks of Parkinsonian pathology is the widespread degeneration of dopaminergic neurons in the midbrain (Poewe et al., 2017). The most conspicuous electrophysiological manifestation in PD patients is thought to be the emergence of beta oscillations. The dependency of abnormally sustained beta oscillations on dopamine depletion has been shown in both the STN, motor cortex and globus pallidus (Brown et al., 2001; Sharott et al., 2005; Mallet et al., 2008a; Lofredi et al., 2018). In human PD patients beta desynchronization has been shown to relate to overall motor performance (Kühn et al., 2004, 2006; Keebaugh et al., 2015; Torrecillos et al., 2018). This sustained beta power synchronisation has been demonstrated time and again to be attenuated by dopaminergic medication and movement onset and its suppression to be associated with treatment induced improvements in bradykinesia and rigidity (Brown et al., 2001; Doyle et al., 2005; Mallet et al., 2008a; Accolla et al., 2016; Cagnan et al., 2018b) and UPDRS III scores have been shown to directly correlate with beta power in the OFF medication state (Neumann et al., 2016; van Wijk et al., 2016). Furthermore, beta oscillation power in the STN has consistently been shown to be suppressed by conventional, high-frequency DBS as a symptomatic treatment for severe PD (Kühn et al., 2008; Tinkhauser et al., 2017a), which will be discussed in further detail in Chapter 1.3.

Interestingly, stimulating cortex at beta-frequencies has in healthy controls using transcranial alternating current stimulation (tACS) (Pogosyan et al., 2009) and STN using DBS in PD patients (Eusebio et al., 2009), been shown to slow movements and worsen PD symptoms, adding to the causal implications of the beta oscillation in motor control and impairment. Evidence from a rodent model of PD showed beta-oscillatory changes did not follow acutely after 6-hydroxydopamine lesions, but rather the beta-exaggeration occurred after several days, suggesting the abnormal beta synchronisations result from maladaptive changes after chronic depletion (Mallet et al., 2008b). Another study found cortical beta oscillations to be significantly amplified during selective activation of striatal cholinergic interneurons using optogenetics and induce parkinsonian symptoms in healthy mice, providing a causal link between basal ganglia activation and cortical beta oscillations (Kondabolu et al., 2016).

Recently, a change has taken place in the study of oscillatory dynamics. From considering oscillations as constant, sustained events focus has shifted towards studying oscillations as transient events in both health and disease that come in periods of bursts (Feingold et al., 2015; Tinkhauser et al., 2017a; Torrecillos et al., 2018; van Ede et al., 2018; Wessel, 2019). It has been suggested that it is not the presence of beta-bursts per se, but rather their prolongation, that is the pathophysiological anti-kinematic manifestation in PD (Tinkhauser et al., 2017a, 2017b). This theory offers a bridge between models of beta-oscillations in health and disease by suggesting that beta-oscillations in themselves are not pathophysiological and only become so as a result of their sustainment and delayed terminations (Tinkhauser et al., 2018b). However, little is known about the neuronal basis for these transient events in PD patients and no studies have examined the activity of other parkinsonian biomarkers during such events. This will be examined in Chapter 3 and 4.

The underlying neuronal basis behind both the normal and abnormally sustained beta oscillations across regions have been subject to debate (Engel and Fries, 2010; Buzsáki et al., 2012; Jones, 2016; Sherman et al., 2016). In a 6-OHDA lesion model of PD subthalamic multiunit discharge locked significantly to the beta-oscillation in the LFP (Mallet et al., 2008b) and beta LFP power is thought to reflect synchronisation across STN synaptic inputs (Weinberger et al., 2006; Mallet et al., 2008a, 2008b; Tinkhauser et al., 2017b; Sharott et al., 2018). In PD patients, STN neurons have also been found to significantly lock to motor and sensory beta cortical oscillations (Lipski et al., 2017). A study found that a large group of MSNs in the indirect pathway synchronised to cortical beta-frequencies following dopamine depletion in rodents (Sharott et al., 2017) and proposed dynamical changes in the indirect pathway to mediate beta-oscillation propagation in the BTC network. Interestingly, this was not the case for direct pathway MSNs. Direct pathway neurons did not synchronise to beta-oscillations and remained at normal activity levels.

A model of spontaneous neocortical beta oscillations brought forward by the Stephanie Jones group proposes beta oscillations to reflect the specifically timed synaptic events to distinct cortical layers, most likely originating from BTC networks (Sherman et al., 2016). But the thalamic hypothesis is in want of experimental evidence and raises questions: Do thalamic inputs indeed manifest in cortical oscillatory activity and if so how? And what parts of thalamus do they originate from? This will be explored in Chapter 5.

1.2.6 Phase-amplitude coupling

It has been proposed that not only oscillations within one frequency band like beta, but also the interactions between oscillations of different frequencies, are computationally important (Canolty et al., 2006; Canolty and Knight, 2010; Buzsáki and Wang, 2012) and that abnormally sustained cross-frequency interactions could be pathological manifestations in conditions like PD (Lopez-Azcarate et al., 2010; de Hemptinne et al., 2015).

Phase-amplitude coupling (PAC), a form of cross-frequency coupling (CFC), where the phase of a lower frequency rhythm is statistically coupled to a higher frequency amplitude has been studied in a wide number of cortical and subcortical structures (Canolty and Knight, 2010). PAC has been implied to have a computational role in functions as various as cognition (Canolty et al., 2006), motor control (de Hemptinne et al., 2015), visual (Voytek, 2010) and other sensory (Seymour et al., 2017) processing and memory consolidation (Tort et al., 2009) to name a few.

In PD patients PAC has been described in both the STN (Lopez-Azcarate et al., 2010; Özkurt et al., 2011; van Wijk et al., 2016) and cortex (Shimamoto et al., 2013; de Hemptinne et al., 2015). Additionally, PAC has been demonstrated to arise in GPe and cortex in MPTP models of PD in non-human primates (Connolly et al., 2015; Escobar et al., 2017) and in 6-OHDA lesion models in rodents (Sanders and Jaeger, 2016).

In PD patients subthalamic PAC has been described between beta phase and HFO amplitude, been linked to motor impairment, and shown to be attenuated by dopaminergic medication and movement (Lopez-Azcarate et al., 2010; van Wijk et al., 2016). Cortical PAC between beta and broadband gamma frequencies (70-150 Hz) has been observed in electrocorticography (ECoG) recordings compared to patients suffering from epilepsy and demonstrated to be attenuated by subthalamic high-frequency DBS (Shimamoto et

al., 2013; de Hemptinne et al., 2015). Also in EEG recordings PAC was found to be diminished by dopaminergic medication (Jackson et al., 2019).

Three prominent explanations for PAC have been given (Canolty, R T, 2012; Jensen et al., 2016):

1) The two statistically coupled signals originate from two different populations of neurons that oscillate synchronised at different frequencies (Buzsáki and Wang, 2012; Spaak et al., 2012).
2) A semi-independent process where the lower frequency is dominated by synaptic input and the higher-frequency arises from background neural unit activity locked to this input. (Ray et al., 2008a; Jensen et al., 2016; Sanders, 2016).
3) The higher frequency component can arise from signal nonlinearities in the lower frequency signal (Kramer et al., 2008; Sheremet et al., 2016; Cole et al., 2017).

PAC between beta oscillations and broadband gamma observed in ECoG recordings in PD patients (de Hemptinne et al., 2015) was later found, at least in part, to originate from the asymmetric features of the lower frequency signal (Cole and Voytek, 2016; Cole et al., 2017; van Wijk, 2017) and could thus be explained by the third PAC generation theory. Furthermore, these asymmetries corresponded with degrees of motor impairment (Cole et al., 2017). This led to the proposal that raw beta waveform asymmetries could serve as a cortical biomarker in PD.

In the STN downward shifts in HFO spectral frequencies have been described following dopamine depletion in PD (Lopez-Azcarate et al., 2010). The neuronal origin of these fast

oscillations remains to be established (Wijk et al., 2017), but is thought to provide a proxy for the assessment of neuronal outputs in LFPs (Buzsáki et al., 2012). In line with this intraburst neuronal firing rates have been shown to fall inside this range (Gale et al., 2009; Sharott et al., 2014). One study, however, suggested that HFOs could be independent spatiotemporal phenomena from neuronal spiking (Wang et al., 2014). On the other hand, a computational study showed that PAC between beta-oscillations and HFO oscillation amplitude could indeed theoretically represent unit intraburst firing frequencies as indexed by HFO synchronisation at beta frequencies (Sanders, 2016). However, experimental evidence for this remains to be had. The existing literature raises important questions: what is the neuronal basis of PAC in the STN? Are HFOs independent from subthalamic neuronal unit activity? What gives rise to cortical waveform asymmetries and thereby statistical PAC? Are these biomarkers constant in time or do they come in transient events like beta-bursts? How do the biomarkers relate to each other and what are neuronal basis thereof? And can the answer to these question guide future closed-loop DBS experiments?

1.3 Biomarker guided closed-loop deep brain stimulation in movement disorders

In the previous subchapter we discussed electrophysiological biomarkers in PD extracted from BTC-networks. In this subchapter we will review existing studies, in which biomarkers have been used for experimental closed-loop DBS interventions for PD and how DBS has been pertained spatially and temporally to such signals. How signals such as PAC and waveform-asymmetries could be utilised for closed-loop interventions will be saved for the general discussion (Chapter 6).

1.3.1 Overview

Deep Brain Stimulation (DBS) has become an established and reversible treatment of motor symptoms in essential tremor, dystonia and severe Parkinson's Disease (PD) resulting in reductions in clinical impairment and increased quality of life in patients (Vidailhet et al., 2005; Kleiner-Fisman et al., 2006; Kupsch et al., 2006; Blomstedt et al., 2007; Williams et al., 2007; Okun and Foote, 2010; Schuepbach et al., 2013). The DBS systems used in current clinical practice effectively operate open-loop, so that stimulation parameters remain constant over time between visits to the clinician. With few exceptions, stimulation is applied at regular and high frequencies, in excess of 100 Hz. Such high frequencies of stimulation are believed to create an acute information lesion, whereby transmission of aberrant neural activity is stopped (Grill et al., 2004; Agnesi et al., 2013; Herrington et al., 2015). At the same time, however, any residual physiological communication may be impaired in the stimulated brain circuit (Chen et al., 2006). It is perhaps no surprise then that the application of DBS in movement disorder patients is limited by side effects such as speech impairment, psychiatric symptoms and antagonistic worsening in motor function, that are all thought to arise from interactions between the

stimulation and local brain circuitries (Chen et al., 2006; Berman et al., 2009; Zauber et al., 2009; Tripoliti et al., 2011; Castrioto et al., 2014; Huebl et al., 2015). Such side-effects could potentially be reduced by sparing neural circuits from high frequency stimulation when dysfunction is limited, or by patterning stimulation so that it is far more selective for dysfunctional neural dynamics. In line with this, recent studies suggest that DBS could potentially be more efficient and efficacious if modulated in response to the inferred state of activity in pathological brain circuits (Little et al., 2013; Beudel and Brown, 2015).

The primary goal of DBS that adapts to the current state of pathological activity, so called closed-loop or adaptive DBS (aDBS), is to increase the specificity of the intervention, and thereby widen the therapeutic window. A secondary goal is to reduce power drains on the implanted pulse generator (IPG). Improvements in battery technology have lessened but not negated the gains to be had from reduced power consumption. A significant proportion of patients are unsuitable for rechargeable IPG systems (Wagle Shukla and Okun, 2014), and those that are would benefit from the ability to recharge less frequently. However, perhaps the most exciting impact of reduced power demands might be the possibility of reducing rechargeable battery size sufficiently to enable skull mounted IPGs (Hariz, 2014; McIntyre et al., 2015; Rossi et al., 2016).

How might aDBS systems infer the current state of activity in the pathological circuits with which they interact? Essentially information can be derived from peripheral measures of motor state, such as the monitoring of tremor or involuntary writhing movements (dyskinesias), directly from recordings of brain activity, or through a combination of these approaches. Where deep brain signals are recorded these must be robust over many years (Steiner et al., 2017), and for this reason local field potential activity is preferred over microelectrode recordings of neurons, even though features of both may correlate with symptoms (Kühn et al., 2006, 2009; Sharott et al., 2014;

Thompson et al., 2014; Neumann et al., 2016). Microelectrode recordings might also carry a greater risk of haemorrhage (Zrinzo et al., 2012), although this is disputed (Deuschl et al., 2006a). Also critical is to consider the nature of those pathological circuits in which activity is inferred. These may be mechanistically or causally related to the symptoms or serve as faithful markers of circuit dysfunction. In the former case stimulation can be specifically patterned to maximally disrupt the underlying causal circuit dynamics, as, for example, in the case of phase-responsive forms of stimulation being pioneered for the treatment of tremor (Little et al., 2016). In the latter case, the DBS intervention is necessarily more generic, and its delivery is controlled by the inferred state of the unmeasured or unknown primary circuit dysfunction. An example of a generic DBS approach is the stereotyped high frequency stimulation that forms conventional DBS. This may be modulated according to the amplitude of signals that need not directly relate to the primary circuit dysfunction, but provide indirect evidence of the severity of the latter. We term this amplitude-responsive adaptive DBS, and distinguish it from the more specific phase-responsive adaptive DBS currently being developed for tremor treatment (Fig. 1.3). An example of amplitude-responsive aDBS is DBS which is delivered according to the level of beta (13-35 Hz) local field potential (LFP) activity recorded in the subthalamic nucleus (STN): we do not know for sure whether beta activity is causally important or not, but it correlates with motor impairment in PD patients undergoing functional neurosurgery (Kühn et al., 2008), as outlined in Chapter 1.2.5, and thereby provides a surrogate for whatever may be mechanistically at play.

The choice between amplitude and phase-responsive approaches primarily depends on the maturity of our knowledge about underlying causal circuit dysfunction. In the case of tremor it is reasonable to attribute the peripheral disturbance to central oscillators which empirical evidence suggests can be controlled at the level of the motor cortex or thalamic

cerebellar receiving areas (Muthuraman et al., 2012; Gövert and Deuschl, 2015). For most conditions, however, we have no compelling evidence as yet that one or other circuit feature lies at the heart of the motor disturbance. For these it is best to use generic high frequency DBS, and to control its delivery through the monitoring of surrogates like the beta activity recorded in the STN LFP.

In this chapter we will first consider the evidence motivating further development of amplitude-responsive and phase-responsive aDBS, the limitations of trials performed to date, and what remains to be studied and done if aDBS is to be translated into clinical practice.

1.3.2 Applications and supporting evidence

Amplitude-responsive aDBS

Amplitude-responsive aDBS was systematically tested in Parkinsonian humans for the first time in an acute trial in 2013 (Little et al., 2013) after a landmark study of aDBS in non-human primates in 2011 yielded promising results (Rosin et al., 2011). Unilateral DBS was performed over about 10 minutes in eight PD patients in the STN up to seven days after electrode implantation. High frequency DBS was delivered whenever the beta activity exceeded a threshold amplitude of beta in the STN. This resulted in a 50 % motor score reduction in the contralateral upper limb Unified Parkinson's Disease Rating Scale (UPDRS) assessed by blinded evaluation compared to no stimulation. Compared to conventional DBS, aDBS was significantly (27 % absolute reduction) more effective, and resulted in a 56 % reduction in time on stimulation. An important element of the study was the comparison of aDBS to random, intermittent stimulation unlocked to LFP bursts of beta activity. Random DBS resulted in trivial UPDRS improvements of 7 % in blinded

assessments despite involving almost exactly the same time on stimulation as aDBS. Hence randomness of stimulation could not account for the clinical efficacy of aDBS.

Nevertheless, this proof of principle study was limited by short stimulation times and unilateral application that did not allow assessment of axial signs and gait. These limitations were addressed in a follow-up study of bilateral aDBS in four PD patients tested over stimulation sessions lasting up to about two hours (Little et al., 2015). Here aDBS improved blinded total UPDRS III scores by 43 % compared to no stimulation (Fig. 1.4), similar to the improvement in conventional DBS studies in which blinded video assessments have been made (Ford et al., 2004; Castrioto, 2011). aDBS also resulted in a 45 % reduction in stimulation time, which could be decreased further by additional administration of levodopa. The bilateral sensing and stimulation, and longer stimulation times in this study enabled the assessment of gait and axial signs which presented an improvement on the earlier study. However, no direct comparisons between aDBS and conventional DBS were made.

An additional animal study trialled amplitude-responsive DBS of the STN in a single non-human primate 1-methyl-4-phenyl-1,2,3,6-tetrahydropyridine (MPTP) model of PD (Johnson et al., 2016). The study found aDBS to be as good, if not better, than cDBS in reducing rigidity despite stimulation being present for only about 50% of the time, and that reaching speed was not changed by either treatment. However, only cDBS reduced the speed of the return from a reach with the upper limb in a cue reaching task.

Together these studies suggest that, at least under acute testing conditions, aDBS is effective despite involving substantially less energy than conventional DBS. This reduction in energy raises the hope that side-effects will be correspondingly less for a given voltage or current of stimulation than with conventional DBS, and that the goal of a widened therapeutic window might be met. Two further studies support this hypothesis.

The first was a case report of bilateral aDBS in a freely moving PD patient (Rosa et al., 2015). Here a scalar approach was chosen where stimulation voltages varied according to LFP beta changes through a personalized algorithm, rather than the binary 'bang/bang' approach of turning DBS on and off used in other studies (Fig. 1.3B, lower green panel). aDBS substantially reduced the dyskinesias otherwise seen in both rest and gait during conventional DBS in the medicated patient. The acute impact of aDBS on speech was assessed in 10 PD patients in a further study (Little et al., 2016). The patients received bilateral aDBS and conventional DBS, but only conventional DBS caused an acute deterioration in speech, assessed through the blinded assessment of the speech intelligibility test. This was despite the better motor improvement with aDBS in this cohort.

One concern with the use of beta activity as a feedback biomarker has been what might happen during movement, when beta activity is suppressed (Johnson et al., 2016). In practice this has not been a problem in patient studies, as much of the motor UPDRS involves active movement, and yet this is improved during beta amplitude-responsive aDBS. This might be because bradykinetic movements are associated with poor beta reactivity, so that impaired movement may still be accompanied by beta activity that is sufficient to trigger stimulation (Doyle et al., 2005; Androulidakis et al., 2007; Anzak et al., 2012; Tan et al., 2013). Dopaminergic medication improves both beta reactivity and movement, but stimulation under these more physiological circumstances is less relevant. Another issue has been how might amplitude-responsive aDBS work in Parkinson's disease. This was addressed in a recent electrophysiological analysis of previously reported data sets (Tinkhauser et al., 2017a). The study showed that aDBS selectively trims long duration beta bursts, and increases the number of short beta bursts, relative to no stimulation and conventional DBS. Critically, the amplitude of beta bursts scales with

their duration, so that longer bursts signal greater pathological oscillatory synchronisation within the local neural population. In line with this, the authors demonstrated that the prevalence of short and long beta bursts negatively and positively correlated with motor impairment, respectively. Furthermore, additional studies are required to better

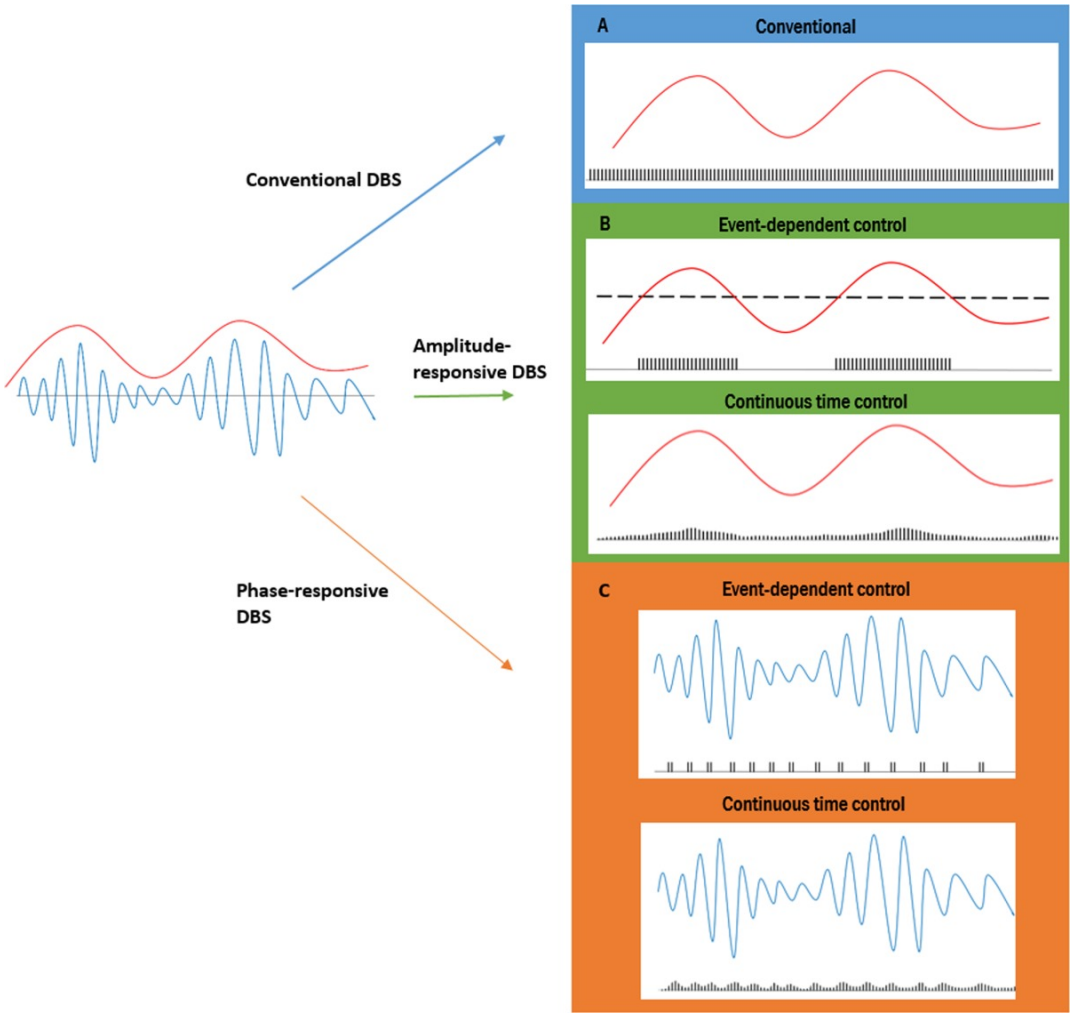


Figure 1.3 - Schematic summary displaying different forms of DBS. **A**) shows conventional DBS where pulses occur at a constant frequency. **B**) depicts two forms of amplitude responsive aDBS; upper green panel, event-dependent control where stimulation is triggered and terminated when a signal, like beta-amplitude, rises above and falls below a threshold, respectively and green lower panel, continuous-time control where stimulation varies proportionately to the amplitude of the signal. **C**) shows phase-responsive aDBS where pulses of high-frequency stimulation are timed to a particular phase by either event-dependent (upper orange panel) or continuous time control (lower orange panel).

characterise the physiological significance of beta burst properties, since additional parameters could be derived to optimise closed loop control policies in future.

In summary, the evidence to date supports the view that aDBS may afford a wider therapeutic window than conventional DBS in PD. However, all studies have been performed in the acute post-operative setting and have important limitations that will be discussed later.

What about amplitude-responsive DBS for tremor? Here there have been several trials. These, unlike the above, have been performed in chronically implanted patients, although they still remain acute in nature. The earliest study used not the severity of tremor itself to trigger stimulation onset, but surface electromyographic (EMG) activity over the deltoid muscle signalling upper limb activation. This was then used to trigger periods of thalamic DBS in five patients with severe intention tremor due to multiple sclerosis, two of whom had pronounced functional benefit (Brice and McLellan, 1980). However, the absence of a control condition without stimulation meant that it was unclear whether benefit was due to lesion effects or adaptive DBS. Subsequent studies have used the severity of tremor recorded with peripheral inertial-based sensors and/or surface EMG activity as the feedback signal, a personal computer to process the signals, extract key features and implement the control algorithm, and electromagnetic telemetric communication with the IPG. Control algorithms usually involve simple thresholding of processed signals, but can be more sophisticated, and utilise additional information about whether the patient is engaged in rest, posture or action (Basu et al., 2013). The nature of the telemetric link and implanted IPG has meant that stimulation is then controlled with a ‘bang/bang’ approach of turning DBS on and off.

The clinical efficacy of aDBS for tremor can be difficult to ascertain from these more recent trials, as some only formally evaluate the success of tremor prediction (Basu et al.,

2013) or report changes in tremor amplitude, rather than changes in clinical rating scales more readily related to disability. Yamamoto et al (2013) aimed to treat intention tremor in patients with severe essential tremor and triggered high frequency thalamic DBS whenever spectral power at tremor frequency in the EMG recorded over biceps brachii exceeded a customised threshold (Yamamoto et al., 2013). This led to complete resolution of intention and action tremor, as assessed unblinded using corresponding elements of the essential tremor rating scale in all four patients tested. The average time on stimulation was not reported, however. Another important trial explored amplitude-responsive aDBS in tremor-dominant PD (Malekmohammadi et al., 2016). Five patients were studied and unilateral high frequency DBS was delivered whenever the tremor power detected by a Smart Watch exceeded a threshold. Tremor power was reduced on average only by 37% relative to baseline, but this was achieved with voltages that were almost 80% lower than those used for conventional DBS. Stimulation was also delivered for only 50 % of the time. However, the system had difficulty in distinguishing tremor from episodes of voluntary movements and these were therefore excluded from analysis.

Phase-responsive aDBS

Where we have good reason to suspect that a particular neural activity directly relates to symptomatology, we can potentially increase the efficiency and selectivity of electrical stimulation by patterning the latter so that it specifically modulates the causal neural activity. In a landmark study from 2011 Rosin et al. performed a form of phase-responsive aDBS in the 1-methyl-4-phenyl-1,2,3,6-tetrahydropyridine (MTPT) model of PD in two non-human primates (Rosin et al., 2011). They showed aDBS to be more effective at attenuating motor symptoms compared to cDBS when applying brief, high-frequency bursts of simulation to the globus pallidus interna, 80 ms after detection of

spikes in single motor neuron recorded in the ipsilateral M1. The 80 ms delay was critical in improving motor impairment and corresponded to the cycle of the 9-15 Hz beta band oscillations typical of this model. More recently phase-responsive aDBS has been applied to treat tremor (Cagnan et al., 2016). The assumption here is that oscillatory activity in brain circuits drives peripheral tremor oscillations with a more-or-less fixed time delay, so that delivering DBS pulses at particular phases of the cycle of the peripheral tremor will also mean that such stimulation is phase locked (albeit with a fixed offset) to the pathological neural activity. Dynamical systems theory and empirical data suggests that there should be phases at which impulses will increase or decrease the amplitude of the oscillations, just as there are points in the excursion of a child's swing at which a push will impede or increase the swing cycle (Cagnan et al., 2013). Phase-responsive aDBS for tremor aims to selectively stimulate at those phases that attenuate tremor amplitude. Stimulation consists of bursts of high frequency pulses timed to a particular phase of the tremor and delivered to the ventrolateral thalamus (Fig. 1.3C, upper orange panel). Sustained locking of DBS to the optimal phase for amplitude suppression led to clinically significant tremor relief in three of the five patients with essential tremor tested despite delivering less than half the energy of conventional high frequency stimulation (Cagnan et al., 2016).

Nevertheless, phase-responsive aDBS has not been delivered for longer than 30s thus far, and longer trials are essential. Only then will it be possible to test whether this form of stimulation will give sustained tremor suppression with an improved side-effect profile due to the lower energy delivery and selectivity for those oscillations that are phase locked to the stimulation. In the longer term it will also be interesting to see if this technique can improve akinesia and rigidity when stimulation is phase-locked to beta activity in the STN.

In practice the successful application of phase-responsive aDBS will also entail consideration of how best to keep pathological oscillators in the desynchronised state. This is because the amplitude attenuating effects of aDBS at suppressive phases build up over many cycles. Phase-responsive aDBS alone would mean a delay in tremor suppression whenever significant tremor emerged. In the study by Cagnan et al (2016) when phase-responsive aDBS induced clinically significant tremor suppression it did so over the course of several seconds in some patients with essential tremor, but then, the weak tremor precluded reliable identification of tremor phase and effectively led to random stimulation at low frequency (Cagnan et al., 2016). Despite this tremor remained suppressed, raising the possibility that random low frequency stimulation is sufficient to keep central tremor oscillators desynchronised once they have been suppressed. In summary, phase-responsive aDBS may be best thought of as a means of suppressing tremor and controlling episodes of break-through tremor, but a necessary adjunct may be intercurrent stimulation to maintain tremor in its attenuated state. In this regard, phase-responsive aDBS might be considered similar to conventional high frequency DBS in that the acute effect of both on tremor is delayed, and the clinical benefits accrue because once tremor is suppressed it is maintained in this state by continued stimulation. The major difference is that aDBS may involve lower overall frequencies of stimulation and less energy delivery.

1.3.3 Limitations and roadblocks

Difficulty in assessing efficacy

Trials of aDBS in which feedback is derived from LFP activity have necessarily been carried out 2-7 days after electrode implantation because of the need to record directly from implanted electrodes. This is problematic. First and foremost, patients may

experience substantial symptom relief as a result of the so-called 'stun effect' resulting from local edema and micro-lesions (Mestre et al., 2016), and it is for this reason that most centres delay postoperative programming (Deuschl et al., 2006b). The stun effect refers to a common phenomenon seen following DBS-surgery where the implantation of the electrodes themselves improve motor-scores without the application of stimulation (Mestre et al., 2016).

The exact duration of the stun effect is not fully established but recent studies have found UPDRS score improvements off stimulation postoperatively compared to the preoperative state for up to six months after electrode placement (Mestre et al., 2016). Similarly, it has been shown that changes in both impedance and LFPs occur after electrode implantation, particularly within the first 24 hours (Williams et al., 2007; Lempka et al., 2010; Rosa et al., 2010). For these reasons, acute peri-operative aDBS findings may not necessarily be representative of the chronic state.

Another disadvantage of studying the effects of aDBS in the acute postoperative setting is the limited time available and the confound of postoperative fatigue leading to drifts in baseline performance. Time constraints and stun effects limit the extent to which conventional DBS may be optimised, and this may explain why conventional DBS fails to have an appreciable therapeutic effect in some studies (Rosa et al., 2015; Little et al., 2016). This complicates the interpretation of the acute peri-operative contrast of the performance of aDBS and conventional DBS, as neither may be representative of that following recurrent optimisation in the chronically treated patient. The above limitations, with the exception of time constraints, could be circumvented by contrasting aDBS and conventional DBS acutely at the time of battery change. Here stun effects are absent and the experimenter benefits from the knowledge of the clinically optimised stimulation parameters. Ultimately the comparative efficacy of aDBS and conventional DBS should

be assessed during chronic treatment at home, where impact on quality of life may also be determined. In future chronically implanted bidirectional devices such as the Responsive Neurostimulation system (RNS) or the Activa PC+S can help overcome such struggles (Cagnan et al., 2019)

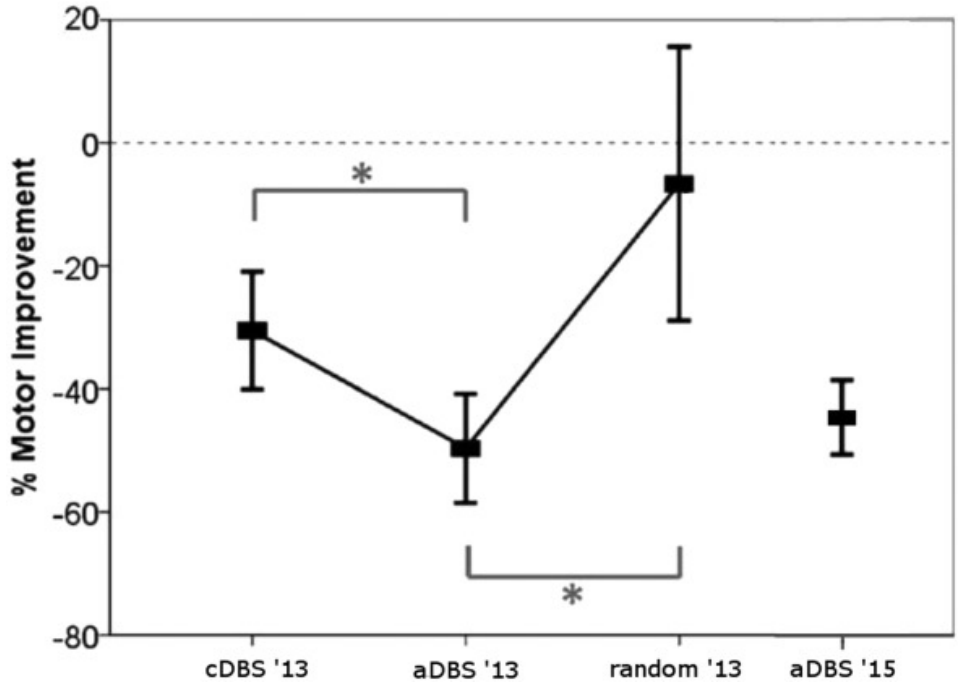


Figure 1.4 - Improvements in motor scores assessed blinded in the studies of Little et al. 2013 and Little et al 2015 (combined figures). Data are presented as the mean ± standard error of the mean percentage change in UPDRS scores.

Difficulty in assessing side-effects

Although there have been some encouraging initial reports of reduced side-effects during aDBS, those side-effects seen and tested in the acute post-implantation period may also be unrepresentative of the chronic state. Dyskinesias may, for example, be problematic when stimulation is combined with dopaminergic medication following surgery, but this will be less so once the stun effect abates and once medication has been titrated over time,

and so the impact of aDBS on this side-effect less remarkable in the chronic state (Rosa et al., 2015). The speech impairment that was shown with acute conventional DBS, and was absent with aDBS, might also disappear with optimisation of conventional DBS stimulation site and parameters over time (Little et al., 2016). In reality side-effects should be assessed during chronic treatment in the patient's everyday environment, with the clinical team afforded the opportunity to optimise both DBS therapy and medication.

Insufficient time for adaptive effects

The mechanisms by which DBS exerts its therapeutic effects are still not fully understood and are very likely multimodal involving various time dependent mechanisms like acute local neuromodulation, changes in synaptic plasticity, and long-term anatomical reorganisation (Herrington et al., 2015). Any potential, adaptive long-term effects cannot be studied in the acute setting and will need to be assessed during chronic treatment. Interestingly, a tendency for the time on stimulation to progressively fall during aDBS has been reported, suggestive of short-term plasticity (Little et al., 2013). Such plasticity has also been noted in computational studies of desynchronizing brain stimulation, including DBS (Hauptmann and Tass, 2007), and may contribute to the carry-over effects of high frequency electrical stimulation triggered by automated seizure detection noted in patients with epilepsy (Osorio et al., 2005).

The converse of the above is maladaptive plasticity, and this is perhaps commonest in the treatment of essential tremor by conventional thalamic DBS. Here it leads to habituation to the effects of DBS over time and gait ataxia (Barbe et al., 2011; Reich et al., 2016), and prolonged trials are necessary to determine whether this also occurs with aDBS.

Use of simplistic feedback biomarkers and control algorithms

Hitherto, feedback signals have generally been one dimensional, such as beta power or tremor severity. However, this may be sub-optimal. For example, beta power in the STN correlates with bradykinesia and rigidity, but it does not do so with tremor (Kühn et al., 2006; Beudel and Brown, 2015). Thus aDBS systems that rely on beta activity feedback run the risk of not controlling tremor. So far, in practice, this has not been the case, perhaps because tremor is one of the features that is most susceptible to the stun effect, or because the stimulation intensity necessary for tremor suppression is below that needed for beta suppression, and bursts of aDBS are given sufficiently frequently for tremor to remain suppressed. Nevertheless, there is a case to be made for combining both beta activity and inertial sensor activity in a dual feedback control loop (Fig 1.5). Indeed, there are many other possible brain and peripheral signals that correlate with motor impairment which could, in principle, be combined for more precise control of different symptoms (Little and Brown, 2012; Beudel and Brown, 2015; Arlotti et al., 2016; Kühn and Volkmann, 2016).

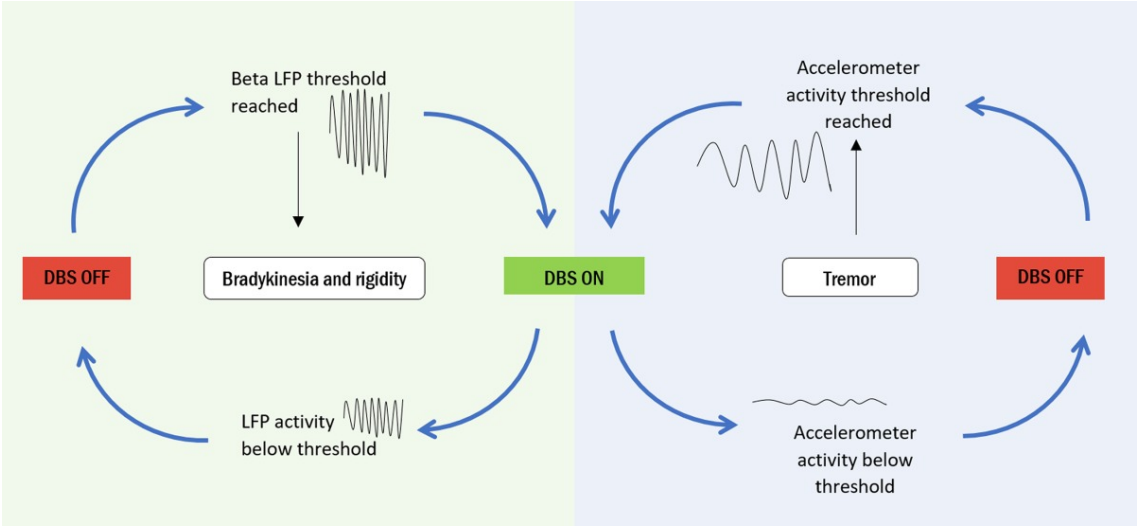


Figure 1.5 - Potential combined beta-tremor control loops. DBS stimulation is triggered whenever one or other or both signals cross independent thresholds and is terminated whenever both signals have fallen below their thresholds.

However, the potential use of multiple feedback signals raises issues of redundancy, sufficiency and tractability. Is the information from additional signals redundant? Are the benefits to be had with existing biomarkers, if borne out with chronic aDBS, sufficient in offering a step improvement in therapy? Are other candidate feedback signals tractable and practical in combination or alone? Consider, for example the recording of the STN high-frequency oscillations (HFO) over 100-400 Hz, and the modulation of these by the amplitude of local beta activity (phase-amplitude coupling or PAC, see Chapter 1.2.4), which have been demonstrated to correlate with bradykinesia and rigidity (Lopez-Azcarate et al., 2010; van Wijk et al., 2016). Detecting the very low amplitude of STN HFOs in the setting of high frequency stimulation delivered through the same electrode is likely to be very difficult, and possibly power demanding. An alternative might be to record PAC at the level of the motor cortex (de Hemptinne et al., 2013), but it is unclear whether cortical HFOs are any different in amplitude to those in the STN. On the other hand, as previously discussed PAC may be at least partly driven by asymmetries in the waveform of beta band oscillations (Lozano-Soldevilla et al., 2016; Cole et al., 2017), and in this case there would certainly be advantages to recording PAC or other measures of this asymmetry at the cortex as cortical beta is of significantly greater magnitude than STN beta, due to the improved spatio-temporal integration afforded by cortical lamination.

In addition to the simplicity of current feedback signals, amplitude-responsive aDBS has most often relied on a bang-bang control policy. This is an 'event-dependant control' whereby the change of state (on/off) of the stimulation depends on beta amplitude, for example, crossing a predefined threshold (Fig 1.2 B, upper green panel). Although this can work well, e.g. in the thermostatic control of central heating, it ignores information

that might be afforded by the continuous evolution of the feedback signal. For example, is room temperature dropping fast, in which case there might be an advantage in turning on the central heating earlier or higher. Continuous evolution of the signal is considered in 'continuous-time control' strategies (Figure 1.2 C, lower green panel). So far, the latter have been implemented in the simple form of the 'proportional' control used by Rosa et al. (2015). Here high frequency stimulation was controlled so that its intensity depended proportionally (with a constant gain) on the amplitude of beta activity at all times. An alternative approach would be to implement Proportional-Integral-Derivative (PID) control, a well-established and successful engineering method (Åström and Hägglund, 1995), recently successfully applied in automated insulin delivery systems (Ly et al., 2016). With PID control stimulation intensity is determined, at any moment in time, by a linear combination of individually weighted factors; a constant proportion of the difference between the set reference/threshold and the actual temporal evolution of the feedback signal (for example, the difference between beta threshold and actually measured beta), the past accumulated error given by integrating the error, and a prediction of the possible future evolution of the error estimated by differentiating the error. Thus, PID control affords continuous control of stimulation intensity that takes into account the present, past and future of the deviation from the set reference or threshold. This form of control responds to and anticipates changes in the feedback signal both rapidly and efficiently. Moreover, continuous-time control lends itself to implement more advanced control approaches like nonlinear stochastic dynamic control or multivariable control. A simple example of the latter would be a 'dual-control system' whereby central beta activity and inertial signals related to peripheral tremor are simultaneously controlled by stimulation, or different spectral elements of the local field potential activity are simultaneously controlled, but with different set references. This versatility of

continuous-time control, however, again underscores the need to consider issues of redundancy, sufficiency and tractability in aDBS design. Furthermore, it is critical that such design considers biological constraints. One specific constraint with respect to DBS is that stimulation effects have a threshold, so that continuous time-control below this threshold may be relatively superfluous and inefficient. Accordingly, future implementations of aDBS may involve hybrid control whereby continuous-time control approaches kick in once a threshold signal value is surpassed.

When considering multidimensional feedback and more sophisticated control systems it is also important to bear in mind limitations on the embedded computing power possible in implanted systems and the battery power burden that these operations may bring. Amplitude-responsive aDBS has been estimated to decrease total electrical energy delivered by about 130μW per side (Little et al., 2013), whilst the energy consumed by a low-energy circuit underpinning a single-channel power classifier should be no more than about 10μW. Thus unidimensional signals and a simple control policy can achieve very significant energy savings, but this remains to be seen if more complex approaches are sought (Afshar et al., 2012).

Lack of optimisation

Hitherto the threshold of bang-bang control or the gain of the proportional control have been determined heuristically. This means that although beneficial they may not still be optimal. Indeed, there are multiple parameters to select and optimise in DBS, including contacts to be stimulated, pulse width, stimulation frequency and stimulation intensity. In amplitude-responsive DBS additional variables are the frequency-band of interest and smoothing of the feedback signal, the threshold, the steepness of any ramp in stimulation introduced to limit side-effects like paraesthesia, and the duration of any lock-out period

before stimulation can be triggered again. In phase-responsive DBS additional variables are the selection of the phase for stimulation, and the number and frequency of pulses to be delivered at that phase. So far choices have been made on empirical grounds, but the very presence of an informative feedback signal offers the possibility of automatic, on-line, comprehensive optimisation of variables to achieve maximal effect on the feedback signal, -something that is just not feasible to achieve through clinical assessments.

Questions about long-term stability

What if the biomarker features and the thresholds or gearings used in aDBS change over time, with medication changes, alteration in the brain-electrode interface or disease progression? At present this question is totally unexplored, as aDBS has only been acutely trialled. However, for aDBS to be clinically useful it must be robust to changes over time, and may need the functionality to perform auto-identification and auto-tuning, so that the system can identify on-line and in real-time optimal control parameters. As a minimum, it may be necessary to include a system that monitors the stability of the control loop. Such a system could, for instance, be implemented in a simple way by using a performance index like the 'Integral Time-weighted Absolute error' (ITAE) which can be performed with very little computing power (Åström and Hägglund, 1995). This would enable a 'fail-safe' approach whereby should the performance index exceed a given value then aDBS could be reverted to cDBS; then, when the performance index returns to a suitable value, the aDBS algorithm would be re-activated.

The optimal biomarker

Numerous electrophysiological biomarkers have been brought forward that could be utilised for closed-loop experimental interventions in PD (Fig. 1.2) (Brown et al., 2001;

Lopez-Azcarate et al., 2010; Little and Brown, 2014; de Hemptinne et al., 2015; Cole et al., 2017; Arlotti et al., 2018; Bouthour et al., 2019; Holt et al., 2019). However, as outlined in this chapter only the beta-oscillation has hitherto been subjected to real-time experimental aDBS applications, and very little is known about the causal or the statistical interdependency of beta and other proposed biomarkers. Are there better outcomes, if indeed any, to be had from focussing stimulation on one biomarker over the other? If so, what would be the best way to interfere with such a biomarker, serving as a parameter of underlying pathophysiological processes? What structures would be most optimal for the biomarkers to be extracted from? What is the neuronal basis for the biomarkers observed? What role, if any at all, do the basal ganglia-thalamo-cortical and cerebello-thalamo-cortical pathways play in the biomarkers' formation? In order to find the most optimal signal such questions remain to be answered.

1.3.4 Conclusion

Adaptive DBS is a promising therapeutic development that may, in time, complement other innovative approaches to deep brain stimulation, such as novel pulse parameters or current steering (Kühn and Volkmann, 2016). The hope, too, is that it might eventually be rolled out to movement disorders other than Parkinsonism and tremor, as knowledge of correlating biomarkers or causal neural patterns matures. Phase-responsive aDBS might also lend itself to the control of some of the intractable childhood epilepsy syndromes characterised by long and rhythmic sequences of epileptic activity. However, the aDBS studies performed to date have significant limitations, and these stem from the fact that the investigations have all necessarily been acute, either because the only way to reliably record low amplitude subcortical LFPs and to rapidly react to changes is to externalise electrode connections in the short-lived peri-operative window, or because

electromagnetic telemetry links to chronically implanted IPGs are slow, sensitive to alignment, and unsuitable for chronic trials in real-life situations. We are therefore fast approaching an impasse in which the utility and chronic viability of aDBS cannot be further explored without suitably functioning, implantable, medical grade devices. Meanwhile, until we have a better understanding of the underlying neuronal basis, only trial and error attempts can guide closed-loop DBS experiments. It is therefore vital to further the understanding of what mechanistically is at play on a neuronal level in order to best inform future stimulation strategies. What is the basis of subthalamic PAC and HFOs and how do they relate to beta-bursts? How do cortical asymmetries relate to subthalamic neuronal firing? Very little is known about the interdependence of all proposed biomarkers. Are the cortical biomarkers indeed reflective of BTC-network activity? Can information be had from utilising one over the other? Or when are we in fact merely looking at two sides of the same coin?

1.4 Main aims and findings

The general introduction has provided an overview of existing biomarkers for closed-loop DBS interventions in Parkinson's disease, their current utilisation in closed-loop applications and raised numerous questions relating to the neurophysiology and pathophysiology behind these signals. The overarching aim of this thesis was to study the neuronal basis of some of the most prominent biomarkers and their interdependency, using cortical and subthalamic recordings in human PD patients and optogenetic stimulation to drive basal ganglia and cerebellar receiving thalamus in mice.

Study 1 (Chapter 3)

In the first study we examined micro and macro electrode recordings of LFPs and single unit activity from the STN in human PD patients undergoing DBS surgery. The aim was to study the neuronal origin of phase-amplitude coupling, a proposed biomarker for closed-loop DBS and relate it to another significant biomarker, beta bursts.

Our findings offer new insight in the pathology of Parkinson's disease by providing numerous lines of evidence that subthalamic PAC reflects the locking of spiking activity to network beta oscillations and that this coupling progressively increases with beta-burst duration. These findings suggest that beta-bursts capture periods of increased subthalamic input/output synchronisation in the beta frequency range and have important implications for therapeutic closed-loop DBS.

Study 2 (Chapter 4)

In the second study we analyse simultaneous cortical ECoG and subthalamic macro- and micro electrode recordings of LFPs and single unit activity in PD patients undergoing

DBS surgery. The aim was to examine how cortical waveform asymmetries, cross-regional phase-amplitude coupling and beta bursts relate to subthalamic neuronal firing and to each other. The approach was here to compare some of the most prominent biomarkers across the BTC-network and to gain a better understanding of their relationship with subthalamic neuronal activity.

We found that cortico-subthalamic PAC increased progressively with beta-burst duration and captured the synchronisation of STN single unit activity to cortical beta oscillations. Furthermore, peak sharpness of cortical beta progressively increased with the duration of cortical beta bursts and reflected the degree of STN subthalamic spike locking to cortex, providing the first link between cortical beta peak sharpness and STN single unit activity. Our findings demonstrate that duration of cortical beta-bursts modulates several other electrophysiological biomarkers of PD and captures increasing levels of pathological neuronal activity.

Study 3 (Chapter 5)

In the third study optogenetic stimulation is applied to basal ganglia recipient thalamus and cerebellar recipient thalamus, respectively, in mice to study simultaneous changes in ECoG and cortical laminar LFP probe recordings. We address the hypothesis that cortical PAC and beta waveform asymmetries, as seen in PD, can be produced by driving motor thalamic input.

The study gives numerous lines of evidence that cortical PAC can arise from stimulation of the basal ganglia recipient thalamus, but not the cerebellar recipient thalamus, by the induction of nonlinearities in the beta-oscillations. This suggests that cortical PAC and asymmetries in beta oscillations could serve as a viable biomarker of the basal ganglia drive of motor thalamic input.

2

General methods

Contents

2.1 Overview

2.2 Ethics

2.3 Electrophysiological recording techniques

2.4 Principles behind optogenetic stimulation

2.5 General data analysis

2.5.1 Phase-amplitude coupling

2.5.2 Time-frequency decompositions

2.5.3 Beta bursts analysis

2.5.4 Waveform asymmetries

2.6 Statistical analysis

2.1 Overview

This chapter gives a brief overview of the theories behind some of the major analysis applied throughout this thesis. Details on the recording setups, specific data analysis, data processing and applied statistics for individual experiments are outlined in respective Chapters 3-5.

All computations were written and performed in Matlab (R2017a, The Mathworks Inc., Natick, USA) if not otherwise specified.

2.2 Ethics

All human data analysed in this thesis was acquired from participants, who all gave their informed written consent in accordance the Code of Ethics of the World Medical Association (Helsinki Declaration, 1967). All animal experiments referenced have been conducted in accordance with the UK Animals (Scientific Procedures) Act 1986 under personal and project licenses issued by the Home Office following ethical reviews. All experimental protocols had been approved by local ethics committees.

2.3 Electrophysiological recording techniques

In addition to the specific experimental methods in the individual chapters, below a brief overview is provided of the various recording techniques used for neurophysiological signal extraction in humans and rodents throughout this thesis. Chapters 3 and 4 are based on local field potentials (LFPs) and electrocorticograms (ECoGs) recordings from human PD patients undergoing DBS electrode implantation surgery. Chapter 5 is based on ECoG and probe channel LFP recordings throughout the laminas of motor cortex in rodents undergoing selective optogenetic-stimulation of either basal ganglia or cerebellar recipient thalamus.

Implantation and externalisation of electrodes in the subthalamic nucleus during DBS surgery as a treatment in PD has allowed scientists and clinicians unprecedented access to extract and study LFPs from macroelectrodes in awake humans. The LFP is thought to represent the summations of extracellular potentials generated by cellular transmembrane currents as described in biophysics under the rules of volume conductor theories (Buzsáki et al., 2012; Einevoll et al., 2013). Generally speaking, the two main contributors to the LFPs are considered to be the cellular-synaptic architectural organization of the network and synchrony of the current sources (Buzsáki et al., 2012). The greatest single factor to LFPs are mostly thought to be changes in transmembrane currents of synaptic inputs onto dendrites according to most experimental studies and studies of inverse and forward modelling (Einevoll et al., 2007, 2013; Potjans and Diesmann, 2012). Others argue that also spiking and intrinsic membrane oscillations can substantially shape the LFPs (Buzsáki et al., 2012). Our biophysical understanding of LFPs does not immediately get less complicated by the temporal decomposition of LFPs into numerous frequency bands that might all have their individual spatial origins (Colgin et al., 2009; Spaak et al., 2012; Jensen et al., 2016). The same can be said for the interdependency and interactions (statistical cross frequency coupling) between these various oscillations within and across regions (Canolty et al., 2006; Canolty, R T, 2012; Hemptinne et al., 2015; Jensen et al., 2016),

The ECoG has been increasingly applied in recent years as neurosurgery has allowed for unprecedented access to cortical structures in human patients (Engel et al., 2005; Buzsáki et al., 2012; Brunet et al., 2015; Watrous et al., 2015; Moses et al., 2019). Th ECoG can either be extracted from subdural grid electrodes on the cortical surface or as in the case

of this thesis from an electrode placed right above the dura in the surgical burr hole (Sharott et al., 2018). ECoG has the great advantage to the EEG, that it measures the electrical activity directly from the surface of the brain and not through the thickness of the signal disturbing skull as is the case with EEG (Buzsáki et al., 2012) and thus offers much higher signal-to-noise ratios and greater spatial and temporal resolutions (Hill et al., 2012; Dubey and Ray, 2019).

2.4 Principles behind optogenetic stimulation

In Chapter 5 optogenetics is applied to selectively stimulate basal-ganglia or cerebellar recipient thalamus at different frequencies, while simultaneously recording ECoG signals and LFPs throughout the laminas of motor cortex. How optogenetic stimulation is applied in this thesis will be described in detail in Chapter 5. The following is intended as a general introduction to optogenetics as a stimulation technique.

Optogenetics has become a viable tool in the investigation of neuronal circuits by allowing for selective neuronal activation or inactivation with high temporal and spatial precision by the use of viral opsins and light stimulation (Miesenböck, 2011; Tye and Deisseroth, 2012; Deisseroth, 2015). The toolbox for such interventions has been rapidly expanding over the last fifteen years with increasingly refined precision to become one of the most revolutionary techniques in neuroscience for the investigation of causal relationships in neuronal circuits (Boyden et al., 2005; Miesenböck, 2011; Deisseroth, 2015).

Microbial opsins can be injected into neuronal tissue in order to render neurons responsive to light of a certain wavelength. The most widely applied opsins include channel-rhodopsin 2 (ChR2) and halo-rhodopsin (NpHR) (Deisseroth, 2015). ChR2 is a transmembrane protein that functions as a light-gated ion channel when activated by blue

laser light with action spectrum peaks at wavelengths between 430–550 nm (Nagel et al., 2003; Klapoetke et al., 2014). When exposed to such light ChR2 opens and allows for the cellular influx of cations (Na^+, K^+, Ca^{2+}, and H^+) (Nagel et al., 2003), which manifests in the induction of time-locked action potentials on the timescale of milliseconds (Boyden et al., 2005; Zhang et al., 2007; Deisseroth, 2015). The activation of NpHR, on the other hand, induces the net Cl^- influxes through active anion channels, leading to neuronal hyperpolarisation and inhibition (Gradinaru et al., 2008; Busskamp et al., 2010).

Since the initial discovery and neuroscientific applications of opsins an increasing need for specificity with regards to neuronal circuitry subdivisions has been met (Deisseroth, 2015). The creation of Cre dependant opsin expression has enabled the selective induction of opsins in specific Cre+ neurons (Atasoy et al., 2008). This can be done through either genetically modified animals to express Cre in selected areas or through the injections of a virus that expresses Cre coupled to a trans-neuronal tracer such as wheat germ agglutinin (WGA) (Gradinaru et al., 2010; Libbrecht et al., 2017). In this thesis the latter approach has been taken, where brain areas can be targeted by injecting a WGA-Cre virus into any area that is connected either anterogradely or retrogradely through long range projections to the brain area of interest (Fig. 2.1) (Gradinaru et al., 2010; Grosenick et al., 2015; Libbrecht et al., 2017). Hereby, Cre is transcellularly delivered to cells that are connected to the first injection area and a second injection of the Cre-dependant opsin into the area of interest ensures that only neurons with connection to the WGA-Cre injected area are induced to express the opsin (Gradinaru et al., 2010; Libbrecht et al., 2017). Consequently, only such cells will be induced to become light sensitive (Tye and Deisseroth, 2012).

Optogenetic stimulation has undeniably been a pioneering tool in neuroscience but has also presented with certain limitations and challenges (Grosenick et al., 2015). For

example, a study found that when light was shed on ChR2 neurons for very long durations, unintended and paradoxical neuronal inactivation might occur (Herman et al., 2014). And despite the advantage of applying light and not electric current simultaneous to carrying out electrophysiological recordings, a study found that simultaneous electrophysiological recordings and light stimulation in the same brain area could manifest in photoelectrical artefacts in electrophysiological signals (Kozai and Vazquez, 2015).

Specific implantations as well as challenges and limitations in this thesis relating to individual optogenetic experiments and their generalisability, will be discussed in Chapters 5 and 6.

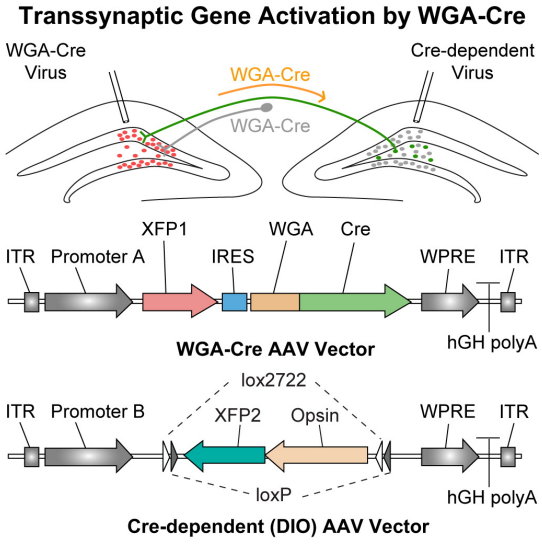


Figure 2.1 – Upper row: Schematic shows injection of the transcellular WGA-Cre fusion gene virus into a brain area that projects in long-range to the brain area of interest. In this second area a Cre-dependent opsin virus is injected. The result is that Cre is transcellularly delivered to activate distant opsin gene expression only in connected neurons that have received the Cre-dependent virus.

Lower row: Schematic of the WGA-Cre and Cre-dependent (bottom) AAV vectors.

The figure is reproduced from Gradinaru et al. 2010 for this thesis with permission from Elsevier (License Number 4713141510364).

2.5 General data analysis

2.5.1 Phase-amplitude coupling

Phase-amplitude coupling (PAC) is a form of cross-frequency coupling (CFC) where the phase of a lower frequency is statically coupled to the amplitude envelope of a higher frequency. In this paper phase amplitude coupling was calculated by either one of two methods: The general linear model or the PLV-modulation index. See individual chapters for discussions of choice of method.

General linear model

The general linear model (GLM) (Penny et al., 2008; van Wijk et al., 2015) allows for parametric estimation of significance by splitting continuous data recordings into epochs of few seconds durations. Furthermore, we used this model to incorporate measures of spike-amplitude coupling.

After the removal of any harmonics, the signal of interest is bandpass filtered to obtain the lower frequency component (x) and the higher frequency component (y). See individual chapters for examples of centre frequencies and frequency increments.
The bandwidth of the amplitude frequency is set to be wide enough to include the centre frequency ± the phase frequency (van Wijk et al., 2015).

The GLM was applied to all phase and amplitude combinations:

$$a_y = \beta_1 \sin(\theta_x) + \beta_2 \cos(\theta_x)$$

With the instantaneous phases being extracted by use of the Hilbert transform using Matlab code:

$$\theta_x = mod(angle\big(hilbert(x)\big), 2\pi)$$

and amplitude of HFO components via

$$a_y = abs(hilbert(y))$$

$\sin(\theta_x)$, $\cos(\theta_x)$ and a_y are transformed to have zero mean and unit variance, for example: $a_y = \big(a_y - \text{mean}\big(a_y\big)\big)/\text{std}\big(a_y\big)$. Beta coefficients are calculated using least squares. And a single PAC value can then be obtained by:

$$r_{PAC} = \sqrt{{\beta_1}^2 + {\beta_2}^2}$$

To test for significance, the time series can be split into non-overlapping epochs of a few second durations to perform parametric statistical testing, yielding separate GLMs and regression coefficients across epochs. An F-test can then be applied to test for beta-coefficient consistency across epochs.

We also extended the GLM-model to incorporate spike-time series into the formula:

$$a_y = \beta_1 \sin(\theta_x) + \beta_2 \cos(\theta_x) + \beta_3 s_x$$

with s_x representing the Z-scored spiking time series. Spike-amplitude coupling was then represented by $\text{Spike}_{\text{AMP}} = \beta_3$ with values ranging from -1 to 1. For individual recordings, a t-test could be performed to test for β_3 consistency across epochs for each amplitude frequency, to determine levels of significance.

PLV PAC modulation index

Another method to test for phase amplitude coupling with greater suitability for shorter data segments is the PLV-modulation index (Penny et al., 2008; Seymour et al., 2017).

The PLV is defined as:

$$PLV = \left| \frac{1}{N} \sum_{n=1}^{N} e^{i(\phi f_p(n) - \phi f_a(n))} \right|$$

ϕf_a represents the phase time series of the higher frequency oscillation amplitude envelope and ϕf_p the beta phase time series. PAC assumes the value of 1 when the phase series are fully locked and 0 if they are completely desynchronised (Tort et al., 2010; Seymour et al., 2017).

Prior to extracting phase and amplitude phase time series the data is bandpass filtered in the frequency ranges of interest. For statistical testing of PAC significance, permutations are performed via 500 surrogate runs of data with circularly shifted permutations of the amplitude data (Penny et al., 2008; Cohen, 2014; Seymour et al., 2017). This involves temporally shifting the power times series by random temporal offsets while keeping the phase angle time series the same. A PAC value is then computed according to the PLV-equation under the null hypothesis from the randomly circshifted data. This is then

repeated 500 times in order to generate a PAC distribution. Standardised z-values of PAC are then derived by taking the original non-circshifted PAC and subtracting the PAC distribution mean and dividing by the standard deviation of the PAC distribution (Cohen, 2014). The normal z-values are then converted to p-values.

2.5.2 Time frequency decompositions

In this this thesis the filter-Hilbert method was used for time-frequency decompositions. In the filter-Hilbert method the data signal sequence is initially bandpass filtered and then so-called Hilbert transformed in order to acquire the complex helical sequence, also referred to as the analytical signal.

$$Y(t) = y(t) + i * H(t)$$

Y(t) represents the analytical signal as a function of time and y(t) represents the real signal (the original data sequence). $iH(t)$ is an imaginary part. The Hilbert-transform, H(t), can be derived from the convolution:

$$H(t) = (\pi * t)^{-1} * y(t)$$

In this thesis the Matlab function *Hilbert* was applied to obtain the analytical signal.

The exact upper and lower range limits of the various frequency bands are somewhat arbitrary in the literature and varies slightly from study to study (Voytek et al., 2010; Buzsáki et al., 2012; de Hemptinne et al., 2013; van Wijk and Wijk, 2017; Zhang et al., 2018). The frequency band definitions applied throughout this thesis if not otherwise specified can be found in Table 2.1.

Frequency band	Frequency range (Hz)
Alpha	8-12
Beta	13-35
Broadband gamma	70-150
HFOs	100-300

Table 2.1 – Frequency band definitions used throughout this thesis if not otherwise specified.

2.5.3 Beta bursts analysis

The beta-burst analysis of the ECoG and LFP data in this thesis is based on the method outlined by Tinkhauser et al. 2017a by applying a 75 % sustained beta-amplitude-threshold criterium. The LFP or ECoG signals are bandpass filtered around the individual beta peak frequency as identified by wavelet frequency decompositions (ft_specest_wavelet script in Fieldtrip - Morlet Wavelet, width = 10, gwidth = 5; Donders Institute for Brain, Cognition and Behaviour, 2010) (Tinkhauser et al., 2017b). The Hilbert amplitude can then be extracted from the filtered signal. If not otherwise specified in individual thesis chapters, the standard criteria for beta bursts periods were defined as time periods exceeding the 75th percentile of the signal amplitude for at least 100 ms. Outside bursting periods if not otherwise defined were defined as the time series, where the beta envelope signal fell below the 50th percentile for longer than 100 ms.

2.5.4 Waveform asymmetries

To assess degrees of waveform asymmetry as a parameter of signal nonlinearities, we apply three measurements adapted from studies by Cole et al. 2017. First the signal of interest is low pass filtered at 100 Hz using a 4th-order Butterworth to exclude high frequency artefacts. Simultaneously, the raw signal is bandpass filtered in the frequency band of interest . The bandpass filtered signal is then used to identify zero crossings in the raw signal in order to go back to the pre-processed signal and identify peaks and troughs. The following measurements is then applied to calculate nonsinusoidal signal features:

$$Sharpness_{peak} = \frac{(V_{peak} - V_{peak-5ms}) + (V_{peak} - V_{peak-5ms})}{2}$$

With sharpness of peaks as the normalised voltage in relation to the normalised voltage 5 milliseconds prior and after to the peak.

The sharpness ratio (SR) being the ratio between sharpness of peaks and troughs:

$$SR = \max\left(\frac{\frac{1}{N_{peaks}}\sum_{peaks} Sharp_{peak}}{\frac{1}{N_{troughs}}\sum_{troughs} Sharp_{troughs}}, \frac{\frac{1}{N_{troughs}}\sum_{troughs} Sharp_{troughs}}{\frac{1}{N_{peaks}}\sum_{peaks} Sharp_{peak}}\right)$$

for an entire recording or a data sequence of interest. Th SR serves as a measure of horizontal signal asymmetry.

To assess vertical cycle asymmetry, we used the rise-decay ratio:

$$RDR = \max\left(\frac{steepness_{decays}}{steepness_{rises}}, \frac{steepness_{rises}}{steepness_{decays}}\right)$$

with steepness defined by as exemplified rise-steepness:

$$steepness_{rise} = max(|V(t+1) - V(t)|, t_{trough} \leq t \leq t_{peak} - 1)$$

The reader is asked to refer to individual methods chapters for the application to the respective data sets.

2.6 Statistical analysis

Statistical analysis throughout this thesis was performed in Matlab. If not otherwise specified, the significance threshold was set at $p < 0.05$. If there were no violations against normality assumptions (as for example assessed by Lilliefors test) t-tests were performed for pair-wise comparisons. In the presence of two or more categorical variables multiway ANOVAs were applied with post-hoc Bonferroni corrections for multiple comparisons to assess the effects of multiple factors on the vector mean.

To determine whether data from several groups have a common mean one-way ANOVAs with repeated measurements were used for parametric estimations of significance with Bonferroni corrections for multiple comparisons. If the dependant variable was ordinal or assumptions of normality were violated a Friedman's test for non-parametric estimation of significance was applied.

For circular data Watson–Williams tests were applied to assess the homogeneity of means of two or more samples and Rayleigh's tests were applied to test for nonuniformity (Berens, 2009). CFC statistics were carried out either via surrogate runs of data with

circularly shifted permutations of the amplitude data and z-value conversion as outlined in Chapter 2.5.1 (Cohen, 2014) or in case of the general linear model via epoch data splitting to perform parametric statistical testing (F-tests) for beta-coefficient consistency across epochs (van Wijk et al., 2015).

All reported correlation coefficients, if not otherwise stated, are Pearson's correlations. If normality assumptions were violated or correlations appeared to be driven by a few outliers a Spearman rank correlation (Spearman's rho) was applied and specifically stated in the text.

3

Synchronised spiking activity, beta bursts and phase amplitude coupling in the subthalamic nucleus of Parkinson's disease patients

Contents

3.1 Introduction
3.2 Methods
- 3.2.1 Surgical procedure and recordings
- 3.2.2 Data selection and processing
- 3.2.3 Phase amplitude coupling by general linear model
- 3.2.4 Spike-amplitude coupling
- 3.2.5 Spike triggered averages
- 3.2.6 Comparison of firing rates and HFO amplitude coupling
- 3.2.7 Unit power spectral densities
- 3.2.8 Spike-phase locking
- 3.2.9 PAC during beta bursts

3.3 Results
- 3.3.1 Defining the presence of STN LFP phase amplitude coupling
- 3.3.2 STN firing predicts HFO amplitude only in the presence of PAC
- 3.3.3 Specific features of PAC are associated with the presence of synchronise beta-oscillations in STN neurons
- 3.3.4 Increased PAC is captured by the duration of beta bursts

3.4 Discussion
- 3.4.1 Physiological basis of PAC in the STN
- 3.4.2 PAC during episodes of transient input synchronisation
- 3.4.3 Subthalamic PAC as a biomarker of pathophysiology

3.1 Introduction

Deep brain stimulation (DBS) is a well-established treatment of severe Parkinson's disease (PD). In recent years several putative biomarkers have emerged for closed-loop applications and new experimental interventions that might further improve DBS efficacy. Beta (13-35 Hz) power in local field potential (LFP) recordings from the subthalamic nucleus (STN) of PD patients correlates with akinetic/rigid motor impairment and is attenuated by DBS and levodopa medication (Kühn et al., 2006, 2008, 2009; Ray et al., 2008a; Steiner et al., 2017). Changes in power of high frequency oscillations (HFOs, 100-300 Hz) have been observed between on and off dopaminergic treatment (Lopez-Azcarate et al., 2010) and during movement initiation and planning (Combrisson et al., 2017). Additionally, neuronal firing patterns in the STN have been linked to symptom severity in PD with intra-burst rates and beta-oscillating unit activity positively relating to bradykinesia, rigidity and axial scores (Sharott et al., 2014).

Phase-amplitude coupling (PAC), where the phase of a low frequency is coupled to the amplitude of higher frequency oscillation, is believed to serve a role in a variety of physiological brain functions (Cohen et al., 2009; Colgin et al., 2009; Tort et al., 2009; Carracedo et al., 2013; Richardson et al., 2017). In PD, however, beta-HFO PAC in the STN (Lopez-Azcarate et al., 2010; van Wijk et al., 2016) and beta-gamma PAC in motor cortex (Shimamoto et al., 2013; de Hemptinne et al., 2015) have been shown to correlate with motor symptom severity in patients and to develop in non-human primates in the STN after dopamine depletion (Escobar et al., 2017). PAC in the STN is attenuated by dopamine replacement (Lopez-Azcarate et al., 2010; van Wijk et al., 2016), and PAC in the motor cortex is reduced by STN DBS (de Hemptinne et al., 2015), providing further evidence for PAC as a biomarker of PD. Whether these correlations reflect a mechanistic

relationship with PD symptoms, and how PAC relates to other established biomarkers of PD symptoms, has not been fully determined.

Interpreting the importance of PAC to PD pathophysiology is complicated by conflicting explanations for the underlying mechanism. Low frequency phase in PAC is often thought to reflect the synchronisation of synaptic potentials that can drive coordinated firing of local neurons (Canolty and Knight, 2010). This mechanism is likely to underlie the phase of beta oscillations in STN LFPs in PD, which have fixed timing relationships to firing of single neurons (Steigerwald et al., 2008; Shimamoto et al., 2013; Yang et al., 2014; Lipski et al., 2017; Sharott et al., 2018). However, recent studies have emphasised the transient nature of beta oscillations, which occur in "bursts" of high amplitude (Tinkhauser et al., 2017a, 2017b). It is currently unclear as to whether PAC is restricted to such bursts or can occur independently of the amplitude of the beta oscillation.

Investigations into the relationship between HFOs and spiking activity in the STN have produced conflicting results. Wang and colleagues (Wang et al., 2014) found that HFOs were independent spatiotemporal phenomena from neuronal spiking. These authors concluded that large pools of desynchronised neuronal clusters give rise to nonstationary HFOs in the LFP that are distinct from the locally-synchronised multiunit activities and are also phase locked to the beta oscillation (Weinberger et al., 2006; Sharott et al., 2014). However, a recent computational study found that synchronized single-cell bursting led to PAC that closely resembled that of parkinsonian mice and primates and could produce PAC resembling that seen in patients (Sanders, 2016).

Using intraoperative macro- and microelectrode recordings in PD patients off medication, we demonstrate that HFO amplitude is related to the firing rate and pattern of single STN neurons in the presence, but not absence of PAC. In addition, PAC and HFO amplitude are higher during beta bursts, suggesting that PAC occurs during enhanced beta synchronisation. These findings suggest that STN PAC could be a proxy for the locking of neurons to network oscillations.

3.2 Methods

3.2.1 Surgical procedure and recordings

Local field potentials and single unit recordings were captured simultaneously from subthalamic nuclei in 15 hemispheres in 10 patients during surgical DBS electrode placement. All patients (6 female, 4 male; mean ± SD age: 66.8 ± 3.4 years) suffered from advanced idiopathic PD and were withdrawn from anti-parkinsonian medication the night before surgery. For patient details see Table 3.1. The surgical procedure yielded 231 local field potential recordings with 157 single units extracted from microelectrode recordings (14 hemispheres in 9 patients were used for analysis of single units. One hemisphere was without unit recordings and was only used for the bursts study). All LFPs/spike train pairs analysed in this paper were recorded by a distance of at least 2 mm to remove spiking contaminations of recorded LFPs in the analysis.

Electrophysiological data from all patients in this study have been reported previously (Sharott et al., 2014, 2018). Operations were performed under local anaesthesia. Details concerning the surgical procedure are reported elsewhere (Sharott et al., 2014, 2018). 10-15 minutes prior to the start of microelectrode recordings at the level of the thalamus (usually 6-12 mm above the centre of the STN as delineated on MRI), systemic sedation with low dose remifentanyl (0.01 - 0.1 μg/kg/min) was completely stopped. No sedatives

or anesthetics were administered during the microelectrode mapping procedure. Participation in the study extended the surgical procedure by approximately 15-25 minutes.

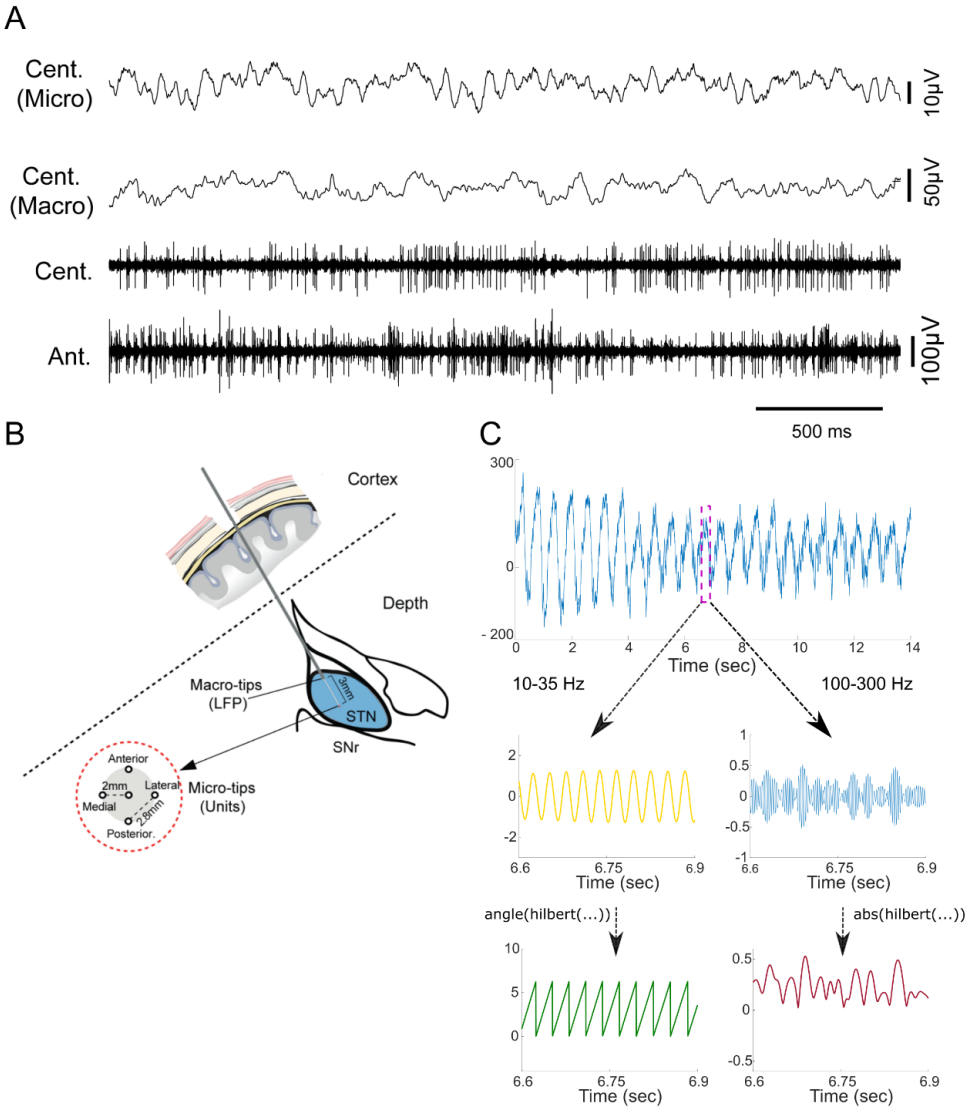


Figure 3.1 – Local field potentials (LFPs) were recorded from the subthalamic nucleus (STN) from micro- and macro-electrode recordings during deep brain stimulation surgery. **A**) Example of micro- and macro electrode recordings of raw LFP signals in one patient and microelectrode multi- and single unit recordings from an anterior and central microelectrode, respectively. The micro electrodes were organised in a concentric array (**B**) with four outer micro electrodes distanced 2 mm from the central micro-electrode. All simultaneous spiking and LFP analyses were made from microelectrodes at least 2 mm apart. **C**) In order to apply the GLM-method to calculate PAC the LFP signal was bandpass filtered and Hilbert transformed in order to extract the instantaneous HFO (100-300 Hz) amplitude and broad beta phase (10-35 Hz).

Microelectrode recordings were performed along five parallel tracks arranged in a concentric array (MicroGuide, Alpha-Omega, Nazareth, Israel) (Fig. 3.1). Four outer platinum–iridium electrodes (impedance = 0.7 ± 0.2 (range, 0.2 - 1.25) megaOhm at 1000 Hz; FHC Inc., Bowdoinham, ME, USA) were separated by 2 mm from a central one, which was aimed at the STN surgical target. Signals were amplified (x20.000), bandpass-filtered (0-300 Hz) and digitized (sampling rate: 24 kHz). An electrode was identified as having entered the STN following a clear increase in the size of the background activity (Moran et al., 2006) and only macroelectrode recordings assessed to originate from within the STN were included in the study. The reader is asked to refer to Moran et al. 2006 for details about the surgical and electro-physiological determination and approach. STN units were distinguished by their tonic irregular, oscillatory or bursty discharge pattern (Fig. 3.1), and this was clearly different from slower bursting and single-spiking of neurons in the overlying thalamus and zona incerta, and from the regular, high frequency spiking of more ventral substantia nigra pars reticulata neurons.

3.2.2 Data selection and processing

All data were collected as part of our routine neuronavigation process which aims to precisely identify the STN. Recordings were only included if they were made during sustained periods during which patients were awake and highly co-operative. In total, 157 STN unit recordings were used in this study. In some recordings, patients were engaged in a simple, brief movement task (flexion/extension of wrist or ankle) as part of the routine mapping procedure. Such epochs comprised a relatively small proportion of individual recordings and we have demonstrated previously that beta oscillations are present in these recordings (Sharott et al., 2014, 2018). Spike detection was performed offline using a voltage threshold method (Offline-Sorter, Plexon Inc., Dallas, TX, USA). The threshold value was set sufficiently high relative to the noise level to avoid false-positives (threshold values > 4 SD of the background level were used). When possible, single unit activities (SUAs) were then separated by manual cluster selection in 3D feature space on the basis of several parameters including signal energy, principal components, peak time and the presence of a central trough in the autocorrelogram. Over half of the unit activities were characterized as SUAs (n = 157). Any portions of injury discharge were discarded.

3.2.3 Phase-amplitude coupling by general linear model

All computation was done in Matlab (R2017a, The Mathworks Inc., Natick, USA). In analyses comparing measures of neuronal activity to PAC, PAC was computed using the General linear model (GLM) method (van Wijk et al., 2015) to allow parametric estimation of significance. After removing 50 Hz harmonics using a 4^{th} order Butterworth filter the LFP signals were initially bandpass filtered around centre frequencies between

10-35 Hz with 1 Hz increments to obtain the beta component and between 100-300 Hz with 4 Hz increments to extract the HFO component. Filter bandwidths were set at ± 1 Hz and ± 35 Hz, respectively, and the instantaneous phase was extracted for the beta components via

$$\theta_x = mod(angle(hilbert(x)), 2\pi)$$

and amplitude of HFO components via

$$a_y = abs(hilbert(y))$$

with *x* representing the beta, and *y* the HFO signal components (Fig. 3.1) as written in Matlab code. The general linear model:

$$a_y = \beta_1 \sin(\theta_x) + \beta_2 \cos(\theta_x)$$

was then applied to all phase and amplitude frequency combinations. Each frequency combination would then yield a single PAC value from

$$r = \sqrt{{\beta_1}^2 + {\beta_2}^2}$$

with beta coefficients calculated via least squares.

$\sin(\theta_x)$, $\cos(\theta_x)$ and a_y were all transformed to have zero mean and unit variance, for example: $a_y = \left(a_y - \text{mean}(a_y)\right)/\text{std}(a_y)$. To test for significance, the time series was divided into non-overlapping epochs of 3 second durations to allow for parametric statistical testing, yielding separate GLMs and regression coefficients across epochs. The recordings had their edges (2*sampling rate) removed to eliminate filter artefacts. An F-test was applied to test for beta-coefficient consistency across epochs. PAC was defined

to be significantly present if a cluster of at least 30 contiguous significant frequency bins of p-values < 0.01 was observed.

Data that fell below 10 connecting significant frequency bins of p-values < 0.01 were categorised as non-significant (Fig. 3.2). Data that fell in between were classified as intermediate and excluded from further analysis. Based on this significance testing, the recordings were allocated to groups of "significant" or "non-significant PAC".

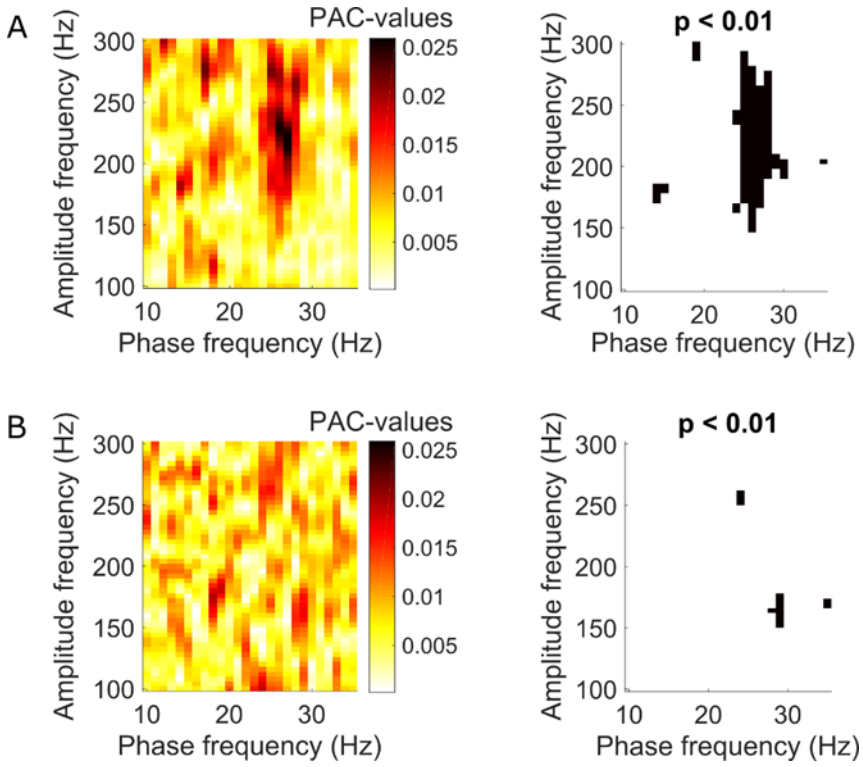


Figure 3.2 – Examples of significant and non-significant PAC-clustering by the GLM method. **A**) Example PAC comodulogram from one recording in one patient with significant coupling between the phase of beta frequencies and HFO amplitude. Frequency bins indicated in black were significant for p < 0.01. **B**) Example comodulogram in the same patient from a different recording without significant PAC-clustering.

3.2.4 Spike-amplitude coupling

The GLM was further extended by including spiking as an additional predictor to test for Spike-amplitude coupling:

$$a_y = \beta_1 \sin(\theta_x) + \beta_2 \cos(\theta_x) + \beta_3 s_x$$

with s_x representing the Z-scored spiking time series. Spike-amplitude coupling was then represented by $\text{Spike}_{\text{AMP}} = \beta_3$ with values ranging from -1 to 1. For individual recordings, a t-test was performed to test for β_3 consistency across epochs for each HFO frequency, to determine levels of significance. For the spike-amplitude-coupling group figures, all the spike-amplitude plots were averaged for the significant and non-significant PAC groups respectively, and a two-sample t-test was performed to determine levels of spike-amplitude significance.

3.2.5 Spike-triggered averages

Spike-triggered averages (STAs) were computed by triggering the amplitude envelope of the band-pass filtered (4th-order Butterworth) HFO (100-300 Hz) at the time of each action potential from a single unit, where the unit and LFP signals were separated by at least 2 mm. The HFO amplitude was averaged around each single-unit spike with time zero marking spike onset. For averaged group data, a two-sample t-test was performed at spike onset.

3.2.6 Comparison of firing rates and HFO amplitude within recordings

Mean firing rates and HFO amplitudes were calculated from single unit and LFP recordings in non-overlapping 3 second epochs. The HFO 180-220 Hz amplitude was chosen for comparison as this was the frequency range where the highest degree of significant PAC was found overall. HFO amplitude was extracted as described in the GLM-method section and averaged for corresponding epochs.

3.2.7 Unit power spectral densities

Power spectral densities of single units were calculated by use of the Welch periodogram method (Matlab function pwelch.m function, using a Hanning window with 50% overlap, window size = 0.2*sampling frequency) by analysing binary spike time files. We also ran shuffled data with randomisation of the spikes to ensure the spectral features were genuine by comparison using the Matlab randn function.

3.2.8 Spike-phase locking

The Hilbert transform was used to extract phase from band-pass filtered LFP signals (beta-frequency corresponding to highest PAC value +/- 5 Hz) and the phases at the times of each action potential were extracted to construct phase histograms. A Rayleigh's test for non-uniformity was applied to determine if the spike-phase locking was significant using the Circstat Matlab toolbox (Berens, 2009). Phase histograms were also made from the Hilbert extracted beta phase with regards to HFO, which was separated into 30 amplitude bins and plotted against the beta phase cycle.

3.2.9 PAC during beta bursts

Beta-bursts were identified in accordance with the method used by Tinkhauser and colleagues (Tinkhauser et al., 2017a). The rectified LFP signal was filtered around the individual beta peak frequency as identified by wavelet frequency decomposition. The Hilbert amplitude was extracted from this filtered signal and used to identify periods of beta-bursts above the set threshold and duration criteria. As standard criteria burst thresholds were set at 75% with durations above 100 ms (Fig. 3.3). Non-bursting periods were identified as periods where the beta Hilbert envelope fell below a 50% threshold. To ensure sufficient data lengths for PAC calculation the bursting and non-bursting periods were concatenated in two different vectors. When comparisons were made between bursting and non-bursting episodes all vector lengths were adjusted to have the same length as the shortest combined vector. The Hilbert phase of the beta component and the phase of Hilbert HFO amplitude were both extracted prior to cutting and concatenating the data to avoid jumps in the signal between periods.

To calculate PAC during bursting and non-bursting periods we chose the phase-locking value (PLV) method between beta phase and the phase of HFO-filtered Hilbert transformed amplitude (Cohen, 2008; Seymour et al., 2017). Like the GLM method, the PLV method is non-susceptible to HFO amplitude levels, which we found to be progressively increased with increased burst thresholds and durations. However, the PLV method has been shown to be superior to the modulation index for short-epoch data (Penny et al., 2008) and the GLM method relies on longer data sets for statistical testing. For the PLV method we tested for statistical significance via 500 runs of surrogate data with circularly shifted permutations of the phase (Penny et al., 2008; Seymour et al., 2017).

The PLV is defined as:

$$PLV = \left| \frac{1}{N} \sum_{n=1}^{N} e^{i(\phi f_p(n) - \phi f_a(n))} \right|$$

ϕf_a represents the phase time series of the HFO amplitude envelope and ϕf_p the beta phase time series. PAC assumes the value of 1 when the phase series are fully locked and 0 if they are completely desynchronised (Tort et al., 2010; Seymour et al., 2017). Before the ϕf_a by way of the Hilbert transform was extracted from the HFO-amplitude time series, the amplitude signal was high- and lowpass filtered as previously described using Butterworth filters to remove non-beta components (Penny et al., 2008). Absolute PAC values were calculated as the mean of the PAC values in the range of the HFO frequency for the max PAC value ±16 Hz.

We also circshifted the beta phase from the HFO amplitude in permutations to exclude that a better-defined beta phase during periods of higher beta amplitude could account for higher levels of PAC.

For estimation of the mean HFO and beta amplitude during bursting and non-bursting episodes the signals were filtered as previously described for the respective components under the GLM method and, after standardizing the entire time series to have zero mean and unit variance, amplitudes were averaged separately for the bursts and non-bursts periods (Fig. 3.3).

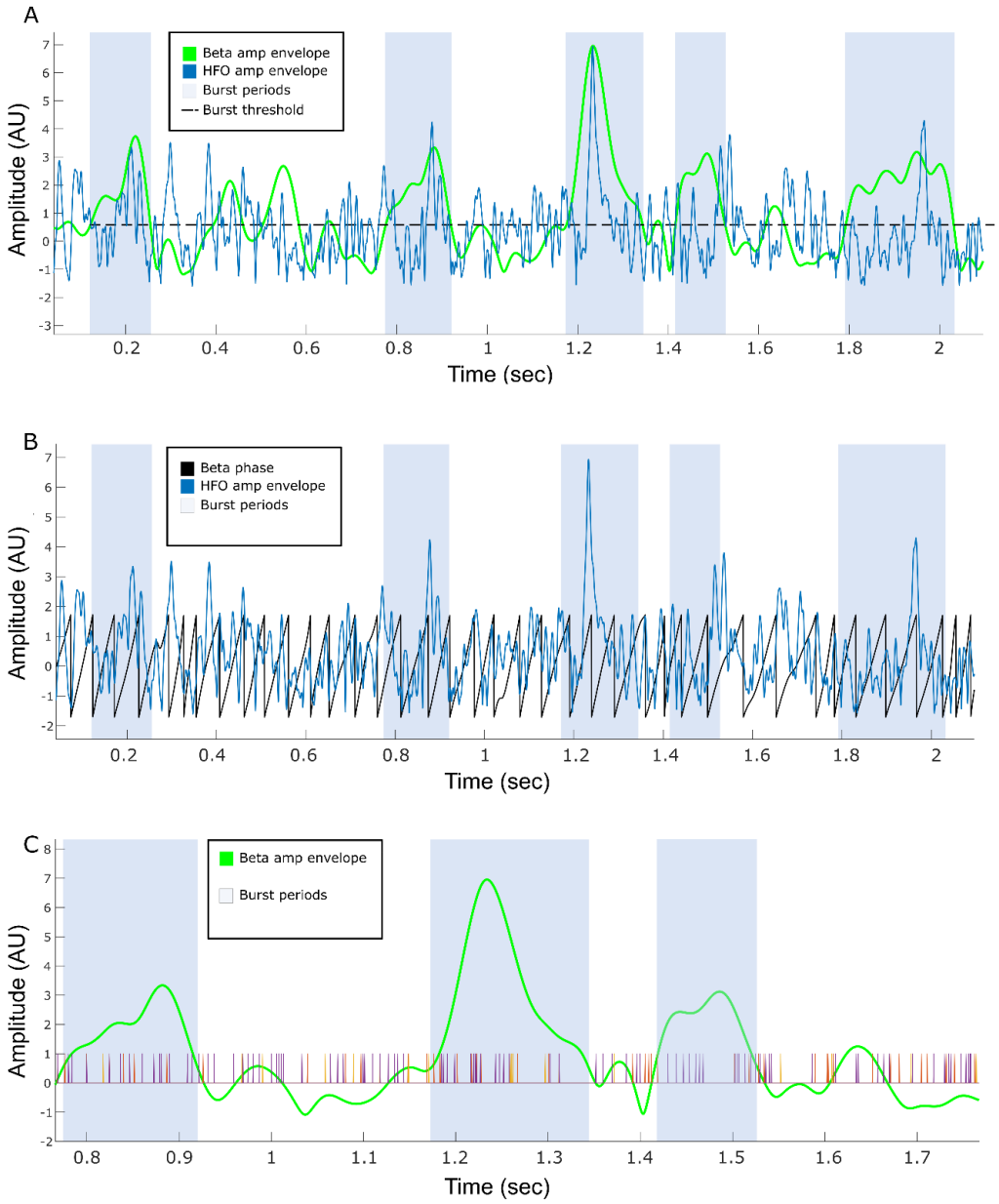


Figure 3.3 - Example of occurrence of HFOs, spiking and beta bursts in single recordings. **A**) Example recording of broadband HFO (100-300 Hz) amplitude time series and HFO amplitude filtered around the beta peak frequency. Shaded blue areas mark periods of beta-bursting of more than 100 ms. The dashed line outlines the 75% burst threshold. **B**) Example of normalised HFO filtered amplitude envelope and beta phase. **C**) Beta amplitude envelope (green), beta bursts (shaded blue areas) and unit firing (orange, yellow and purple).

Case	Age (Yrs) and Sex	Disease Duration (Yrs)	Motor UPDRS OFF	Motor UPDRS ON	Medication pre-operation/day	Hoehn/ Yahr Score	Dominant side	Major Symptoms	Hemispheres analysed
1	61F	25	50	30	Levodopa 700 mg Carbidopa 150 mg Entacapone 1000 mg Benserazide 25 mg Pramipexole 0.26 mg	5	Left	Tremor, Akinesia/rigidity Fluctuations	Right
2	70F	26	45	24	Entacaponee 1600 mg Amantadin 300 mg Pramipexole 0.9625 mg Levodopa 900 mg Selegilin 5 mg	4	Left	Tremor, Akinesia/rigidity	Left
+3	72F	18	41	19	Levodopa 700mg Carbidopa 175mg	4	Left	Equivalence type Fluctuations, Dyskensia	Left
4	70F	8	38	21	Ropinirole 8mg Alpha-dihydroergocryptine 40 mg Amantadine 600 mg Levodopa 250mg Carbidopa 150mg	3	Left	Bradykinesia Fluctuations Dyskinesia	Both
5	66M	17	49	20	Levodopa 700 mg Carbidopa 50 mg Pramipexole 4.4 mg Amantadine 300 mg	4	Left	Dyskinesias Rigidity	Both
6	64M	15	53	39	Amantadine 300 mg Levodopa 550 mg Ropinirole 20 mg Entacapone 900 mg Carbidopa 112.5 mg Benserazide 25 mg	4	Left	Akinesia/rigidity Camptocormia	Left
7	69F	9	21.5	7	Levodopa 450 mg Lisuride 0.9 mg Rotigotine 4 mg Amantadine 300 mg	3	Right	Fluctuations Dyskinesia	Both
8	66M	11	28	14	Amantadine 150 mg Levodopa 1450 mg Tolcapone 300mg Carbidopa 312.5 Benserazide 50mg	4	Right	Akinesia/rigidity Fluctuations	Both
9	63F	17	35	16	Rotigotine 4mg Ropinirole 25mg Levodopa 350mg	3	Left	Akinesia/rigidity, Bradykinesia, Fluctuations, Dyskinesia	Both
10	67,M	10	19	4	Entacapone 1200 mg Levodopa 700 mg Carbidopa 175 mg	3	Right	Bradykinesia Rigidity Fluctuations	Right

Table 3.1 – Patient details.

3.3 Results

3.3.1 Defining the presence of STN LFP phase-amplitude coupling

We analysed 114 micro- and macroelectrode recordings to investigate phase-amplitude coupling of LFP signals in the subthalamic nucleus (Fig. 3.1). Note that 114 of the 231 recordings were identified to be from the STN. Recordings were divided based on whether or not significant PAC was detected using significant frequency-bin clustering. Significant PAC-clustering in the STN on a grand average was predominantly found between beta (20-35 Hz) phase and 160-220 Hz amplitude with individual maximum PAC values peaking on average across the HFO frequency range at either 180 or 220 Hz (Fig. 3.2).

Previous work has suggested that the timing of beta synchronised HFOs and spiking activity in STN are independent (Yang et al., 2014). Our aim was to re-examine this issue and to define precisely how the spiking of STN units is related to PAC. As using spikes and LFPs recordings from the same electrode can obviously introduce contamination between spikes and any other signals, including HFOs, all unit/LFP pairs analysed here were recorded from different electrodes. The configuration of our recording system dictated that these were at least 2mm apart, excluding the possibility of substantial LFP signal contamination (Fig. 3.1, Einevoll et al., 2013).

3.3.2 STN firing predicts HFO amplitude only in the presence of PAC

We first examined whether simple correlations in the time domain between HFOs and spike times only occurred in recordings when PAC was present. To achieve this, spike triggered averages of the HFO amplitude (STA-HFO) were compared across PAC and non-PAC recordings (Fig. 3.4). In single recordings, peaks could be observed at zero lag in the presence of significant PAC (Fig. 3.4A), but not when PAC was absent (Fig. 3.4B). Over all recordings, HFO amplitude was significantly locked to spike-onset in the presence of significant PAC, but not in the absence thereof ($p = 0.0014$, two sample t-test, n(Non-PAC) =38 n(PAC) = 39). In recordings with PAC, secondary peaks could be observed at latencies consistent with the spike triggered HFO oscillating at beta frequencies (e.g. multiples around ~33 ms corresponding to ~30Hz, Fig. 3.4C, D). Furthermore, the area under the STA-HFO around time zero was positively correlated to the number of connected significant PAC frequency bins ($p = 0.0103$, $r = 0.42811$, $n = 33$, F-test, Fig. 3.4E) based on microelectrode recordings, demonstrating that the larger the span of significant PAC across frequencies, the greater the STA HFO amplitude peaks. Importantly, the lack of STA-HFO peaks in the absence of PAC demonstrates that the presence of spikes does not lead to increased HFO amplitude *per se,* rather that spikes and HFOs are specifically associated when PAC is present.

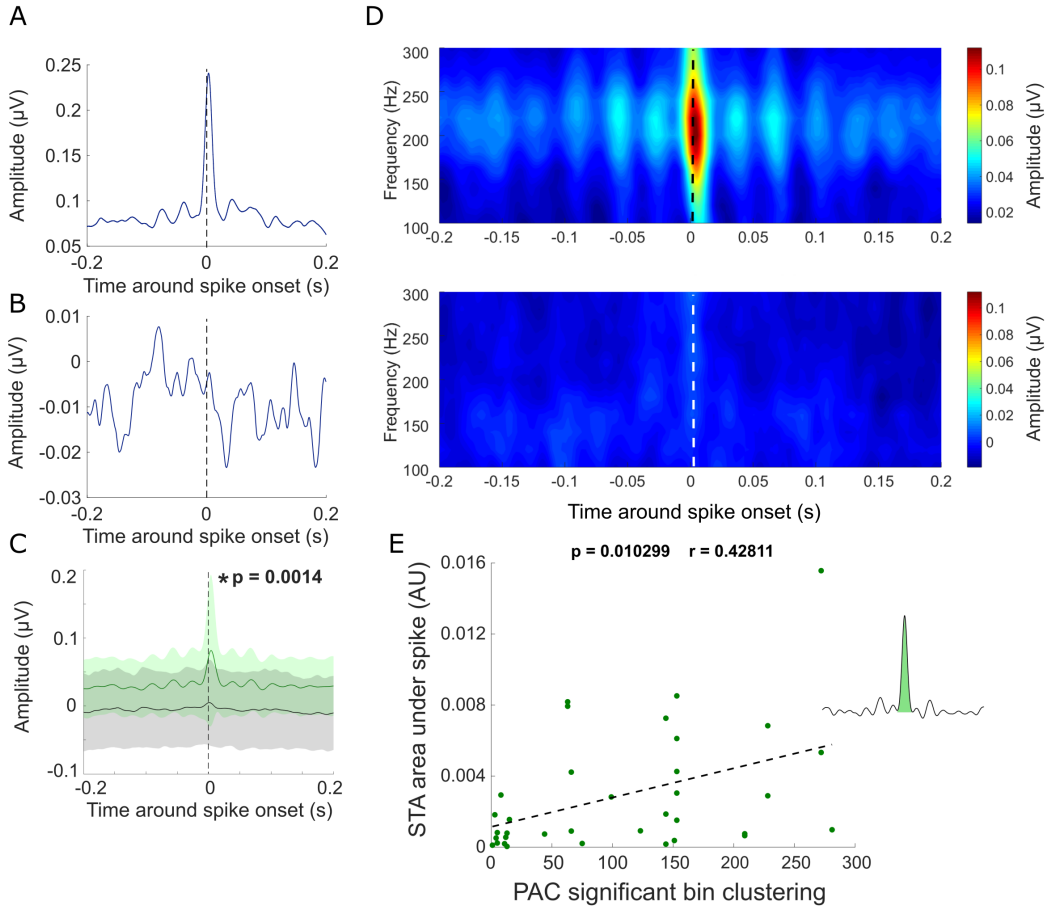


Figure 3.4 - Spike-trigged HFO amplitude is increased during periods of PAC. A-B) Two example spike-triggered averages (STA) from recordings with (**A**) and without (**B**) PAC. The band pass filtered LFP HFO (100-300 Hz) amplitude was averaged around each single-unit spike, indicated by zero on the x-axis. **C)** Grand mean across all recordings of spike triggered HFO amplitude averages for recordings with significant PAC (green) +/- standard deviation and without significant PAC (black) +/- standard deviation. * p = 0.0014 unpaired t-test at time zero. **D)** Grand average of spike triggered amplitude across HFO frequencies from all recordings containing significant PAC (upper) and non-significant PAC-clustering (lower) with time zero denoting spike onset. Notice the repeating side peak-intervals, corresponding to beta frequency of ~30 Hz. **E)** The area under the spike of the spike triggered average significantly relates to the degree of significant PAC clustering calculated from microelectrode recordings (p = 0.0103, r = 0.4281).

In addition to averaging the HFO amplitude around individual spike-onsets, we extended the GLM-method to investigate how spike-amplitude coupling compared to GLM-calculated PAC patterns across all HFO frequencies and found a clear concordance between the significant spike-amplitude curves and significant PAC plots as exemplified in one recording from one patient (Fig 3.3, where significant PAC levels corresponded to spike-amplitude coupling peaks. This pattern was reproduced on the grand average level with significantly greater spike-amplitude coupling in the PAC group compared to the non-PAC group for HFO frequencies ranging from 120-224 Hz (t-test, $p < 0.05$ n(Non-PAC) = 38 n(PAC) = 39) (Fig. 3.5 C), mimicking the PAC peaks for HFOs in the PAC comodulograms. Interestingly, spike-HFO-amplitude coupling peaked at the same 220 Hz frequency for which the maximal PAC values were found (Fig. 3.5 C-D). Taken together these findings suggest that, in the presence of PAC, HFO amplitude and the timing of single unit activity are comodulated by beta phase.

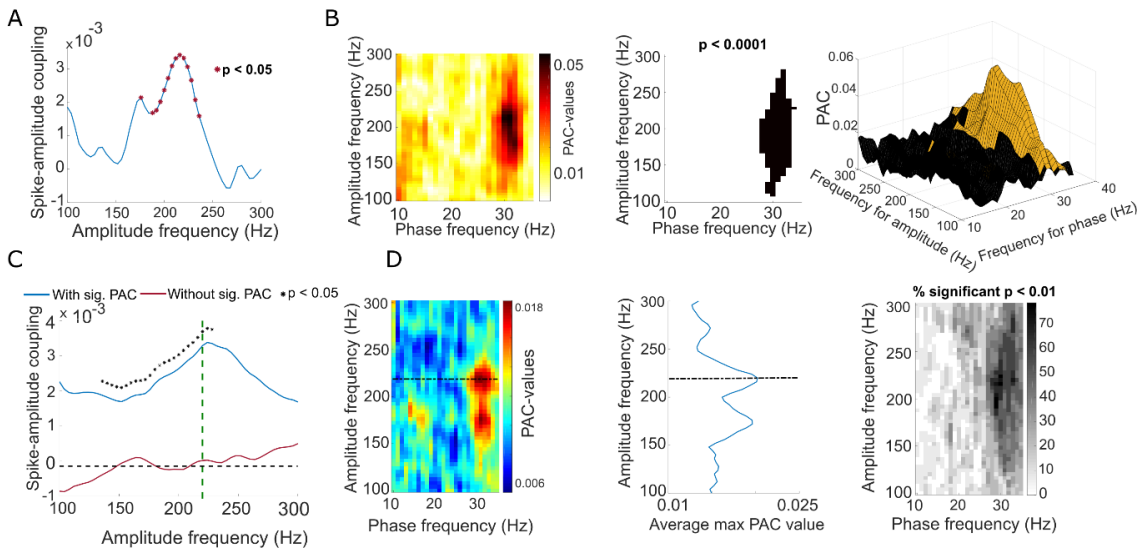


Figure 3.5 - Contribution of spiking to PAC is revealed by multivariate analysis. Statistical coupling between single unit spiking and LFP HFO bandpass filtered amplitude - recorded at distance of at least 2 mm from each other – is seen to be significantly higher in the presence of significant PAC. Also, spike-amplitude coupling peaks at the same HFO frequency as maximum PAC-values**. A)** Example of spike-amplitude coupling plot across HFO frequencies. * denotes values that are significantly different from 0 ($p < 0.05$, t-test). **B)** The corresponding PAC comodulogram for A, PAC significance testing with $p < 0.0001$ (middle) and combined 3D PAC and p-value (brown: $p < 0.01$) representation. Note that spike-amplitude coupling peaks around the same HFO frequency (220 Hz) as the maximum PAC value in the comodulogram. **C)** Group averages of statistical spike-amplitude coupling for significant PAC (blue) and non-significant PAC (red) data sets (* p value < 0.05, two-sample t-test). The green dotted line marks the HFO frequency corresponding to the maximum PAC value from **D)** the grand across recordings averaged significant PAC comodulogram (left) with grey scaled frequency bins displaying percentages of significant p-values <0.01 (right) and averaged max PAC-values across HFO-frequencies (middle).

Given that, in the presence of PAC, spike times predicted periods of high-amplitude HFOs lasting a few milliseconds, we hypothesised that increases in the number of spikes would lead to higher HFO amplitude over longer timescales. To this end, within individual recordings we assessed the relationship between the firing rate of STN neurons and HFO amplitude (180-220 Hz) in the neighbouring LFP (Fig. 3.6). Firing rates when PAC was present and absent were not significantly different (Average mean firing rate of single units (PAC) = 29.15 Hz, non-PAC = 26.06 Hz, $p = 0.5155$, two-sided test). However, in recordings where PAC was present, we found an overall positive relationship between firing rate and HFO power across epochs of 3 seconds (PAC example Fig. 3.6A, $r = 0.6115$, $p < 0.0001$, F-test). In the absence of significant PAC clustering, however, no relationship between overall between firing rate and HFO power could be found (Non-

PAC example Fig. 3.6B, r = 0.0544, p = 0.6520). Across all recordings, we found r-values to be normally distributed around zero for the non-PAC group (Non-PAC mean-r = -0.0305, n = 38, Fig. 3.6C), but shifted to the right for recordings in which PAC was present (PAC mean r = 0.1906, n = 39, Fig. 3.6C). In line with this result, r-values in the presence of significant PAC were significantly greater than in its absence (p = 0.0007, two-sample t-test).

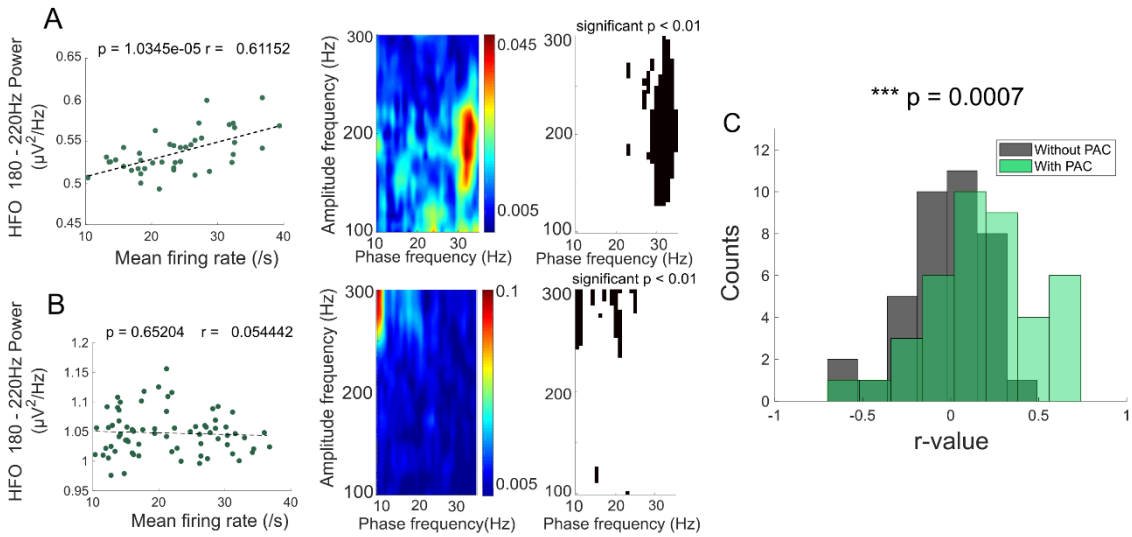


Figure 3.6 - Firing rate predicts HFO amplitude in the presence of PAC. A higher degree of synchronisation of STN spiking with high frequency oscillations is seen when the latter is modulated by the phase of beta frequencies. **A**) Example correlation between mean firing rate and HFO (180-220 Hz) amplitude correlation ($p < 0.0001$, r-value = 0.61152), each dot represents an epoch of 3 seconds. The corresponding PAC comodulogram and significance plot is on the right. **B**) As in A, but for a recording where PAC was absent. **C**) Population histogram of r-values from the correlation between mean firing rate and HFO power in the presence (green, mean r = 0.1906) and absence (grey, mean r = -0.0323) of significant PAC for all recordings. Note that r-values in the presence of significant PAC clustering are shifted to the right compared to the non-significant PAC data (p = 0.0007, two-sample t-test).

Moreover, across recordings, we found that the span of significant PAC clustering and mean firing rate values were positively correlated for the PAC group (defined as clustering exceeding 30 frequency bins, p = 0.018, r = 0.408, Fig. 3.7) but not the non-PAC group (defined as clustering below ten significant frequency bins, p = 0.789, r = 0.048, Fig. 3.7).

Overall, increased spiking activity correlated with the amplitude of HFOs only when PAC was present. These results suggest that spiking does not predict HFO amplitude *per se*, but only under conditions that also lead to significant PAC.

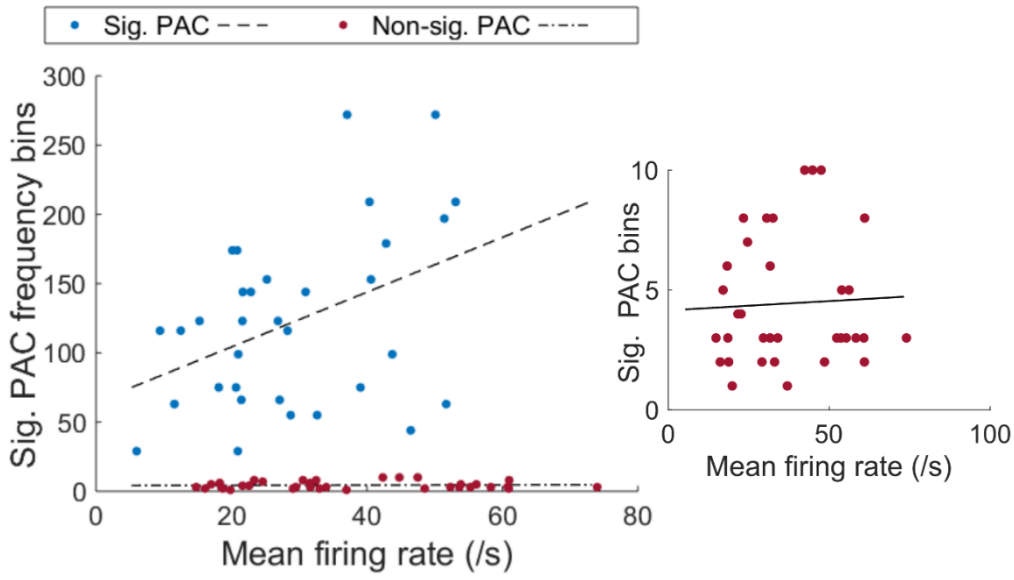


Figure 3.7 - Extent of PAC predicts firing rate across whole recordings. Extent of significant PAC clustering correlates with mean firing rate when clustering exceeds 30 contiguous frequency bins (blue dots, p = 0.018, r = 0.408). In the case of fewer than 10 contiguous significant PAC bins (red dots, no significant PAC) there was no relationship between mean firing rate and the extent of PAC clustering (red dots, p = 0.789, r = 0.048). PAC and mean firing rate calculated from different electrodes.

3.3.3 Specific features of PAC are associated with the presence of synchronised beta oscillations in STN neurons

Next, we tested whether the phase and frequency parameters of PAC could be explained by their association with the spiking patterns of STN neurons. First, we examined whether there was a correlation between the angle of phase locking of the spikes and HFOs in recordings with and without PAC. In recordings with both PAC and phase locked units, both the spikes and HFOs were mostly clustered around the peak of the LFP beta oscillation (Fig. 3.8A) and the differences in their peak phases was not significant ($p = 0.1889$, Watson–Williams test). In contrast, in recordings where no PAC or phase locking was present (Fig. 3.8B-D), both units and HFOs were locked to all phases except for this peak and the differences in preferred phase were significant ($p = 0.0124$, Watson–Williams test) (Fig. 3.8B). This analysis further indicates that STN spiking underlies the time course of HFO amplitude under conditions where STN spiking is locked to local beta oscillations.

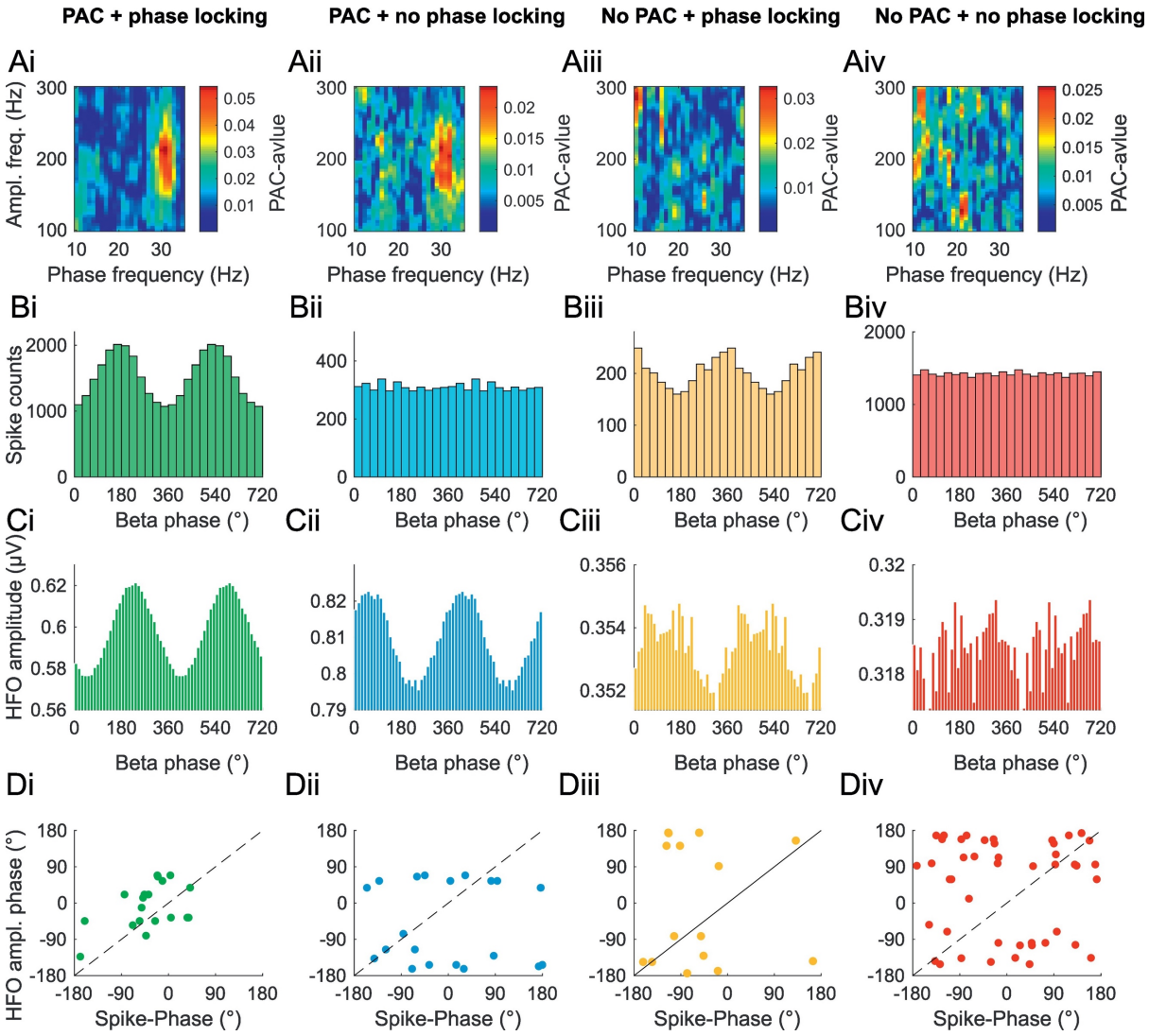


Figure 3.8 - Phase-locked spiking and high HFO amplitude cluster around the same phase of the LFP beta oscillation. The figure is divided into columns with regards to whether PAC and/or spike-phase locking were significant in a pair of LFP/unit recordings. i) Significant PAC and significant spike phase-locking, column ii) significant PAC without significant phase-spike locking, column iii) no significant PAC but significant phase-spike-locking and column iv) no significant PAC and no significant phase locking. A) PAC comodulogram examples. B) Spike-phase-plots for same recordings as in A. C) Beta-phase HFO-amplitude histograms for the same recordings. Di-iv) Mean phase of spiking plotted against the phase with the highest HFO amplitude for each recording meeting the criteria labelled at the top of the column. Diagonals mark complete phase alignments. Note that Di shows that both spikes and the highest HFO amplitude occur around 0° when both PAC and spike-phase locking are present.

A consistent feature of STN LFP PAC is that the HFO frequency peaks > 200Hz (Lopez-Azcarate et al., 2010; Özkurt et al., 2011; Yang et al., 2014; van Wijk et al., 2016), are considerably higher than the broadband gamma (70-150 Hz) activity statistically coupled to beta phase frequencies observed in cortex (Manning et al., 2009; de Hemptinne et al., 2015). Having established a temporal correlation between beta-locked STN spikes and HFOs, we next investigated whether the spectral properties of these phase-locked neurons could explain the frequency of STN HFOs. To this end we compared the power spectra across single unit recordings in recordings with and without significant PAC (Fig. 3.9). The single units at sites with PAC showed both a clear peak between 150 and 250Hz and a peak at beta frequency (Fig. 3.9A). Both peaks were significantly greater than in the non-PAC group ($p < 0.05$, F-test, Fig. 3.9B), which did not show an obvious peak above 100Hz. In recordings with PAC, the peak frequency of the unit power spectra was significantly correlated with that of the HFO (Fig. 3.9C), while there was no such correlation when PAC was absent. Furthermore, analysing the frequencies of interspike intervals (ISI) in the ranges 1-80 Hz and 100-500 Hz across single units we found that these significantly peaked at 24-32 Hz within the high-beta range (Fig. 3.9E) and at 166-204 Hz in the HFO range ($p < 0.0001$, paired T-test) in the presence of significant PAC. We argue that these ISI intervals serve as proxies for inter and intrabursts spike periods, respectively. Interestingly these ISI frequency peaks correlate to the significant PAC frequencies and support similar findings from computational studies (Saunders et al. 2016).

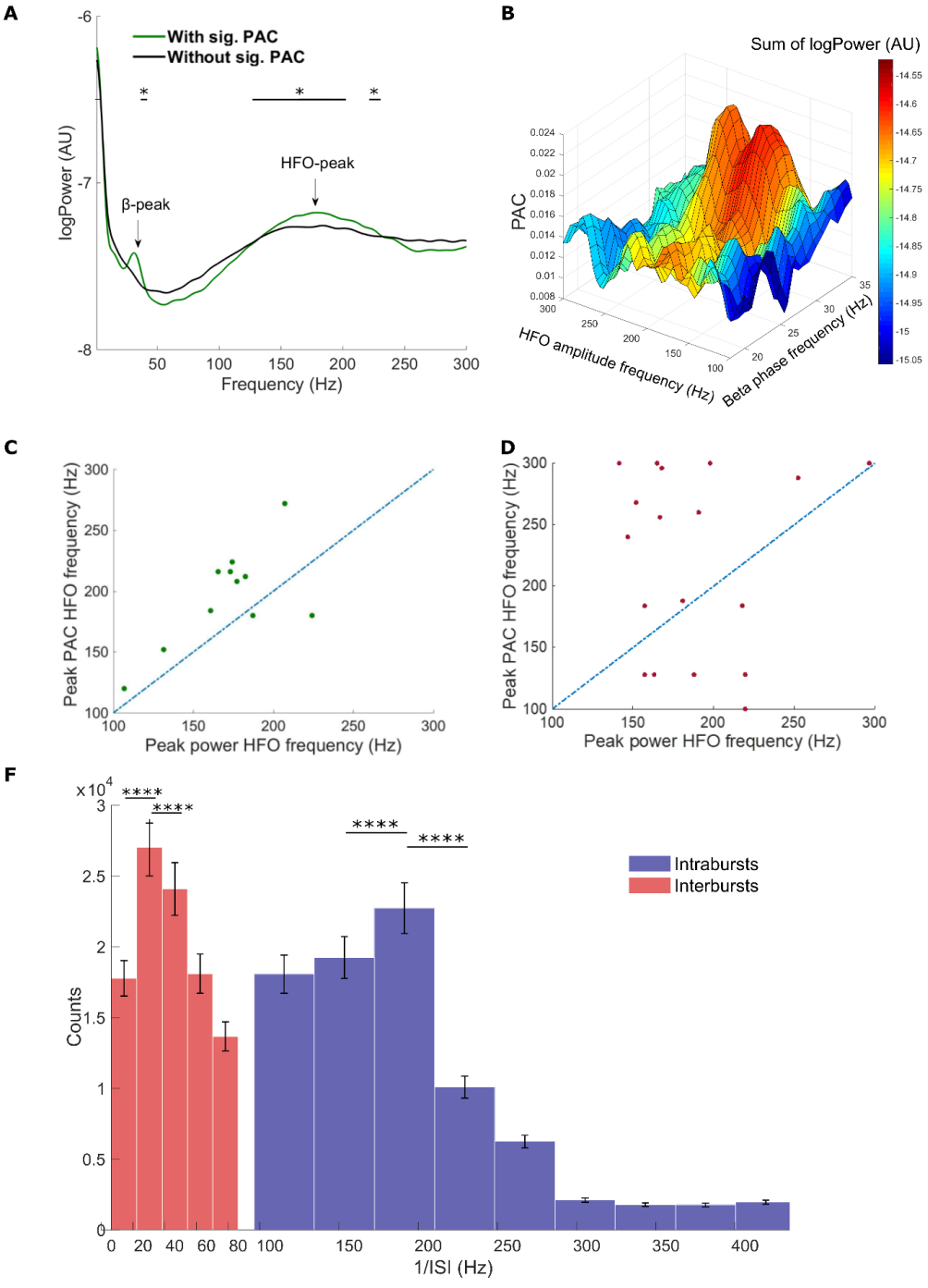

A
With sig. PAC
Without sig. PAC
logPower (AU)
Frequency (Hz)
β-peak
HFO-peak
B
Sum of logPower (AU)
PAC
HFO amplitude frequency (Hz)
Beta phase frequency (Hz)
C
Peak PAC HFO frequency (Hz)
Peak power HFO frequency (Hz)
D
Peak PAC HFO frequency (Hz)
Peak power HFO frequency (Hz)
F
Intrabursts
Interbursts
Counts
1/ISI (Hz)

Figure 3.9 - The power spectral density features of single unit activity reflect HFO frequency. **A**) Group averaged single unit spectral densities at PAC (green) or non-PAC (black) clustering recorded sites. Note that only single units at PAC sites demonstrate a beta peak and a larger gamma peak. * $p < 0.05$, Two-sample F test for equal variances. **B**) 4D representation of grand average microelectrode phase-amplitude coupling for the significant PAC group and the overlapping power spectrum summation with x-values = beta-phase frequency, y-values = HFO amplitude frequency, z-values = PAC-values. The single unit spectral power densities for the beta and HFO frequencies represented by the colour bar (c-axis). The graph shows how the PSD intensity corresponds with PAC-values. **C** + **D**) Peak PAC HFO frequencies plotted against peak power HFO frequencies for microelectrode recordings from the significant PAC group (C, n = 11) and the non-significant PAC group (D, n = 18) demonstrating a higher degree of correspondence between HFO power peak frequencies and PAC peak HFO frequencies for the significant PAC-data. Proximity of dots to the blue line indicates a correspondence between peaks in PAC and power. The dotted lines represent potential frequency alignments. F) Histogram of inter-spike intervals (ISI) as proxies for interbursts (red) and intrabursts (purple) spiking averaged across recordings ± SEM in presence of significant PAC. The intrabrusts ISI significantly peaked at the 166-204 Hz range and the interbursts ISI rate significantly peaked at high beta frequencies of 24-32 Hz. **** $p < 0.0001$.

3.3.4 Increased PAC is captured by the duration of beta bursts

Recent studies have demonstrated that beta oscillations are not continuous, but occur in transient, high amplitude bursts of several cycles that are thought to reflect transient synchronisation of synaptic inputs to the STN (Tinkhauser et al., 2017a, 2017b). We next asked whether the occurrence of PAC was independent to that of beta bursts, or whether the two measures could reflect the same underlying process. Here, we calculated PAC by the PLV-method, which is preferable for short time series. For individual recordings, calculation of PAC inside and outside beta bursts in the same recording led to clearly

different comodulograms, with considerably larger PAC in the burst periods (Fig. 3.10A). This result was consistent across the data set, with significantly higher PAC during beta-bursts than outside bursts across hemispheres in the presence of a beta-peak (PAC during bursts = 0.2055, PAC outside bursts = 0.0989, p = 0.0234, paired t-test) (Fig. 3.10B).

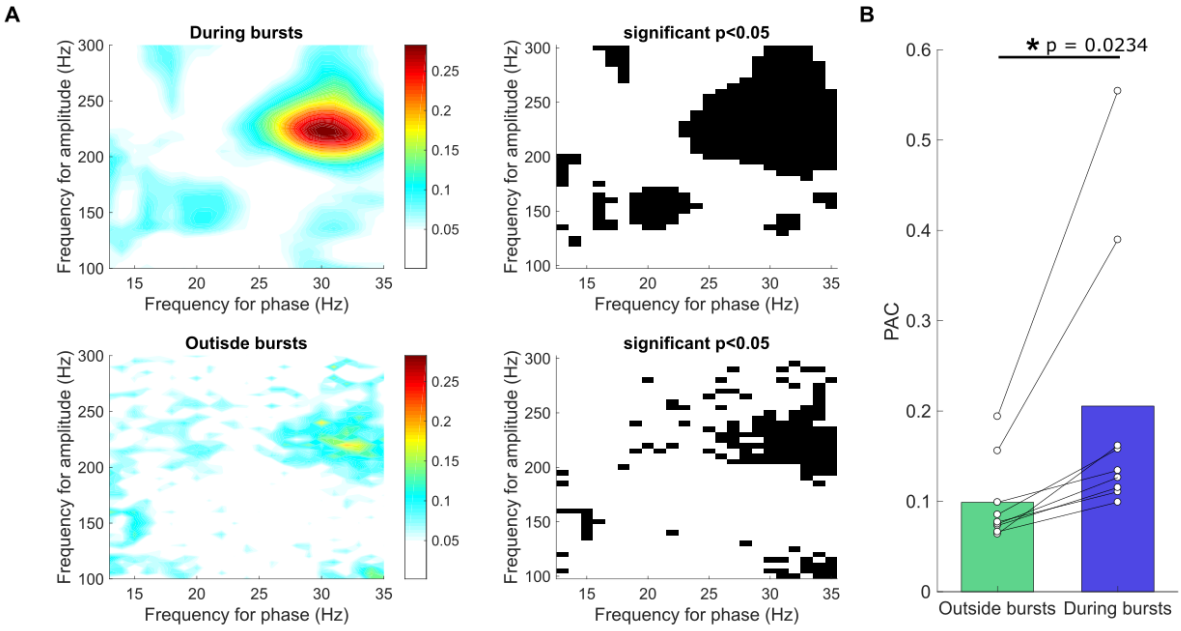


Figure 3.10 - PAC is significantly higher during beta bursts. **A**) Example PAC comodulogram inside and outside bursting period from the same recordings, calculated by the PLV method. **B**) Average around maximum (± 16 Hz) PAC calculated from 9 hemispheres with recordings that demonstrated a beta peak. PAC was found to be significantly higher during periods of beta bursting compared to outside periods of bursting (PAC during bursts = 0.2055, PAC outside bursts = 0.0989 p = 0.0234, paired t-test, n = 9) in the presence of a beta peak.

We acknowledge that a better-defined phase during periods of beta bursting, when the beta oscillation amplitude is higher, could contribute to higher observed PAC values and that this factor should be taken into account. However, by running circularly shifted permutations, where we shift the beta phase from the HFO amplitude, we find that phase-

consistency is not sufficient to explain the increases in PAC and that a better defined phase during bursting in this study could not account for observed differences between the inside and outside bursts states (Fig. 3.10).

Moreover, we found that there was a significant increase in PAC with burst duration and when progressively higher thresholds were used to define the burst epochs, following a correction for the shortening of the data segments as the threshold and durations were increased (One-way ANOVA, $p < 0.0001$, Fig. 3.11). Longer bursts and higher amplitude thresholds consequently captured higher levels of synchronisation between the beta phase and amplitude of the HFOs. Finally, we also found progressive increases in both HFO and beta power with increasing burst durations (One-way ANOVA, $p < 0.0001$, Fig. 3.12). Overall correlations between different measures in the paper are summarised in Table 3.2. In summary, PAC was higher within beta bursts and increased progressively with the magnitude (set by threshold) and duration of the bursts.

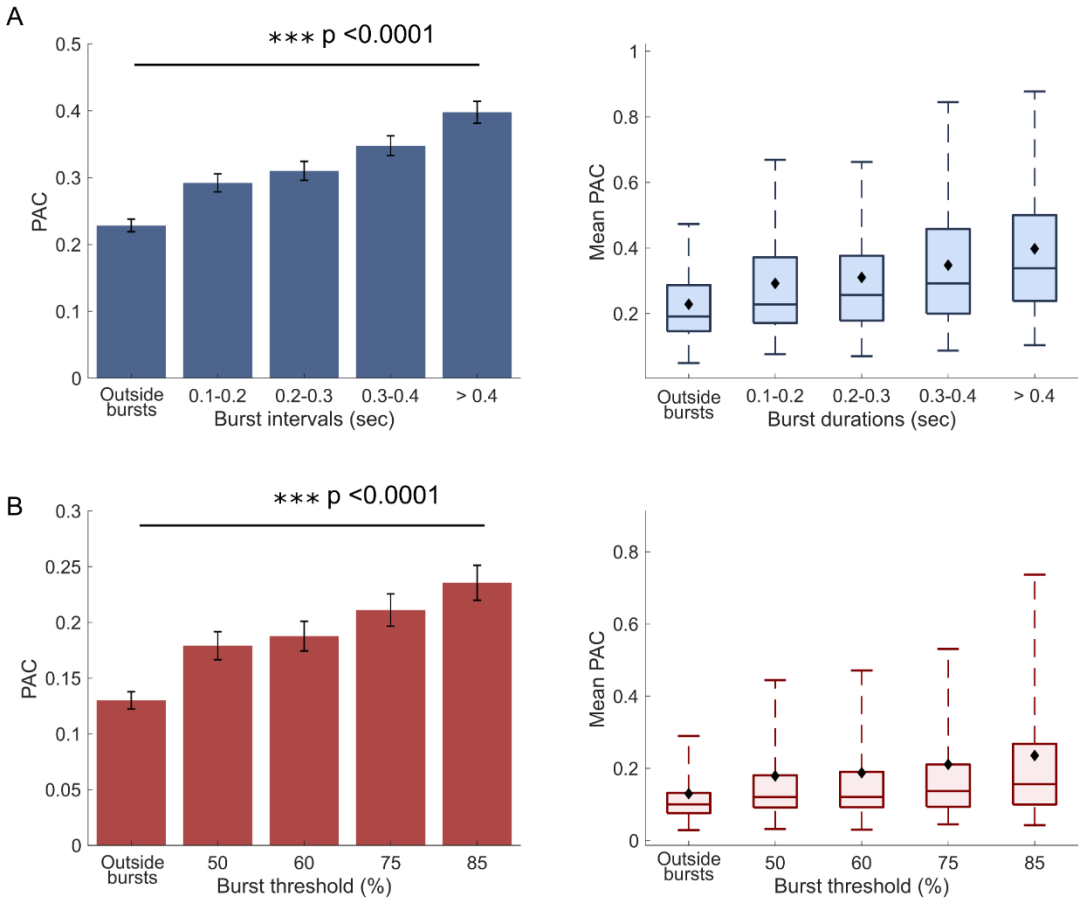


Figure 3.11 - PAC increases progressively with both burst duration and thresholds increments. **A**) Bar and box plots of PAC at different burst durations. PAC significantly increases with burst duration with longer bursts capturing higher levels of coupling. **B**) Bar and box plots of PAC at different burst thresholds. PAC increases significantly with threshold increments. All concentrated burst vectors were length adjusted.

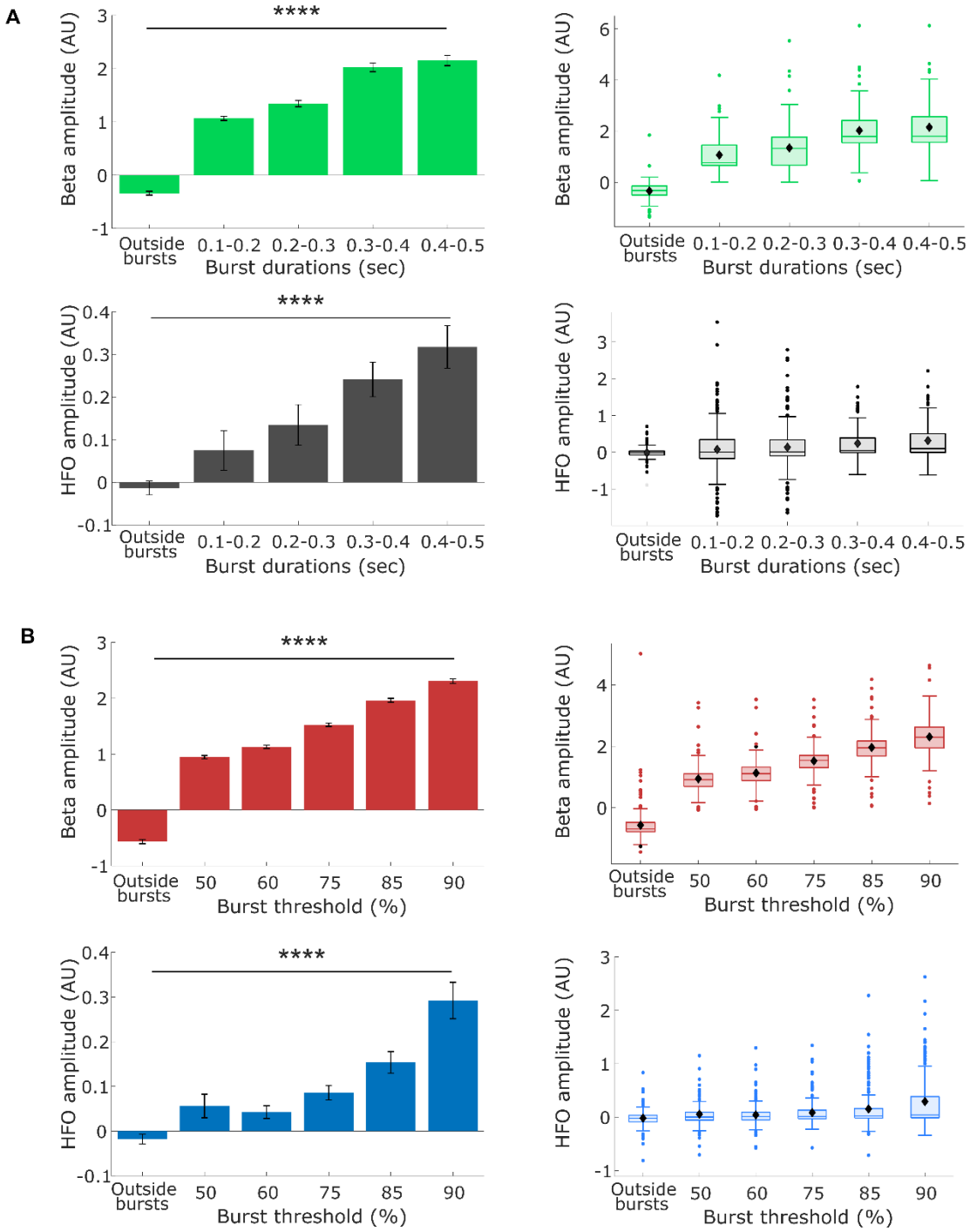


Figure 3.12 - Both normalised beta and HFO amplitude increase significantly with both burst duration and thresholds. **A**) Bar and box plots of average beta (green) and HFO (grey) amplitudes for different burst durations. **B**) Bar and box plots for average beta (red) and HFO (blue) amplitude for different burst thresholds. **** $p < 0.0001$, One-way ANOVA.

PAC parameters	Spiking activity		Spectra/Phase		Beta bursts		
	Spike times	Mean firing rate	Spike phase	Unit high frequency peak	Beta-burst in/out	Beta-burst amp.	Beta-burst length
PAC	N/A	✓	✓	N/A	✓	✓	✖
HFO amplitude	✓	✓	N/A	N/A	✓	✓	✓
HFO frequency	N/A	N/A	N/A	✓	N/A	N/A	N/A
HFO beta phase	N/A	N/A	✓	N/A	N/A	N/A	N/A

Table 3.2 - Associations between measures of PAC, spiking activity and beta bursts. Ticks and crosses show when two measures, denoted by the row and column labels, were/were not associated based on analysis of PAC vs non-PAC recordings or temporal/phase/frequency correlations within recordings.

3.4 Discussion

In this study, we investigated how different aspects of PAC in the STN LFP related to the spiking activity of STN neurons. We analysed the relationship between STN beta oscillations, HFOs and spiking activity in the presence and absence of PAC and investigated how PAC differed inside and outside of beta bursts. Our results suggest that PAC reflects the oscillatory recruitment of STN spiking activity at beta frequencies and that this coupling is stronger during transient beta-burst events. These findings raise specific issues regarding the relationship of PAC to other biomarkers of pathophysiological activity in PD.

3.4.1 Physiological basis of PAC in the STN

PAC has been demonstrated in many brain areas including several cortical regions (Canolty et al., 2006; Canolty and Knight, 2010; Szczepanski and Knight, 2014; Voytek et al., 2015), basal ganglia in the non-parkinsonian state (Tort et al., 2009; Nicolai et al., 2014) and hippocampus (Kramer et al., 2008; Colgin et al., 2009; Scheffer-Teixeira and Tort, 2016). Across this range of structures, there is considerable variability in the frequency of both the phase and amplitude signals. Several biological and nonbiological mechanisms can lead to significant PAC in a given time series. The first common interpretation is that there is functional coupling between neural populations oscillating at different frequencies. Such coupling has been convincingly demonstrated in the hippocampus, where the power of gamma frequencies is locked to specific phases of the ongoing theta oscillation, depending on the location of the recording electrodes (Colgin et al., 2009; Buzsáki and Wang, 2012; Scheffer-Teixeira and Tort, 2016). In this case, both carrier and amplitude are underpinned by the synchronised firing of the underlying neurons. A second common interpretation is that higher frequency oscillations in neocortex are generated by background spiking (Ray et al., 2008a, 2008b; Ray and Maunsell, 2010) and PAC is the result of the locking of this activity to a low frequency carrier oscillation. Nevertheless, here the two oscillations represent semi-independent processes, i.e. the carrier oscillation is dominated by synaptic input and the high frequency oscillation by background spiking. The third interpretation is that the shape of the carrier signal creates a high frequency spectral component that has a consistent phase (Aru et al, 2015). This was recently demonstrated for cortical PAC in PD patients, where the asymmetry of the beta oscillation was shown to create the phase locked high frequency spectral content (Cole et al., 2017; van Wijk, 2017).

In regard to STN PAC, we provide several lines of evidence for the second interpretation; that beta oscillations, representing coordinated synaptic input, drive spiking activity, which manifests as high frequency oscillations. Firstly, only when PAC was present was spiking correlated with HFO amplitude. It is worth reiterating that the spike was at least 2 mm away from the LFP channel, eliminating the possibility of direct electrical contamination. The time of spikes at a distant site, thus predicted the timing of high HFO power with millisecond precision. It is important to note that, while the 2mm distance removed the possibility of contamination, it was probably suboptimal for detecting HFOs generated directly from the pool of neurons around the microelectrode. Rather, our analysis likely relied on the highly uniform phase locking of STN neurons both to the LFP, and to each other, across the nucleus (Weinberger et al., 2006; Mallet et al., 2008; Sharott et al., 2018), which allowed us to detect phase and temporal correlations even at these relatively long distances. Importantly, peaks were not seen when PAC was absent, suggesting that spiking only leads to peaks in HFO in certain contexts. Secondly, over time windows of a few seconds, firing rate was positively correlated with HFO power in the presence of PAC. As these correlations were absent when PAC was not present, such correlations are more likely the result of correlated activity, rather than any spiking, which is caused by beta synchronisation. Moreover, there were no significant differences in mean firing rate between the PAC and non-PAC groups, highlighting that this result must be due to temporal dynamics, rather than excitability per se. These conclusions are supported by the finding that the phase of HFO locking to the beta carrier predicts that of single units. Furthermore, we show that the spiking of single STN neurons can produce spectral frequencies that match those of the HFO. This is a novel and important finding, as the HFO frequency is much higher in STN than in cortex. Our results suggest that the frequency of the HFO in STN could be determined by the interspike intervals of bursts

of spikes that are phase-locked to the LFP beta oscillation. This provides an important link between PAC, LFP beta oscillations and high frequency spike bursts, the frequency of which correlates with motor symptom severity (Sharott et al., 2014). The correlation between bursting and PAC is supported by a recent computational study demonstrating that spike bursts with the intraburst and interburst intervals seen in STN neurons in PD patients can generate PAC (Sanders, 2016). In line with this, we found, in the presence of PAC, that peaks in the inter spike interval histograms of STN units predicted the frequency of the HFOs recorded in the LFP. Interestingly, dopamine replacement shifts the frequency of HFOs considerably, to around 300-350Hz (Lopez-Azcarate et al., 2010). We speculate that two, non-mutually exclusive mechanisms could underlie this observation. Firstly, the reintroduction of dopamine could change the excitability of STN neurons and the resulting changes in firing rate and pattern could manifest as higher HFO frequency. Secondly, the concurrent increase in beta frequency following dopamine replacement (Sharott et al., 2005; Lopez-Azcarate et al., 2010) could lead to phase-locking of STN spikes at even lower intraburst intervals. The dependence of PAC and HFO on phase-locked spikes described here provides indirect evidence for the latter hypothesis.

Our findings are different to those of Yang and colleagues (Yang et al., 2014) who suggest, using similar data to our own, that spike locking to beta oscillations is independent from HFO locking. There could be several reasons for this discrepancy. Here we only used LFPs that were recorded within the STN, as defined by the characteristic spiking of STN neurons. Although we concur with Yang and colleagues that the LFP dorsal to the STN probably contains volume conducted activity from that structure, it may likely have a greater contribution from other sources such as thalamus and zona incerta. The GLM

method and the commonly used modulation index (as determined by the circular mean method), are in essence the same when the latter is properly normalised, and similar results have been yielded by both methods (Penny et al., 2008). However, we used a more stringent criterion for defining significant PAC, which may have reduced our calculations of the HFO beta phase to those with the strongest locking, and thus most stable phase. Given the larger data set in Yang et al, further characterisation of STN PAC, possibly in animal models where more single neurons can be recorded, would be highly valuable for resolving this issue.

3.4.2 PAC during episodes of transient input synchronisation

Synchronisation across STN synaptic inputs is thought to be indexed by beta LFP power (Weinberger et al., 2006; Mallet et al., 2008a, 2008b; Tinkhauser et al., 2017b; Sharott et al., 2018). Recently, much attention has been focussed on the interpretation of neuronal oscillations as transient, burst-like events (van Ede et al., 2018). This has been found to be particularly true of oscillations in the beta range, both in the healthy (Feingold et al., 2015; Mirzaei et al., 2017) and Parkinsonian (Tinkhauser et al., 2017a, 2017b, 2018b) cortico-basal ganglia network. The transient nature of these oscillatory events suggests that these bursts are periods where synaptic inputs are most synchronised and that it is these sustained periods of synchronisation in PD that impairs movement processing. We found that beta bursts also have significantly higher PAC and that the PAC increases progressively with duration and amplitude (assessed by increments in burst threshold) of the bursts. In line with this, dopamine replacement in PD patients supresses both burst length (Cagnan et al., 2015; Tinkhauser et al., 2017b) and PAC (Lopez-Azcarate et al., 2010; van Wijk et al., 2016). Overall, PAC and beta bursts may thus reflect periods of increased input/output synchronisation, or transfer, in the beta frequency range.

Tinkhauser and colleagues showed that that adaptive DBS truncated longer bursts in favour of bursts of shorter durations and lower amplitudes (Tinkhauser et al., 2017a). As longer bursts proportionately capture higher levels of input/output synchronisation, as indexed by PAC, our analysis suggests that successful stimulation strategies will reduce burst length and PAC magnitude in parallel. It is important to note that the phase consistency that accompanies beta bursts is likely to be necessary for high PAC, in order for the HFO amplitude to phase-lock consistently. Our surrogate analysis, however, shows that phase-consistency is not sufficient to increase PAC without synchronisation of the HFO. Even taking into account the possible dependency of phase-consistency in the relationship between beta bursts and PAC, for any bioengineering uses of PAC and/or beta bursts, we provide a useful demonstration that they are not independent.

3.4.3 Subthalamic PAC as a biomarker of pathophysiology

PAC is increasingly suggested as a primary biomarker for pathophysiology in PD patients. At the level of STN, our results suggest that this may be due to PAC being a proxy for the locking of local spiking activity to beta oscillations, which is supported by computational evidence (Sanders, 2016). The importance of this interpretation is that beta oscillations, as measured in basal ganglia LFPs or EEG/ECoG, are synchronised across the entire cortical basal ganglia network (Mallet et al., 2008b, 2008a; Brazhnik et al., 2016; Sharott et al., 2017) and such spike-field locking is a robust marker of the Parkinsonian state across experimental animals and patients. Using the timing of cortical spiking activity locked to such network oscillations as a biomarker for closed-loop deep brain stimulation relieves motor impairment to a greater degree than conventional 130Hz stimulation (Rosin et al., 2011). PAC may thus serve as a useful way of detecting the locking of local spiking activity to network oscillations from wideband signals. In terms

of its use as a biomarker for closed-loop stimulation, the main question is whether the HFO locking provides information that cannot be extracted from the beta oscillation alone, using metrics of amplitude, phase and possible cycle asymmetry. The possible masking of significant PAC by stimulation may also impede its use to control stimulation timing (Sanders, 2016). Nevertheless, given the proliferation of devices allowing long term recording of STN LFPs, our results suggest that PAC and beta-bursts can provide a useful parameter for measuring the synchronisation and/or oscillation of underlying unit activity in the absence of direct access to measurements of spiking.

4

Cortical beta burst duration modulates other candidate electrophysiological biomarkers for closed-loop deep brain stimulation in Parkinson's disease

Contents

4.1 Introduction

4.2 Methods
- 4.2.1 Surgical procedure and micro recordings
- 4.2.2 Beta-bursts identification
- 4.2.3 Non-sinusoidal features
- 4.2.4 PAC within and between areas
- 4.2.5 Spike-triggered averages
- 4.2.6 Power spectral densities
- 4.2.7 Spike-phase locking

4.3 Results
- 4.3.1 Cortical beta bursts capture higher levels of non-sinusoidal sharpness
- 4.3.2 Cortico-subthalamic PAC predicts the locking of single units to HFO amplitude at beta frequencies
- 4.3.3 PAC and sharpness
- 4.3.4 Cortico-subthalamic PAC increases with cortical beta burst duration

4.4 Discussion

4.1 Introduction

Continuous high-frequency deep brain stimulation (cDBS) has established itself as a reversible treatment of severe motor symptoms. However, as discussed in detail in Chapter 1, the clinical application of cDBS is restricted by side effects like psychiatric symptoms, speech impairment and brittle dyskinesias. Lately, in an attempt to minimise side-effects and maximise the efficiency of the treatment, much attention has been given to closed-loop or adaptive DBS (aDBS) where stimulation in real-time is controlled by feedback from biomarkers of pathological brain circuit dynamics. Various biomarkers across cortical and subcortical regions have been proposed including beta-bursts, nonsinusoidal sharp oscillation features, high-frequency oscillations (HFOs), neuronal firing patterns and phase-amplitude coupling (Rosin et al., 2011; Little et al., 2013; de Hemptinne et al., 2015; Cole et al., 2017; Kühn and Volkmann, 2017; Meidahl et al., 2017; Bouthour et al., 2019).

A key feature of the pathophysiology of PD is the emergence of exaggerated beta-oscillations (13-35 Hz) across cortico-basal ganglia structures (Brown et al., 2001; Kühn et al., 2006; Mallet et al., 2008a). In PD patients subthalamic spiking activity recorded from microelectrodes during electrode implantation has been shown to be synchronised to the phase of the motor cortex in the beta range, as recorded simultaneously by subdural electrocorticography (ECoG), and to be movement modulated (Shimamoto et al., 2013; Lipski et al., 2017). Furthermore, it has been demonstrated in rodent models of PD that cortical beta rhythms are abnormally synchronised to subthalamic single unit discharge compared to normal controls (Mallet et al., 2008b). Lately, it has become clear that beta activity is not constantly elevated but comes in transient periods or bursts (Feingold et al., 2015; Lundqvist et al., 2016; Sherman et al., 2016; Tinkhauser et al., 2017a; Torrecillos

et al., 2018). As the duration of beta bursts in the subthalamic nucleus (STN) was found to correlate with motor impairment and to be truncated by aDBS and dopaminergic medication (Tinkhauser et al., 2017a, 2017b), it has been suggested that it is not the presence of beta oscillations *per se* but rather duration of episodically elevated beta activity that is then propagated across the cortical-basal ganglia circuit that is a manifestation of the underlying the pathophysiology in parkinsonism (Tinkhauser et al., 2017b; Cagnan et al., 2018a; Deffains et al., 2018).

Another potential central biomarker in PD is phase-amplitude coupling (PAC), where the phase of a lower frequency oscillation is statistically coupled to the amplitude envelope of a higher frequency. In PD patients, both PAC between beta phase and broadband gamma (70-150 Hz) amplitude in cortex and beta phase and high-frequency oscillation (HFO, 100-300 Hz) amplitude in the STN have been linked to symptom severity and demonstrated to be attenuated by DBS, contralateral movements, and dopaminergic replacement therapy (Lopez-Azcarate et al., 2010; de Hemptinne et al., 2015; van Wijk et al., 2016). Cortical PAC has also been observed to develop in MPTP-models of parkinsonism in non-human primates (Devergnas et al., 2017).

The broadband gamma (70-150 Hz) component of cortical PAC in PD patients, however, has lately been understood to arise from the stereotypical non-sinusoidal shape of the beta oscillation (Cole et al., 2017; van Wijk, 2017). Meanwhile, both computational and electrophysiological studies have demonstrated that beta-HFO PAC within the STN reflects the locking of spiking activity to LFP beta oscillations (Sanders, 2016; Meidahl et al., 2019).

Lately, attention has returned to the asymmetric morphology and nonlinearities of the raw electrophysiological signal as it has been argued that important physiological or pathophysiological information could be lost in the signal bandpass filtering process

(Cole and Voytek, 2016; Dowsett and Herrmann, 2016; Sheremet et al., 2016; Sherman et al., 2016; Jackson et al., 2019). In PD patients sharpness ratios between troughs and peaks (a measure of horizontal asymmetry) relate significantly to measures of contralateral rigidity scores (Cole et al., 2017; van Wijk, 2017). Consequently, cortical oscillatory sharpness has been proposed as a real-time biomarker for closed-loop DBS (Jackson et al., 2019).

In this chapter we expand on the data set described in Chapter 3 of this thesis by analysing simultaneous ECoG-recordings from the motor cortex as well as macro and microelectrode recordings of LFPs and single unit activity from the STN in human PD patients undergoing DBS surgery. We investigate how five competing biomarkers for closed-loop DBS applications relate to one another: 1) cortical beta-bursts, 2) cortical oscillatory sharpness 3) STN spiking activity 4) Cortico-subthalamic PAC (CTX-STN PAC) and 5) STN HFOs. We show that cortical beta bursts capture higher levels of non-sinusoidal sharpness, which increases progressively, not only with the burst duration, but also with the locking of STN single units to cortical beta oscillations. CTX-STN PAC also increases progressively with burst duration and reflects the locking of synchronised single unit spiking and HFOs amplitude to cortical beta oscillations.

4.2 Methods

In this study we analysed ECoG recordings from motor cortex and LFPs from macro- and micro electrode recordings from the STN in in a subset of PD patients from Chapter 3 with simultaneous LFP and ECoG recordings (13 hemispheres in 9 patients, 5 female, 4 male; mean ± SD age: 67 ± 3.4 years) during surgical DBS electrode implantation surgery (Fig. 4.1).

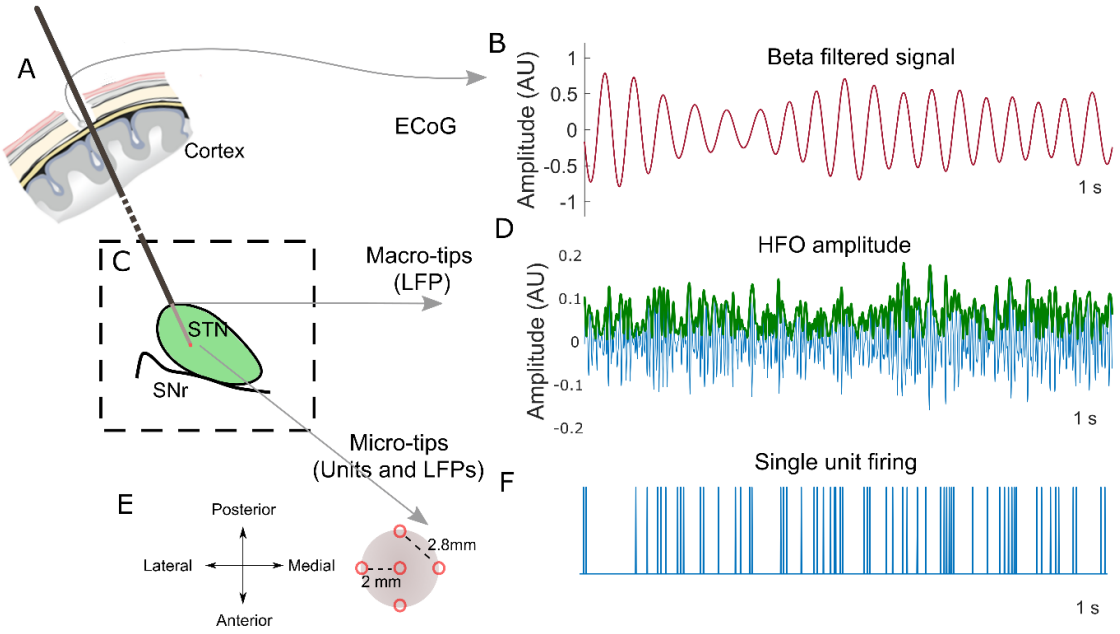


Figure 4.1 - Cortico-subthalamic recordings in PD patients. Schematic overview of deep brain stimulation recordings setup. **A)** ECoG recordings from motor cortex. **B)** Example of the cortical extracted beta-oscillation (13-35 Hz) using the Hilbert transform. **C)** Macro and microelectrodes were used to capture local field potentials (LFPs) from the STN **D**) Examples of signals extracted from the STN LFPs: HFOs (blue) and the HFO amplitude envelope (dark green). **E)** The micro electrodes were organised in a concentric array with four outer micro electrodes distanced 2 mm from the central micro-electrode. All simultaneous spiking and LFP analyses were made from electrodes at least 2 mm apart. **F)** Example of single unit spike time series.

4.2.1 Surgical procedure and electrophysiological recordings

Patient details specific to this chapter are presented in table 4.1. The reader is asked to refer to Chapter 3 for details of the surgical procedure, data selection and data processing. In addition to the subthalamic recordings described there, an electrocorticogram (ECoG) was recorded simultaneously from the dura right above the craniotomy, approximately over the dorsolateral prefrontal cortex (Engel et al., 2005; Sharott et al., 2018). The ECoG was referenced to the simultaneously placed EEG channel placed approximately in the Cz position (Sharott et al., 2018). The mean recording time was 177 seconds. Only patients with simultaneous subthalamic LFP and ECoG recordings were included in this study.

Case	Age (Yrs) and Sex	Disease Duration (Yrs)	Motor UPDRS OFF	Motor UPDRS ON	Medication pre-operation	Hoehn/ Yahr Score	Dominant side	Major Symptoms	Hemispheres analysed
1	61F	25	50	30	Levodopa 700 mg Carbidopa 150 mg Entacapone 1000 mg Benserazide 25 mg Pramipexol 0.26 mg	5	Left	Tremor, Akinesia/rigidity Fluctuations	Right
2	70F	26	45	24	Entacapon 200 mg 8x1 Amantadin 100 mg 3x1 Pramipexol 0.35 mg 5x0.5 Madopar 125 T (Levodopa 100 mg + Benserazid 25 mg)8x0.5 Nacom 100 retard (Levodopa 100 mg + Carbidopa 25 mg) 1x1 Selegilin 10 mg 1x0.5	4	Left	Tremor, Akinesia/rigidity	Left
3	72F	18	41	19	Levodopa 700mg Carbidopa 175mg	4	Left	Equivalence type Fluctuations, Dyskensia	Left
4	70F	8	38	21	Ropinirole 8mg Alpha-dihydroergocryptine 40 mg Amantadine 600 mg Levodopa 250mg Carbidopa 150mg	3	Left	Bradykinesia Fluctuations Dyskinesia	Both
5	66M	17	49	20	Levodopa 700 mg Carbidopa 50 mg Pramipexole 4.4 mg Amantadine 300 mg	4	Left	Dyskinesias Rigidity	Both
6	64M	15	53	39	Amantadine 300 mg Levodopa 550 mg Ropinirole 20 mg Entacapone 900 mg Carbidopa 112.5 mg Benserazide 25 mg	4	Left	Akinesia/rigidity Camptocormia	Left
7	69F	9	21.5	7	Levodopa 450 mg Lisuride 0.9 mg Rotigotine 4 mg Amantadine 300 mg	3	Right	Equivalence type Fluctuations Dyskinesia	Both
8	66M	11	28	14	Amantadine 150 mg Levodopa 1450 mg Tolcapone 300mg Carbidopa 312.5 Benserazide 50mg	4	Right	Akinesia/rigidity Fluctuations	Both
9	67,M	10	19	4	Entacapone 1200 mg Levodopa 700 mg Carbidopa 175 mg	3	Right	Bradykinesia Rigidity Fluctuations	Right

Table 4.1 - Patient details

4.2.2 Beta-bursts identification

Periods of beta-bursts were calculated in accordance with the method outlined by Tinkhauser and colleagues (Tinkhauser et al., 2017a) and described in Chapter 2 and 3 of this thesis. Accordingly, wavelet frequency decomposition was applied (ft_specest_wavelet script in Fieldtrip - Morlet Wavelet, width = 10, gwidth = 5; Donders Institute for Brain, Cognition and Behaviour, 2010) to identify individual peak beta frequencies. The signal was then bandpass filtered around this peak ± 3 Hz (2^{nd}-order Butterworth, range: beta peak frequency ± 3 Hz) (Little et al., 2013; Tinkhauser et al., 2017a). We extracted the Hilbert amplitude from this signal and used this to identify the beta-burst event in accordance with our standard criteria (if not otherwise specified the amplitude percentile threshold criterion was set at 75 % with minimum durations above 100 ms, Fig. 4.2A). Periods outside bursting were defined as those where the Hilbert envelope fell below a 50 % threshold.

4.2.3 Non-sinusoidal features

To study the non-sinusoidal features of beta oscillations we followed the approach outlined by the Voytek group (Cole et al., 2017). We initially low-pass filtered the raw signal from the ECoG recordings at 100 Hz (4^{th} order, Butterworth) to exclude high frequency artefacts and applied notch filters ± 2 Hz to remove 50 Hz harmonics (4^{th} order, Butterworth). To identify time points of rising and falling zero-crossings the raw signal was also bandpass filtered in the beta range (2^{nd}-order Butterworth, range: beta peak frequency ± 3 Hz). Having identified these, we went back to the raw, pre-processed signal

to identify peaks and troughs as the maximal and minimal voltage between rising and falling and falling and rising zero-crossings, respectively (Fig. 4.2A).

The reader is asked to refer to the General Methods subchapter 2.5.4 for mathematical definitions of sharpness, sharpness ratio (SR), steepness and rise-decay ratios (RDR).

We then studied the non-sinusoidal features of the signal inside and outside periods of beta bursts. Non-sinusoidal features were calculated for each cycle within and outside bursts and meaned for bursts and non-bursts within recordings.

Furthermore, as the asymmetric features extracted from cortex have been shown to account for cortical PAC (Cole et al., 2017) the non-sinusoidal features of ECoG and STN LFP signals were compared to cortical PAC and cortico-subthalamic PAC (CTX-STN PAC), respectively.

T-tests were performed for pair-wise comparisons. In the presence of two or more categorical variables multiway ANOVAs were applied with post-hoc Bonferroni corrections for multiple comparisons to assess the effects of multiple factors on the vector mean. To determine whether data from several groups have a common mean one-way ANOVAs with repeated measurements were used for parametric estimations of significance. If the dependant variable was ordinal or assumptions of normality were violated a Friedman's test for non-parametric estimation of significance was applied.

For correlations between PAC values and levels of asymmetry, Pearson's correlations were calculated. If assumptions of normality were violated (Lilliefors test) or correlations appeared to be driven by a few outliers, Spearman's rank correlation (Spearman's rho) was performed.

4.2.4 PAC within and between areas

In order to calculate the degree of phase-amplitude coupling between beta phase and the phase of HFO-filtered Hilbert transformed amplitude we chose the phase-locking value (PLV) method (Cohen, 2008; Seymour et al., 2017) in accordance with Chapter 2. For the PLV method we tested for statistical significance via 500 runs of surrogate data with circularly shifted permutations of the phase (Penny et al., 2008; Seymour et al., 2017). Please refer to Chapter 2.5.1 for the PLV-PAC equation.

For the calculation of cortico-subthalamic PAC (CTX-STN-PAC) the beta-phase was extracted from the cortical ECoG signal, whereas the HFOs were extracted from the STN LFPs. Within cortical PAC, where both phase and amplitude signals are extracted from the same source, was calculated by using the ECoG signal to extract both beta phase and HFO amplitude. The PLV-PAC modulation index assumes the value of 1 when the phase series are fully locked and 0 if they are completely desynchronised (Tort et al., 2010; Seymour et al., 2017). The LFP was filtered between 100 and 300 Hz with 4 Hz increments to extract the HFOs using 4th order Butterworth filters with bandwidths of ± 35 Hz.

Before the ϕf_a by way of the Hilbert transform was extracted from the HFO-amplitude time series, the amplitude signal was high- and lowpass filtered using Butterworth filters to remove non-beta components (Penny et al., 2008; Cohen, 2014). To ensure sufficient data lengths to calculate PAC during bursting and non-bursting periods, the bursting periods were cut and concatenated in one vector and non-bursting periods in another. The length of the vectors was adjusted to match that of the shortest one to eliminate the influence of data lengths in the PAC estimates. Importantly, the Hilbert phase of the beta component and the phase of Hilbert HFO amplitude were both extracted prior to cutting and concatenating the data to avoid jumps in the signal between periods.

4.2.5 Spike-triggered averages

Spike-triggered averages (STAs) were computed by triggering the amplitude envelope of the band-pass filtered (4th-order Butterworth) HFO (100-300 Hz) at the time of each action potential from a single unit, where the unit and LFP signals were separated by at least 2 mm. The HFO amplitude was averaged around each single-unit spike with time zero marking spike onset. Within subjects a t-test was carried out to test for consistency across epochs of 3 seconds durations. For averaged group data, a two-sample t-test was performed at spike onset.

4.2.6 Power spectral densities

Power spectral densities of single units were calculated by use of the Welch periodogram method (Matlab function pwelch.m function, using a Hanning window with 50% overlap, window size = 0.2*sampling frequency) by analysing binary spike time files.

4.2.7 Spike-phase locking

The Hilbert transform was used to extract phase from band-pass filtered LFP signals (beta-frequency corresponding to highest PAC value +/- 5 Hz) and the phases at the times of each action potential were extracted to construct phase histograms. For circular data Watson–Williams tests were applied to assess the homogeneity of means of two or more samples. Rayleigh's test for non-uniformity was applied to determine if the spike-phase locking (SPL) was significant using the Circstat Matlab toolbox (Berens, 2009). Phase histograms were also made from the Hilbert-extracted beta phase with regards to HFOs, which were separated into 30 amplitude bins and plotted against the beta phase cycle. To relate subthalamic spike-locking to cortical beta bursts of different durations the mean

vector length (MVL) was calculated using the same Circstat Matlab toolbox for subthalamic single units. This metric was related to cortical mean burst sharpness and number of cycles in bursts. Vectors of cortical beta phases of binary subthalamic spiking were concatenated and assigned according to the cortical bursts durations under which they occurred. Only vectors of at least 20 spike-phases were included. Mean firing rates were calculated for different burst durations and assigned on a cycle-by-cycle basis during beta-bursts and 3 cycles prior and 3 cycles after bursts.

4.3 Results

Only LFP recordings from micro- and macro-electrodes within the STN were included in the study. Whenever microelectrode recordings were used for both spiking and LFP-signal comparisons they were made from different microelectrodes separated by at least 2 mm (Fig. 4.1) to eliminate signal contamination.

4.3.1 Cortical beta bursts capture higher levels of non-sinusoidal sharpness

Our overarching aim was to define the relationship between different electrophysiological biomarkers across cortex and STN. Both raw beta sharpness ratios and beta burst longevity have been linked to symptom severity in PD (Cole et al., 2017; Tinkhauser et al., 2017b). We therefore began by studying how cortical beta-bursts related to measures of non-sinusoidal features by analysing absolute peak sharpness, sharpness ratios (SR) and rise-decay ratios (RDR) inside and outside periods of beta bursting. Beta-peaks were found in 45 % of all ECoG recordings (Suppl. Fig. 1).

There was a significant effect of burst duration on both peak sharpness (ANOVA $p < 0.0001$, Fig. 4.2C) and sharpness ratios (ANOVA, $p = 0.0015$, Fig. 4.2D), and we found a significantly higher sharpness ratio (Fig. 4.2D, Bonferroni, $p < 0.0001$, mean SR(during bursts) = 0.6291, meanSR (outside bursts) = 0.5586, n = 96 recordings) and absolute peak sharpness (Fig. 4.2C, Bonferroni, $p < 0.0001$, meanSharpness (during bursts) = 0.0212, meanSharpness (outside bursts) = 0.0148, n = 96) during periods of bursting compared to non-bursts after adjustment for multiple comparisons using Bonferroni correction. Burst-duration also had a significant effect on rise-decay-ratios (ANOVA, $p < 0.0001$), and outside-burst periods captured higher levels of rise-decay ratios indicating slightly greater vertical symmetry in periods of bursting (Fig. 4.2E, Bonferroni, $p < 0.0001$, meanRDR (during bursts) = 0.1883, meanRDR (outside bursts) = 0.3041, n = 96).

Given the correlation between PAC and beta waveform asymmetry (Cole et al., 2017) and PAC and phase locking of STN units during beta bursts (see below and Chapter 3), we hypothesised that these three biomarker signals are comodulated in time by beta bursts. In support of this hypothesis, we found that absolute sharpness increased significantly and progressively with beta-burst duration (See Fig. 4.2C for pairwise comparisons after Bonferroni corrections for multiple comparisons).

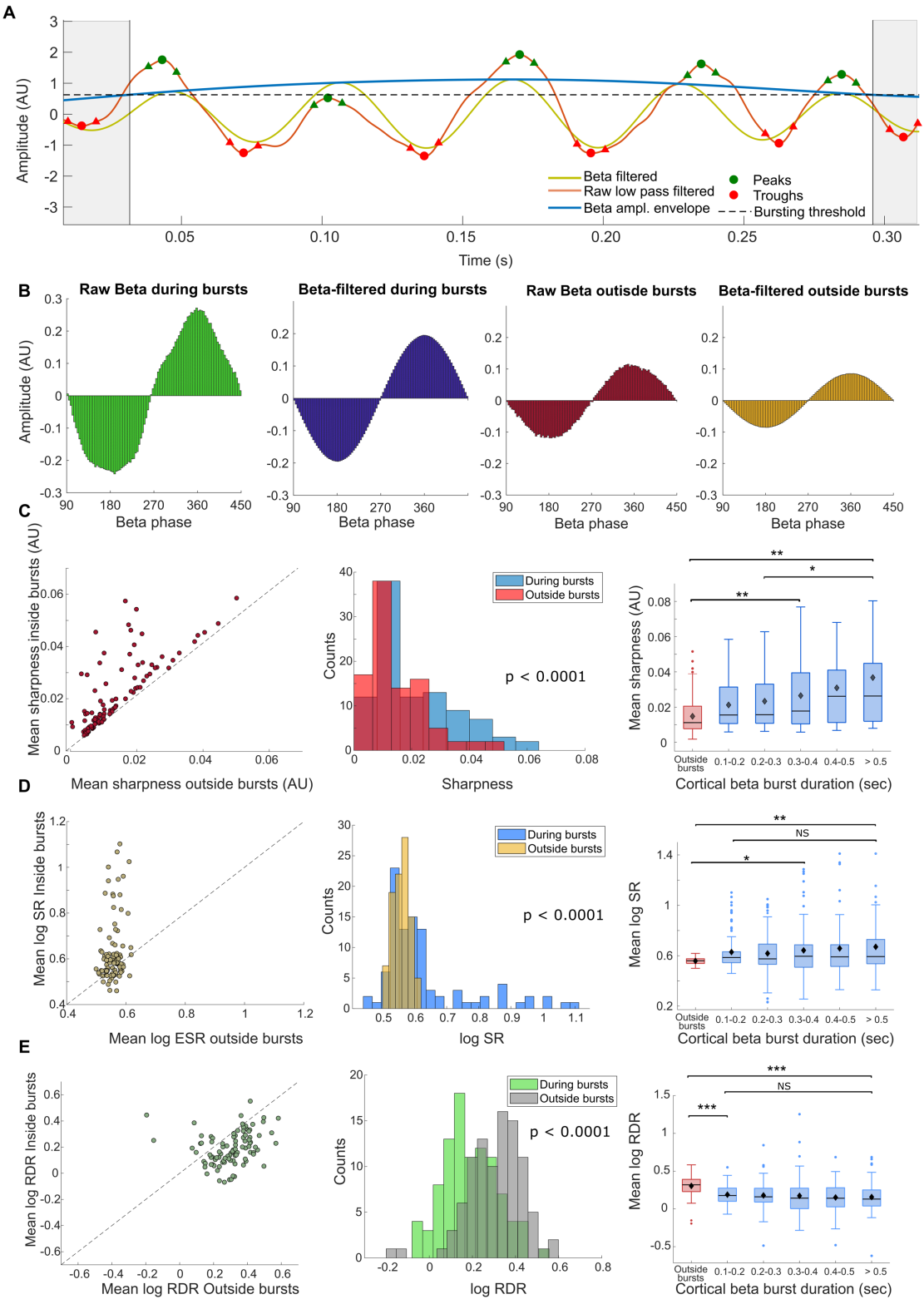

A
Amplitude (AU)
Time (s)
Beta filtered
Raw low pass filtered
Beta ampl. envelope
Peaks
Troughs
Bursting threshold
B
Raw Beta during bursts
Beta-filtered during bursts
Raw Beta outisde bursts
Beta-filtered outside bursts
Amplitude (AU)
Beta phase
C
Mean sharpness inside bursts (AU)
Mean sharpness outside bursts (AU)
During bursts
Outside bursts
Counts
p < 0.0001
Sharpness
Mean sharpness (AU)
Outside bursts
0.1-0.2
0.2-0.3
0.3-0.4
0.4-0.5
> 0.5
Cortical beta burst duration (sec)
D
Mean log SR Inside bursts
Mean log ESR outside bursts
During bursts
Outside bursts
Counts
p < 0.0001
log SR
Mean log SR
NS
Cortical beta burst duration (sec)
E
Mean log RDR Inside bursts
Mean log RDR Outside bursts
During bursts
Outside bursts
Counts
p < 0.0001
log RDR
Mean log RDR
NS
Cortical beta burst duration (sec)

Figure 4.2. Non-sinusoidal features of cortical beta-oscillations during and outside periods of cortical beta-bursts. **A**) Example of the raw low pass filtered signal during a beta burst, the beta-filtered signal with marked peaks and troughs ± 5 ms, the beta amplitude-envelope, and the bursting 75 % percentile amplitude threshold criterion. White background marks the period inside the burst. **B**) Example of averaged binned amplitudes from raw data (green) and beta filtered (blue) averaged across one cycle during beta bursts and raw (red) and beta-filtered (yellow) data averaged across one beta cycle outside bursts. **C**) Mean absolute peak sharpness during and outside periods and bursting as well as mean absolute peak sharpness by burst duration. **D**) Mean log sharpness ratios (SR) during and outside bursts and SR by burst duration. **E**) Mean log rise-decay-ratios (RDR) during and outside bursts and as a function of burst duration. P-values for pair wise comparisons were adjusted for multiple comparisons using Bonferroni correction. *** $p < 0.001$, ** $p < 0.01$, * $p < 0.05$, $n = 96$. **SR = Sharpness ratio. RDR = Rise decay ratio**

When sharpness was studied on a cycle-by-cycle basis, we found the peak sharpness was significantly correlated with burst duration ($r = 0.9458$, $p < 0.0001$, Pearson's correlation coefficient) and that higher values of both measures were associated with higher values of subthalamic unit locking to cortical beta phase (Fig. 4.3A). In line with this, we found cortical beta sharpness to be significantly positively correlated with the locking of subthalamic single units to cortical beta-oscillations ($r = 0.8578$, $p = 0.0007$, Pearson's correlation coefficient, Fig. 4.3B). The correlation between sharpness and number of cycles in the burst indicates that the former should closely follow the time course of the burst amplitude. We found this to be the case, with sharpness peaking in the middle of the individual bursts for all lengths (Fig. 4.3C, $p < 0.0001$, Friedman ANOVA, significance levels are adjusted for multiple comparisons by post-hoc Bonferroni correction). This relationship was not seen for the other measures of waveform

asymmetry (Fig. 4.3D + E). Finally, no correlation was found between mean single unit firing rates of subthalamic single units and cortical beta bursts sharpness on a cycle-by-cycle basis (Fig 4.3E).

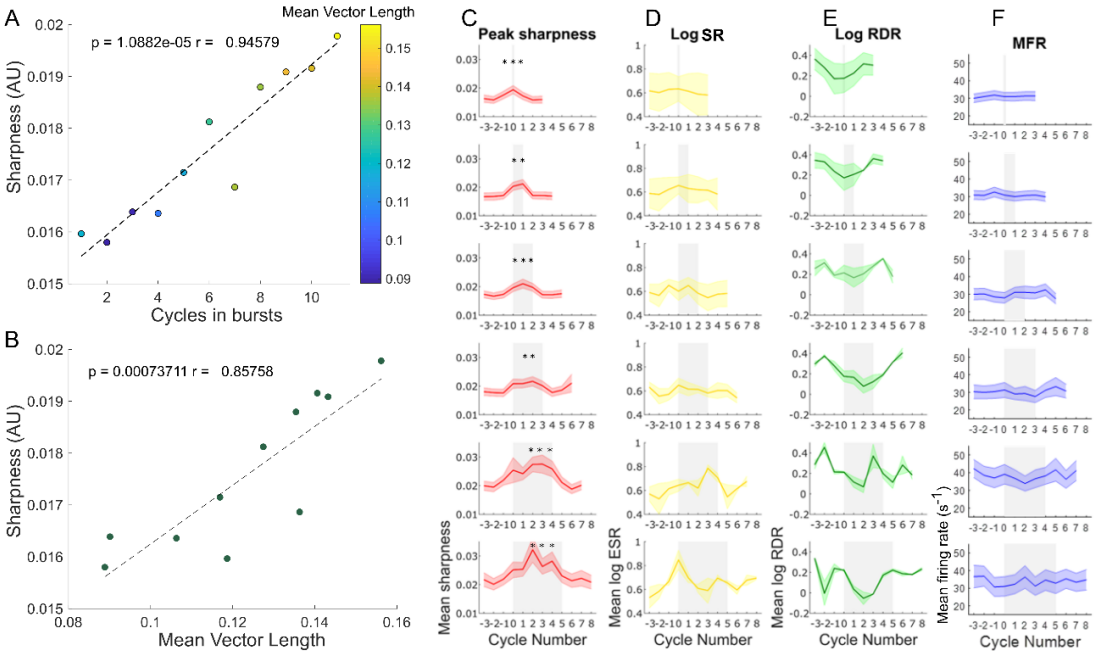


Figure 4.3 - Peak sharpness in beta-bursts progresses with burst duration and subthalamic unit locking to cortical beta and is greatest in the middle of bursts. A-B) Mean peak sharpness as a function of total cycle number in beta-bursts and mean-vector length**.** Correlations are Pearson's correlation coefficients. **C-F)** Peak sharpness, log SR (sharpness ratio), log RDR (rise decay ratio) and mean firing rate (MFR) as a function of beta burst cycle progression. Grand average +- SEM according to beta cycle duration in periods of beta bursts. n = 96. ***** p < 0.05, Friedman's test with Bonferroni correction for multiple comparisons. Grey squares mark beta-bursting periods staring with cycle 0. Negative numbers on the x-axis mark cycle numbers leading up to bursts (i.e. -3 is cycle number 3 before burst onset).

4.3.2 Cortico-subthalamic PAC predicts the locking of single units to HFO amplitude at beta frequencies

Cortical signal asymmetries have been demonstrated to account at least in part for levels of cortical PAC in PD patients (de Hemptinne et al., 2015; Cole et al., 2017), whereas we recently demonstrated that STN PAC could reflect the locking of single units to subthalamic beta-oscillations. Here we introduce a cross-regional measure of PAC between cortical beta phase and subthalamic HFO (CTX-STN PAC) to investigate to what extent cortical beta bursts could predict the locking to subthalamic spiking activity. Significant CTX-STN PAC (> 20 connected frequency bins with $p < 0.05$) was found in 43 out of 93 recordings (Fig. 4.4).

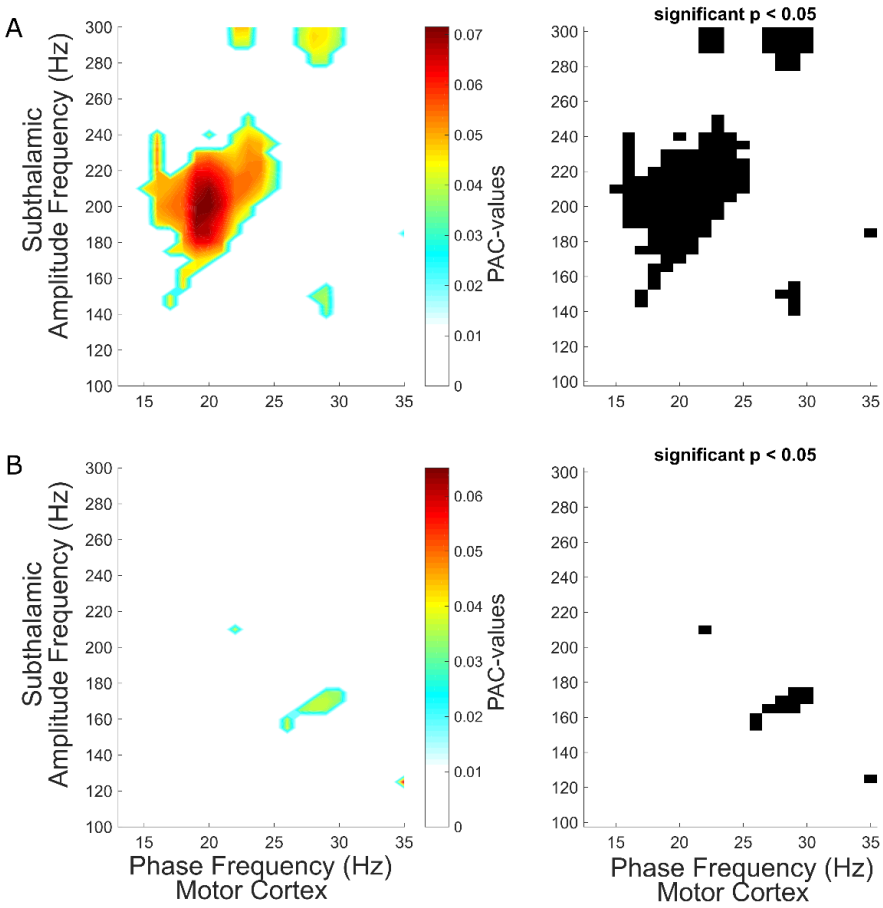


Figure 4.4 - Determination of significant cortico-subthalamic PAC (CTX-STN-PAC). **A)** Example comodulogram from recording with significant CTX-STN PAC determined by significant frequency bin clustering. **B)** Example of recording without any significant CTX-STN-PAC.

We started out by examining the locking of STN spikes to the STN HFO amplitude in the presence and absence of significant CTX-STN PAC. As seen in the grand spike triggered averages (Fig. 4.5), the STN HFO amplitude (180-260 Hz) was significantly locked to spike onsets, with rippling patterns corresponding to beta frequencies (20 – 33 Hz). This was significant across cases (180-260 Hz, ~80-100 % significant bins, paired t-test per frequency bin for consistency across epochs, significance criteria: $p < 0.05$ Fig. 4.5A, n= 55, STN units with sig. STN-CTX PAC). The absolute mean HFO power (100-300 Hz) was not found to be significantly different across the spike time window for recordings with and without significant CTX-STN PAC at spike onsets ($p = 0.9185$, two-sample t-test). Moreover, no beta-ripples were found and any synchronisation to spike onset was insignificant across cases (180-260 Hz, 5-10 %, paired t-test per frequency bin for consistency across epochs, significance criteria: $p > 0.05$, Fig. 4.5B, n = 62, STN units with non-sig. CTX-STN PAC).

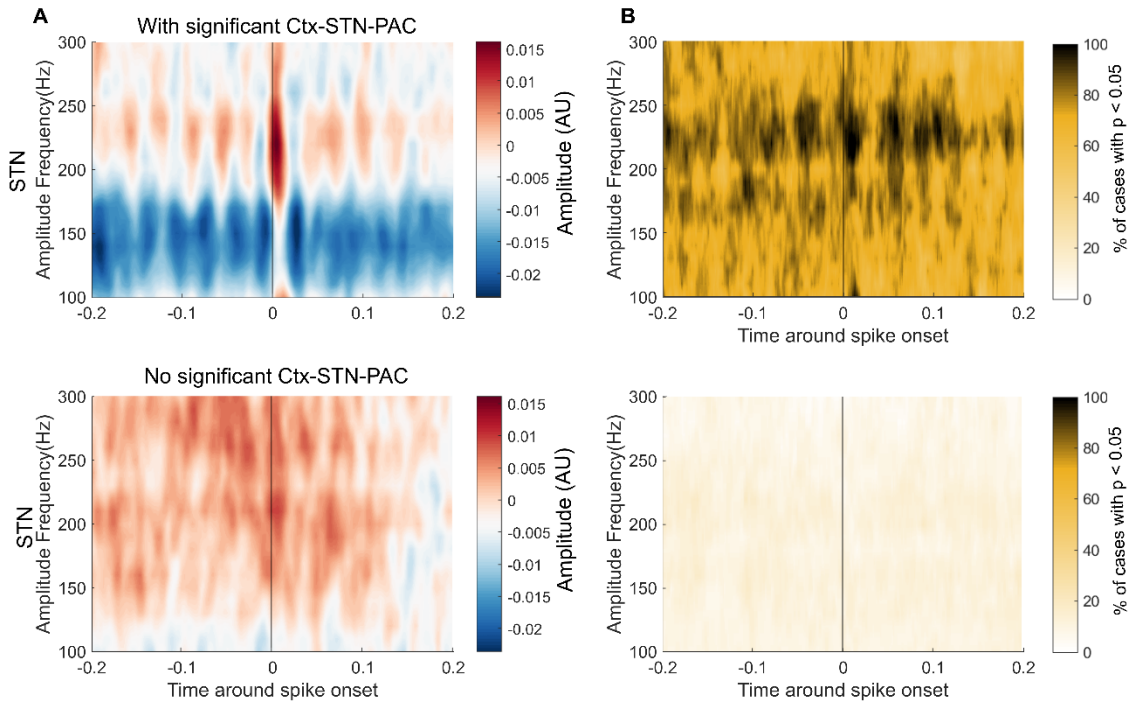


Figure 4.5 Subthalamic spiking locks significantly to HFO amplitude at cortical beta frequencies in the presence of significant CTX-STN-PAC. Grand average across all recordings. Upper row: Grand average of spike triggered-average (STA) in the presence of significant CTX STN-PAC (left) and percentages of cases where this finding was significant (right). Note that the rippling pattern in the synchronisation that corresponds to beta frequencies (20 – 33 Hz). Lower row: STA in the absence of significant CTX-STN-PAC. Note that the synchronisation is not significant in any patterns across cases (right).

The temporal correlation between the timing of STN HFOs and spikes in the presence of CTX-STN PAC suggests that the phase of the cortical beta oscillation is a common reference point for the two STN signals. In line with this, in the presence of significant CTX-STN PAC there was no significant difference between the mean cortical beta phases at which the peak amplitude of STN HFOs and spikes of significantly phase-locked STN

units occurred ($p = 0.67422$, Watson–Williams test, Fig 4.6A). The power spectral density of STN units during this enhanced cortico-subthalamic coupling manifested in enhanced beta oscillations in STN neurons (Fig. 4.6B). A significant beta-peak was found in the STN neuron power spectrum in the presence of CTX-STN PAC, but not in the absence thereof ($p = 0.00273$, two sample t-test, comparison of groups with significant and non-significant CTX-STN PAC, Fig. 4.6A). Similarly, a significant beta-peak was present for neurons locked to beta phase for which the strongest CTX-STN PAC was found compared to non-locked neurons ($p < 0.0001$, two sample t-test, n = 36/24 STN units significantly/non-significantly locked to cortical beta [Rayleigh's test, $p < 0.05$], Fig. 4.6B). The relative difference in beta-oscillatory firing was even stronger when we compared cortical beta-phase locked neurons with significant CTX-STN PAC to those that were neither phase locked and or recorded in the presence of significant CTX-STN PAC ($p = 0.0005$, two sample t-test, Fig. 4.6C n = 24/15 STN units significantly/non-significantly locked to cortical beta [Rayleigh's test, $p < 0.05$] with/without CTX STN PAC).

Overall, these results suggest that CTX-STN PAC provides a proxy measurement for the locking of STN neurons to cortical beta oscillations.

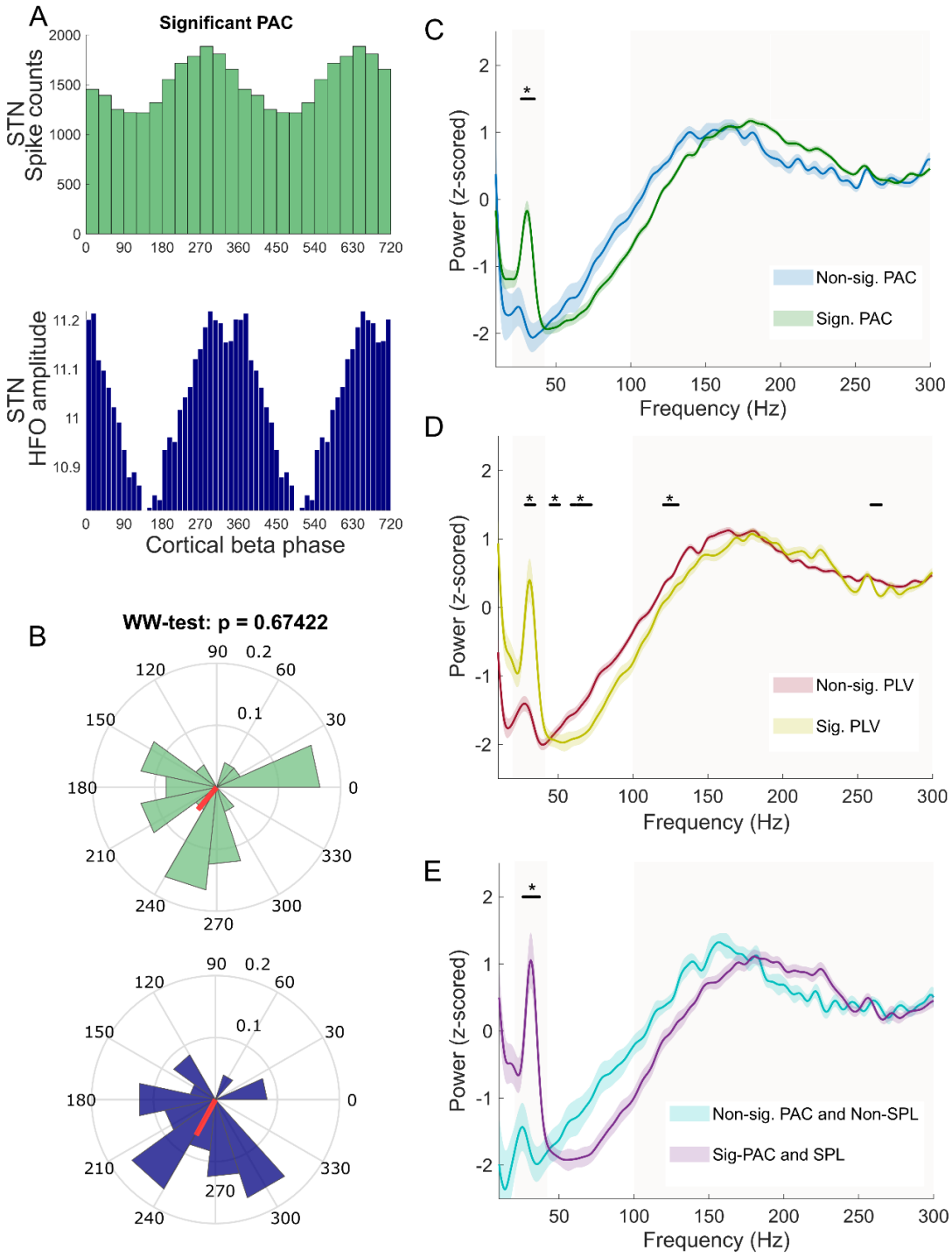

A
Significant PAC
STN Spike counts
2000
1500
1000
500
0
0 90 180 270 360 450 540 630 720
STN HFO amplitude
11.2
11.1
11
10.9
0 90 180 270 360 450 540 630 720
Cortical beta phase
B
WW-test: p = 0.67422
90 0.2 60
120
0.1
150
30
180
0
210
330
240
300
270
C
Power (z-scored)
Frequency (Hz)
Non-sig. PAC
Sign. PAC
D
Power (z-scored)
Frequency (Hz)
Non-sig. PLV
Sig. PLV
E
Power (z-scored)
Frequency (Hz)
Non-sig. PAC and Non-SPL
Sig-PAC and SPL

Figure 4.6. – Subthalamic HFO amplitudes and spikes are synchronised to the same phase when locked to cortical beta oscillations, and single unit power spectra predict significant CTX-STN PAC frequencies. **A**) Examples of spike-phase locking and HFO-phase locking in the presence of significant CTX-STN PAC and significant spike-phase locking (SPL). **B**) Circular representation of all recordings exhibiting both significant CTX-STN PAC and significant SPL. Colours correspond to the examples in A so that green shows phase peaks for spikes and blue phase peaks for the HFO amplitude envelope. When both HFO and spikes are locked to the same cortical beta-phase they do so at the same phases of the cortical beta oscillation (Watson Williams-test, $p = 0.6742$). **C**) Single unit power spectral densities +/-SEM according to significance of CTX-STN PAC only. ***** F-test $p < 0.05$. **D**) Single unit power spectral densities according to significance of cortical beta-phase subthalamic spike locking only. E) Single unit power spectral densities according to both the significance of CTX-STN PAC and cortical beta-phase subthalamic spike locking.

4.3.3 PAC and sharpness

Non-sinusoidal features of ECoG-recorded signals in PD patients have recently been shown at least in part to explain the measured PAC within cortex with the sharpness ratio being significantly correlated to PAC values (Cole and Voytek, 2016; Cole et al., 2017; van Wijk, 2017). The sharpness ratio between peaks and troughs was found to be positively correlated to clinical rigidity scores in PD patients off stimulation (Cole et al., 2017). We established that the features of beta waveform asymmetry, and their relationship to PAC, described by Voytek and colleagues were present in our dataset. As described by Cole et al., we found that the cortical sharpness ratio was significantly correlated to absolute cortical beta-high gamma PAC values ($r = 0.3356$, $p = 0.0122$,

Pearson's correlation, Fig. 4.7) albeit using a different method to calculate the levels of PAC. However, this correlation in our study appeared to be heavily driven by one data point. When Spearman's rho is applied this correlation is weakened (rho = 0.2265, p = 0.0964, Spearman's rank correlation). Sharpness ratios of the cortical signal were not able to explain the cortico-subthalamic PAC-values (r = 0.0445, p = 0.7610, Pearson's correlation, Fig. 4.8).

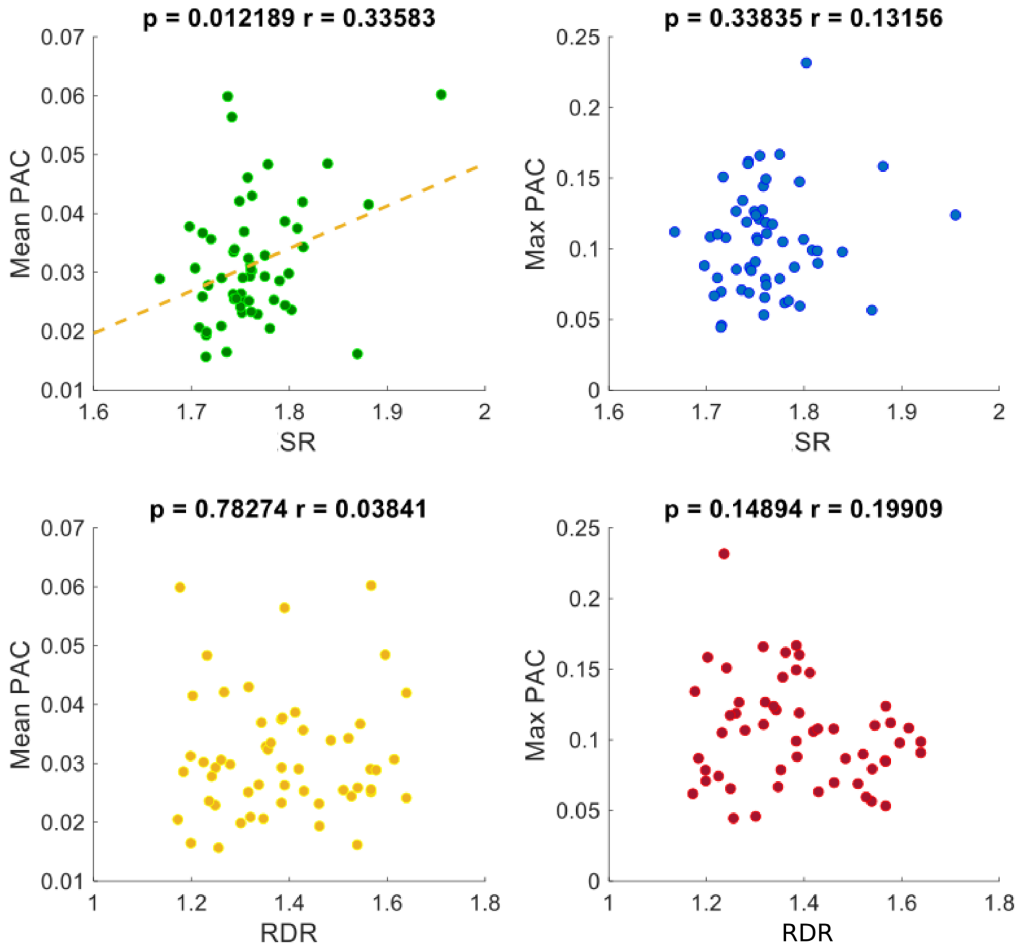


Figure 4.7. Within cortical PAC and nonsinusoidal features (SR and RDR). Within-cortical PAC is significantly related to the peak-trough extreme sharpness ratio of the raw beta oscillations. Pearson's correlation coefficients. SR = Sharpness ratio. RDR = Rise decay ratio.

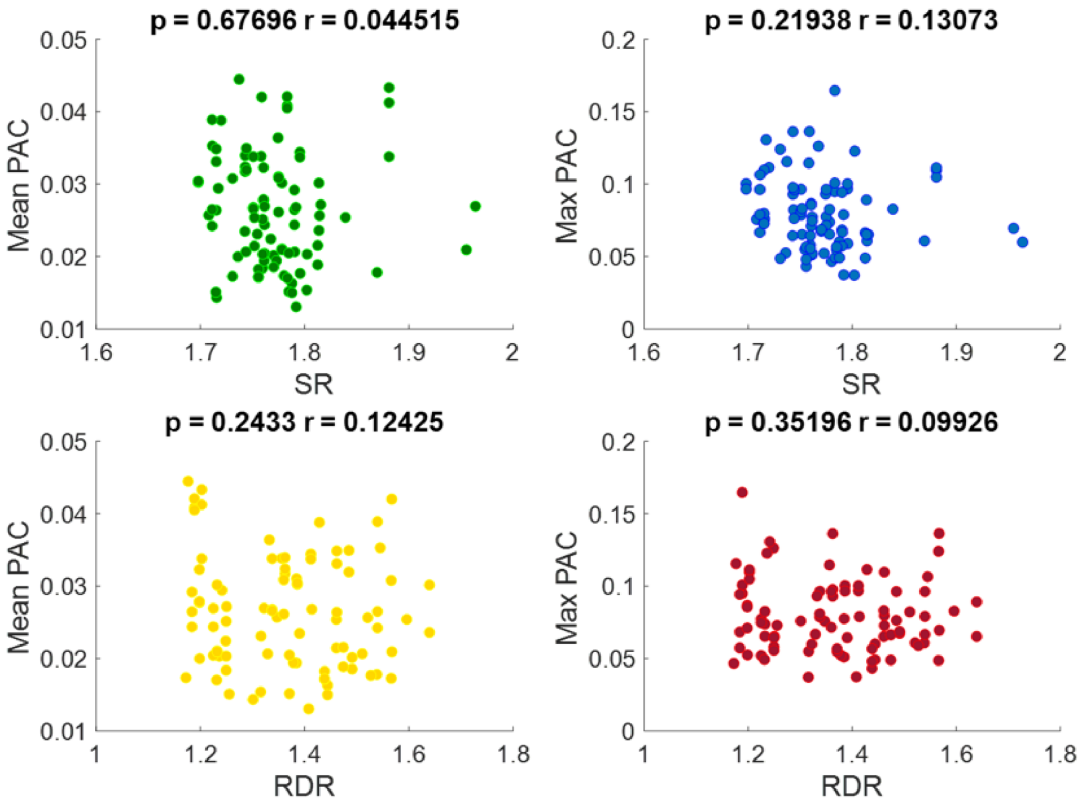


Figure 4.8 – CTX-STN PAC and measures of nonsinusoidal features. No significant correlation between PAC, ESR and RDR were found. Pearson's correlation coefficients. SR = Sharpness ratio. RDR = Rise decay ratio.

4.3.4 Cortico-subthalamic PAC increases with cortical beta burst duration

Several recent studies have demonstrated that the temporal dynamics of beta oscillations, particularly the length of beta bursts is a key metric in the pathophysiology of PD (Tinkhauser et al., 2017b). Having established the utility of CTX-STN PAC in defining cortico-subthalamic phase-locking, we investigated how CTX-STN PAC related to the time course of beta bursts in cortex. Fig. 4.9A shows two comodulograms from the same hemisphere recording of CTX-STN PAC inside and outside cortical beta-bursts, where CTX-STN PAC was only significant inside bursts, as compared to surrogate data. Across brain hemispheres we found that CTX-STN PAC was significantly higher in periods of cortical beta-bursting compared to periods outside (Fig. 4.9A-B, $PAC_{Inside} = 0.2143$, $PAC_{Outside} = 0.1792$, $p = 0.0177$, paired t-test, $n = 7$, hemispheres) in recordings with the presence of a beta-peak. We also found CTX-STN PAC values increased progressively and significantly with the duration of the bursts after vector length adjustment (data vectors were adjusted to have the same length as the shortest combined vector, ANOVA, $p < 0.0001$, Fig. 4.9C, $n = 96$ recordings). Refer to Fig. 4.9C for pairwise comparisons of CTX-STN PAC levels at increasing burst intervals (p-values are adjusted for multiple comparisons using Bonferroni correction). In summary, CTX-STN PAC was higher inside than outside cortical beta bursts suggesting that, as previously found within the STN, beta bursts and phase amplitude coupling are not independent biomarkers at the cortico-subthalamic network level.

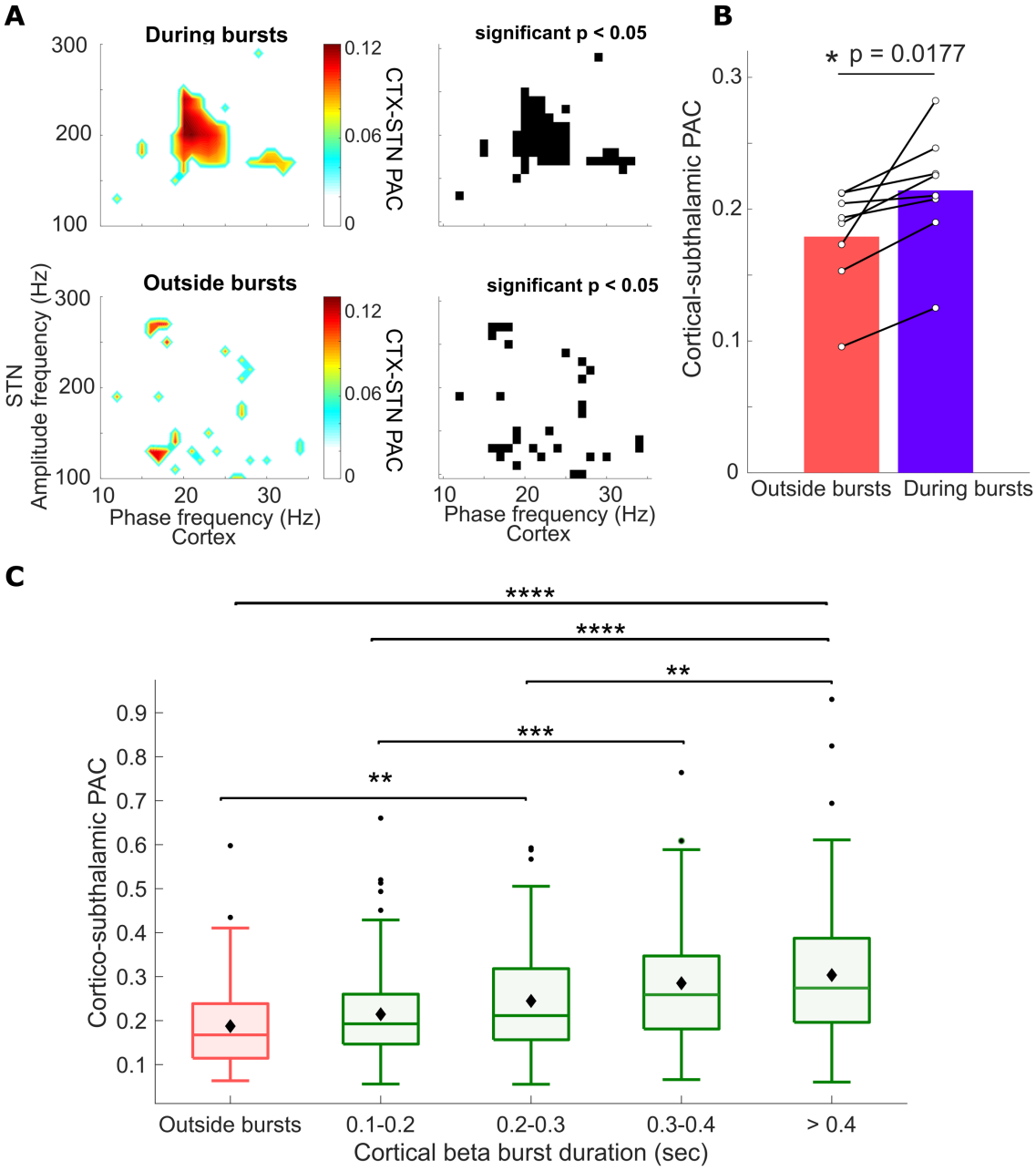


Figure 4.9 - Cortico-subthalamic PAC is higher during cortical beta-bursts periods and increases with bursts duration. A) Example of CTX-STN PAC during beta bursts (upper row) and outside beta-bursts (lower row) from the same recording. B) Average around maximum (± 16 Hz) CTX-STN PAC calculated from 7 hemispheres with recordings that demonstrated a beta peak. CTX-STN PAC was found to be significantly higher during periods of beta bursting compared to outside periods of bursting ($p = 0.0177$, paired t-test). C) CTX-STN PAC significantly increased with burst duration (ANOVA, $p < 0.0001$). Average around maximum (± 16 Hz) CTX-STN PAC during bursts of different durations across recordings ($n = 96$). Pairwise comparisons are adjusted for multiple comparisons using Bonferroni correction.* $p < 0.05$, ** $p < 0.01$, *** $p < 0.001$, **** $p < 0.0001$.

4.4 Discussion

With a growing worldwide burden of Parkinson's disease (PD) and a rising clinical, industrial and scientific interest in adaptive forms of DBS there is a need for robust biomarkers of pathophysiological activity. In this paper we analysed the relationship between some of the most prominent electrophysiological biomarkers of PD: cortical beta bursts, nonsinusoidal sharpness features, PAC, and the locking of subthalamic spike-amplitude synchronisation to cortical beta phases. Importantly, we focused on the relationship between these biomarkers on the timescale of beta bursts, which are proven to be effective as a closed-loop biomarker (Little et al., 2013). In addition, by using combinations of cortical and subthalamic signals, we are able to demonstrate that cortical biomarkers can be used to infer physiological changes at the level of STN units. Our findings suggest that both cortical beta peak sharpness and CTX-STN PAC reflect subthalamic spike synchronisation to cortical beta oscillations, and that these measurements increase with the duration of transient, cortical beta-bursts events.

Several theories have been brought forward regarding the propagation mechanisms behind beta-oscillations and transient beta burst events across brain regions in health and disease (Engel and Fries, 2010; Holgado et al., 2010; Sherman et al., 2016; Cagnan et al., 2018a). In PD beta-oscillations are thought to arise as a result of synchronised transient synaptic inputs across the cortical basal ganglia circuits in the setting of nigrostriatal dopaminergic depletion. Recently, studies have found amplitude-responsive aDBS to trim the longevity of beta-bursts (Tinkhauser et al., 2017a) and PD motor symptoms and freezing of gate to correspond to the duration of the bursts (Tinkhauser et al., 2017b; Anidi et al., 2018). These studies suggest that it may not be the beta bursts per se, but their sustained propagation that is a pathophysiological feature in PD. As the degree of subthalamic spike-locking to cortical beta-oscillations progresses with both cortical beta-

burst duration and sharpness it could be that it is the sustained locking of subthalamic neuronal activity to cortical beta oscillations which is the pathophysiological feature captured during the longer beta-bursts.

Meanwhile, PAC has also been widely studied in various brain regions such as cortex, hippocampus and basal ganglia structures (Canolty et al., 2006; Canolty and Knight, 2010; Lopez-Azcarate et al., 2010; Belluscio et al., 2012; Watrous et al., 2015; Zhang et al., 2018). Interpretations and inferences vary depending on the investigated frequencies, states and structures but commonly involve either the functional coupling between neuronal populations oscillating at different frequencies, the synchronisation of background unit activity to lower frequencies dominated by synaptic inputs or the product of signal non-linearities, whether or not the latter carries pathophysiological information (Canolty, R T, 2012; Aru et al., 2015; Cole et al., 2017). In the motor cortex of PD patients the broadband gamma amplitude component of PAC is at least in part driven by the nonlinearities of the beta oscillation (Cole et al., 2017; van Wijk, 2017; Jackson et al., 2019). We here found some confirmation of the statistical relation between within-cortical PAC and nonsinusoidal features of the cortical beta oscillations using Pearson's correlations, but not Spearman's correlations. This lack of significance between SR and mean PAC could perhaps stem from the measure of sharpness used, which involves a fixed 5 ms step from the peak. Depending on the value of the beta peak, 5 ms is a different fraction of the cycle period for different participants. This could somewhat hinder the comparison between subjects and make the findings less conclusive. CTX-STN PAC, on the other hand, was associated with synchronisation of subthalamic spiking activity to the HFO amplitude at cortical beta frequencies. In the presence of significant CTX-STN PAC the HFO amplitude peaked centred on the timing of spikes from single units. Significantly, the STA time resolved spectrograms demonstrated cortical beta-ripples only in the

presence of cortical-subthalamic PAC. Furthermore, the spike-triggered amplitude was locked to the same phase of cortical beta as the significantly cortical phase-locked STN neurons and no significant differences were found in the overall levels of HFO amplitude in either the single unit spectrograms or the LFPs between the two groups. This demonstrates that CTX-STN PAC, unlike within-cortical PAC, mimics the features attributed to STN PAC in recent computational and analytical studies (Sanders, 2016; Meidahl et al., 2019). It is worth emphasising that the statistically coupled amplitude frequency here was higher (150-300 Hz) than the broadband gamma observed in ECoGs (70-150 Hz) (de Hemptinne et al., 2013). Shimamoto et al. found STN spiking to be significantly synchronised to both the beta and broadband gamma activity of the motor cortex with the cortical gamma activity demonstrating an oscillatory envelope at beta frequencies (Shimamoto et al., 2013). With the latest discoveries of the non-sinusoidal features giving rise, at least in part, to the within-cortical beta-gamma PAC, it may well be that they observed the neuronal phase-locking to beta asymmetries.

This study shows that both peak sharpness, a non-sinusoidal feature, and CTX-STN PAC increases with the duration of the bursts, demonstrating that transient events in cortical activity in the form of beta-bursts capture progressively higher levels of cortico-subthalamic synchronisation. Beta-bursts consequently share the non-linearity giving rise to cortical beta-gamma PAC and subthalamic spike-HFO synchronisation at cortical beta phases. We acknowledge that one contributing factor to the observed increase in sharpness asymmetries during bursts could be that the waveform morphology is easier and more stable to detect in periods of high amplitude (Schaworonkow and Nikulin, 2019).

Beta bursts, beta-phase, HFO-amplitude, CTX-STN-PAC, sharpness and spiking activity have all been proposed as central biomarkers for aDBS interventions (Kühn and

Volkmann, 2017; Meidahl et al., 2017; Bouthour et al., 2019). We have provided evidence to suggest that all six phenomena are related and hence focusing stimulation on one might target them all. Thus, amplitude responsive aDBS that triggers stimulation during beta-bursts would also implicitly be triggered by periods of elevated PAC, cortical-subthalamic spike synchronisation and peak sharpness. Conversely, triggering stimulation by peak-sharpness would likely also capture longer periods of beta bursts. As these biomarkers are also attenuated by subthalamic cDBS (de Hemptinne et al., 2015; Cole et al., 2017) they might be considered interchangeable in the context of adaptive DBS, with their selection being best determined on methodological grounds dictated by the need to quantify these measures in ultra-low power devices. A key constraint is the amplitude of the signal feature, and in this regard asymmetries in cortical beta activity are a good starting point, given that this signal is several orders of magnitude greater than comparable subthalamic features and more tractable than spike recordings.

As closed-loop approaches to deep brain stimulation evolve, so do the proposed electrophysiological signals for feedback. In order to find the most optimal signal for future experimental interventions, studies are needed that compare individual signals with symptom severity in real-time, taking their individual read-out feasibility into account, using adaptive stimulation parameters. In future, machine learning and artificial intelligence might negate the need to extract particular aspects of macro signals and allow for a more multi-dimensional signal feedback approach. In the meantime, based on our findings, hybrid sensing of beta amplitude and sharpness could be promising biomarkers in future closed-loop DBS experiments in Parkinson's disease.

5

Cortical phase-amplitude coupling and signal asymmetries during selective optogenetic stimulation of basal ganglia and cerebellar recipient thalamus

Contents

5.1 Introduction

5.2 Materials and methods
- 5.2.1 Animals
- 5.2.2 Viral Constructs
- 5.2.3 Surgical procedures
- 5.2.4 In vivo electrophysiology and optogenetic stimulation of BZ neurons
- 5.2.5 Data analysis

5.3 Results
- 5.3.1 Cortical power spectral changes in ECoG signals during motor thalamic stimulation
- 5.3.2 Selective stimulation of basal ganglia receiving thalamus generates PAC in ipsilateral ECoG signals
- 5.3.3 Laminar-specific changes in PAC and oscillations in motor cortex during motor thalamic stimulation
- 5.3.4 BZ thalamic stimulation induces cortical waveform asymmetries
- 5.3.5 Basal ganglia thalamic projections to cortex give rise to ECoG asymmetries and PAC
- 5.3.6 Laminar PAC throughout motor cortex is not explained by waveform asymmetries

5.4 Discussion
- 5.4.1 Cortical PAC and asymmetries as biomarkers of basal ganglia-thalamo-cortical network activity
- 5.4.2 Origins of cortical beta oscillations
- 5.4.3 Theories of PAC generation
- 5.4.4 Implications for Parkinson's disease and closed-loop modulations

5.1 Introduction

Cortical electrophysiological signals have been extensively studied for almost a century since Hans Berger's first electroencephalogram recordings (Berger, 1929). Since then, the analysis of cortical electrophysiological signals has evolved and been adapted as routine investigations across the neuroscientific field in the study of both health and disease. Thalamus has been proposed to play a vital role in the generation and formation of both alpha and beta oscillations in cortex, and phase-amplitude coupling (PAC), where the lower frequency is statistically coupled to higher broadband frequencies, has been proposed as a method for computational transfer of neuronal information between subcortical and cortical regions (Steriade et al., 1993; Fries, 2005, 2015; Canolty et al., 2006; FitzGerald et al., 2013; Malekmohammadi et al., 2015; Sherman et al., 2016; Opri et al., 2019).

Beta oscillations (13-35 Hz) have, as stated in previous chapters, time and again been implicated in motor control (Sanes and Donoghue, 1993; Baker et al., 1997, 2003; Kühn et al., 2004; Engel and Fries, 2010; Anzak et al., 2012; Tan et al., 2014; Khanna and Carmena, 2017; Torrecillos et al., 2018; Fischer et al., 2018, 2019). Lately beta oscillations have been proposed to reflect timed synaptic events to distinct cortical layers, theorised to originate from basal ganglia-thalamo-cortical projections (Sherman et al., 2016). The basal ganglia are known to send GABAergic projections to both ventromedial (VM) thalamus and inhibitory afferent-dominant zone of the ventral anterior (VA) thalamus (Kuramoto et al., 2009, 2015) as part of the basal ganglia-thalamo-cortical (BTC) network. In this chapter we refer to the part of VM thalamus that receives basal ganglia input as the basal ganglia-recipient zone (BZ) (Nakamura et al., 2014). The deep cerebellar nuclei project to the excitatory subcortical afferent-dominant zone of the

ventrolateral (VL) as part of the cerebello-thalamo-cortical (CTC) network (Kuramoto et al., 2015), and here we refer to the cerebellar-recipient part of VL thalamus as the cerebellar-recipient zone (CZ) (Nakamura et al., 2014). Furthermore, intralaminar thalamic nuclei are known to receive both basal ganglia and cerebellar input (Smith et al., 1998). Thalamic nuclei in BTC and CTC networks have been shown to project to different layers of cortex: with basal ganglia receiving ventromedial thalamus predominantly projecting to layer 1 and cerebellar receiving ventrolateral thalamus projecting to neocortical layers 2-5 (Kuramoto et al., 2009, 2015). What role, if indeed any, basal ganglia and cerebellar recipient thalamus plays in the generation of such oscillations in neocortex remains unclear and is lacking in experimental support. This is also the case for the role of motor thalamus with regards to the initiation and maintenance of broadband gamma oscillations (Minlebaev et al., 2011; Buzsáki and Wang, 2012). In this chapter of the thesis we define high-gamma as frequencies in the range of 70-150 Hz in referral to previous papers on cortical spectral content (Canolty et al., 2006; Buzsáki and Wang, 2012; de Hemptinne et al., 2015) and make a spectral, albeit slightly overlapping, differentiation from HFOs (100-300 Hz) as defined in the STN in Chapters 3 and 4.

It has been argued that the coupling of lower frequencies, such as beta, to higher broadband frequencies is computationally important for neural information transfer (Canolty et al., 2006; Canolty and Knight, 2010; Spaak et al., 2012; Fries, 2015; Watrous et al., 2015; Opri et al., 2019). PAC has been studied in a wide area of cortical regions and has been implied in functions as various as cognition (Canolty et al., 2006), motor control (Lopez-Azcarate et al., 2010; de Hemptinne et al., 2015; Opri et al., 2019), visual processing (Voytek, 2010), other sensory functions (Seymour et al., 2017) and memory consolidation (Tort et al., 2009) to name a few. Thalamus has been proposed to play an important role in cortical PAC generation and been suggested as a driver for cortical

neuronal excitability (FitzGerald et al., 2013; Malekmohammadi et al., 2015; Opri et al., 2019). One study in humans found cortical PAC to be dependent on thalamo-cortical coherence in the carrier frequency range and to represent spatially and temporally distinct cortical phenomena (Malekmohammadi et al., 2015). Another study found high broadband activity in motor cortex to be statistically coupled to low frequency oscillations in the ventral intermediate nucleus in thalamus and to be attenuated during periods of contralateral movements in humans (Opri et al., 2019), thus proposing thalamo-cortical PAC to play an anti-kinematic role, or at least be statistically reflective of anti-kinematic processes.

Regarding the neuronal origin of PAC, the reader is asked to refer to thesis Chapter 1.2.6 for general PAC theories. Theta-gamma coupling in hippocampus has been found to be dependent on the inhibitory activity of GABAergic parvalbumin interneurons (Wulff et al., 2009). But even though several human studies have correlated cortical PAC to motor functions, the origin of neocortical PAC, and what role thalamus might play in its neuronal generation for each frequency, remains largely speculative (Canolty and Knight, 2010; Malekmohammadi et al., 2015) and is mainly based on inferences from studies with correlations between high-gamma frequencies and spiking activity in hippocampus (Colgin et al., 2009; Canolty and Knight, 2010) as well as deductions from studies of axo-axonal gap junctions between pyramidal neurons (Schmitz et al., 2001). Lately, however, studies have given greater support to the theory of thalamus playing an important role in the cortical PAC formation (Malekmohammadi et al., 2015; Opri et al., 2019) and any disturbances in thalamo-cortical projections are likely to interfere with cortical PAC generation or sustainment (de Hemptinne et al., 2015).

While signals such as beta and PAC may be important in aspects of human brain function, both have also been established to be exaggerated in Parkinson's disease (PD).

In the introductory chapter of this thesis we discussed how beta oscillations have been established to be exaggerated across basal ganglia cortical structures in PD patients and relate to levels of dopamine depletion (Brown et al., 2001; Kühn et al., 2004; Sharott et al., 2005; Mallet et al., 2008b; Tinkhauser et al., 2017b). Furthermore, it was discussed how cortical PAC, between beta phase and high gamma amplitude, in electrocorticography (ECoG) recordings, has been shown to be exaggerated in PD, relate to motor impairment and to be attenuated by subthalamic deep brain stimulation (DBS) (de Hemptinne et al., 2013, 2015). The observed PAC in these studies, however, was later in large attributed to waveform asymmetries in the lower frequency oscillation (Cole et al., 2017; van Wijk, 2017). The same asymmetries were shown to relate to degrees of motor impairment (Cole et al., 2017). There has lately been a resurgence in the investigation of asymmetric morphology and nonlinearities of the raw electrophysiological signal as it has been argued that important physiological or pathophysiological information could be lost in the signal bandpass filtering process (Cole and Voytek, 2016; Dowsett and Herrmann, 2016; Sheremet et al., 2016; Sherman et al., 2016).

Beta power, phase-amplitude coupling, and waveform asymmetries have all been implied in neuronal information transfer, and their sustained exaggerations have been proposed as individual biomarkers for closed-loop DBS control in PD (Little et al., 2013; de Hemptinne et al., 2015; Cole et al., 2017; Arlotti et al., 2018). However, their individual origins and the role that basal ganglia and cerebellar receiving thalamic nuclei play in the induction and maintenance of the biomarkers is widely unknown in both health and disease. Here, applying optogenetics selectively to thalamic nuclei based on their

predominant afferent inputs, we address the hypothesis that cortical PAC, as seen in PD, can be produced by driving motor thalamic input.

5.2 Materials and methods

5.2.1 Animals

The experiments were conducted in accordance with the UK Animals (Scientific Procedures) Act 1986 under personal and project licenses issued by the Home Office following ethical reviews. All rodents studied in the experiments were C57BL/6J mice (Charles River, UK). Animals in the study were housed with their littermates up until the first surgical procedure with free access to food and water in a dedicated housing room with a light/dark cycle (lights on 7 a.m. to 7 p.m.).

A total of 9 mice were included in the experiments. 4 mice received injections of Cre-expression dependant AAV-ChR2 into the VM-thalamus (basal ganglia tagged) and 5 in the VL-thalamus (cerebellar tagged) (Fig. 5.1). The general principles behind optogenetics are outlined in Chapter 2.4 of this thesis. To selectively target neurons in the VM-thalamus to express channel-rhodopsin, a WGA-Cre expressing AA-virus (AAV-EF1A-mCherry-IRES-WGA-Cre) was first injected into the SNr. This was followed by an injection of a Cre-dependant channel-rhodopsin AA-virus (AAV-Ef1a-DIO-Chr2_EYFP) into the VM. The WGA-Cre expressing AA-virus is transported through the neurons, synoptically secreted and taken up by connected neurons (Gradinaru et al., 2010; Libbrecht et al., 2017). As the channel-rhodopsin AA-virus is cre-dependant, channel-rhodopsin would only be expressed in neurons with SNr-connections (Gradinaru et al., 2010; Grosenick et al., 2015).

Likewise, to induce channel-rhodopsin in CZ-thalamus, a WGA-Cre expressing AA-virus (AAV-EF1A-mCherry-IRES-WGA-Cre) was injected into the deep cerebellar nuclei

(DCN) contralateral to the thalamic injection (note the midline crossing by the decussation of the superior cerebellar peduncle), followed by the injection of the Cre-dependant channel-rhodopsin AA-virus (AAV-Ef1a-DIO-Chr2_EYFP) into VL-thalamus. The mechanisms through which these viruses were used to express channel-rhodopsin selectively in BZ or CZ is depicted in figure 5.1 and more generally in figure 2.1.

5.2.2 Viral Constructs

The following AAVs were used: rAAV5-EF1a-DIO-hChR2(E123T/T159C)–EYFP (UNC Vector Core; 6.2 x 1012 vg/ml; was a gift from Dr Karl Deisseroth) and AAV2/5-Ef1a-mCherry-IRES-WGA-Cre ((UNC Vector Core; 1.6 x 1012 vg/ml; was a gift from Dr Karl Deisseroth).

5.2.3 Surgical procedures

Isoflurane (IsoFlo ®, induction 3%, maintenance 1.5%; Abbott Laboratories) in oxygen-enriched air (Novo Lite, Mark 5) was used to anaesthetize mice fixed in a stereotactic frame (Kopf Instruments 1430 series). A feedback-controlled heating pad (Harvard Apparatus) ensured maintenance of core body temperature at 36 °C. A volume of 50–200 nl virus solution (depending on respective viral titre and observed expression strength) was pressure-injected intracranially using calibrated glass pipets (15-20 µm tip microcapillary tube) at a rate no faster than 1ul/min, and pipette was removed slowly no sooner than 8 minutes post-injection. Coordinates for virus injections were: SNr (AP −3.4 mm, ML ±1.6 mm, DV −4.5 mm), DCN (AP -5.88mm, ML 2.2mm, DV 2.2mm), VM (AP -1.3mm, ML 0.9mm, DV 4.1mm) and VL (AP-1.4mm, ML 1.1mm, Dv 3.9mm).

5.2.4 In vivo electrophysiology and optogenetic stimulation of BZ neurons

A mouse injected with ChR2/WGA-Cre 8 weeks previously was anesthetized with urethane (1.5 g/kg induction, 10% supplemental injections as needed). ECoG screws (1.0x3mm) were implanted bilaterally over the frontal lobe (AP +2.0mm, ML +2.0mm) and cerebellum. Bilateral burr holes were also drilled over M1 (AP +1.0mm, ML 1.0mm) and thalamus (AP -1.3mm, ML 0.9mm). For optical manipulation during electrophysiological recordings, a unilateral optic fibre was inserted 3.5mm below the brain surface above VM thalamus. All fibres were tested for effective light transduction before implantation. For optical stimulation of ChR2, laser light of 473 nm (Cobolt, Sweden) was applied driven by TTL pulses (50 trains of 5 x 5ms pulses at 10Hz and 25Hz) from a CED Power 1401 mkII console controlled by Spike 2 software (v8.03, Cambridge Electronic Devices). Light intensity was adjusted with an integrating-sphere optical power meter (Thorlabs PM100USB and S140C) to reach 20 mW at the end of the implanted optic fibre (200um, 0.22NA). Unilateral local field potential recordings were made with a linear silicon probe (A1x16-3mm-100- 413-A16; Neuronexus, Ann Arbour, MI) positioned in M1 (ipsilateral or contralateral to the optic fibre stimulation) with the top recording site at the brain surface (0-μm depth). The extracellular signals picked up by each electrode were buffered directly above the head of the animal through an A16-Omnetics32 adapter (Neuronexus, Ann Arbour, MI) connected to an analogue to digital headstage (RHD2164, Intan Technologies) and sent to an interface board (RHD2000; Intan Technologies) where they were synchronized with signals from laser stimulation and filtered data was saved to a computer with a 20kHz sampling rate (DSP cutoff 1Hz, Low-pass filter 0.1 Hz, High-pass filter 7500Hz).

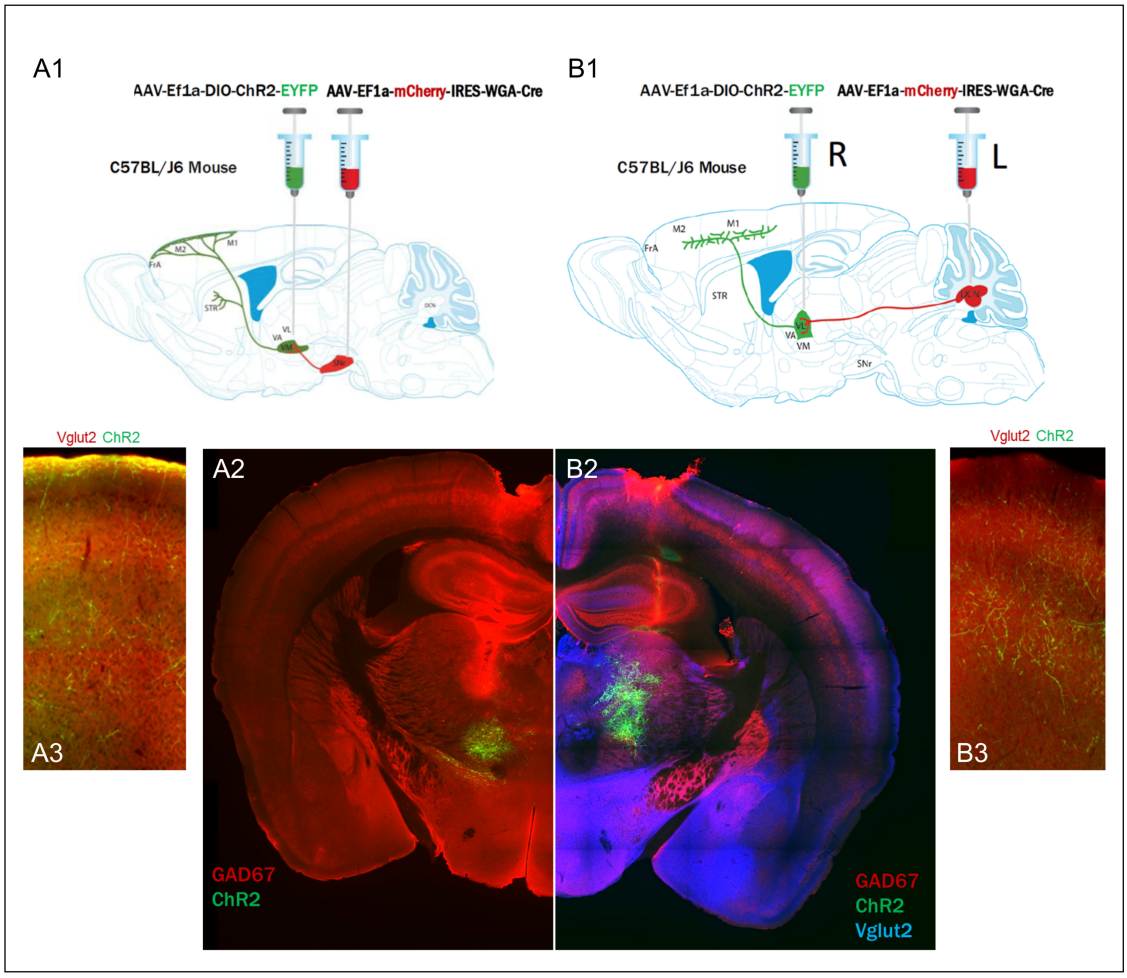


Figure 5.1 - Induction of ChR2 in basal ganglia (A) and cerebellar (B) recipient thalamus. A1) Schematic of injection of WGA-cre virus into SNr and Cre-dependant Chr2 into VM-thalamus. B1) Schematic of injection of WGA-cre virus into deep cerebellar nuclei and Cre-dependant Chr2 into VL-thalamus. A2) Immunohistochemical visualisation of induced neuronal expression of ChR2 in VM thalamus. B2) Immunohistochemical visualisation of induced neuronal expression of ChR2 in VL thalamus. A3) Immunohistochemical visualisation of axonal ChR2 expression motor cortex after targeting of basal ganglia receiving thalamus. B3) Immunohistochemical visualisation of axonal ChR2 expression motor cortex after targeting of cerebellar receiving thalamus. Figures produced by Rahul Shah.

5.2.5 Data analysis

Time-frequency decomposition

All recordings were down sampled from 20000 to 2000 Hz and normalised to have zero mean and unit variance. The ECoG and probe signals were bandpass filtered (using a 2nd order Butterworth filter) around centre frequencies between 5-15 Hz with 1 Hz increments to extract alpha frequencies and between 13-35 Hz with 1 Hz increments to extract beta frequencies and bandwidths at ± 1 Hz. Band widths of ± 2 and 3 were also trialled and yielded similar results (not shown is this thesis). The gamma and HFO components were extracted around centre frequencies using a 4th order Butterworth filter from between 50-200 Hz (with 10 Hz stim) or 80-250 Hz (with 25 Hz stim) with 2 Hz increments and filter bandwidths at ± 7 % of centre frequencies.

Instantaneous phase and amplitude envelope time series were then extracted from the bandpass filtered signals using Hilbert transform via the Matlab functions *angle*(*hilbert(x)) and abs(Hilbert(x))*. Time-frequency power was plotted in time windows of 0.5 seconds before and after thalamic stimulation onset and averaged across trials (n = 50) at stimulation pulse onsets. One-sample paired t-tests were applied to test for statistical significance ($p < 0.05$) time-frequency bins across stimulation trials (n = 50) against the time window power spectral mean for each frequency. For grand average power spectral plots across subjects, these statistics were reported as percentages of frequency bin significance out of all subjects (% of t-test with $p < 0.05$).

PAC-analysis

The PLV-method was chosen to calculate PAC (see Chapter 2). Before the ϕf_a by way of the Hilbert transform was extracted from the HFO-amplitude time series, the amplitude

signal was high- and lowpass filtered as previously described using Butterworth filters to remove non-beta components (Penny et al., 2008).

For accurate PAC calculation (Seymour et al., 2017) the periods during and outside opto-stimulation were concatenated in two different vectors after Hilbert beta phase and the phase of the Hilbert amplitude extractions to ensure sufficient data lengths and exclude signal jumps. For statistical testing of PAC significance, permutations were performed via 500 surrogate runs of data with circularly shifted (circshifted) permutations of the amplitude data (Penny et al., 2008; Cohen, 2014; Seymour et al., 2017). This involves temporally shifting the power times series by random temporal offsets while keeping the phase angle time series the same. A PAC value is then computed according to the PLV-equation under the null hypothesis from the randomly circshifted data. In this experiment, that is repeated 500 times in order to generate a PAC distribution. Standardised z-values of PAC are then derived by taking the original non-circshifted PAC and subtracting the PAC distribution mean and dividing by the standard deviation of the PAC distribution (Cohen, 2014). The normal z-values are then converted to p-values.

Analysis of data asymmetries

To analyse the nonsinusoidal components of the signal we applied the measures of signal asymmetries as outlined by Cole et al and described in Chapter 2 of this thesis. We started by low pass filtering the raw signal from the probe and ECoG recordings at 100 Hz using a 4^{th}-order Butterworth to exclude high frequency artefacts. We extracted alpha or beta bandpass filtered signal as outlined above to identify rising and falling zero crossings. These time points were used to locate peaks and troughs in the pre-processed signal. Peak sharpness, sharpness ratios (SR) and rise-decay-ratios (RDR) were then calculated (See Chapter 2).

These measurements were then averaged across recordings and animals during and outside periods of thalamic stimulation (50 trials per recordings with 5 pulses of 10 and 25 Hz-stimulation, respectively) and compared to corresponding mean PAC values.

Furthermore, the pre-processed signal was averaged across all filtered alpha and beta-time series to visualise the morphology of the asymmetries.

For statistical analysis of asymmetries during and outside BZ and CZ stimulation multiway ANOVAs were applied with post-hoc Bonferroni corrections for multiple comparisons. All reported correlation coefficients are Pearson's correlations.

5.3 Results

We analysed ECoG and cortical probe recordings during and outside selective optogenetic stimulation of the BZ or CZ thalamus in a total of 9 mice (n(BZ) = 4 , n(CZ) = 5) to address the hypothesis that cortical PAC, as seen in PD, can be generated by driving motor thalamic input.

5.3.1 Cortical power spectral changes in ECoG signals during motor thalamic stimulation

We started out by examining the effects of motor thalamic stimulation on power spectral changes in ECoG signals in the time frequency domain. We first applied brief epochs of 25 Hz and 10 Hz opto-stimulation to BZ or CZ thalamus, respectively, and analysed time-frequency decompositions in ECoGs using the Hilbert transform of signals filtered from 13-35 Hz and between 5-15 Hz with 1 Hz increments and between 50/80 Hz to 200/250 Hz for the high-frequency content as outlined in the methods section . Time windows of 0.5 seconds were chosen before and after stimulation onset (5 opto-stim pulses were

applied at either alpha or beta frequencies and averaged across 50 trials per recording). As seen in figure 5.2 (example of averaged time-frequency spectrogram across 50 trials in one subject) and figure 5.3 (grand average time-frequency spectrogram across subjects) we found that 25 Hz stimulation of BZ thalamus resulted in both significant beta (Across recordings: Mean normalised beta power during stim = 0 0.9587, mean normalised beta power baseline = -0.1839, p = 0.0349, paired t-test, n = 4) and high-gamma (Across subjects: mean normalised peak HFO power during stim = 0.8589, mean normalised HFO baseline = – 0.0119, p = 0.0488, paired t-test, n = 4) power synchronisations in the ipsilateral ECoG signal with high consistency across subjects (Beta: 100 % frequency bins of $p < 0.05$, high-gamma: 80 % frequency bins of $p < 0.05$, paired t-test across 50 trials compared to baseline across subjects, n = 4, figure 5.3), but not contralateral across recordings (across subjects 0 % of frequency bins of $p < 0.05$, n = 4, Fig. 5.3). CZ stimulation on the other hand did not produce any significant power spectral changes in neither the contralateral nor the ipsilateral beta range (across subjects: mean normalised beta power during stim = 0 0.0983, mean normalised beta power baseline = – 0.0454, p = 0.3869, paired t-test, n = 5) and HFO ECoG signal (Across subjects: normalised mean peak HFO power during stim = 0.0294, mean normalised HFO baseline = – 0.0187, p = 0.6728, paired t-test, n = 5, 0-20 % of frequency bins of $p < 0.05$, n = 5, paired t-test across 50 trials compared to baseline across subjects Fig. 5.3).

10 Hz BZ-stimulation induced power increases in both the alpha and HFO domain (Grand average across subjects. Mean normalised alpha power during stim = 0.3033, mean normalised alpha power baseline = – 0.0810. Stats across subjects Figure 5.4: 100 % of frequency bins $p < 0.05$, high-gamma: 50-75 % , paired t-test across 50 trials compared to baseline across subjects, n = 4) in the ipsilateral ECoG signal. As exemplified in Figure 5.5 gamma oscillations (gamma cycle intervals = 12 ms => 83 Hz) were generated at 10

Hz intervals, indicative of a statistical coupling between alpha and high-gamma frequencies. As was the case for beta-stimulation of CZ-thalamus, 10 Hz-stimulation of CZ-thalamus did not manifest in significant ECoG power spectral changes (See stats in Figure 5.4 and 5.5).

In summary, driving motor thalamic input at low frequencies (10 and 25 Hz) in basal ganglia, but not cerebellar, thalamo-cortical networks manifested in oscillation amplitude changes in the domain of the input-drive frequencies as well as gamma range similar to the PAC frequencies in human PD patients (de Hemptinne et al., 2013, 2015).

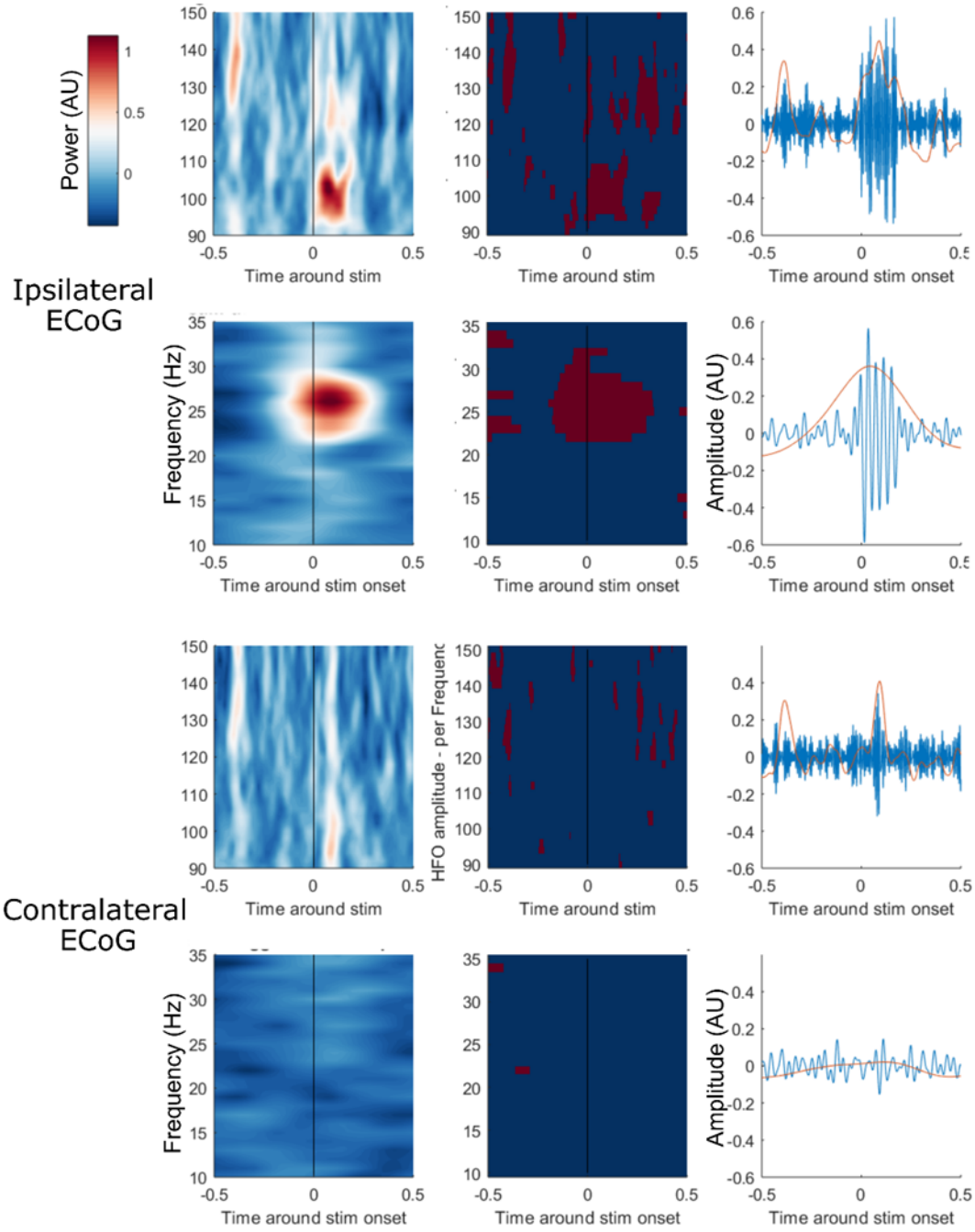


Figure 5.2 – ECoG example of beta and high-gamma spectral changes during 25 Hz optogenetic stimulation of BZ thalamus across 50 stimulation trials in one subject. A) Ipsilateral ECoG time-frequency decomposition around stimulation onset in the beta (lower row) and gamma (upper row) range. Left column: Gamma and beta amplitude envelope of Hilbert transform. Middle column statistical significance $p < 0.05$. B) As above but recorded simultaneously from the contralateral ECoG. The example data is averaged across 50 stimulation trials of 25 Hz stimulation from one recording.

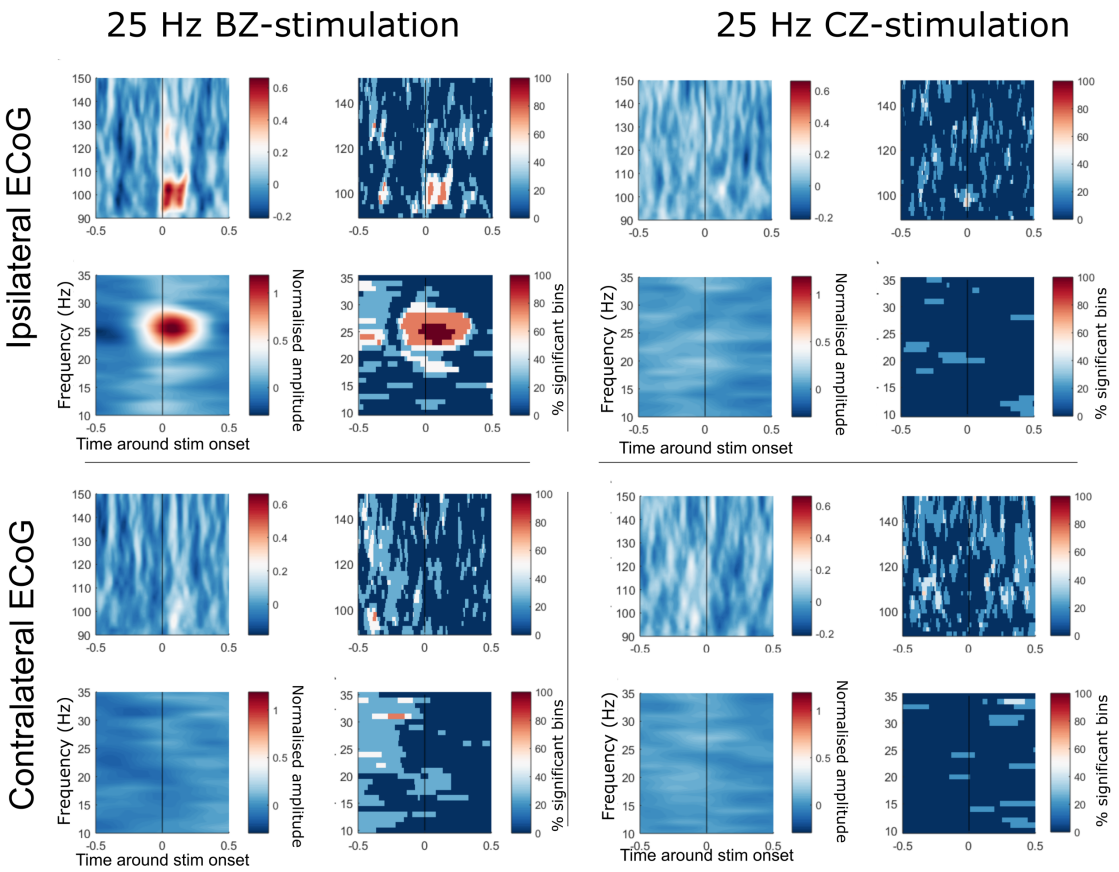


Figure 5.3 – 25 Hz stimulation of BZ-thalamus induces beta and gamma synchronisation in the ipsilateral ECoG signal. Time frequency decompositions of the beta and high-gamma ranges 0.5 seconds before and after thalamic beta stimulation onset and corresponding significance plots. Time zero marks onset of stimulation. A) Ipsilateral BG thalamic stimulation 25 Hz stimulation. B) Ipsilateral CZ thalamic stimulation 25 Hz stimulation. C) Contralateral BZ thalamic stimulation 25 Hz stimulation. Contralateral CZ thalamic stimulation 25 Hz stimulation. Significance plots mark percentages with significant frequency bins ($p < 0.05$) across subjects, n(BZ) = 4, n(CZ) = 5.

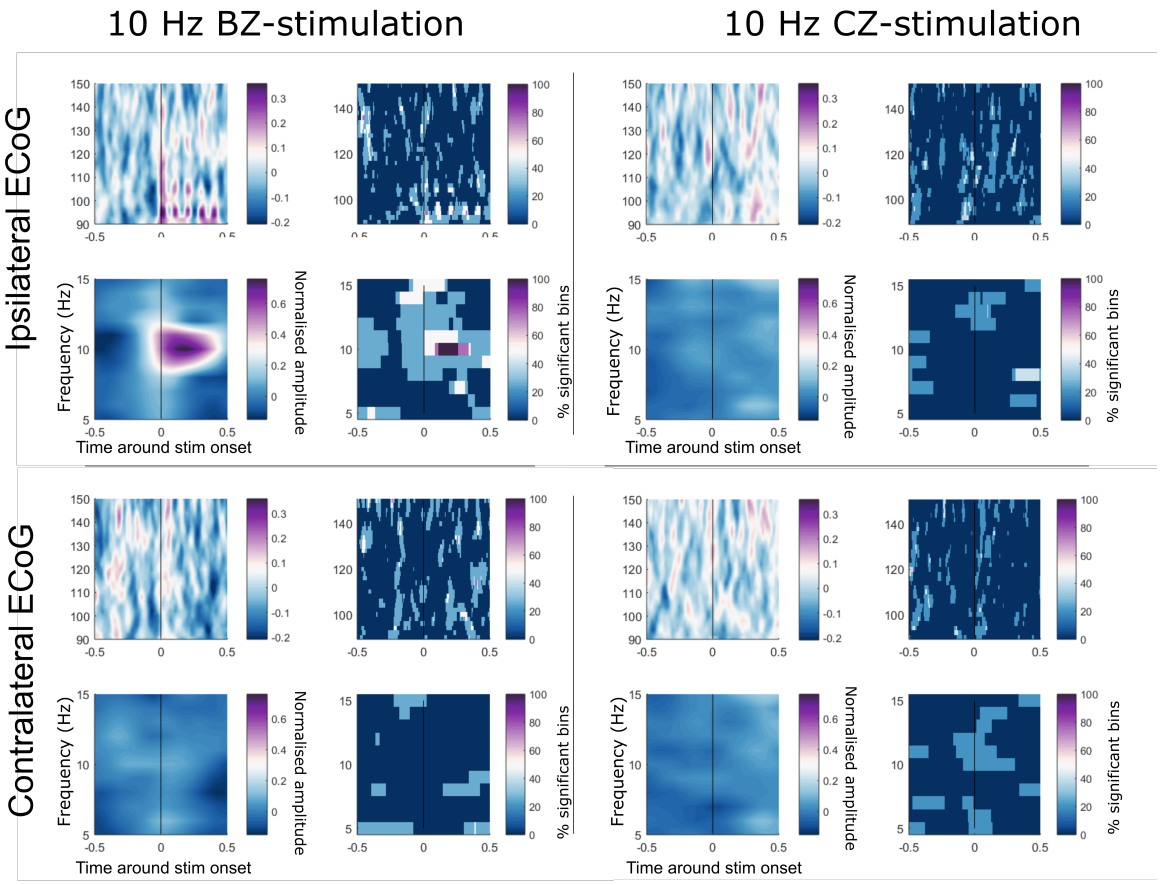


Figure 5.4 – BZ-thalamic optogenetic alpha stimulation induces power spectral changes in the alpha and high-gamma range in ipsilateral ECoG signal. Grand average across subjects shwoing time frequency decompositions in the alpha and high-gamma ranges 0.5 seconds before and after thalamic 10 Hz stimulation onset and corresponding significance plots. Time zero marks onset of stimulation. A) Ipsilateral BZ-thalamic stimulation 10 Hz stimulation. B) Ipsilateral CZ-thalamic stimulation 10 Hz stimulation. C) Contralateral BZ-thalamic stimulation 10 Hz stimulation. Contralateral CZ-thalamic stimulation 10 Hz stimulation. Significance plots mark percentages with significant frequency bins ($p < 0.05$) across subjects, n(BZ) = 4, n(CZ) = 5.

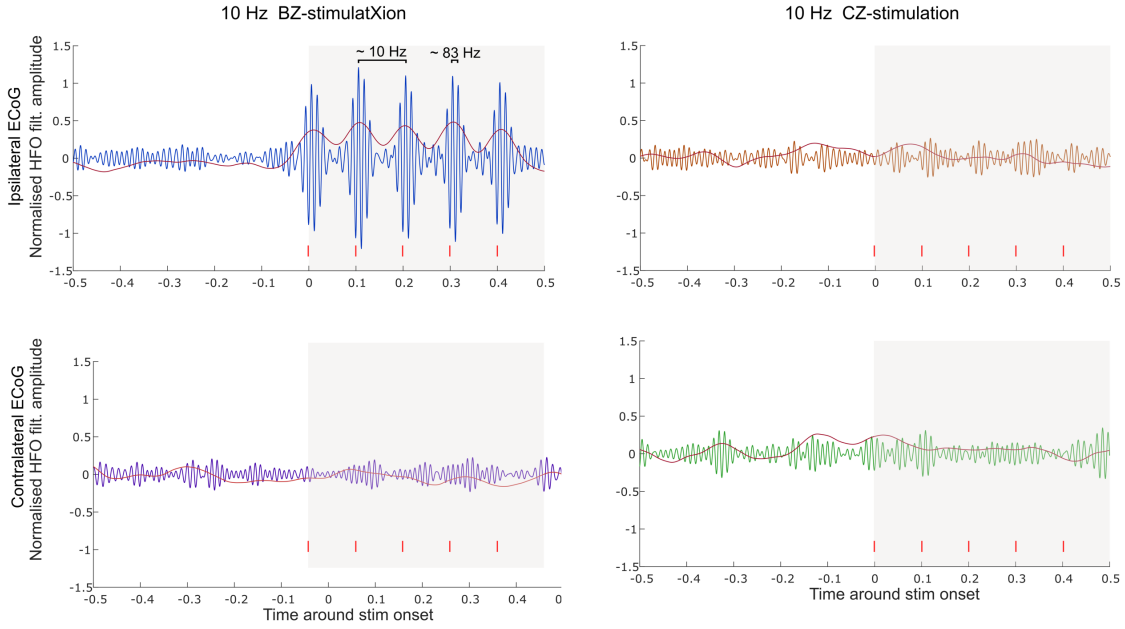


Figure 5.5 – 10 Hz BZ-thalamic stimulation induces cortical HFO-oscillations at alpha amplitude frequencies. Example recording from one subject averaged across 50 stimulation trials. Upper row: Ipsilateral ECoG recordings of filtered data (80-130 Hz) 500 ms before and after 10 Hz BZ-thalamus stimulation and BG-thalamus stimulation. Lower row: Contralateral ECoG recordings of HFO-filtered data before and after BZ-thalamus and BG-thalamus stimulation. Red lines above signal curves mark the HFO-amplitude envelope. Vertical red lines mark stimulation pulses.

5.3.2 Selective stimulation of basal ganglia receiving thalamus generates PAC in ipsilateral ECoG signals

We then proceeded to study the impact of selective motor thalamic stimulation of BTC and CTC networks on PAC in ECoG recordings. To do so, PAC was calculated in ipsilateral and contralateral ECoG-recordings during and outside 10 Hz and 25 Hz stimulation of BZ and CZ thalamus. When applying 25 Hz BZ stimulation PAC clustering in ipsilateral ECoG recordings was highly significant across animals ($p < 0.05$, 100 %, $n = 4$, Fig. 5.6A) between beta phase frequencies (20-30 Hz) and high gamma amplitude (70-110 Hz). These PAC frequencies, interestingly, correspond to those observed in ECoG recordings from human PD patients, where coupling between beta and high-gamma frequencies were observed (de Hemptinne et al., 2015). In comparison, in the contralateral ECoG no significant simultaneous PAC clustering was detected (Fig. 5.6A). To see if the observed PAC was stimulation-frequency specific we also analysed ECoG recordings during 10 Hz BZ-stimulation and found significant PAC (Across subjects: 80-100 %, $p < 0.05$, $n = 4$, Figure 5.7A) between the phase of alpha frequencies and the high gamma amplitude (50-100 Hz). Notably, the frequencies of the observed PAC corresponded to the applied opto-stimulation frequency in thalamus. No significant PAC was found in the contralateral ECoG recordings. This was expected as both BZ and CZ thalamus are known to project to the ipsilateral cortex (Kuramoto et al., 2015), but served as a real-time signal control.

PAC was then analysed in the ECoG signal during and outside both 25 Hz and 10 Hz stimulation of CZ thalamus. Here we did not observe any significant PAC compared to the contralateral ECoG recordings for neither 25 Hz stimulation (Figure 5.6B) nor 10 Hz stimulation (Figure 5.7B).

In summary cortical PAC was observed in ipsilateral ECoG recordings during frequency specific optogenetic stimulation of basal ganglia receiving thalamus and the gamma amplitude frequencies were similar to those coupled to beta phase in ECoG recordings in human PD patients (de Hemptinne et al., 2015).

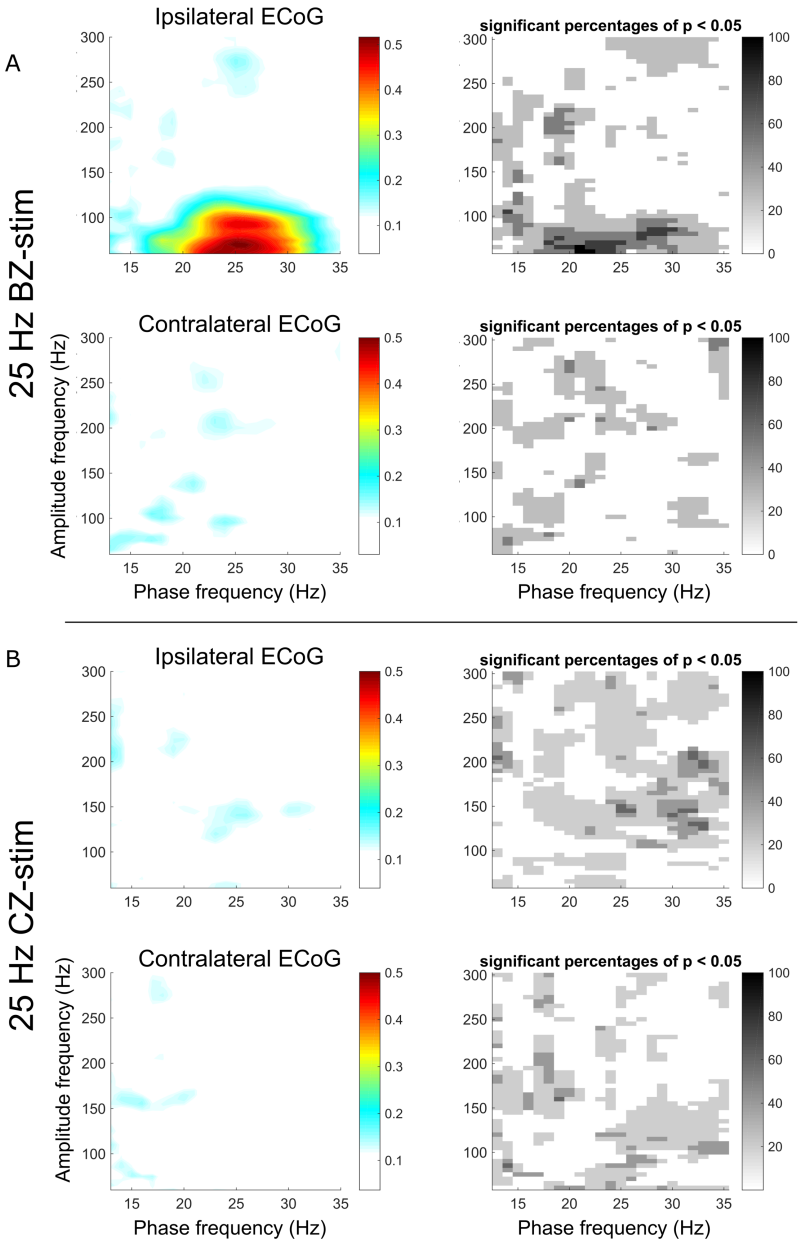


Figure 5.6 – Selective 25 Hz stimulation of basal ganglia receiving thalamus but not cerebellar thalamus, induces significant PAC. Grand average PAC comodulograms across subjects from ipsilateral and contralateral ECoG recordings during A) BZ-thalamic 25 Hz stimulation and B) CZ-thalamic 25 Hz stimulation. Significant plots mark percentages of recordings with significant frequency bins ($p < 0.05$) based on circular shifted permutations, n(BZ) = 4, n(CZ) = 5.

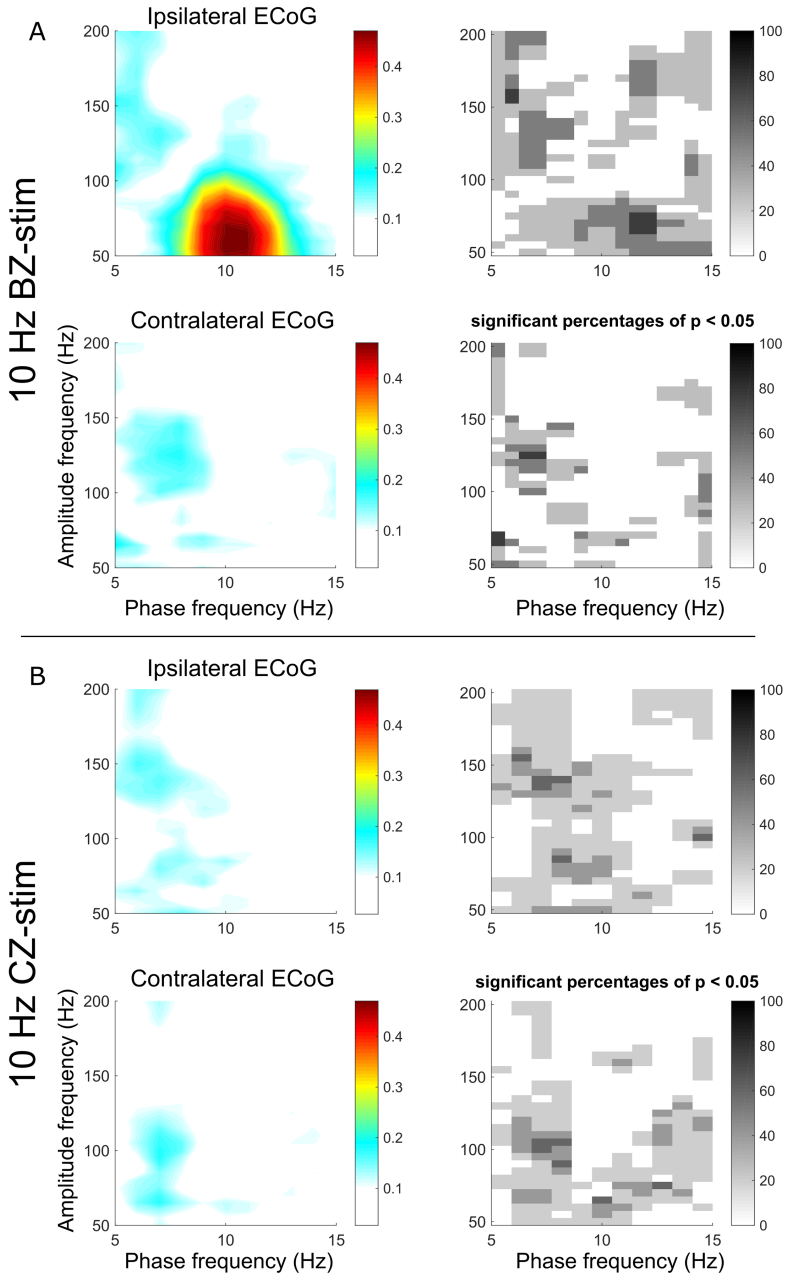


Figure 5.7 – Selective 10 Hz stimulation of basal ganglia receiving thalamus but not cerebellar thalamus, induces significant phase amplitude coupling. Grand average of PAC comodulograms across subjects from ipsilateral and contralateral ECoG recordings during A) BZ-thalamic 10 Hz stimulation and B) CZ-thalamic 10 Hz stimulation. Significant plots mark percentages of recordings with significant frequency bins ($p < 0.05$) based on circular shifted permutations. n(BZ) = 4, n(CZ) = 5.

5.3.3 Laminar-specific changes in PAC and oscillations in motor cortex during motor thalamic stimulation

Cortical PAC studies in human PD patients have been carried out using ECoG recordings from the surface of the brain. Since BZ and CZ thalamus project to different cortical layers (Kuramoto et al., 2015), we used probe LFP recordings to study PAC and power spectral changes throughout the layers of cortex to see if these signals were restricted to certain cortical layers.

A silicon probe with 30 linearly arranged contacts (spacing 100 μm) was used to record LFPs across all the laminar of motor cortex. These were analysed during and outside of thalamic stimulation as outlined above with channel 1 being the most superficial and channel 30 being the deepest. 25 marks the lower boundary of cortex (i.e. 1-25 span through all layers of cortex and channels 26-30 channels are subcortical).

Grand averages of time-resolved frequency decompositions across subjects and their percentages of significance were plotted before and during 10 Hz and 25 Hz stimulation of BZ and CZ thalamus (Fig. 5.8 and 5.9). Both 10 Hz and 25 Hz stimulation manifested in significant alpha and beta power increases throughout the layers of motor cortex, albeit with the greatest average strength in the deepest half (channels 17-25) and the outmost superficial (channels 1-5) laminas. The consistency was greatest in the most superficial layers (Fig. 5.10).

Overall power increases during both 10 and 25 Hz CZ stimulation were less than for BZ stimulation (Fig. 5.8 and 5.9). 10 Hz CZ stimulation induced the greatest alpha power increases in the channels 4-9 but achieved only very low significance across subjects (Fig. 5.9 and 5.10). 25 Hz CZ stimulation manifested in the greatest beta spectral changes in

channels 5-9, but also 15-17 and 21, but this again happened with low significance and consistency across subjects (Fig. 5.9 and 5.10).

We then went on to study the levels of PAC throughout the layers of motor cortex during motor thalamic stimulation. As seen in figure 10, PAC was induced in the deeper channels 20 to 30 during BZ-stimulation but not in the more superficial channel LFPs. Some PAC was also observed, albeit to a much a lesser extent, in channel 20 during 25 Hz CZ-stimulation (Fig. 5.11). Interestingly, PAC was not observed in the superficial channels during neither BZ nor CZ stimulation suggesting that power spectral increases in the carrier phase frequency domain in itself is not sufficient to give rise to PAC (compare with Fig. 5.8).

In brief, stimulation of basal ganglia receiving thalamus induced PAC in the lower half of motor cortex along with power spectral changes in the input stimulation frequencies in the deeper half and utmost superficial laminas of motor cortex. Cerebellar receiving thalamic opto-stimulation produced discreet power spectral changes in the mid-upper half and very little PAC in the deeper layers. It is noteworthy that power spectral changes could be induced in channels without being accompanied by PAC.

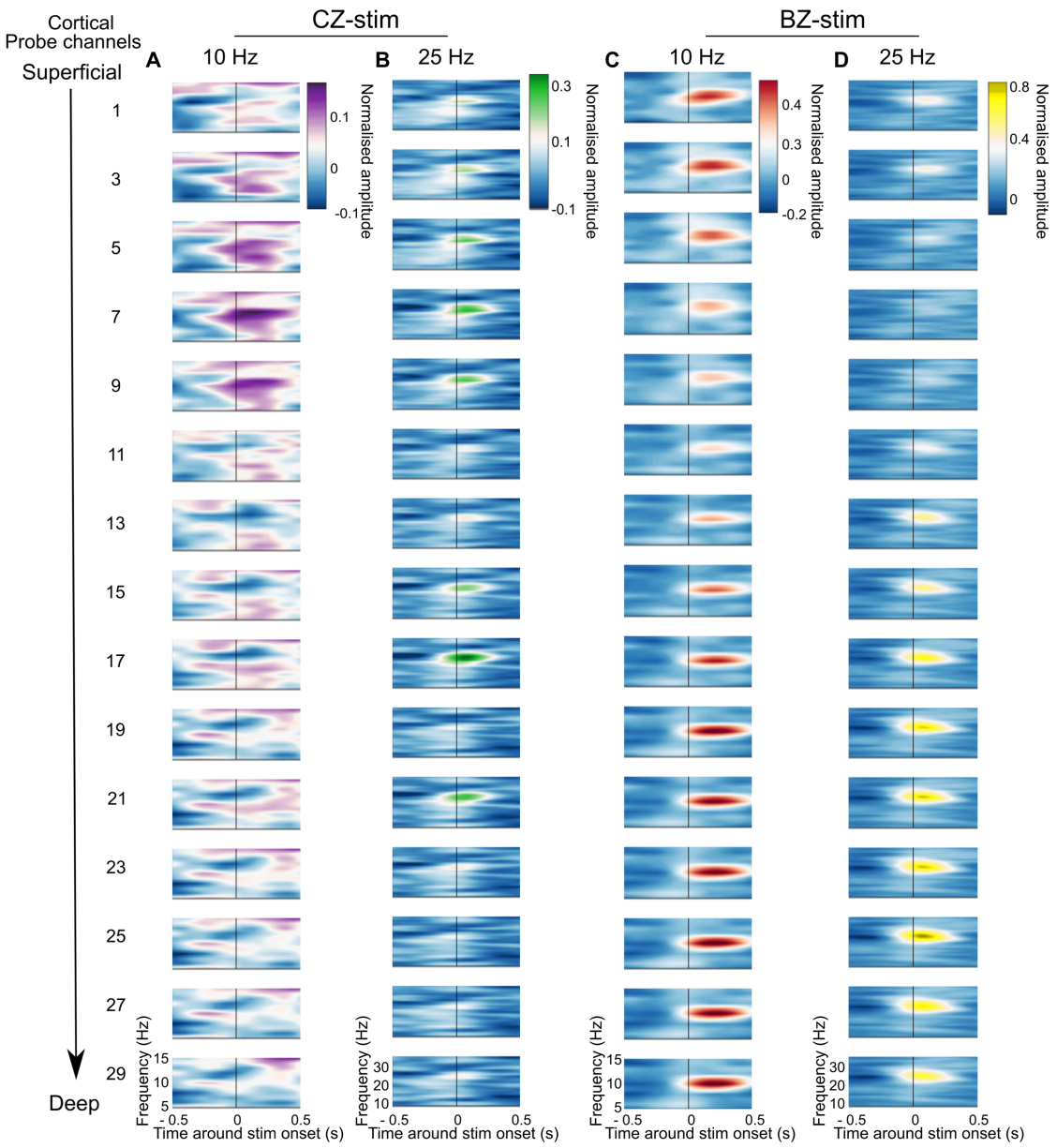


Figure 5.8 – Grand average across subjects of time-resolved laminar-specific power spectral changes in motor cortex following stimulation of basal ganglia and cerebellar receiving thalamus. Time-frequency spectrograms from cortical probe LFPs during A) 10 Hz CZ-thalamic opto-stimulation, B) 25 Hz CZ-thalamic opto-stimulation, C) 10 Hz BZ-thalamic opto-stimulation and D) 25 Hz BZ-thalamic opto-stimulation across 15 probe recordings throughout the layers of motor cortex. n(BZ) = 4, n(CZ) = 5. Refer to figure 5.9 for statistics across subjects.

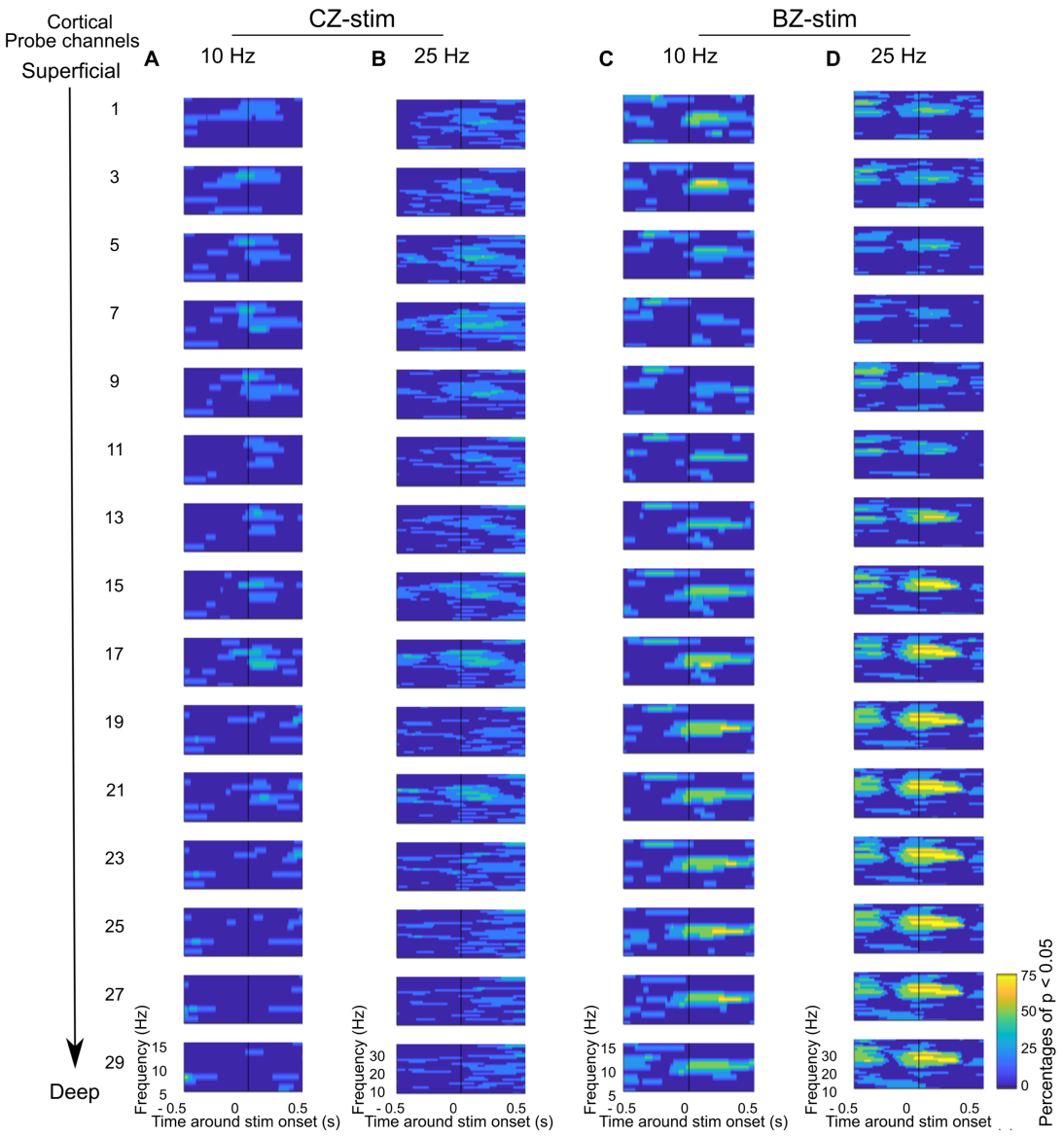


Figure 5.9 – Grand average statistics across subjects for laminar-specific time-resolved power spectral changes in motor cortex following stimulation of basal ganglia and cerebellar receiving thalamus. Statistics for time-frequency spectrograms from cortical probe LFPs during A) 10 Hz CZ-thalamic opto-stimulation, B) 25 Hz CZ-thalamic opto-stimulation, C) 10 Hz BZ-thalamic opto-stimulation and D) 25 Hz BZ-thalamic opto-stimulation across 15 probe recordings throughout cortical layers. C-values mark percentages of significant frequency bins ($p < 0.05$) across subjects n(BZ) = 4, n(CZ) = 5, as assessed in stimulation trials (n = 50) in individual subjects, paired t-test.

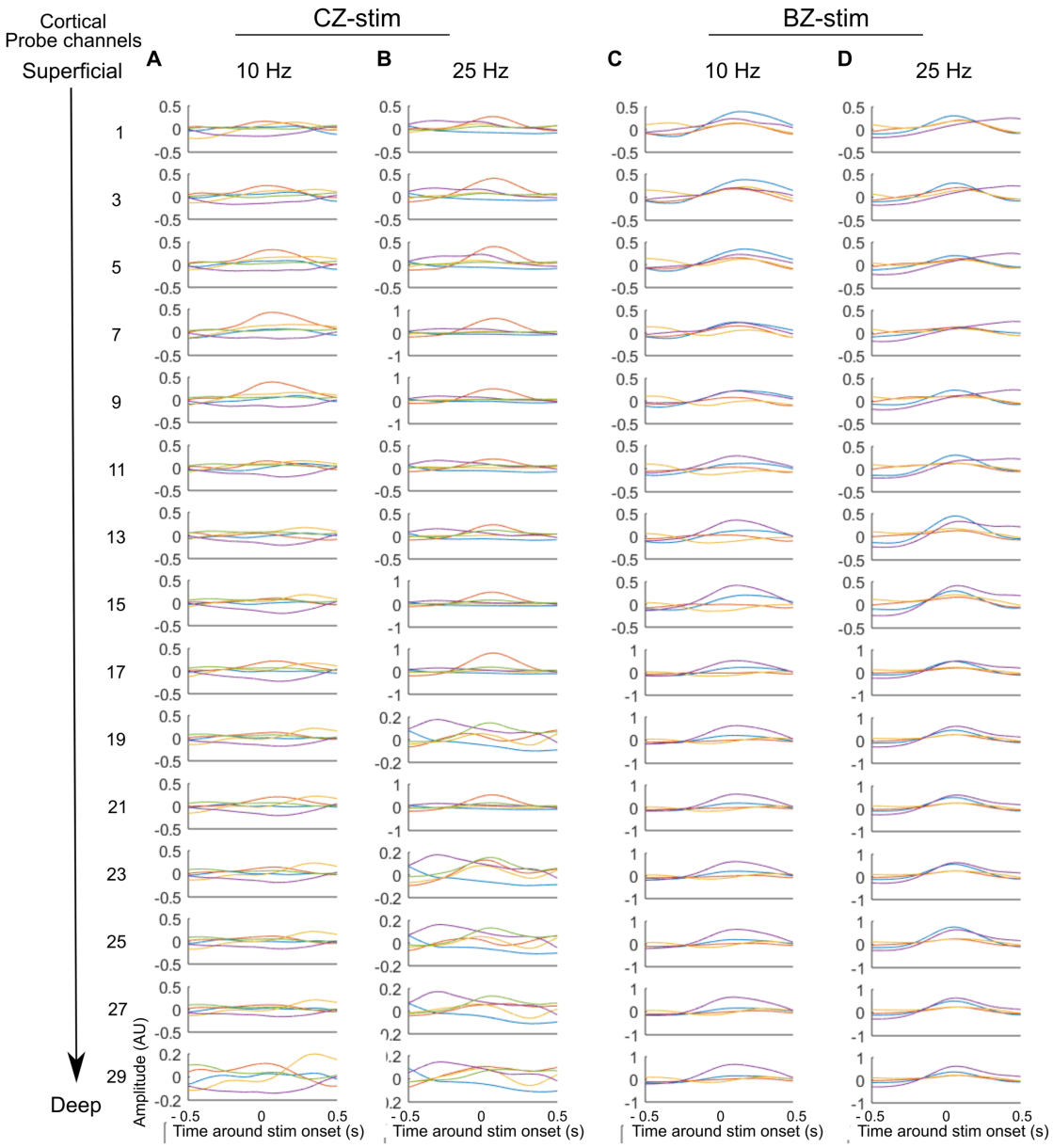


Figure 5.10 – Individual time-resolved laminar-specific power spectral changes in motor cortex following stimulation of basal ganglia and cerebellar receiving thalamus for individual subjects. Time-frequency spectrograms from cortical probe LFPs during A) 10 Hz CZ-thalamic opto-stimulation averaged for 8-12 Hz, B) 25 Hz CZ-thalamic opto-stimulation averaged for 20-30 Hz, C) 10 Hz BZ-thalamic opto-stimulation averaged for 8-12 Hz and D) 25 Hz BZ-thalamic opto-stimulation averaged for 20-30 Hz across 15 probe recordings throughout the layers of motor cortex. n(BZ) = 4, n(CZ) = 5.

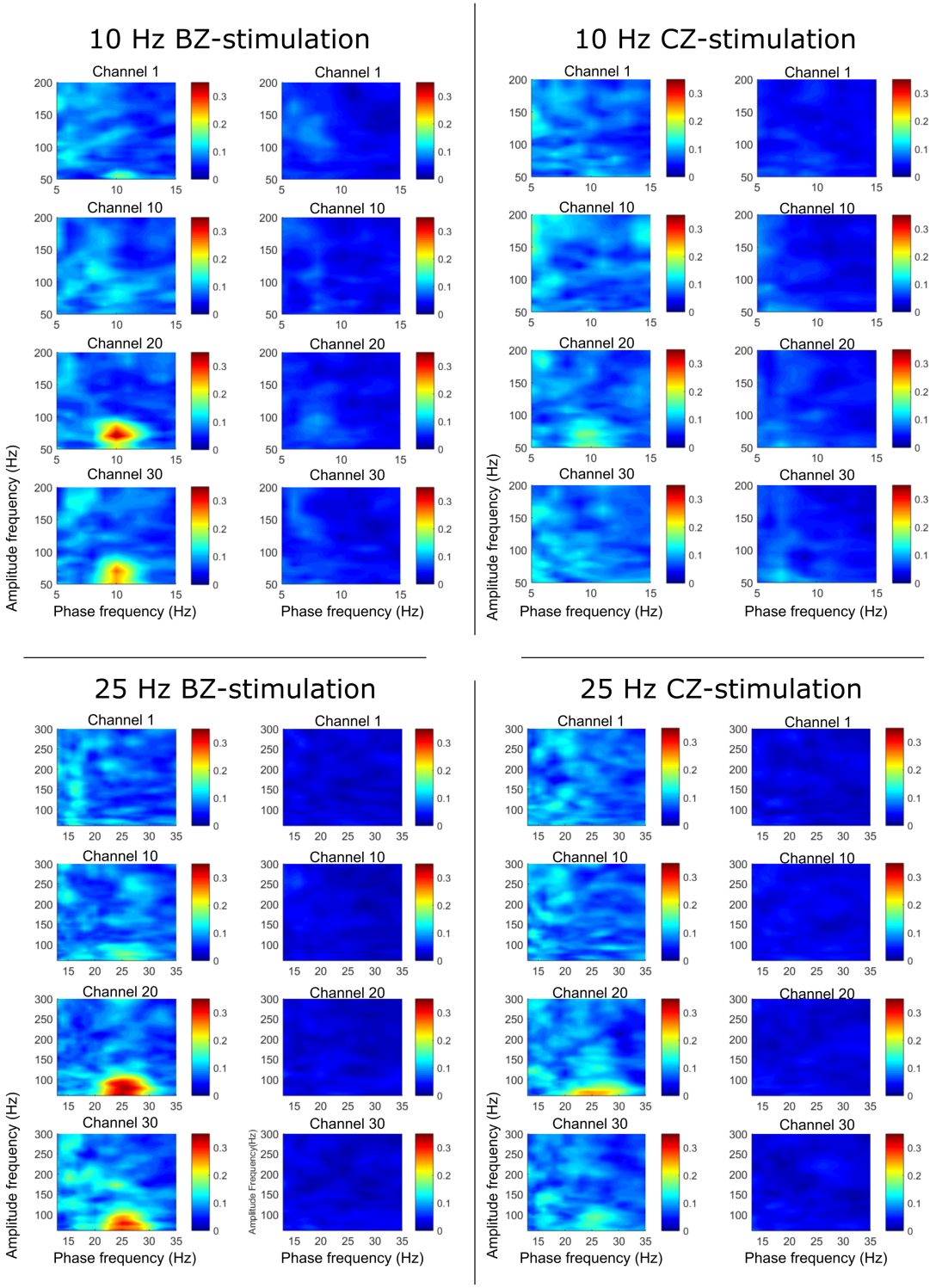


Figure 5.11 – BZ-thalamic stimulation induces PAC in the deepest layers of motor cortex. Grand average across subjects of probe LFP PAC comodulograms during and outside A) 10 Hz stimulation of BZ thalamus, B) 25 Hz stimulation of BZ thalamus, C) 10 Hz stim of CZ thalamus and D) 25 Hz CZ-stimulation in every 10 channels. Channel 1 is most superficial and channel 30 the deepest. n(BZ) = 4, n(CZ) = 5.

5.3.4 BZ thalamic stimulation induces cortical waveform asymmetries

As discussed in more detail in Chapters 1 and 4 of this thesis, renewed attention has been given to the fact that electrophysiological brain signals across brain structures rarely are perfectly sinusoidal and that nonlinearities could carry important physiological or pathophysiological information (Cole and Voytek, 2016; Dowsett and Herrmann, 2016; Sheremet et al., 2016; Sherman et al., 2016). In PD, asymmetries have been proposed as real-time biomarkers for closed-loop DBS (Cole et al., 2017; Jackson et al., 2019). Furthermore, ECoG PAC in human PD patients has been shown to arise from the non-linearities of the lower-frequency carrier signal. Indeed, it has been demonstrated that the entire high frequency oscillation content of signals can arise solely from sharp edges in the data (Kramer et al., 2008). As waveform asymmetries have been proposed as independent biomarkers in PD and been shown to explain cortical PAC in PD patients, we went on to investigate to what extent thalamic stimulation affects the non-linearities of cortical signal.

As demonstrated in example recordings, the raw pre-processed data with concurrent high levels of PAC displayed greater waveform asymmetries with sharper peaks than troughs during BZ-thalamic stimulation compared to CZ stim and VM stim with low PAC levels (Fig. 5.12). There was an effect of BZ-stimulation on sharpness ratios (ANOVA, $p = 0.0284$) and post-hoc testing with adjustments for multiple comparisons showed that sharpness ratios were significantly higher during BZ-stimulation than outside (Bonferroni, $p = 0.0474$, SR = 0.8465 during stimulation versus SR = 0.5546 outside stimulation, $n = 9$, combined 10 Hz and 25 Hz trials, Fig. 5.13). This was not the case for CZ-stimulation (Bonferroni, $p = 1.000$, SR= 0.6307 during stimulation versus SR = 0.6561 outside, $n = 9$, combined 10 Hz and 25 Hz trials, Fig. 5.13).

Cole et al. 2017 observed a higher peak:trough sharpness ratio in PD patient ECoG data and found this ratio to be attenuated by subthalamic DBS and the ratio to correspond with symptoms of rigidity. Our findings of significantly higher peak:trough sharpness ratios observed during BTC stimulation is in line with the waveform asymmetries found in PD patients (Cole et al., 2017). Consequently, this suggest that increased ECoG and EEG waveform asymmetries in PD patients (Jackson et al., 2019) could result from increased beta activity in the BTC network. Thus, waveform asymmetries could potentially serve as a biomarker of increases in BTC activity.

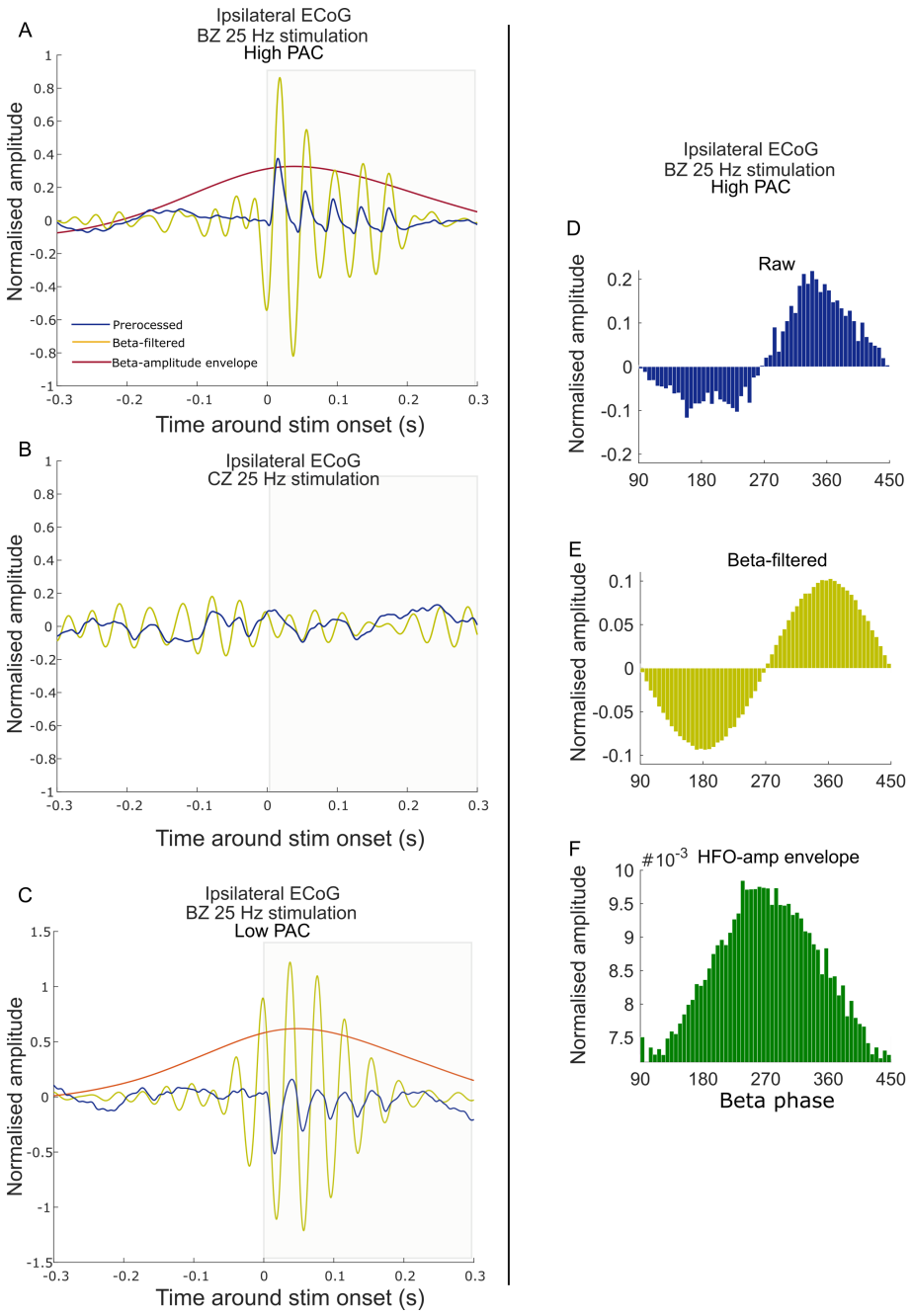

A
Ipsilateral ECoG
BZ 25 Hz stimulation
High PAC
Normalised amplitude
Prerocessed
Beta-filtered
Beta-amplitude envelope
Time around stim onset (s)
B
Ipsilateral ECoG
CZ 25 Hz stimulation
Normalised amplitude
Time around stim onset (s)
C
Ipsilateral ECoG
BZ 25 Hz stimulation
Low PAC
Normalised amplitude
Time around stim onset (s)
D
Ipsilateral ECoG
BZ 25 Hz stimulation
High PAC
Raw
Normalised amplitude
E
Beta-filtered
Normalised amplitude
F
#10-3 HFO-amp envelope
Normalised amplitude
Beta phase

Figure 5.12 – 25 Hz stimulation of basal ganglia recipient thalamus generates cortical beta waveform asymmetries. A) Example of ipsilateral ECoG recording of beta filtered (golden) and pre-processed (blue) signal aligned to onset of stimulation of BZ-thalamus at 25 Hz. B) Example ipsilateral ECoG recording of 25 Hz stimulation of CZ-thalamus. C) Example of BZ-stimulation without significant PAC-clustering. Note the absence of peak-trough sharpness asymmetries. D) The raw prepossessed data from A aligned to the beta-filtered phase. Note sharper peaks than troughs and steeper rises than decays. E) Average beta filtered amplitude aligned to beta phase. F) HFO amplitude envelope aligned to the beta filtered phase. The HFO envelope peaks at the same phase as the sharp asymmetric rise of the raw data in C.

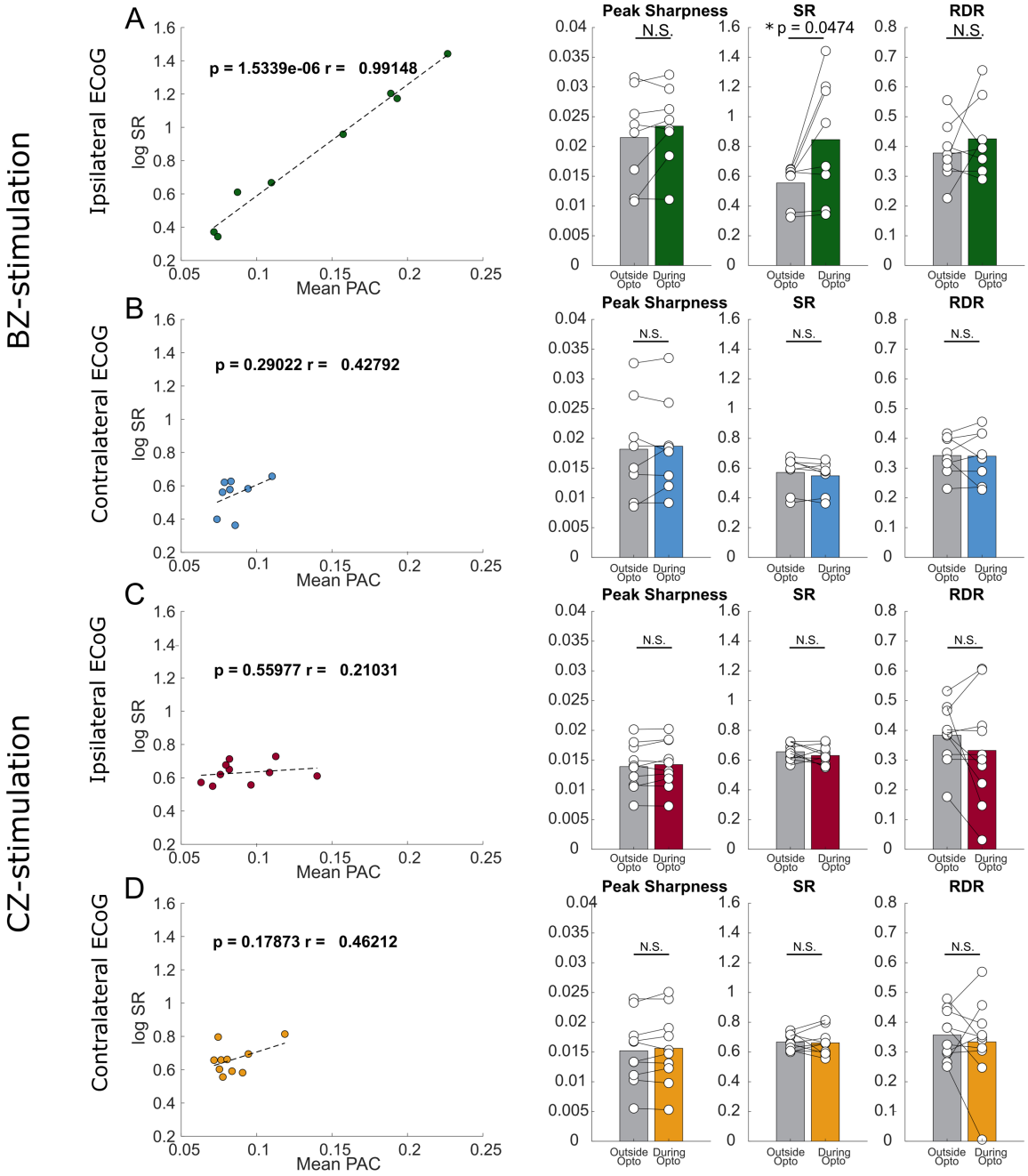

BZ-stimulation
CZ-stimulation
A
B
C
D
Ipsilateral ECoG
Contralateral ECoG
log SR
Mean PAC
p = 1.5339e-06 r = 0.99148
p = 0.29022 r = 0.42792
p = 0.55977 r = 0.21031
p = 0.17873 r = 0.46212
Peak Sharpness
SR
RDR
N.S.
* p = 0.0474
Outside Opto
During Opto

Figure 5.13 – BZ-stimulation induces significant cortical beta waveform asymmetries, that are correlated with the degree of PAC. Correlations between mean PAC values and sharpness ratios during 10 and 25 Hz opto-stimulation and bar plots of differences in waveform asymmetries outside and during thalamic opto-stimulation. Data from A) ipsilateral ECoG during BZ-stimulation, B) contralateral ECoG during BZ-stimulation, C) ipsilateral ECoG during CZ-stimulation, and D) contralateral ECoG during CZ-stimulation. SR = log sharpness ratio between troughs and peaks. RDR = rise decay ratios. All correlations are Pearson's correlations. * $p < 0.05$. P-values for pair wise comparisons were adjusted for multiple comparisons using Bonferroni correction.

5.3.5 Basal ganglia thalamic projections to cortex give rise to ECoG asymmetries and PAC

As statistical PAC has been shown in both theoretical and experimental studies to be able to arise from signal nonlinearities (Kramer et al., 2008; Aru et al., 2015; Cole and Voytek, 2016; Jensen et al., 2016; Lozano-Soldevilla et al., 2016) we asked if the observed PAC in this study induced by BZ stimulation could be attributed to parameters of signal nonlinearities.

We found a near perfect relationship between peak:trough sharpness ratios and mean PAC values during BZ stimulation ($r = 0.9915$, $p < 0.0001$, Pearson's correlation coefficient, Fig. 5.13) for combined 10 Hz and 25 Hz stimulation providing evidence that the observed ECoG PAC arises from signal asymmetries. This was not the case for CZ-stimulation ($r = 0.2103$, $p = 0.5598$, Pearson's correlation coefficient), where also no significant PAC was observed. We found that ECoG PAC arose after BZ opto-stimulation but not CZ opto-stimulation. This PAC can be explained by the non-linearities in the frequency signal by which is applied. Thus, signal nonlinearities are reflected in statistical

PAC-values which again along with asymmetry changes are reflective of the cortical BZ oscillatory input from increases in BTC network activity.

5.3.6 Laminar PAC throughout motor cortex is not explained by waveform asymmetries

We then proceeded to investigate if the observed PAC values in the probe channel LFP recordings could also be explained by changes in waveform asymmetries (Jensen et al., 2016; Cole et al., 2017). No significant relationship, however, was observed between mean PAC values and peak sharpness ratios for any of the probe channel LFPs (Fig. 5.14 and 5.15) despite time resolved power spectral increases (reference Fig. 8 and 9) and any signal asymmetry differences found during stimulation compared to no stimulation periods were found no to be statistically significant for neither BZ nor CZ stimulation after correction for multiple comparisons. The observed PAC within the cortical layers could then perhaps be attributed to other factors (Jensen et al., 2016) such as phase-locked spiking (Sanders, 2016). But this remains to be investigated.

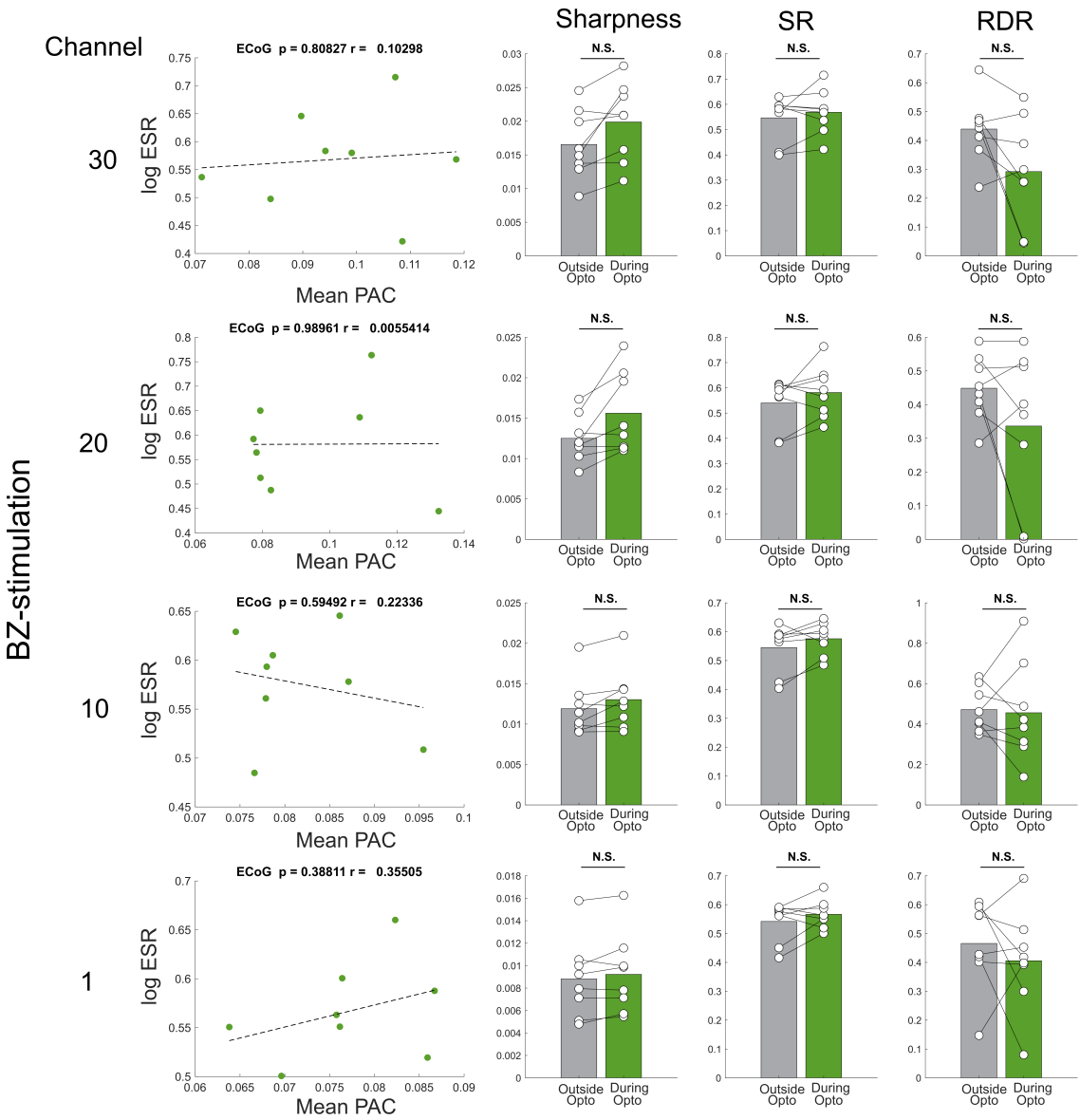


Figure 5.14 – No significant differences in waveform asymmetries were found between periods during and outside BZ-thalamus opto-stimulation and asymmetries failed to explain the observed mean PAC values in probe LFP recordings. Data from 10 and 25 Hz stimulation at various probe LFP levels. Channel 1 is superficial and channel 30 is deep. SR = log sharpness ratio between troughs and peaks. RDR = rise decay ratios. All correlations are Pearson's correlations. Pairwise comparisons were adjusted for multiple comparisons using Bonferroni correction. Probe channel 1 = most superficial. Channel 30 = deepest.

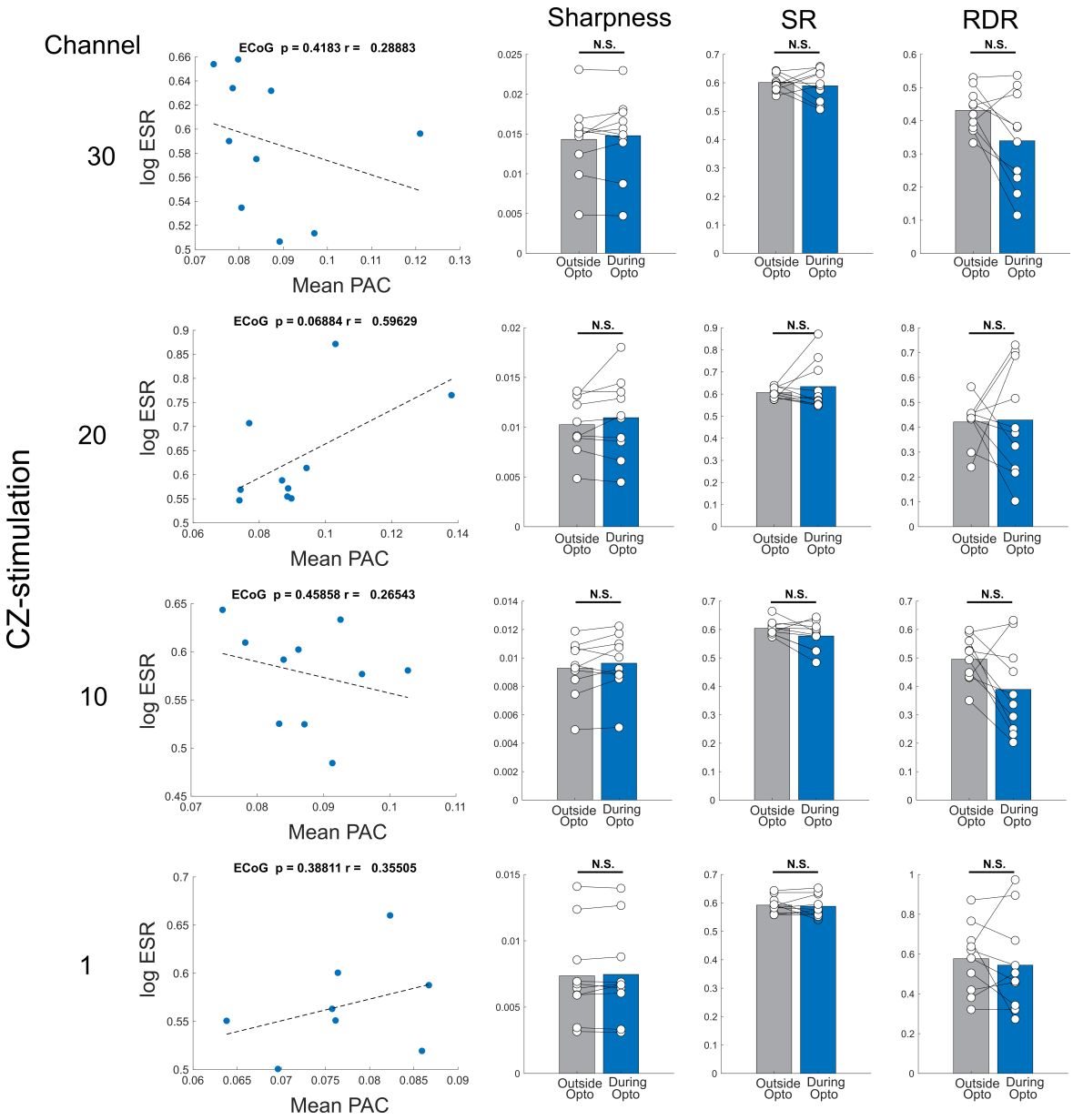


Figure 5.15 – No significant differences in waveform asymmetries were found between periods during and outside CZ-thalamus opto-stimulation and asymmetries failed to explain the observed mean PAC values in probe LFP recordings. Data from 10 and 25 Hz stimulation at various probe LFP levels. Channel 1 is superficial and channel 30 is deep. SR = log sharpness ratio between troughs and peaks. RDR = rise decay ratios. All correlations are Pearson's correlations. Pairwise comparisons were adjusted for multiple comparisons using Bonferroni correction. Probe channel 1 = most superficial. Channel 30 = deepest.

5.4 Discussion

5.4.1 Cortical PAC and asymmetries as biomarkers of basal ganglia-thalamo-cortical network activity

Several theories about the physiological and pathophysiological origin of PAC in both cortical and subcortical brain structures have been brought forward (Canolty, R T, 2012). We show that stimulation of the basal ganglia receiving thalamus, but not the cerebellar receiving thalamus, induces significant PAC in the ECoG signal by generating nonlinearities in the waveform of oscillations of frequencies corresponding to those applied to drive thalamic neuronal activity. Pathophysiological beta oscillations have been demonstrated to arise across cortical, thalamic and basal ganglia structures in PD. Cortical beta waveform asymmetries have been observed in both ECoG and EEG recordings in PD patients and correspond to motor impairment (Cole et al., 2017; Jackson et al., 2019). Cortical PAC between beta and broadband high-gamma has been shown to arise in PD patients in ECoG signals and to be attenuated by subthalamic cDBS and contralateral body movements (de Hemptinne et al., 2015). This study shows that optogenetics-induced thalamic beta oscillations in the basal ganglia receiving thalamus creates cortical PAC in the ECoG signal by inducing beta waveform asymmetries. Importantly, this was not the case for the cerebellar thalamo-cortical circuit. This indicates that ECoG PAC/asymmetries could serve as a biomarker of underlying frequency specific activity in the basal ganglia-thalamic-cortical network in health and disease.

5.4.2 Origins of cortical beta oscillations

Several, and sometimes conflicting, theories regarding the neuronal origin of cortical LFPs have been brought forward based on experimental findings and inverse and forward modelling (Buzsáki et al., 2012; Einevoll et al., 2013) with cortical LFPs resulting from transmembrane currents of synaptic inputs onto dendrites being the dominant factor according to most theories (Einevoll et al., 2007, 2013; Potjans and Diesmann, 2012). Others point to additional contributors in the form of neuronal action potentials and intrinsic membrane oscillations (Buzsáki et al., 2012). The task of finding the greatest contributor is further complicated by the differentiation between distinct oscillatory frequencies that make up the raw LFPs, and the determination of the origin of the various oscillations and their interdependency (Belluscio et al., 2012; Buzsáki and Wang, 2012). A model of neocortical beta oscillations brought forward by Jones and colleagues proposes that beta oscillations reflect the specifically timed synaptic events to distinct cortical layers, most likely originating from BTC networks (Sherman et al., 2016). Specifically the BZ thalamus is being highlighted as an ideal candidate based on its dominant and diffuse projections to supragranular layers in motor and sensory cortex (Sherman et al., 2016). Motor thalamic nuclei project to different layers in cortex (Herkenham, 1980; Kuramoto et al., 2015). While the basal ganglia receiving thalamus projects predominantly to the supragranular layer 1, the cerebellar receiving thalamus projects to layers 2-5 (Kuramoto et al., 2015). Our analysis shows that specific neuronal oscillations, generated by driving basal ganglia receiving thalamic activity by use of optogenetics, manifests in corresponding frequency power changes in the supragranular as well as more profound neocortical layers, which is in some ways aligned with the Sherman et al. theory of beta propagation. Perhaps surprisingly, however, CZ-stimulation did not result in deeper layer power spectral changes.

But if basal ganglia-receiving thalamus projects predominantly to layer 1, while cerebellar-receiving-thalamus projects to layers 2-5 (Kuramoto et al., 2015), why then does stimulation of BZ thalamus result in power spectral changes at not just the supragranular levels, but also, and to a greater extent, in the deeper layers of motor cortex? One possibility is the further downstream signal transmission to deep pyramidal neurons (Buzsáki et al., 2012) and the following signal transmission cascade and transmembrane voltage change within the microcircuits of cortex (Potjans and Diesmann, 2012; Einevoll et al., 2013). The answer will hopefully be given in future as our understanding of cortical layer dynamics and conduction models of LFPs matures.

Another study found that selective stimulation via optogenetics of striatal cholinergic interneurons was able to amplify cortical beta and gamma oscillations and induce parkinsonian symptoms in healthy mice (Kondabolu et al., 2016). The impact of changes in basal ganglia dynamics to cortex go through BZ-thalamus and we demonstrate that beta frequency evoked potentials in BZ-thalamus manifest in ECoG registered beta bursts and broadband gamma increases, providing a route for transmission of these changes in network dynamics. Importantly, selective CZ-stimulation at neither beta nor alpha frequencies resulted in significant supragranular power spectral changes across subjects.

5.4.3 Theories of PAC generation

Three dominant theories of the origin of PAC in brain structures exist: 1) Different neural populations oscillating synchronised at different frequencies have convincingly been demonstrated in the hippocampus (Buzsáki and Wang, 2012). 2) The higher frequency could arise from phase locked background unit activity locked to a lower frequency dominated by synaptic input (Ray et al., 2008a; Sanders, 2016; Meidahl et al., 2019). 3)

The high frequency component arises from non-linearities and results in spurious statistical PAC (Sheremet et al., 2016).

Our study supports the third explanation as the predominant reason for any observed cortical PAC during thalamic stimulation in ECoG signals. However, this does not rule out underlying smaller contributions from any of the other forms. Furthermore, sharp edges failed to explain PAC within cortical layers, and consequently it may be that information from extracted measures of PAC here could provide valuable physiological information that can not readily be extracted from the lower frequency signal alone.

Interestingly, both the PAC frequency clustering and waveform morphology observed during optogenetic VM-stimulation resembled that described in ECoG recordings from human PD patients (de Hemptinne et al., 2015; Cole et al., 2017). The broadband high-gamma amplitude statistically coupled to beta phase in the ECoG PAC comodulograms was very similar to the broadband gamma frequencies in PD patients (de Hemptinne et al., 2013, 2015) and considerably lower in amplitude frequencies than those observed in PAC in the STN (Lopez-Azcarate et al., 2010; van Wijk et al., 2016; Meidahl et al., 2019) where beta phase was coupled to HFOs. In canonical cortical PAC computational work the beta phase was found to couple to frequencies much higher than those of broadband gamma (Cole et al., 2017) and to be more similar to those HFOs observed within the STN (Meidahl et al., 2019). Meanwhile, they found sharp edges in the lower frequency beta oscillation, at least in part, could explain the broadband high-gamma content (Cole et al., 2017).

5.4.4 Implications for Parkinson's disease and closed-loop modulations

The degeneration of dopaminergic fibre projections from substantia nigra pars compacta has time and again in both humans and animals been shown to manifest itself in beta oscillation propagation throughout the BTC network (Brown et al., 2001; Doyle et al., 2005; Mallet et al., 2008b; Tinkhauser et al., 2017b). We show that evoked beta oscillations in basal ganglia receiving thalamus transmit to ECoG recordings in the form of asymmetric beta waves, implying that basal ganglia-thalamocortical-projections could play a vital part in the propagation of beta-synchronisation in transient bursts to cortex and consequently across the BTC networks.

ECoG recordings play an increasingly larger role in neuroscience (Moses et al., 2019) and investigations for closed-loop feedback modulations in movement disorders (Buzsáki et al., 2012; Meidahl et al., 2017; Bouthour et al., 2019). We provide evidence that asymmetric beta oscillations, and statistical PAC, in ECoG signals is a parameter of activity in specific BZ-thalamic cortical projections.

It is questionable if there are any immediate benefits from using cortical PAC over cortical asymmetries for real-time closed-loop DBS feedback as their exaggeration in cortex appear to be reflective of one another. The simplicity of the asymmetric signal makes it much advantageous to PAC extraction and real-time prediction. Cortical beta asymmetries in PD has lately been shown to be picked up by non-invasive EEG-electrodes in PD patients (Jackson et al., 2019), where the EEG beta asymmetries were attenuated by dopaminergic medication. EEG has a lower signal to noise ratio, which could make the extraction of beta asymmetries advantageous compared to the extraction of beta power. Consequently, EEG beta oscillation waveform asymmetries might be more beneficial as a non-invasive biomarker for future experimental and clinically trialled

closed-loop modulation interventions. Meanwhile PAC extracted from cortical layers during thalamic opto-stimulation could not be accounted for by signal non-linearities. It remains to be investigated if any clinical benefits could be had from extracting this signal compared to that of the ECoG. Speaking against this is the invasiveness of the signal extraction and spatial limitations of the probe implantations. In contrast, the ECoG grid can span without inflicting cortical layer damage over the entire motor cortex. Ultimately, clinical trials using different stimulation modalities to various biomarker features will decide the utility and feasibility of the individual biomarkers in closed-loop applications and the decisive test of any clinical trials will be symptom attenuation, side effect profiles and quality of life impacts and not mere signal attenuations.

In summary we provide several lines of evidence that ECoG PAC arises during stimulation of the basal ganglia-recipient thalamus, but not the cerebellar-recipient thalamus. In ECoG signals, this PAC appears to result from the induction of nonlinearities in both the beta and alpha frequency range. ECoG PAC and waveform asymmetries have been proposed as advantageous biomarkers for closed-loop interventions in PD (de Hemptinne et al., 2015; Cole et al., 2017). By applying selective optogenetic stimulation to motor thalamus our study gives evidence that cortical PAC and cortical signal asymmetries can result from beta oscillations generated by frequency specific activity in basal ganglia thalamocortical projections. We therefor propose that cortical asymmetric beta oscillations in ECoG signals could serve as a viable biomarker of synchronised basal ganglia-thalamo-cortical network activity.

6

General discussion

Contents

6.1 General summary of results

6.2 Implications for basal ganglia network models

6.3 Biomarkers in PD: One to rule them all?

6.3.1 Overview

6.3.2 PAC-responsive DBS

6.3.3 Implications for beta-responsive DBS

6.3.4 Waveform asymmetry responsive DBS

6.3.5 Spatial and multimodal considerations

6.3.6 Conclusion

6.4 Symptom versus signal attenuation

6.5 Limitations

6.6 Open questions

6.7 AI, machine learning and future technologies

6.8 Final remarks

6.1 General summary of results

In this thesis, simultaneous ECoG-recordings as well as recordings of subthalamic local field potentials and single unit activity were analysed in awake human PD patients undergoing DBS electrode implantations.

We show that STN PAC, which has been linked to motor impairment in PD, is reflective of subthalamic input-output synchronisation by being a proxy of the locking of spiking activity to beta-oscillations. We give several lines of evidence that beta oscillations drive spiking activity, which manifests as high frequency oscillations in the STN. STN PAC could therefore serve as a biomarker of input/output synchronisation in the beta frequency range. Thus, we reveal a neuronal basis for one of the most prominently proposed biomarkers in PD. Furthermore, we found transient periods of beta bursting, a clinically trialled biomarker for closed-loop DBS, to capture progressively higher levels of this input-output manifestation, suggesting that STN PAC occurs in transient events during periods of high beta-input.

Furthermore, by analysing simultaneous ECoG signals we investigated the dependency between leading cortical and subcortical electrophysiological biomarkers in PD. We provide a first link between cortical waveform sharpness and subthalamic neuronal synchronizations by showing that cortical waveform sharpness is reflective of the locking of single unit activity to cortical beta oscillations. Furthermore, we show that cortical beta-bursts capture higher levels of subthalamic cortical spike-phase locking, as indexed by cortico-subthalamic PAC, and cortical sharpness, with direct implications for future closed-loop DBS trials.

Finally, we give evidence that cortical PAC, as seen in PD, can be produced by driving basal-ganglia inputs to motor thalamus and that this is not the case when driving cerebellar recipient thalamus. The findings add evidence, in rodents at least, to a model

of beta generations brought forward by the Stephanie Jones group, that proposes neocortical beta oscillations to be reflective of specifically timed synaptic events to distinct cortical layers, most likely originating from BTC networks (Sherman et al., 2016). We furthermore show, that cortical beta asymmetries arise by driving basal-ganglia inputs to motor thalamus and that these nonlinear features correlate with the observed cortical PAC. Thus, cortical PAC, and indeed sharp oscillations, could serve as a biomarker of the frequency specific drive of basal ganglia on thalamus. Based on these results we propose sharp beta oscillations in cortex could serve as a promising biomarker in future closed-loop DBS experiments.

6.2 Implications for basal ganglia network models

The dualistic rate model offers an intuitive and simplified theory of basal ganglia function but fails to explain several paradoxical observations (Cui et al., 2013; Calabresi et al., 2014; Nelson and Kreitzer, 2014). Most notably that transient increases in activity in both the direct and indirect pathways happen during movement (Cui et al., 2013). It has been argued in theoretical neuroscience that coherence in timing is of vital importance for effective neuronal transmission throughout dynamic brain networks (Fries, 2005). Could it be that the dynamics of activation patterns are the determinant for basal ganglia functional outcomes and not their dichotomous active vs. inactive states?

PAC in the STN has been found to be a pathophysiological manifestation in Parkinson's disease. We uncover STN PAC to represent the locking of local neuronal activity to beta-oscillations and thereby represent a measure of input-output synchrony. This, importantly, was in spite of neurons in the absence of PAC firing at similar rates. Consequently, it was not neuronal excitability per se that manifested in the pathophysiological activity but the

ways in which certain neurons engaged with input activity patterns. Thus, a dichotomous active versus inactive approach to the STN would fail to account for the pathophysiological changes. Our findings thereby speak in favour of the communication through coherence-theory. Furthermore, the PAC activity was not constant over time and happened during transient bursting events of the carrier frequency. The longer the events the more sustained was PAC. This calls for transient considerations of swift oscillatory changes in the study of brain network dynamics.

When we drive basal ganglia input to motor thalamus, we show that cortical manifestations are determined by both structural and temporal input properties. Structural differences were important (differences in cerebellar versus basal ganglia input drive and cortical recording sites) for signal manifestations, but so was the way in which input was driven by different frequencies of stimulation. Again, active vs. inactive would not account for the dynamic manifestations observed. It is therefore likely that the dynamic way in which the indirect and direct pathways engage with motor thalamus is a highly determining factor for cortical outcomes.

The rate model and structural projection flowcharts (Fig. 1.1, Chapter 1) should be complemented by models of neurodynamics informed by experimental studies (Fries, 2015; West et al., 2018; Reis et al., 2019; Whittington and Bogacz, 2019) . I argue that traditional basal ganglia models have been limited by focusing on structural and spatial differences, so that an impasse has been reached and the time has come for much more dynamic and temporal approaches to basal ganglia function.

6.3 Biomarkers for closed loop DBS: one signal to rule them all?

6.3.1 Overview

Closed-loop DBS is evolving and could offer a way to better engage with pathophysiological processes in neural networks and spare interference with healthy physiological circuits in order to minimise side effects (Rosin et al., 2011; Little et al., 2013, 2016; Rosa et al., 2015; Meidahl et al., 2017; Arlotti et al., 2018; Bouthour et al., 2019).

Beta-oscillation amplitude has already been trialled as feedback signals for closed-loop DBS in Parkinson's disease in both amplitude-responsive and phase-responsive manners in proof of principle studies (Rosin et al., 2011; Little et al., 2013, 2015, 2016; Arlotti et al., 2018; Holt et al., 2019). The findings of this thesis hold numerous implications for future closed-loop interventions. In the following we will discuss such implications and their potential applications in closed-loop DBS experiments.

6.3.2 PAC-responsive aDBS

Both subthalamic and cortical PAC have been suggested as biomarkers in PD based on symptom correlations. Based on previous studies and the findings of this thesis we will discuss PAC extracted from STN and cortex as feedback signals for closed loop, or aDBS, in PD patients.

Subthalamic PAC

Subthalamic PAC relates to PD motor impairment and is attenuated by both contralateral movement and dopaminergic medication (Lopez-Azcarate et al., 2010; van Wijk et al., 2016). Our study of PAC in the human STN in PD patients backed the second hypothesis for PAC origin (see Chapter 1.2.6), and indicated STN PAC to represent a semi-

independent process where the lower frequency is dominated by synaptic input and the higher-frequency arises from background neural unit activity locked to this input (Jensen et al., 2016).

We found STN PAC, a measure of motor impairment in PD, to be reflective of subthalamic input-output synchronisation by being a proxy of the locking of spiking activity to beta-oscillations. Consequently, aDBS pertained to PAC in real time, could enable DBS to interfere at times of high pathophysiological input/output synchrony in the STN. STN PAC, however, was found to progress with beta bursts duration. By focussing closed-loop DBS on subthalamic beta-bursts, one would implicitly also focus stimulation on higher levels of subthalamic PAC, simply by virtue of the statistical higher co-occurrence.

Would there be any benefits to focussing stimulation to this subthalamic input-output synchrony indexed by PAC as opposed to pertaining stimulation to the beta input synchrony alone?

Speaking against the idea of using beta as a surrogate of PAC is the fact that PAC and beta have been found to have slightly different spatial profiles within the STN (Wijk et al., 2017). It is therefore possible that PAC signals capture neuronal synchronisations to beta inputs that are not ubiquitously captured across the STN by beta power alone. In other words, you could have beta inputs that do not engage in neuronal oscillatory outputs. It might then be that PAC is more informative as a biomarker of the neuronal information transfer than the supposed input oscillation alone.

Speaking for the use of beta-power alone is our demonstration, that periods of beta-bursting capture progressively higher levels of PAC and HFO power, suggesting that any form of bursts event-responsive aDBS would implicitly also focus stimulation on higher levels of PAC. One thing is of course to identify periods and proxies of

pathophysiological activity regardless of causality. Another is of course to ask how best to apply stimulation during such events. It might be that subthalamic beta-bursts capture higher levels subthalamic PAC, but if one wants to apply DBS in order to attenuate the signal (and the mechanistic basis thereof) it might prove too simplistic to use one signal as a proxy of the other simply by virtue of their co-occurrence. Especially if it is needed to apply event-dependant or continuous control to engage with particular features of that signal.

We have already discussed ways in which to engage with the beta-oscillation alone in thesis chapter 1 (Fig. 1.3). Here we will expand our theories regarding ways to focus stimulation on signals reflective of PAC (Fig 6.1). Overall exploratory PAC calculations using existing methods are computationally heavy, especially across the wide frequency ranges as those observed in the typical PAC-comodulograms. One way to circumvent this could be to identify the phase and amplitude frequency corresponding to the peak PAC values and identify at what phases of beta the gamma or HFO amplitude peaks. This information could then be a guide in specifying two oscillations for bandpass filtering in real time (e.g. if PAC peaks between 20 Hz beta phase and 220 Hz amplitude, one could simply process these signals in real time and apply stimulation when synchronisations occur).

The simplest way to apply stimulation would perhaps be *PAC-responsive event dependent control*. During periods of detected PAC, stimulation could simply be applied in an On-Off manner (Fig. 6.1A). Another way would be to scale the stimulation voltage to the levels to the higher frequency amplitude envelope, *PAC-responsive event dependent continuous control* (Fig. 6.1B). A third option is to engage with the phase of the lower frequency signal during periods of detected PAC, *PAC-phase responsive event dependent control*.

Ultimately, however, clinical assessments and side-effects profiles together with considerations of engineering feasibilities would determine the most suitable biomarker.

Cortical PAC

Cortical PAC, between beta phase and broadband gamma, in PD relates to motor impairment and is attenuated by subthalamic DBS, contralateral movement and dopaminergic medication (de Hemptinne et al., 2013, 2015) as discussed in the general introduction, and can at least in part be explained by cortical waveform asymmetries (Cole et al., 2017).

We demonstrated that cortical PAC, as seen in PD, could be produced by driving basal-ganglia inputs to motor thalamus by using optogenetic stimulation. A beta-oscillatory drive is widely established in the basal ganglia structures in PD and we provide a link between propagation of beta synchrony in basal ganglia and cortical PAC formation via thalamus. When thalamus is driven by beta-synchronised inputs, cortical beta waveform asymmetries are seen. These in turn give rise to beta-broadband gamma PAC as described by the Voytek group (Cole et al., 2017). The results of this thesis suggest those asymmetries arise from beta synchronised input to thalamus from basal ganglia networks. ECoG recorded PAC could theoretically be utilised as a biomarker to guide STN DBS in the same manner as described above for STN PAC regardless of a spurious nonsinusoidal basis as long as the signal in real time correlates with motor impairment. However, it is unlikely that any additional information could be gained that could not be extracted from the nonsinusoidal features of the carrier oscillation itself. Thus, a more advantageous biomarker of physiological and pathophysiological synchrony in BTC networks than cortical PAC would be cortical asymmetries which will be discussed below.

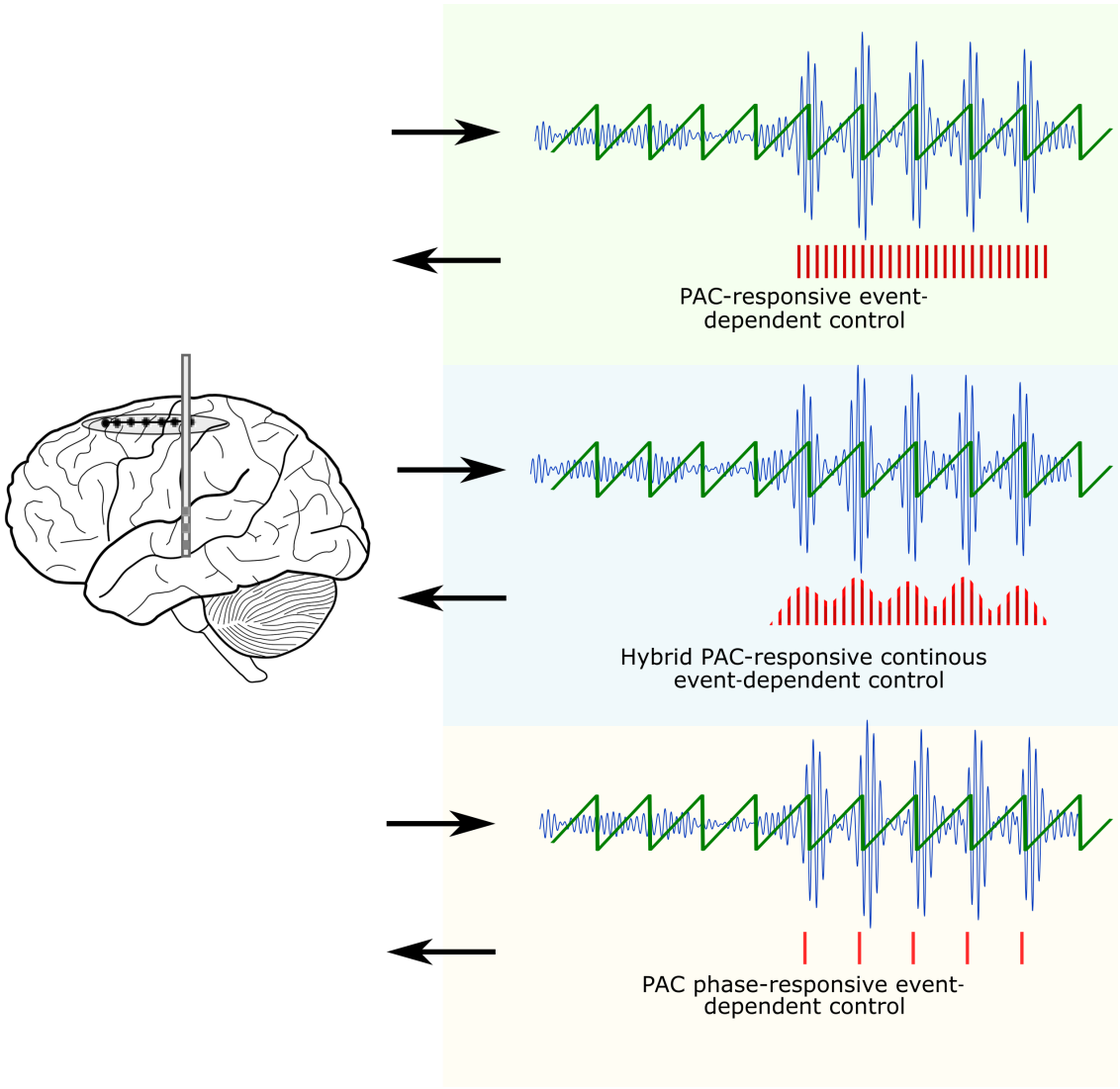


Figure 6.1 - Schematic of proposed forms of PAC-responsive DBS based on signals read out from either STN LFPs or cortical ECoGs. Blue signals represent band pass filtered HFOs, green beta filtered phase and red vertical lines applied stimulation pulses. **A**) Stimulation is applied in an on-off setting during events of detected PAC. **B**) Stimulation is applied during periods of increased PAC but varies proportionately to the amplitude envelope of the HFOs. **C**) Stimulation is applied during periods of PAC timed to specific phases of the carrier-oscillation.

CTX-STN PAC

In simultaneous recordings from cortical ECoGs and STN LFPs, we show that CTX-STN PAC is a surrogate of the synchronisations of subthalamic unit activity to cortical beta oscillations. It might therefore be the case that a double signal extraction of cortical beta phase and subthalamic HFOs could be utilised as a feedback biomarker for aDBS as a surrogate of such pathophysiological cortico-subthalamic unit synchronisation. Stimulation could be signal focussed as in figure 6.1 with the only difference being dual site signal extraction. Extracting beta-oscillations from cortex comes with certain disadvantages (see section 6.3.3 and 6.3.5 below) and it is uncertain if any useful information would be gained that could not be extracted from STN PAC alone. As our understanding of BTC oscillatory network propagation matures, it might be possible to answer such questions from physiological predictions. In the meantime, clinical experiments should guide the answer to such questions.

6.3.3 Implications for beta-responsive aDBS

Beta-filtered oscillation offers a fairly straightforward biomarker for real time amplitude or phase responsive DBS (see Fig. 1.3, Chapter 1) and has been tested in proof of principles studies in humans (Little et al., 2013, 2015; Arlotti et al., 2018; Holt et al., 2019). It is however less clear to what extent this biomarker captures the complexity of the neurophysiological manifestations in PD across the BTC-networks. We demonstrate that subthalamic beta bursts capture higher levels of subthalamic PAC and HFO power. We also show how cortical beta bursts encompass higher levels of cortico-subthalamic phase-spike synchrony as indexed by CTX-STN PAC as well as higher levels of raw beta waveform asymmetries. It could then be inferred that any stimulation applied during these bursting events could also interfere with whatever mechanisms the other biomarkers are

reflective of. That may be true for an ON/OFF application setting. But what if one specifically wishes to engage with the statistical coupling between signals (e.g. PAC) or the aberrant asymmetries during such events? It might not then be that a beta-burst amplitude event-dependant stimulation form would be preferable. Perhaps applying stimulation in real time to particularities of these individual signal features could prove superior in symptom attenuation, side-effect profiles or battery sparing.

The relationship between beta-power and symptom impairment is much more established than it is for any other biomarker in PD and from an engineering point of view, applying beta-responsive stimulation is certainly advantageous in its simplicity to PAC-responsive DBS. And further comparative studies of links between motor impairment and PAC is warranted. But as discussed in the PAC-responsive subchapter above, it is possible that in the STN information about input/output synchrony is lost by looking at the beta oscillation alone, and that subthalamic PAC could prove to be superior for sophisticated closed-loop signal engagements. The litmus test will be the application of both in comparable clinical settings.

6.3.4 Waveform asymmetry responsive aDBS

We showed in awake human PD patients off medication that raw cortical beta waveform sharpness is reflective of subthalamic unit synchronisation to cortical beta oscillations. Furthermore, cortical oscillatory peak sharpness asymmetries could be induced by driving input to basal ganglia receiving thalamus. The Voytek group has previously shown that ECoG nonsinusoidal beta sharpness related to motor impairment (Cole et al., 2017) and more recently that such sharpness was dopamine responsive and could be detected using non-invasive EEG (Jackson et al., 2019). It remains to be demonstrated if such features in the EEG, as is the case with ECoG, also relate progressively to motor impairment.

Cortical PAC, between beta-phase and broadband gamma, has been shown to result from the waveform asymmetries in the carrier signal (Cole and Voytek, 2016; Cole et al., 2017). We confirmed this finding in human PD patients. It might therefore be much more advantageous to use cortical asymmetries than within-cortical PAC to guide closed-loop DBS. Focussing stimulation to cortical beta-sharpness would certainly be less computationally demanding than applying it to the synchronisations of two bandpass signal, whose real-time synchronisations would be indicative of PAC.

The simplest way of applying waveform-asymmetry responsive DBS might be to apply it through an on-off control setting during periods of sustained waveform asymmetry (Fig. 6.2A). A perhaps more refined approach would be to apply stimulation continuously so that the intensity of stimulation varies proportionately with the raw beta amplitude features (Fig. 6.2C).

Longer beta-bursts capture higher levels of horizontal waveform asymmetry as well as progressively sharper peaks. One could therefor argue for the use of cortical beta-bursts over the use of signal nonlinearities. However, from a theoretical point of view, a hybrid application might be a more promising tool. Hybrid burst-asymmetry simulation could be pertained to the biomarker signals in various ways and forms. One way would be to apply stimulation in an event dependant manner during detected periods of beta-bursting (the sustained crossing of a beta-power threshold). During these periods, subthalamic stimulation could then be focussed on sharp cortical signal features that we in this thesis have demonstrated to be reflective of the locking of subthalamic unit activity to cortex (Fig. 6.2B). Alternatively, stimulation could be applied during sharp rises or decays. A continuous approach as outlined above could also be taken trough an event-dependant manner during periods of beta-bursting (not shown).

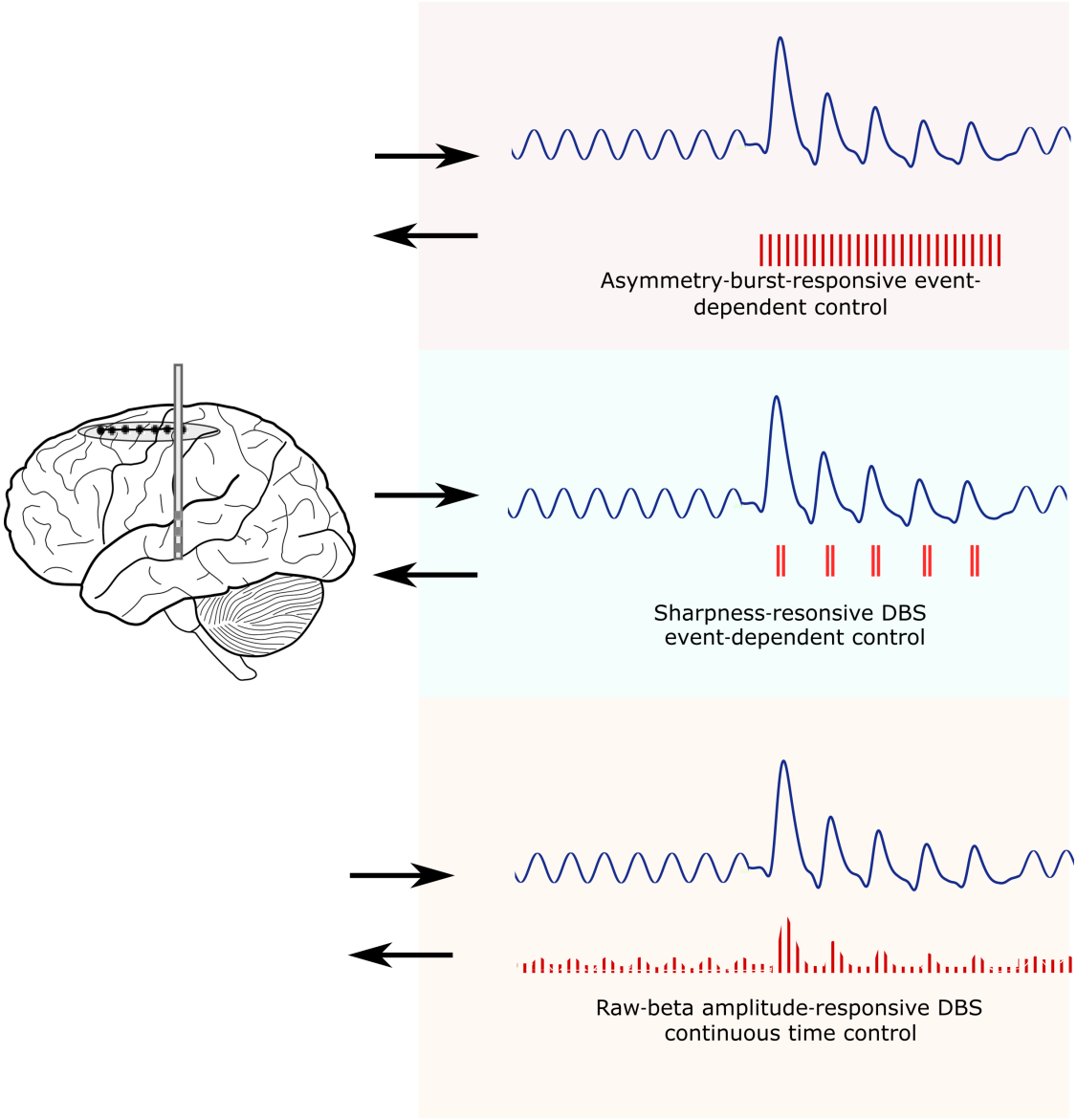


Figure 6.2 - Schematic of proposed forms of asymmetry-responsive DBS based on signals read out from either STN LFPs or cortical ECoGs. Blue signals represent the pre-processed data and red vertical lines applied stimulation pulses. **A**) Stimulation is applied on-off during periods of increased asymmetry or sharpness. **B**) Stimulation is applied during periods of high asymmetry and timed to the peaks of the signals. **C**) Stimulation is applied continuously and proportionately to the amplitude of the signal.

6.3.5 Spatial and multimodal considerations

When it comes to closed-loop DBS applications, one consideration is temporal, another is spatial. In this thesis we have analysed neurophysiological recordings from both cortex and the STN in human PD patients and cortex in mice undergoing optogenetic stimulation of motor thalamus.

The poet William Golding is quoted as saying "the greatest ideas are the simplest". Whether this dogma readily can be extracted from poetry and applied to neuroscience is a matter for debate. It is however clear, that relying on same site signal readouts and stimulation would be preferable to multiple sites, if no differences were found in outcomes.

However, it might be advantageous to extract signals from one site and stimulate at another. Indeed, it might be that the best outcome could be achieved by the extraction and stimulation at several basal ganglia sites simultaneously. But any such benefits could be negated by the invasiveness, impracticalities, surgical risks, and potential complications. This is the multisite trade-off.

Cortical beta is significantly greater in magnitude than STN beta due to the improved spatio-temporal integration afforded by cortical lamination and it might thus be advantageous to use any cortical beta features over that of the STN. Furthermore, extracting the signal from cortex while stimulating in STN could spare any problems with signal readouts during periods of stimulation. Reading out signals from STN while applying subthalamic simulation minimises the combination options of applying stimulation (Tinkhauser et al., 2017a, 2018a). The cortical homunculus, however, is, as opposed to the STN, expansive and might require an entire ECoG implanted grid with additional surgical, infectious risks. This could perhaps be circumvented by using EEG-

signals, that have recently been shown to display dopamine-sensitive beta asymmetries in human PD patients (Jackson et al., 2019).

We found some biomarkers like PAC not to represent the same underlying phenomena in cortex and STN. Consequently, as PAC could have a different neuronal basis at different sites, aDBS stimulation outcomes cannot be expected to be the same.

Beta power correlates well with bradykinesia and rigidity but not with tremor (Kühn et al., 2006; Beudel and Brown, 2015). No existing literature compares PAC or nonsinusoidal features directly with tremor assessments. Consequently, it could prove necessary to take a multidimensional approach and apply stimulation to signal extracted from both central and peripheral sensors (Malekmohammadi et al., 2016). This approach might, however, begin to compromise our vision of simplicity.

Another potentially pioneering supplement to the stimulation arsenal is field steering (Tinkhauser et al., 2018a; Cagnan et al., 2019) that would allow for more optimally focused stimulation applications. In the far future new stimulation modalities such as closed-loop optogenetics might also be introduced in the human setting (Kravitz et al., 2010; Grosenick et al., 2015) but numerous obstacles would have to be overcome and so far there are no signs of any such transitions in the near future (Tye and Deisseroth, 2012; Galvan et al., 2017).

6.3.6 Conclusion

According to our findings cortical PAC and asymmetries reflect propagation of pathological activity from the basal ganglia through motor thalamus, whereas STN PAC reflects pathophysiological input/input synchronisations.

We propose that 1) sharp features of beta oscillations in cortical ECoG recordings or 2) subthalamic PAC could be promising biomarkers for subthalamic closed-loop DBS in addition to beta-bursts.

6.4 Symptom versus signal attenuation

Our understanding of electrophysiological and pathophysiological signals in PD is maturing. But we are fast approaching an impasse to the extent that neurophysiological signal analysis can help guide and predict closed-loop DBS experimental outcomes. A constant bidirectional flow between the neurophysiological signal analysis and experimental trials could pave the way forward. Success in these experiments should be measured by the clinical outcomes such as symptom attenuation, side effects and battery longevity and not signal attenuation alone.

The ultimate test should not be signal attenuation or in fact immediate symptom attenuation, but long-term improvements quality of life in patients.

6.5 Limitations

Recording in awake human PD patients were performed during surgical electrode implantation. To what extent any correlations persist in the everyday setting remains unanswered. Continuous readouts of macro signals from chronically implanted IPG-devices will undoubtedly change that in future.

Our studies of the relationships between signals in human recordings across and within sites imply correlation but not necessary causation. We cannot for example be sure about any causations between the phase-locked subthalamic neurons and any observed cortical asymmetries as they could turn out to be occurring as a result of different pathophysiological, albeit related, changes. But for practical applications any correlation could be sufficient for closed-loop DBS guidance.

We analysed PAC in the STN using long recordings to determine PACs statistical consistency and divided recordings dichotomously into PAC and non-PAC. There is likely a grey zone that falls somewhere in the middle. Innovations in real-time PAC methods that could rely on much shorter data lengths without the need for data averaging would be helpful. We used optogenetic stimulation to drive inputs from basal ganglia to motor thalamus and examined cortical changes in the contralateral and ipsilateral side. During everyday tasks and with changes in cognition we cannot rule out contributions to such biomarkers from other cortical and subcortical projections apart from those studied. Additionally, the study in Chapter 5 was performed in healthy mice. How neurodegenerative events could affect the studied dynamics in the experimental setup remains to be investigated.

6.6 Open questions

This thesis raises as many questions as it answers. How do individual biomarkers compare to each other with regards to prediction of symptom severity? What is the better predictor of symptom severity and how do such biomarkers relate to often over-looked non-motor symptoms? No studies have to our knowledge directly compared individual biomarker-symptom correlations in PD. It is important that any firm conclusions are based on very large sets of patient data. Scientific literature is well known to underreport negative

findings (Duyx et al., 2017; Mlinarić et al., 2017) and it is important that all correlations in clinical studies get reported to make the best future predictions and optimisations for future aDBS studies.

How does applied opto-stimulation in non-motor regions of thalamus influence cortical electrophysiological signals and how are the signal changes influenced by behaviour and in the dopamine depleted state?

Are the signals studied causal in both physiology and pathophysiology or do they merely represent epiphenomena correlated statistically to underlying changes?

We studied the effects of stimulation of basal ganglia receiving thalamus on cortical signals. How does stimulation of the direct and indirect pathways, respectively, at different frequencies affect cortical biomarker signals in PD? Experimental evidence suggests that beta propagation in PD is through to the indirect pathway (Sharott et al., 2017). Future optogenetic studies could help further elucidate that.

6.7 AI, machine learning and future technologies

Currently the state-of-the-art extrapolations of biomarkers for closed-loop DBS has relied on retrospective correlations between symptom scores and manually extracted neurophysiological signals, compared to each other offline. The industry is pioneering chronically implantable, readily adjustable DBS-devices (Cagnan et al., 2019), and peripheral sensor systems are being developed for objective motor impairment assessments (Di Biase et al., 2017; Schlachetzki et al., 2017). In the future it might therefore be possible to make correlations between signals and symptoms in real time. Furthermore, innovations such as field steering will increase special stimulation specificities (Tinkhauser et al., 2018a; Cagnan et al., 2019).

The application of AI algorithms and machine learning techniques across scientific and neuroscientific fields is moving fast (Ghahramani, 2015; Savage, 2019). Recently, machine learning algorithms have been able to predict hand gripping force based on subthalamic LFPs (Shah et al., 2018) and to decode language from ECoG signals (Moses et al., 2019). With the prospect of real-time signal readouts and objective, continuous symptom assessments by peripheral sensors, AI algorithms could find hitherto-unseen correlations between signal features and symptoms. In fact, it might negate the necessity for scientists to extract any particular signal features and have any knowledge of such signal features for practical programming purposes. Based on signal readouts, stimulation effects, symptom assessments and patient feedback the AI could help set the most optimal aDBS stimulation parameters and make continuous real-time adjustments (Figure 6.3) (Neumann et al., 2019).

In future other and more specific neuronal interventions such as optogenetic-stimulation might even be translated to the human setting (Grosenick et al., 2015).

Closed-loop DBS could be expanded to other diseases (Cagnan et al., 2019) and might even pave the way for bidirectional computer-brain interfaces in healthy individuals, with numerous foreseeable and unforeseeable ethical and moral implications.

In the meantime, closed-loop DBS must be pioneered in the experimental setting based on electrophysiological biomarkers, symptom and side effect inferences, and life quality assessments in double-blinded, randomised trials, under continuous ethical approval, to stand the test of time.

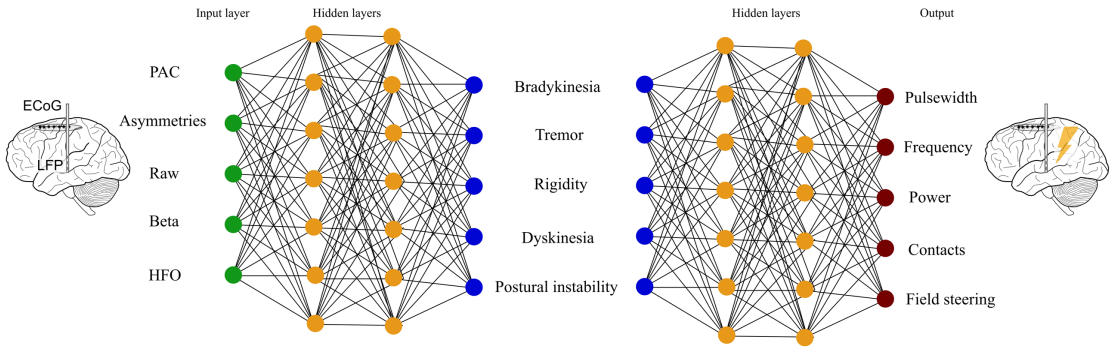


Figure 6.3 - Simplified schematic of an AI Deep Learning Network based on pathophysiological biomarkers recorded from subthalamic LFPs or ECoG (left) and symptom assessments (middle) from peripheral sensors. Hierarchical classifications and predictions could ultimately guide aDBS stimulation parameters (right) in a bidirectional flow. Inspired by (Neumann et al., 2019).

6.8 Final remarks

This thesis has explored and furthered the understanding of the neuronal basis, interdependency and propagation of significant neurophysiological biomarkers in Parkinson's disease. Based on the findings it proposes new ways for closed-loop DBS to interfere with pathophysiological changes in real-time.

As our understanding of neural circuit physiology matures and technology evolves, so does the potential for therapeutic, reversible interventions in brain disorders.

7. References

Accolla EA, Herrojo Ruiz M, Horn A, Schneider G-H, Schmitz-Hübsch T, Draganski B, Kühn AA (2016) Brain networks modulated by subthalamic nucleus deep brain stimulation. Brain 139:2503–2515 Available at: http://brain.oxfordjournals.org/%5Cnhttp://www.brain.oxfordjournals.org/lookup/doi/10.1093/brain/aww182.

Afshar P, Khambhati A, Stanslaski S, Carlson D, Jensen R, Linde D, Dani S, Lazarewicz M, Cong P, Giftakis J, Stypulkowski P, Denison T (2012) A translational platform for prototyping closed-loop neuromodulation systems. Front Neural Circuits 6:117 Available at: http://www.pubmedcentral.nih.gov/articlerender.fcgi?artid=3551193&tool=pmcentrez&rendertype=abstract.

Agnesi F, Connolly AT, Baker KB, Vitek JL, Johnson MD (2013) Deep Brain Stimulation Imposes Complex Informational Lesions. PLoS One 8:1–11.

Akam T, Kullmann DM (2014) Oscillatory multiplexing of population codes for selective communication in the mammalian brain. Nat Rev Neurosci 15:111–122 Available at: http://dx.doi.org/10.1038/nrn3668.

Albin RL, Young AB, Penney JB (1989) The functional anatomy of basal ganglia disorders. Trends Neurosci 12:366–375.

Alexander GE, Crutcher MD (1990) Functional architecture of basal ganglia circuits: neural substrates of parallel processing. Trends Neurosci 13:266–271 Available at: https://linkinghub.elsevier.com/retrieve/pii/016622369090107L.

Alexander GE, DeLong MR (1985) Microstimulation of the primate neostriatum. I. Physiological properties of striatal microexcitable zones. J Neurophysiol 53:1401–1416 Available at: https://www.physiology.org/doi/10.1152/jn.1985.53.6.1401.

Androulidakis AG, Kühn AA, Chen CC, Blomstedt P, Kempf F, Kupsch A, Schneider GH, Doyle L, Dowsey-Limousin P, Hariz MI, Brown P (2007) Dopaminergic therapy promotes lateralized motor activity in the subthalamic area in Parkinson's disease. Brain 130:457–468.

Anidi C, O'Day JJ, Anderson RW, Afzal MF, Syrkin-Nikolau J, Velisar A, Bronte-Stewart HM (2018) Neuromodulation targets pathological not physiological beta bursts during gait in Parkinson's disease. Neurobiol Dis 120:107–117.

Anzak A, Tan H, Pogosyan A, Foltynie T, Limousin P, Zrinzo L, Hariz M, Ashkan K, Bogdanovic M, Green AL, Aziz T, Brown P (2012) Subthalamic nucleus activity optimizes maximal effort motor responses in Parkinson's disease. Brain 135:2766–2778.

Arlotti M, Marceglia S, Foffani G, Volkmann J, Lozano AM, Moro E, Cogiamanian F, Prenassi M, Bocci T, Cortese F, Rampini P, Barbieri S, Priori A (2018) Eight-hours adaptive deep brain stimulation in patients with Parkinson disease. Neurology:10.1212/WNL.0000000000005121 Available at: http://www.ncbi.nlm.nih.gov/pubmed/29444973%0Ahttp://www.neurology.org/lookup/doi/10.1212/WNL.0000000000005121.

Arlotti M, Rosa M, Marceglia S, Barbieri S, Priori A (2016) The adaptive deep brain stimulation challenge. Park Relat Disord 28:12–17 Available at: http://dx.doi.org/10.1016/j.parkreldis.2016.03.020.

Aru J, Aru J, Priesemann V, Wibral M, Lana L, Pipa G, Singer W, Vicente R (2015)

Untangling cross-frequency coupling in neuroscience. Curr Opin Neurobiol 31:51–61 Available at: http://dx.doi.org/10.1016/j.conb.2014.08.002.
Åström K, Hägglund T (1995) PID Controllers: Theory, Design, and Tuning. Res Triangle Park NC Int Soc Meas Control:1995.
Atasoy D, Aponte Y, Su HH, Sternson SM (2008) A FLEX switch targets channelrhodopsin-2 to multiple cell types for imaging and long-range circuit mapping. J Neurosci 28:7025–7030.
Baker SN, Olivier E, Lemon RN (1997) Coherent oscillations in monkey motor cortex and hand muscle EMG show task-dependent modulation. J Physiol 501:225–241.
Baker SN, Pinches EM, Lemon RN (2003) Synchronization in monkey motor cortex during a precision grip task. II. Effect of oscillatory activity on corticospinal output. J Neurophysiol 89:1941–1953.
Bar-Gad I, Morris G, Bergman H (2003) Information processing, dimensionality reduction and reinforcement learning in the basal ganglia. Prog Neurobiol 71:439–473.
Barbe MT, Liebhart L, Runge M, Pauls KAM, Wojtecki L, Schnitzler A, Allert N, Fink GR, Sturm V, Maarouf M, Timmermann L (2011) Deep brain stimulation in the nucleus ventralis intermedius in patients with essential tremor: Habituation of tremor suppression. J Neurol 258:434–439.
Basu I, Graupe D, Tuninetti D, Shukla P, Slavin K V, Metman LV, Corcos DM (2013) Pathological tremor prediction using surface electromyogram and acceleration: potential use in `ON-OFF' demand driven deep brain stimulator design. J Neural Eng 10:036019 Available at: http://www.ncbi.nlm.nih.gov/pubmed/23658233.
Belluscio MA, Mizuseki K, Schmidt R, Kempter R, Buzsáki G (2012) Cross-frequency phase-phase coupling between θ and γ oscillations in the hippocampus. J Neurosci 32:423–435 Available at: http://www.jneurosci.org/content/32/2/423.long.
Berens P (2009) CircStat : A MATLAB Toolbox for Circular Statistics . J Stat Softw 31.
Berger H (1929) Elektrenkephalogramm des Menschen. Arch Psychiatr Nerv 87:527–570.
Berman BD, Starr PA, Marks WJ, Ostrem JL (2009) Induction of bradykinesia with pallidal deep brain stimulation in patients with cranial-cervical dystonia. Stereotact Funct Neurosurg 87:37–44.
Beudel M, Brown P (2015) Adaptive deep brain stimulation in Parkinson's disease. Parkinsonism Relat Disord 22:1–4 Available at: http://dx.doi.org/10.1016/j.parkreldis.2015.09.028.
Bevan MD, Hallworth NE, Baufreton J (2007) GABAergic control of the subthalamic nucleus. Prog Brain Res 160:173–188 Available at: https://www.sciencedirect.com/science/article/pii/S0079612306600101?via%3Dihub [Accessed September 10, 2019].
Blomstedt P, Hariz G-M, Hariz MI, Koskinen L-OD (2007) Thalamic deep brain stimulation in the treatment of essential tremor: a long-term follow-up. Br J Neurosurg 21:504–509.
Bolam JP, Brown MTC, Moss J, Magill PJ (2009) Basal Ganglia : Internal Organization. Neuroscience 2:97–104 Available at: http://scholar.google.com/scholar?hl=en&btnG=Search&q=intitle:Basal+Ganglia:+Internal+Organization#0.
Bouthour W, Mégevand P, Donoghue J, Lüscher C, Birbaumer N, Krack P (2019) Biomarkers for closed-loop deep brain stimulation in Parkinson disease and beyond. Nat Rev Neurol Available at: http://dx.doi.org/10.1038/s41582-019-0166-

4.
Boyden ES, Zhang F, Bamberg E, Nagel G, Deisseroth K (2005) Millisecond-timescale, genetically targeted optical control of neural activity. Nat Neurosci 8:1263–1268 Available at: http://www.nature.com/articles/nn1525.
Braak H, Tredici K Del, Rüb U, de Vos RA., Jansen Steur EN., Braak E (2003) Staging of brain pathology related to sporadic Parkinson's disease. Neurobiol Aging 24:197–211 Available at: https://www.sciencedirect.com/science/article/pii/S0197458002000659?via%3Dihub [Accessed September 11, 2019].
Brazhnik E, McCoy AJ, Novikov N, Hatch CE, Walters JR (2016) Ventral medial thalamic nucleus promotes synchronization of increased high beta oscillatory activity in the basal ganglia-thalamocortical network of the hemiparkinsonian rat. J Neurosci 36:4196–4208.
Brice J, McLellan L (1980) SUPPRESSION OF INTENTION TREMOR BY CONTINGENT DEEP-BRAIN STIMULATION. Lancet:1221–1222.
Brown P, Oliviero A, Mazzone P, Insola A, Tonali P, Di Lazzaro V (2001) Dopamine dependency of oscillations between subthalamic nucleus and pallidum in Parkinson's disease. J Neurosci 21:1033–1038.
Brunet N, Bosman CA, Roberts M, Oostenveld R, Womelsdorf T, De Weerd P, Fries P (2015) Visual cortical gamma-band activity during free viewing of natural images. Cereb Cortex 25:918–926.
Busskamp V, Duebel J, Balya D, Fradot M, Viney TJ, Siegert S, Groner AC, Cabuy E, Forster V, Seeliger M, Biel M, Humphries P, Paques M, Mohand-Said S, Trono D, Deisseroth K, Sahel JA, Picaud S, Roska B (2010) Genetic Reactivation of Cone Photoreceptors Restores Visual Responses in Retinitis Pigmentosa. Science (80-) 329:413–417 Available at: http://www.sciencemag.org/cgi/doi/10.1126/science.1190897.
Buzsáki G, Anastassiou CA, Koch C (2012) The origin of extracellular fields and currents — EEG, ECoG, LFP and spikes. Nat Rev Neurosci 13:407–420 Available at: http://www.nature.com/doifinder/10.1038/nrn3241.
Buzsáki G, Wang X-J (2012) Mechanisms of Gamma Oscillations. Annu Rev Neurosci 35:203–225 Available at: http://www.annualreviews.org/doi/10.1146/annurev-neuro-062111-150444.
Cagnan H, Brittain JS, Little S, Foltynie T, Limousin P, Zrinzo L, Hariz M, Joint C, Fitzgerald J, Green AL, Aziz T, Brown P (2013) Phase dependent modulation of tremor amplitude in essential tremor through thalamic stimulation. Brain 136:3062–3075.
Cagnan H, Denison T, Mcintyre C, Brown P (2019) Emerging technologies for improved deep brain stimulation. Nat Biotechnol 37 Available at: http://dx.doi.org/10.1038/s41587-019-0244-6.
Cagnan H, Duff EP, Brown P (2015) The relative phases of basal ganglia activities dynamically shape effective connectivity in Parkinson's disease. Brain 138:1667–1678.
Cagnan H, Gerloff C, Engel AK, Hamel W, Magill PJ (2018a) Temporal evolution of beta bursts in the parkinsonian cortico-basal ganglia network. :1–28.
Cagnan H, Mallet N, Moll CKE, Gulberti A, Westphal M, Gerloff C, Engel AK, Hamel W, Magill PJ, Brown P, Sharott A (2018b) Temporal evolution of beta bursts in the parkinsonian cortico-basal ganglia network. PNAS:458414 Available at: https://www.biorxiv.org/content/early/2018/10/31/458414.
Cagnan H, Pedrosa D, Little S, Pogosyan A, Cheeran B, Aziz T, Green A, Fitzgerald J,

Foltynie T, Limousin P, Zrinzo L, Hariz M, Friston KJ, Denison T, Brown P (2016) Stimulating at the right time: phase-specific deep brain stimulation. Brain:1–14 Available at: http://fdslive.oup.com/www.oup.com/pdf/production_in_progress.pdf.

Calabresi P, Picconi B, Tozzi A, Ghiglieri V, Di Filippo M (2014) Direct and indirect pathways of basal ganglia: A critical reappraisal. Nat Neurosci 17:1022–1030 Available at: http://dx.doi.org/10.1038/nn.3743.

Canolty, R T KR (2012) The functional role of cross-frequncy coupling. Trends Cogn Sci 14:506–515 Available at: http://www.pubmedcentral.nih.gov/articlerender.fcgi?artid=3359652&tool=pmcentrez&rendertype=abstract.

Canolty RT, Edwards E, Dalal SS, Soltani M, Nagarajan SS, Berger MS, Barbaro NM, Knight RT (2006) High Gamma Power Is Phase-Locked to Theta. Science (80-) 1128115:313 Available at: ftp://ftp.sourcesignal.com/aos/Canolty Gamma Theta Science 2006.pdf.

Canolty RT, Knight RT (2010) The functional role of cross-frequency coupling. Trends Cogn Sci 14:506–515 Available at: http://dx.doi.org/10.1016/j.tics.2010.09.001.

Carracedo LM, Kjeldsen H, Cunnington L, Jenkins A, Schofield I, Cunningham MO, Davies CH, Traub RD, Whittington MA (2013) A Neocortical Delta Rhythm Facilitates Reciprocal Interlaminar Interactions via Nested Theta Rhythms. J Neurosci 33:10750–10761 Available at: http://www.jneurosci.org/cgi/doi/10.1523/JNEUROSCI.0735-13.2013.

Castrioto A (2011) Ten-Year Outcome of Subthalamic Stimulation in Parkinson Disease. Arch Neurol 68:1550 Available at: http://archneur.jamanetwork.com/article.aspx?doi=10.1001/archneurol.2011.182.

Castrioto A, Lhommée E, Moro E, Krack P (2014) Mood and behavioural effects of subthalamic stimulation in Parkinson's disease. Lancet Neurol 13:287–305.

Chen CC, Brücke C, Kempf F, Kupsch A, Lu CS, Lee ST, Tisch S, Limousin P, Hariz M, Brown P (2006) Deep brain stimulation of the subthalamic nucleus: a two-edged sword. Curr Biol 16:R952-3 Available at: http://www.ncbi.nlm.nih.gov/pubmed/17113373.

Cohen MX (2008) Assessing transient cross-frequency coupling in EEG data. J Neurosci Methods 168:494–499.

Cohen MX (2014) Analyzing Neural Time Series Data: Theory and Practice. Cambridge, Massachusetts MIT Press.

Cohen MX, Axmacher N, Lenartz D, Elger CE, Sturm V, Schlaepfer TE (2009) Good vibrations: cross-frequency coupling in the human nucleus accumbens during reward processing. J Cogn Neurosci 21:875–889 Available at: http://www.mitpressjournals.org/doi/abs/10.1162/jocn.2009.21062%5Cnpapers3://publication/doi/10.1162/jocn.2009.21062.

Cole S, Voytek B (2016) Brain oscillations and the importance of waveform shape. Trends Cogn Sci 21:137–149 Available at: http://dx.doi.org/10.1016/j.tics.2016.12.008.

Cole SR, van der Meij R, Peterson EJ, de Hemptinne C, Starr PA, Voytek B (2017) Nonsinusoidal beta oscillations reflect cortical pathophysiology in Parkinson's disease. J Neurosci 37:2208–2216 Available at: http://www.jneurosci.org/lookup/doi/10.1523/JNEUROSCI.2208-16.2017.

Colgin LL, Denninger T, Fyhn M, Hafting T, Bonnevie T, Jensen O, Moser M-BB, Moser EI (2009) Frequency of gamma oscillations routes flow of information in the hippocampus. Nature 462:353–357 Available at:

http://www.nature.com/doifinder/10.1038/nature08573.
Combrisson E, Perrone-Bertolotti M, Soto JL, Alamian G, Kahane P, Lachaux JP, Guillot A, Jerbi K (2017) From intentions to actions: Neural oscillations encode motor processes through phase, amplitude and phase-amplitude coupling. Neuroimage 147:473–487 Available at: http://dx.doi.org/10.1016/j.neuroimage.2016.11.042.
Connolly AT, Jensen AL, Bello EM, Netoff TI, Baker KB, Johnson MD, Vitek JL (2015) Modulations in oscillatory frequency and coupling in globus pallidus with increasing Parkinsonian severity. J Neurosci 35:6231–6240.
Cui G, Jun SB, Jin X, Pham MD, Vogel SS, Lovinger DM, Costa RM, Guohong C (2013) Concurrent activation of striatal direct and indirect pathways during action initiation. Nature 494:238–242 Available at: http://www.nature.com/doifinder/10.1038/nature11846.
de Hemptinne C, Ryapolova-Webb ES, Air EL, Garcia PA, Miller KJ, Ojemann JG, Ostrem JL, Galifianakis NB, Starr PA (2013) Exaggerated phase-amplitude coupling in the primary motor cortex in Parkinson disease. Proc Natl Acad Sci U S A 110:4780–4785 Available at: http://www.pnas.org/content/110/12/4780.abstract.
de Hemptinne C, Swann NC, Ostrem JL, Ryapolova-Webb ES, San Luciano M, Galifianakis NB, Starr P a (2015) Therapeutic deep brain stimulation reduces cortical phase-amplitude coupling in Parkinson's disease. Nat Neurosci 18:779–786 Available at: http://dx.doi.org/10.1038/nn.3997.
Deffains M, Iskhakova L, Katabi S, Israel Z, Bergman H (2018) Longer β oscillatory episodes reliably identify pathological subthalamic activity in Parkinsonism. Mov Disord 33:1609–1618 Available at: http://doi.wiley.com/10.1002/mds.27418.
Deisseroth K (2015) Optogenetics: 10 years of microbial opsins in neuroscience. Nat Neurosci 18:1213–1225 Available at: http://www.nature.com/doifinder/10.1038/nn.4091.
DeLong MR (1990) Primate models of movement disorders of basal ganglia origin. Trends Neurosci 13:281–285.
Deuschl G et al. (2006a) A Randomized Trial of Deep-Brain Stimulation for Parkinson's Disease. N Engl J Med 355:896–908 Available at: http://www.nejm.org/doi/abs/10.1056/NEJMoa060281.
Deuschl G, Herzog J, Kleiner-Fisman G, Kubu C, Lozano AM, Lyons KE, Rodriguez-Oroz MC, Tamma F, Tröster AI, Vitek JL, Volkmann J, Voon V (2006b) Deep brain stimulation: Postoperative issues. Mov Disord 21.
Devergnas A, Caiola M, Pittard D, Wichmann T (2017) Cortical Phase–Amplitude Coupling in a Progressive Model of Parkinsonism in Nonhuman Primates. Cereb Cortex:1–11 Available at: http://academic.oup.com/cercor/advance-article/doi/10.1093/cercor/bhx314/4668704.
Di Biase L, Brittain JS, Shah SA, Pedrosa DJ, Cagnan H, Mathy A, Chen CC, Martín-Rodríguez JF, Mir P, Timmerman L, Schwingenschuh P, Bhatia K, Di Lazzaro V, Brown P (2017) Tremor stability index: A new tool for differential diagnosis in tremor syndromes. Brain 140:1977–1986.
Dowsett J, Herrmann CS (2016) Transcranial alternating current stimulation with sawtooth waves: Simultaneous stimulation and EEG recording. Front Hum Neurosci 10:1–10.
Doyle LMF, Kühn AA, Hariz M, Kupsch A, Schneider GH, Brown P (2005) Levodopa-induced modulation of subthalamic beta oscillations during self-paced movements in patients with Parkinson's disease. Eur J Neurosci 21:1403–1412.
Dubey A, Ray S (2019) Cortical electrocorticogram (Ecog) is a local signal. J Neurosci

39:4299–4311.
Duyx B, Urlings MJE, Swaen GMH, Bouter LM, Zeegers MP (2017) Scientific citations favor positive results: a systematic review and meta-analysis. J Clin Epidemiol 88:92–101 Available at: http://dx.doi.org/10.1016/j.jclinepi.2017.06.002.
Einevoll GT, Kayser C, Logothetis NK, Panzeri S (2013) Modelling and analysis of local field potentials for studying the function of cortical circuits. Nat Rev Neurosci 14:770–785 Available at: http://www.nature.com/doifinder/10.1038/nrn3599.
Einevoll GT, Pettersen KH, Devor A, Ulbert I, Halgren E, Dale AM (2007) Laminar population analysis: Estimating firing rates and evoked synaptic activity from multielectrode recordings in rat barrel cortex. J Neurophysiol 97:2174–2190.
Engel AK, Fries P (2010) Beta-band oscillations-signalling the status quo? Curr Opin Neurobiol 20:156–165.
Engel AK, Moll CKE, Fried I, Ojemann GA (2005) Invasive recordings from the human brain: Clinical insights and beyond. Nat Rev Neurosci 6:35–47.
Escobar D, Johnson LA, Nebeck SD, Zhang J, Johnson MD, Baker KB, Molnar GF, Vitek JL (2017) Parkinsonism and Vigilance: Alteration in neural oscillatory activity and phase-amplitude coupling in the basal ganglia and motor cortex. J Neurophysiol Available at: http://jn.physiology.org/content/early/2017/08/21/jn.00388.2017.
Eusebio A, Pogosyan A, Wang S, Averbeck B, Gaynor LD, Cantiniaux S, Witjas T, Limousin P, Azulay JP, Brown P (2009) Resonance in subthalamo-cortical circuits in Parkinsons disease. Brain 132:2139–2150.
Feingold J, Gibson DJ, DePasquale B, Graybiel AM (2015) Bursts of beta oscillation differentiate postperformance activity in the striatum and motor cortex of monkeys performing movement tasks. Proc Natl Acad Sci 112:13687–13692.
Fischer P, Chen CC, Chang YJ, Yeh CH, Pogosyan A, Herz DM, Cheeran B, Green AL, Aziz TZ, Hyam J, Little S, Foltynie T, Limousin P, Zrinzo L, Hasegawa H, Samuel M, Ashkan K, Brown P, Tan H (2018) Alternating modulation of subthalamic nucleus beta oscillations during stepping. J Neurosci 38:5111–5121.
Fischer P, Pogosyan A, Green AL, Aziz TZ, Hyam J, Foltynie T, Limousin P, Zrinzo L, Samuel M, Ashkan K, Da Lio M, De Cecco M, Fornaser A, Brown P, Tan H (2019) Beta synchrony in the cortico-basal ganglia network during regulation of force control on and off dopamine. Neurobiol Dis 127:253–263 Available at: https://doi.org/10.1016/j.nbd.2019.03.004.
FitzGerald THB, Valentin A, Selway R, Richardson MP (2013) Cross-frequency coupling within and between the human thalamus and neocortex. Front Neuroeng 7:1–13.
Ford B, Winfield L, Pullman SL, Frucht SJ, Du Y, Greene P, Cheringal JH, Yu Q, Cote LJ, Fahn S, McKhann GM, Goodman RR (2004) Subthalamic nucleus stimulation in advanced Parkinson's disease: blinded assessments at one year follow up. J Neurol Neurosurg Psychiatry 75:1255–1259 Available at: http://www.pubmedcentral.nih.gov/articlerender.fcgi?artid=1739226&tool=pmcentrez&rendertype=abstract.
Frank MJ (2007) Hold Your Horses: Impulsivity, Deep Brain Stimulation, and Medication in Parkinsonism. Science (80-) 1309:1309–1312 Available at: http://www.ncbi.nlm.nih.gov/pubmed/17962524.
Fries P (2005) A mechanism for cognitive dynamics: neuronal communication through neuronal coherence. Trends Cogn Sci 9:474–480 Available at:

https://www.sciencedirect.com/science/article/pii/S1364661305002421 [Accessed September 11, 2019].
Fries P (2015) Rhythms for Cognition: Communication through Coherence. Neuron 88:220–235 Available at: http://dx.doi.org/10.1016/j.neuron.2015.09.034.
Fujimoto K, Kita H (1993) Response characteristics of subthalamic neurons to the stimulation of the sensorimotor cortex in the rat. Brain Res 609:185–192 Available at: https://linkinghub.elsevier.com/retrieve/pii/000689939390872K.
Fujiyama F, Sohn J, Nakano T, Furuta T, Nakamura KC, Matsuda W, Kaneko T (2011) Exclusive and common targets of neostriatofugal projections of rat striosome neurons: A single neuron-tracing study using a viral vector. Eur J Neurosci 33:668–677.
Gale JT, Shields DC, Jain FA, Amirnovin R, Eskandar EN (2009) Subthalamic nucleus discharge patterns during movement in the normal monkey and Parkinsonian patient. Brain Res 1260:15–23 Available at: https://www.sciencedirect.com/science/article/pii/S0006899308031375?via%3Dihub [Accessed September 12, 2019].
Galvan A, Stauffer WR, Acker L, El-Shamayleh Y, Inoue KI, Ohayon S, Schmid MC (2017) Nonhuman primate optogenetics: Recent advances and future directions. J Neurosci 37:10894–10903.
Ghahramani Z (2015) Probabilistic machine learning and artificial intelligence. Nature 521:452–459.
Gövert F, Deuschl G (2015) Tremor entities and their classification. Curr Opin Neurol:1 Available at: http://content.wkhealth.com/linkback/openurl?sid=WKPTLP:landingpage&an=00019052-900000000-99421.
Gradinaru V, Thompson KR, Deisseroth K (2008) eNpHR: a Natronomonas halorhodopsin enhanced for optogenetic applications. Brain Cell Biol 36:129–139 Available at: http://link.springer.com/10.1007/s11068-008-9027-6.
Gradinaru V, Zhang F, Ramakrishnan C, Mattis J, Prakash R, Diester I, Goshen I, Thompson KR, Deisseroth K (2010) Molecular and Cellular Approaches for Diversifying and Extending Optogenetics. Cell 141:154–165.
Grill WM, Snyder AN, Miocinovic S (2004) Deep brain stimulation creates an informational lesion of the stimulated nucleus. Neuroreport 15:1137–1140.
Groenewegen HJ, Wright CI, Beijer AVJ, Voorn P (1999) Convergence and segregation of ventral striatal inputs and outputs. Ann N Y Acad Sci 877:49–63.
Grosenick L, Marshel JH, Deisseroth K (2015) Closed-loop and activity-guided optogenetic control. Neuron 86:106–139 Available at: http://dx.doi.org/10.1016/j.neuron.2015.03.034.
Hamani C, Saint-Cyr JA, Fraser J, Kaplitt M, Lozano AM (2004) The subthalamic nucleus in the context of movement disorders. Brain 127:4–20.
Hariz M (2014) Deep brain stimulation: new techniques. Park Realt Disord 20:S192–S196 Available at: http://dx.doi.org/10.1016/S1353-8020(13)70045-2.
Hauptmann C, Tass PA (2007) Therapeutic rewiring by means of desynchronizing brain stimulation. BioSystems 89:173–181.
Hemptinne C De, Swann N, Ostrem JL, Ryapolova-webb ES, Luciano S, Galifianakis N, Starr PA, Francisco S, Francisco S, Francisco S (2015) HHS Public Access. 18:779–786.
Herkenham M (1980) Laminar organization of thalamic projections to the rat neocortex. Science (80-) 207:532–535 Available at: http://www.sciencemag.org/cgi/doi/10.1126/science.7352263.

Herman AM, Huang L, Murphey DK, Garcia I, Arenkiel BR (2014) Cell type-specific and time-dependent light exposure contribute to silencing in neurons expressing Channelrhodopsin-2: (A) Crh-Cre+/−; ROSALSL-ChR2-EYFP mice express the ChR2-EYFP fusion protein in CRH-expressing interneurons of the external plexiform lay. Elife 3:1–18.

Herrington T, Cheng JJ, Eskandar EN (2015) Mechanisms of deep brain stimulation. J Neurophysiol 17:19–38.

Herz DM, Little S, Pedrosa DJ, Tinkhauser G, Cheeran B, Foltynie T, Bogacz R, Brown P (2018) Mechanisms Underlying Decision-Making as Revealed by Deep-Brain Stimulation in Patients with Parkinson's Disease. Curr Biol 28:1169-1178.e6 Available at: https://www.sciencedirect.com/science/article/pii/S0960982218302422?via%3Dihub [Accessed September 10, 2019].

Hill JN, Gupta D, Brunner P, Gunduz A, Adamo MA, Ritaccio A, Schalk G (2012) Recording human electrocorticographic (ECoG) signals for neuroscientific research and real-time functional cortical mapping. J Vis Exp:1–5.

Holgado AJN, Terry JR, Bogacz R (2010) Conditions for the Generation of Beta Oscillations in the Subthalamic Nucleus–Globus Pallidus Network. Int J Environ Waste Manag 10 Available at: http://www.inderscience.com/link.php?id=46395.

Holt AB, Kormann E, Gulberti A, Pötter-Nerger M, McNamara CG, Cagnan H, Baaske MK, Little S, Köppen JA, Buhmann C, Westphal M, Gerloff C, Engel AK, Brown P, Hamel W, Moll CKE, Sharott A (2019) Phase-dependent suppression of beta oscillations in parkinson's disease patients. J Neurosci 39:1119–1134.

Huebl J, Brücke C, Schneider GH, Blahak C, Krauss JK, Kühn AA (2015) Bradykinesia induced by frequency-specific pallidal stimulation in patients with cervical and segmental dystonia. Park Relat Disord 21:800–803 Available at: http://dx.doi.org/10.1016/j.parkreldis.2015.04.023.

Humphries MD, Gurney KN (2001) A pulsed neural network model of bursting in the basal ganglia. Neural Networks 14:845–863.

Iwamuro H, Tachibana Y, Ugawa Y, Saito N, Nambu A (2017) Information processing from the motor cortices to the subthalamic nucleus and globus pallidus and their somatotopic organizations revealed electrophysiologically in monkeys. Eur J Neurosci 46:2684–2701.

Jackson N, Cole SR, Voytek B, Swann NC (2019) Characteristics of waveform shape in Parkinson's disease detected with scalp electroencephalography. eNeuro 6:1–11.

Jensen O, Spaak E, Park H (2016) Discriminating valid from spurious indices of phase-amplitude coupling. Eneuro 3:ENEURO.0334-16.2016 Available at: http://eneuro.sfn.org/lookup/doi/10.1523/ENEURO.0334-16.2016.

Johnson LA, Nebeck SD, Muralidharan A, Johnson MD, Baker KB, Vitek JL (2016) Closed-Loop Deep Brain Stimulation Effects on Parkinsonian Motor Symptoms in a Non-Human Primate – is Beta Enough? Brain Stimul 9:892–896 Available at: http://dx.doi.org/10.1016/j.brs.2016.06.051.

Jones SR (2016) When brain rhythms aren't 'rhythmic': implication for their mechanisms and meaning. Curr Opin Neurobiol.

Keebaugh AC, Barrett CE, LaPrairie JL, Jenkins JJ, Young LJ (2015) RNAi knockdown of oxytocin receptor in the nucleus accumbens inhibits social attachment and parental care in monogamous female prairie voles. Soc Neurosci:150415084538009 Available at: http://www.tandfonline.com/doi/full/10.1080/17470919.2015.1040893.

Khanna P, Carmena JM (2017) Beta band oscillations in motor cortex reflect neural

population signals that delay movement onset. Elife 6:1–31.
Kim S, Kwon S-H, Kam T-I, Panicker N, Karuppagounder SS, Lee S, Lee JH, Kim WR, Kook M, Foss CA, Shen C, Lee H, Kulkarni S, Pasricha PJ, Lee G, Pomper MG, Dawson VL, Dawson TM, Ko HS (2019) Transneuronal Propagation of Pathologic α-Synuclein from the Gut to the Brain Models Parkinson's Disease. Neuron 103:627-641.e7 Available at: https://doi.org/10.1016/j.neuron.2019.05.035.
Kitai ST, Deniau JM (1981) Cortical inputs to the subthalamus: intracellular analysis. Brain Res 214:411–415 Available at: https://linkinghub.elsevier.com/retrieve/pii/000689938191204X.
Klapoetke NC et al. (2014) Independent optical excitation of distinct neural populations. Nat Methods 11:338–346 Available at: https://linkinghub.elsevier.com/retrieve/pii/S0959438809001263.
Kleiner-Fisman G, Herzog J, Fisman DN, Tamma F, Lyons KE, Pahwa R, Lang AE, Deuschl G (2006) Subthalamic nucleus deep brain stimulation: Summary and meta-analysis of outcomes. Mov Disord 21:290–304.
Knudsen K, Fedorova TD, Hansen AK, Sommerauer M, Otto M, Svendsen KB, Nahimi A, Stokholm MG, Pavese N, Beier CP, Brooks DJ, Borghammer P (2018) In-vivo staging of pathology in REM sleep behaviour disorder: a multimodality imaging case-control study. Lancet Neurol 17:618–628 Available at: http://www.ncbi.nlm.nih.gov/pubmed/29866443 [Accessed September 11, 2019].
Kondabolu K, Roberts EA, Bucklin M, McCarthy MM, Kopell N, Han X (2016) Striatal cholinergic interneurons generate beta and gamma oscillations in the corticostriatal circuit and produce motor deficits. Proc Natl Acad Sci 113:E3159–E3168 Available at: http://www.pnas.org/lookup/doi/10.1073/pnas.1605658113.
Kozai TDY, Vazquez AL (2015) Photoelectric artefact from optogenetics and imaging on microelectrodes and bioelectronics: new challenges and opportunities. J Mater Chem B 3:4965–4978 Available at: http://xlink.rsc.org/?DOI=C5TB00108K.
Kramer MA, Tort ABL, Kopell NJ (2008) Sharp edge artifacts and spurious coupling in EEG frequency comodulation measures. J Neurosci Methods 170:352–357.
Kravitz A V., Freeze BS, Parker PRL, Kay K, Thwin MT, Deisseroth K, Kreitzer AC (2010) Regulation of parkinsonian motor behaviours by optogenetic control of basal ganglia circuitry. Nature 466:622–626.
Kravitz A V., Freeze BS, Parker PRLL, Kay K, Myo T, Deisseroth K, Kreitzer AC, Kreitzer AC, Thwin MT, Deisseroth K, Kreitzer AC (2013) Regulation of Parkinsonian motor behaviors by optogenetic control of basal ganglia circuitry. Nature 67:622–626 Available at: http://dx.doi.org/10.1038/nature09159.
Kress GJ, Yamawaki N, Wokosin DL, Wickersham IR, Shepherd GMG, Surmeier DJ (2013) Convergent cortical innervation of striatal projection neurons. Nat Neurosci 16:665–667 Available at: http://dx.doi.org/10.1038/nn.3397.
Kühn AA, Kempf F, Brücke C, Doyle LG, Martinez-Torres I, Pogosyan A, Trottenberg T, Kupsch A, Schneider G-H, Hariz MI, Vandenberghe W, Nuttin B, Brown P (2008) High-Frequency Stimulation of the Subthalamic Nucleus Suppresses Oscillatory β Activity in Patients with Parkinson's Disease in Parallel with Improvement in Motor Performance. J Neurosci 28:6165–6173 Available at: http://www.jneurosci.org/content/28/24/6165%5Cnhttp://www.jneurosci.org/content/28/24/6165.full.pdf%5Cnhttp://www.jneurosci.org/content/28/24/6165.long%5Cnhttp://www.ncbi.nlm.nih.gov/pubmed/18550758.
Kühn AA, Kupsch A, Schneider GH, Brown P (2006) Reduction in subthalamic 8-35 Hz oscillatory activity correlates with clinical improvement in Parkinson's disease.

Eur J Neurosci 23:1956–1960.
Kühn AA, Tsui A, Aziz T, Ray N, Brücke C, Kupsch A, Schneider GH, Brown P (2009) Pathological synchronisation in the subthalamic nucleus of patients with Parkinson's disease relates to both bradykinesia and rigidity. Exp Neurol 215:380–387 Available at: http://dx.doi.org/10.1016/j.expneurol.2008.11.008.
Kühn AA, Volkmann J (2016) Innovations in deep brain stimulation methodology. Mov Disord 00:1–9 Available at: http://doi.wiley.com/10.1002/mds.26703.
Kühn AA, Volkmann J (2017) Innovations in deep brain stimulation methodology. Mov Disord 32:11–19.
Kühn AA, Williams D, Kupsch A, Limousin P, Hariz M, Schneider GH, Yarrow K, Brown P (2004) Event-related beta desynchronization in human subthalamic nucleus correlates with motor performance. Brain 127:735–746.
Kupsch A et al. (2006) Pallidal deep-brain stimulation in primary generalized or segmental dystonia. N Engl J Med 355:1978–1990.
Kuramoto E, Furuta T, Nakamura KC, Unzai T, Hioki H, Kaneko T (2009) Two types of thalamocortical projections from the motor thalamic nuclei of the rat: A single neuron-tracing study using viral vectors. Cereb Cortex 19:2065–2077.
Kuramoto E, Ohno S, Furuta T, Unzai T, Tanaka YR, Hioki H, Kaneko T (2015) Ventral medial nucleus neurons send thalamocortical afferents more widely and more preferentially to layer 1 than neurons of the ventral anterior-ventral lateral nuclear complex in the rat. Cereb Cortex 25:221–235.
Lempka SF, Miocinovic S, Johnson MD, Vitek JL, Mcintyre CC, Engineering B, Foundation CC (2010) In vivo impedance spectroscopy of deep brain stimulation electrodes. 6:1–20.
Levy R, Dostrovsky JO, Lang AE, Sime E, Hutchison WD, Lozano AM (2001) Effects of apomorphine on subthalamic nucleus and globus pallidus internus neurons in patients with Parkinson's disease. J Neurophysiol 86:249–260.
Libbrecht S, Van den Haute C, Malinouskaya L, Gijsbers R, Baekelandt V (2017) Evaluation of WGA–Cre-dependent topological transgene expression in the rodent brain. Brain Struct Funct 222:717–733.
Lipski WJ, Wozny TA, Alhourani A, Kondylis E, Turner RS, Crammond DJ, Richardson RM (2017) Dynamics of human subthalamic neuron phase-locking to motor and sensory cortical oscillations during movement. J Neurophysiol:jn.00964.2016 Available at: http://www.ncbi.nlm.nih.gov/pubmed/28592690%0Ahttp://jn.physiology.org/lookup/doi/10.1152/jn.00964.2016.
Little S, Beudel M, Zrinzo L, Foltynie T, Limousin P, Hariz M, Neal S, Cheeran B, Cagnan H, Gratwicke J, Aziz TZ, Pogosyan A, Brown P (2015) Bilateral adaptive deep brain stimulation is effective in Parkinson's disease. J Neurol Neurosurg Psychiatry:jnnp-2015-310972 Available at: http://jnnp.bmj.com/lookup/doi/10.1136/jnnp-2015-310972.
Little S, Brown P (2012) What brain signals are suitable for feedback controzl of deep brain stimulation in Parkinson's disease? Ann N Y Acad Sci 1265:9–24.
Little S, Brown P (2014) Focusing brain therapeutic interventions in space and time for Parkinson's disease. Curr Biol 24:R898–R909 Available at: http://dx.doi.org/10.1016/j.cub.2014.08.002.
Little S, Pogosyan A, Neal S, Zavala B, Zrinzo L, Hariz M, Foltynie T, Limousin P, Ashkan K, Fitzgerald J, Green AL, Aziz TZ, Brown P (2013) Adaptive deep brain stimulation in advanced Parkinson disease. Ann Neurol:449–457.
Little S, Tripoliti E, Beudel M, Pogosyan A, Cagnan H, Herz D, Bestmann S, Aziz T,

Cheeran B, Zrinzo L, Hariz M, Hyam J, Limousin P, Foltynie T, Brown P (2016) Adaptive deep brain stimulation for Parkinson's disease demonstrates reduced speech side effects compared to conventional stimulation in the acute setting. J Neurol Neurosurg Psychiatry 0:jnnp-2016-313518 Available at: http://jnnp.bmj.com/lookup/doi/10.1136/jnnp-2016-313518.

Lofredi R, Neumann WJ, Brücke C, Huebl J, Krauss JK, Schneider GH, Kühn AA (2018) Pallidal beta bursts in Parkinson's disease and dystonia. Mov Disord:1–5.

Lopez-Azcarate J, Tainta M, Rodriguez-Oroz MC, Valencia M, Gonzalez R, Guridi J, Iriarte J, Obeso JA, Artieda J, Alegre M (2010) Coupling between beta and high-frequency activity in the human subthalamic nucleus may be a pathophysiological mechanism in Parkinson's disease. J Neurosci 30:6667–6677 Available at: http://www.ncbi.nlm.nih.gov/pubmed/20463229.

Lozano-Soldevilla D, Huurne N, Oostenveld R (2016) Neuronal Oscillations with Non-sinusoidal Morphology Produce Spurious Phase-to-Amplitude Coupling and Directionality. Front Comput Neurosci 10:1–17.

Lundqvist M, Rose J, Herman P, Brincat SL, Buschman TJ, Miller EK (2016) Gamma and Beta Bursts Underlie Working Memory. Neuron 90:152–164 Available at: http://dx.doi.org/10.1016/j.neuron.2016.02.028.

Ly TT, Weinzimer SA, Maahs DM, Sherr JL, Roy A, Grosman B, Cantwell M, Kurtz N, Carria L, Messer L, von Eyben R, Buckingham BA (2016) Automated hybrid closed-loop control with a proportional-integral-derivative based system in adolescents and adults with type 1 diabetes: individualizing settings for optimal performance. Pediatr Diabetes:1–8 Available at: http://doi.wiley.com/10.1111/pedi.12399.

Malekmohammadi M, Elias WJ, Pouratian N (2015) Human thalamus regulates cortical activity via spatially specific and structurally constrained phase-amplitude coupling. Cereb Cortex 25:1618–1628.

Malekmohammadi M, Herron J, Velisar A, Blumenfeld Z, Trager MH, Chizeck HJ, Bront??-Stewart H (2016) Kinematic Adaptive Deep Brain Stimulation for Resting Tremor in Parkinson's Disease. Mov Disord 31:426–428.

Mallet N, Pogosyan A, Marton LF, Bolam JP, Brown P, Magill PJ (2008a) Parkinsonian Beta Oscillations in the External Globus Pallidus and Their Relationship with Subthalamic Nucleus Activity. J Neurosci 28:14245–14258 Available at: http://www.jneurosci.org/cgi/doi/10.1523/JNEUROSCI.4199-08.2008.

Mallet N, Pogosyan A, Sharott A, Csicsvari J, Bolam JP, Brown P, Magill PJ (2008b) Disrupted Dopamine Transmission and the Emergence of Exaggerated Beta Oscillations in Subthalamic Nucleus and Cerebral Cortex. J Neurosci 28:4795–4806 Available at: http://www.jneurosci.org/cgi/doi/10.1523/JNEUROSCI.0123-08.2008.

Manning JR, Jacobs J, Fried I, Kahana MJ (2009) Broadband Shifts in Local Field Potential Power Spectra Are Correlated with Single-Neuron Spiking in Humans. J Neurosci 29:13613–13620 Available at: http://www.jneurosci.org/cgi/doi/10.1523/JNEUROSCI.2041-09.2009.

McIntyre CC, Chaturvedi A, Shamir RR, Lempka SF (2015) Engineering the Next Generation of Clinical Deep Brain Stimulation Technology. Brain Stimul 8:21–26.

McIntyre CC, Hahn PJ (2010) Network perspectives on the mechanisms of deep brain stimulation. Neurobiol Dis 38:329–337 Available at: http://dx.doi.org/10.1016/j.nbd.2009.09.022.

Meidahl AC, Moll CKE, van Wijk BCM, Gulberti A, Tinkhauser G, Westphal M, Engel AK, Hamel W, Brown P, Sharott A (2019) Synchronised spiking activity underlies

phase amplitude coupling in the subthalamic nucleus of Parkinson's disease patients. Neurobiol Dis 127:101–113.
Meidahl AC, Tinkhauser G, Herz DM, Cagnan H, Debarros J, Brown P (2017) Adaptive Deep Brain Stimulation for Movement Disorders: The Long Road to Clinical Therapy. Mov Disord 32:810–819 Available at: http://doi.wiley.com/10.1002/mds.27022.
Mestre TA, Lang AE, Okun MS (2016) Factors influencing the outcome of deep brain stimulation: Placebo, nocebo, lessebo, and lesion effects. Mov Disord 31:290–298.
Miesenböck G (2011) Optogenetic Control of Cells and Circuits. Annu Rev Cell Dev Biol 27:731–758 Available at: http://www.annualreviews.org/doi/10.1146/annurev-cellbio-100109-104051.
Mink JW (1996) The basal ganglia: Focused selection and inhibition of competing motor programs. Prog Neurobiol 50:381–425.
Minlebaev M, Colonnese M, Tsintsadze T, Sirota A, Khazipov R (2011) Early Gamma Oscillations Synchronize Developing Thalamus and Cortex. Science (80-) 334:226–229.
Mirzaei A, Kumar A, Leventhal D, Mallet N, Aertsen A, Berke J, Schmidt R (2017) Sensorimotor processing in the basal ganglia leads to transient beta oscillations during behavior. J Neurosci 37:11220–11232.
Mlinarić A, Horvat M, Šupak Smolčić V (2017) Dealing with the positive publication bias: Why you should really publish your negative results. Biochem Medica 27:1–6 Available at: http://www.biochemia-medica.com/en/journal/27/3/10.11613/BM.2017.030201.
Monakow KH, Akert K, K□nzle H (1978) Projections of the precentral motor cortex and other cortical areas of the frontal lobe to the subthalamic nucleus in the monkey. Exp Brain Res 33 Available at: http://link.springer.com/10.1007/BF00235561.
Moran A, Bar-Gad I, Bergman H, Israel Z (2006) Real-time refinement of subthalamic nucleus targeting using Bayesian decision-making on the root mean square measure. Mov Disord 21:1425–1431.
Moses DA, Leonard MK, Makin JG, Chang EF (2019) Real-time decoding of question-and-answer speech dialogue using human cortical activity. Nat Commun 10 Available at: http://dx.doi.org/10.1038/s41467-019-10994-4.
Muller L, Piantoni G, Koller D, Cash SS, Halgren E, Sejnowski TJ (2016) Rotating waves during human sleep spindles organize global patterns of activity that repeat precisely through the night. Elife 5:1–16.
Muthuraman M, Tamas G, Hellriegel H, Deuschl G, Raethjen J (2012) Source analysis of beta-synchronisation and cortico-muscular coherence after movement termination based on high resolution electroencephalography. PLoS One 7:1–8.
Nagel G, Szellas T, Huhn W, Kateriya S, Adeishvili N, Berthold P, Ollig D, Hegemann P, Bamberg E (2003) Channelrhodopsin-2, a directly light-gated cation-selective membrane channel. Proc Natl Acad Sci U S A 100:13940–13945.
Nakamura KC, Sharott A, Magill PJ (2014) Temporal coupling with cortex distinguishes spontaneous neuronal activities in identified basal ganglia-recipient and cerebellar-recipient zones of the motor thalamus. Cereb Cortex 24:81–97.
Nambu A (2008) Seven problems on the basal ganglia. Curr Opin Neurobiol 18:595–604.
Nambu A, Takada M, Inase M, Tokuno H (1996) Dual somatotopical representations in the primate subthalamic nucleus: Evidence for ordered but reversed body-map transformations from the primary motor cortex and the supplementary motor area.

J Neurosci 16:2671–2683.
Nambu A, Tokuno H, Hamada I, Kita H, Imanishi M, Akazawa T, Ikeuchi Y, Hasegawa N (2000) Excitatory conical inputs to pallidal neurons via the subthalamic nucleus in the monkey. J Neurophysiol 84:289–300.
Nambu A, Tokuno H, Takada M (2002) Functional significance of the cortico-subthalamo-pallidal "hyperdirect" pathway. Neurosci Res 43:111–117.
Nelson AB, Kreitzer AC (2014) Reassessing Models of Basal Ganglia Function and Dysfunction. Annu Rev Neurosci 37:117–135.
Neumann W-J, Degen K, Schneider G-H, Brücke C, Huebl J, Brown P, Kühn AA (2016) Subthalamic synchronized oscillatory activity correlates with motor impairment in patients with Parkinson's disease. Mov Disord 00:1–4 Available at: http://doi.wiley.com/10.1002/mds.26759.
Neumann W, Turner RS, Blankertz B, Mitchell T, Kühn AA, Richardson RM (2019) Toward Electrophysiology-Based Intelligent Adaptive Deep Brain Stimulation for Movement Disorders. Neurotherapeutics 16:105–118 Available at: http://link.springer.com/10.1007/s13311-018-00705-0.
Nicolai C Von, Engler G, Sharott A, Engel AK, Moll CK, Siegel M (2014) Corticostriatal Coordination through Coherent Phase-Amplitude Coupling. 34:5938–5948.
Okun MS, Foote KD (2010) Parkinson's disease DBS: what, when, who and why? The time has come to tailor DBS targets. Expert Rev Neurother 10:1847–1857 Available at: http://www.pubmedcentral.nih.gov/articlerender.fcgi?artid=3076937&tool=pmcentrez&rendertype=abstract.
Opri E, Cernera S, Okun MS, Foote KD, Gunduz A (2019) The Functional Role of Thalamocortical Coupling in the Human Motor Network. J Neurosci:1119–1153 Available at: http://www.jneurosci.org/content/early/2019/08/30/JNEUROSCI.1153-19.2019.abstract.
Osorio I, Frei MG, Sunderam S, Giftakis J, Bhavaraju NC, Schaffner SF, Wilkinson SB (2005) Automated seizure abatement in humans using electrical stimulation. Ann Neurol 57:258–268.
Oswal A, Brown P, Litvak V (2013) Synchronized neural oscillations and the pathophysiology of Parkinson's disease. Curr Opin Neurol 26:662–670 Available at: http://content.wkhealth.com/linkback/openurl?sid=WKPTLP:landingpage&an=00019052-201312000-00012.
Özkurt TE, Butz M, Homburger M, Elben S, Vesper J, Wojtecki L, Schnitzler A (2011) High frequency oscillations in the subthalamic nucleus: A neurophysiological marker of the motor state in Parkinson's disease. Exp Neurol 229:324–331 Available at: http://dx.doi.org/10.1016/j.expneurol.2011.02.015.
Panigrahi B, Martin KA, Li Y, Graves AR, Vollmer A, Olson L, Mensh BD, Karpova AY, Dudman JT (2015) Dopamine Is Required for the Neural Representation and Control of Movement Vigor. Cell 162:1418–1430.
Penny WD, Duzel E, Miller KJ, Ojemann JG (2008) Testing for nested oscillation. J Neurosci Methods 174:50–61 Available at: http://dx.doi.org/10.1016/j.jneumeth.2008.06.035.
Plenz D, Kital ST (1999) A basal ganglia pacemaker formed by the subthalamic nucleus and external globus pallidus. Nature 400:677–682.
Poewe W, Seppi K, Tanner CM, Halliday GM, Brundin P, Volkmann J, Schrag AE,

Lang AE (2017) Parkinson disease. Nat Rev Dis Prim 3:1–21.
Pogosyan A, Gaynor LD, Eusebio A, Brown P (2009) Boosting Cortical Activity at Beta-Band Frequencies Slows Movement in Humans. Curr Biol 19:1637–1641 Available at: https://www.sciencedirect.com/science/article/pii/S0960982209016996?via%3Dihub [Accessed September 12, 2019].
Postuma RB, Berg D, Stern M, Poewe W, Marek K, Litvan I, Deuschl G (2015) MDS Clinical Diagnostic Criteria for Parkinson's Disease. 30 Available at: https://escholarship.org/uc/item/1zd719dv.
Potjans TC, Diesmann M (2012) The Cell-Type Specific Cortical Microcircuit: Relating Structure and Activity in a Full-Scale Spiking Network Model. Cereb Cortex 24:785–806 Available at: https://academic.oup.com/cercor/article-lookup/doi/10.1093/cercor/bhs358.
Pringsheim T, Jette N, Frolkis A, Steeves TDL (2014) The prevalence of Parkinson's disease: A systematic review and meta-analysis. Mov Disord 29:1583–1590 Available at: http://doi.wiley.com/10.1002/mds.25945.
Ray NJ, Jenkinson N, Wang S, Holland P, Brittain JS, Joint C, Stein JF, Aziz T (2008a) Local field potential beta activity in the subthalamic nucleus of patients with Parkinson's disease is associated with improvements in bradykinesia after dopamine and deep brain stimulation. Exp Neurol 213:108–113.
Ray S, Maunsell JHR (2010) Differences in Gamma Frequencies across Visual Cortex Restrict Their Possible Use in Computation. Neuron 67:885–896 Available at: http://dx.doi.org/10.1016/j.neuron.2010.08.004.
Ray S, Niebur E, Hsiao SS, Sinai A, Crone NE (2008b) High-frequency gamma activity (80-150 Hz) is increased in human cortex during selective attention. Clin Neurophysiol 119:116–133.
Redgrave P, Rodriguez M, Smith Y, Rodriguez-Oroz MC, Lehericy S, Bergman H, Agid Y, Delong MR, Obeso JA (2010) Goal-directed and habitual control in the basal ganglia: Implications for Parkinson's disease. Nat Rev Neurosci 11:760–772 Available at: http://dx.doi.org/10.1038/nrn2915.
Reich MM, Brumberg J, Pozzi NG, Marotta G, Roothans J, Åström M, Musacchio T, Lopiano L, Lanotte M, Lehrke R, Buck AK, Volkmann J, Isaias IU (2016) Progressive gait ataxia following deep brain stimulation for essential tremor: adverse effect or lack of efficacy? Brain:aww223 Available at: http://www.brain.oxfordjournals.org/lookup/doi/10.1093/brain/aww223.
Reis C, Sharott A, Magill PJ, van Wijk BCM, Parr T, Zeidman P, Friston KJ, Cagnan H (2019) Thalamocortical dynamics underlying spontaneous transitions in beta power in Parkinsonism. Neuroimage 193:103–114 Available at: https://doi.org/10.1016/j.neuroimage.2019.03.009.
Richardson AG, Liu X, Weigand PK, Hudgins ED, Stein JM, Das SR, Proekt A, Kelz MB, Zhang M, Van der Spiegel J, Lucas TH (2017) Hippocampal gamma-slow oscillation coupling in macaques during sedation and sleep. Hippocampus:1125–1139.
Rosa M, Arlotti M, Ardolino G, Cogiamanian F, Marceglia S, Di Fonzo A, Cortese F, Rampini PM, Priori A (2015) Adaptive deep brain stimulation in a freely moving parkinsonian patient. Mov Disord 30:2014–2016.
Rosa M, Marceglia S, Servello D, Foffani G, Rossi L, Sassi M, Mrakic-Sposta S, Zangaglia R, Pacchetti C, Porta M, Priori A (2010) Time dependent subthalamic local field potential changes after DBS surgery in Parkinson's disease. Exp Neurol 222:184–190 Available at: http://dx.doi.org/10.1016/j.expneurol.2009.12.013.

Rosin B, Slovik M, Mitelman R, Rivlin-Etzion M, Haber SN, Israel Z, Vaadia E, Bergman H (2011) Closed-loop deep brain stimulation is superior in ameliorating parkinsonism. Neuron 72:370–384 Available at: http://dx.doi.org/10.1016/j.neuron.2011.08.023.
Rossi PJ et al. (2016) Proceedings of the third annual deep brain stimulation think tank: A review of emerging issues and technologies. Front Neurosci 10:1–15.
Sanders TH (2016) Phase-amplitude coupling, an indication of bursting in parkinsonism, is masked by periodic pulses. J Neurophysiol 115:1587–1595 Available at: http://jn.physiology.org/lookup/doi/10.1152/jn.00801.2015.
Sanders TH, Jaeger D (2016) Optogenetic stimulation of cortico-subthalamic projections is sufficient to ameliorate bradykinesia in 6-ohda lesioned mice. Neurobiol Dis 95:225–237 Available at: http://dx.doi.org/10.1016/j.nbd.2016.07.021.
Sanes JN, Donoghue JP (1993) Oscillations in local field potentials of the primate motor cortex during voluntary movement. Proc Natl Acad Sci U S A 90:4470–4474 Available at: http://www.ncbi.nlm.nih.gov/pubmed/8506287 [Accessed September 12, 2019].
Savage N (2019) Marriage of mind and machine. Nature 571.
Schapira AHV, Chaudhuri KR, Jenner P (2017) Non-motor features of Parkinson disease. Nat Rev Neurosci 18:435–450 Available at: http://dx.doi.org/10.1038/nrn.2017.62.
Schaworonkow N, Nikulin V V. (2019) Spatial neuronal synchronization and the waveform of oscillations: Implications for EEG and MEG. PLoS Comput Biol 15:1–22.
Scheffer-Teixeira R, Tort ABL (2016) On cross-frequency phase-phase coupling between theta and gamma oscillations in the hippocampus. Elife 5:423–435.
Schlachetzki JCM, Barth J, Marxreiter F, Gossler J, Kohl Z, Reinfelder S, Gassner H, Aminian K, Eskofier BM, Winkler J, Klucken J (2017) Wearable sensors objectively measure gait parameters in Parkinson's disease Toft M, ed. PLoS One 12:e0183989 Available at: https://dx.plos.org/10.1371/journal.pone.0183989 [Accessed September 17, 2019].
Schmitz D, Schuchmann S, Fisahn A, Draguhn A, Buhl EH, Petrasch-Parwez E, Dermietzel R, Heinemann U, Traub RD (2001) Axo-axonal coupling: A novel mechanism for ultrafast neuronal communication. Neuron 31:831–840.
Schuepbach WMM, Rau J, Knudsen K, Volkmann J, Krack P, Timmermann L, Hälbig TD, Hesekamp H, Navarro SM, Meier N, Falk D, Mehdorn M, Paschen S (2013) Neurostimulation for Parkinson's Disease with Early Motor Complication. N Engl J Med 368:610–622 Available at: http://www.nejm.org/doi/pdf/10.1056/NEJMoa1205158.
Seymour RA, Rippon G, Kessler K (2017) The detection of phase amplitude coupling during sensory processing. Front Neurosci 11:1–11.
Shah SA, Tan H, Tinkhauser G, Brown P (2018) Towards Real-Time, Continuous Decoding of Gripping Force from Deep Brain Local Field Potentials. IEEE Trans Neural Syst Rehabil Eng 26:1460–1468.
Sharott A, Gulberti A, Hamel W, Köppen JA, Münchau A, Buhmann C, Pötter-Nerger M, Westphal M, Gerloff C, Moll CKE, Engel AK (2018) Spatio-temporal dynamics of cortical drive to human subthalamic nucleus neurons in Parkinson's disease. Neurobiol Dis 112:49–62.
Sharott A, Gulberti A, Zittel S, Tudor Jones AA, Fickel U, Munchau A, Koppen JA, Gerloff C, Westphal M, Buhmann C, Hamel W, Engel AK, Moll CKE (2014)

Activity Parameters of Subthalamic Nucleus Neurons Selectively Predict Motor Symptom Severity in Parkinson's Disease. J Neurosci 34:6273–6285 Available at: http://www.jneurosci.org/cgi/doi/10.1523/JNEUROSCI.1803-13.2014.
Sharott A, Magill PJ, Harnack D, Kupsch A, Meissner W, Brown P (2005) Dopamine depletion increases the power and coherence of β-oscillations in the cerebral cortex and subthalamic nucleus of the awake rat. Eur J Neurosci 21:1413–1422.
Sharott A, Vinciati F, Nakamura KC, Magill PJ (2017) A population of indirect pathway striatal projection neurons is selectively entrained to parkinsonian beta oscillations. J Neurosci 37:0658–17 Available at: http://www.jneurosci.org.insb.bib.cnrs.fr/content/early/2017/08/28/JNEUROSCI.0658-17.2017.
Sheremet A, Burke SN, Maurer AP (2016) Movement enhances the nonlinearity of hippocampal theta. J Neurosci 36:4218–4230.
Sherman MA, Lee S, Law R, Haegens S, Thorn CA, Hämäläinen MS, Moore CI, Jones SR (2016) Neural mechanisms of transient neocortical beta rhythms: Converging evidence from humans, computational modeling, monkeys, and mice. Proc Natl Acad Sci:201604135 Available at: http://www.ncbi.nlm.nih.gov/pubmed/27469163%5Cnhttp://www.pnas.org/lookup/doi/10.1073/pnas.1604135113.
Shimamoto SA, Ryapolova-Webb ES, Ostrem JL, Galifianakis NB, Miller KJ, Starr PA (2013) Subthalamic nucleus neurons are synchronized to primary motor cortex local field potentials in Parkinson's disease. J Neurosci 33:7220–7233 Available at: /pmc/articles/PMC3673303/?report=abstract.
Shink E, Bevan MD, Bolam JP, Smith Y (1996) The subthalamic nucleus and the external pallidum: two tightly interconnected structures that control the output of the basal ganglia in the monkey. Neuroscience 73:335–357 Available at: https://www.sciencedirect.com/science/article/pii/030645229600022X?via%3Dihub [Accessed September 10, 2019].
Sibley DR, Monsma FJ (1992) Molecular biology of dopamine receptors. Trends Pharmacol Sci 13:61–69.
Smith Y, Bevan MD, Shink E, Bolam JP (1998) Microcircuitry of the direct and indirect pathways of the basal ganglia. Neuroscience 86:353–387.
Spaak E, Bonnefond M, Maier A, Leopold DA, Jensen O (2012) Layer-Specific Entrainment of Gamma-Band Neural Activity by the Alpha Rhythm in Monkey Visual Cortex. Curr Biol 22:2313–2318 Available at: https://www.sciencedirect.com/science/article/pii/S0960982212012055?via%3Dihub [Accessed September 12, 2019].
Steigerwald F, Potter M, Herzog J, Pinsker M, Kopper F, Mehdorn H, Deuschl G, Volkmann J (2008) Neuronal Activity of the Human Subthalamic Nucleus in the Parkinsonian and Nonparkinsonian State. J Neurophysiol 100:2515–2524 Available at: http://jn.physiology.org/cgi/doi/10.1152/jn.90574.2008.
Steiner LA, Barreda Tomás FJ, Planert H, Alle H, Vida I, Geiger JRP (2019) Connectivity and dynamics underlying synaptic control of the subthalamic nucleus. J Neurosci 39:2470–2481.
Steiner LA, Neumann W-J, Staub-Bartelt F, Herz DM, Tan H, Pogosyan A, Kuhn AA, Brown P (2017) Subthalamic Beta Dynamics Mirror Parkinsonian Bradykinesia Months After Neurostimulator Implantation. 32:1183–1190.
Steriade M, McCormick DA, Sejnowski TJ (1993) Thalamocortical oscillations in the sleeping and aroused brain. Science (80-) 262:679–685.
Szczepanski SM, Knight RT (2014) Insights into Human Behavior from Lesions to the

Prefrontal Cortex. Neuron 83:1002–1018 Available at: http://dx.doi.org/10.1016/j.neuron.2014.08.011.
Tan H, Jenkinson N, Brown P (2014) Dynamic neural correlates of motor error monitoring and adaptation during trial-to-trial learning. J Neurosci 34:5678–5688.
Tan H, Pogosyan A, Anzak A, Ashkan K, Bogdanovic M, Green AL, Aziz T, Foltynie T, Limousin P, Zrinzo L, Brown P (2013) Complementary roles of different oscillatory activities in the subthalamic nucleus in coding motor effort in Parkinsonism. Exp Neurol 248:187–195 Available at: http://dx.doi.org/10.1016/j.expneurol.2013.06.010.
Thompson JA, Lanctin D, Ince NF, Abosch A (2014) Clinical implications of local field potentials for understanding and treating movement disorders. Stereotact Funct Neurosurg 92:251–263.
Tinkhauser G, Pogosyan A, Debove I, Nowacki A, Shah SA, Seidel K, Tan H, Brittain JS, Petermann K, di Biase L, Oertel M, Pollo C, Brown P, Schuepbach M (2018a) Directional local field potentials: A tool to optimize deep brain stimulation. Mov Disord 33:159–164.
Tinkhauser G, Pogosyan A, Little S, Beudel M, Herz D, Tan H, Brown P (2017a) The modulatory effect of adaptive deep brain stimulation on beta bursts in Parkinson's disease. Brain:2017.
Tinkhauser G, Pogosyan A, Tan H, Herz DM, Kühn AA, Brown P (2017b) Beta burst dynamics in Parkinson's disease off and on dopaminergic medication. Brain 140:2968–2981.
Tinkhauser G, Torrecillos F, Duclos Y, Tan H, Pogosyan A, Fischer P, Carron R, Welter ML, Karachi C, Vandenberghe W, Nuttin B, Witjas T, Régis J, Azulay JP, Eusebio A, Brown P (2018b) Beta burst coupling across the motor circuit in Parkinson's disease. Neurobiol Dis 117:217–225 Available at: https://doi.org/10.1016/j.nbd.2018.06.007.
Torrecillos F, Tinkhauser G, Fischer P, Green AL, Aziz TZ, Foltynie T, Limousin P, Zrinzo L, Ashkan K, Brown P, Tan H (2018) Modulation of Beta Bursts in the Subthalamic Nucleus Predicts Motor Performance. J Neurosci 38:8905–8917 Available at: http://www.jneurosci.org/lookup/doi/10.1523/JNEUROSCI.1314-18.2018.
Tort ABL, Komorowski R, Eichenbaum H, Kopell N (2010) Measuring Phase-Amplitude Coupling Between Neuronal Oscillations of Different Frequencies. J Neurophysiol 104:1195–1210 Available at: http://jn.physiology.org/cgi/doi/10.1152/jn.00106.2010.
Tort ABL, Komorowski RW, Manns JR, Kopell NJ, Eichenbaum H (2009) Theta-gamma coupling increases during the learning of item-context associations. Proc Natl Acad Sci 106:20942–20947 Available at: http://www.pnas.org/cgi/doi/10.1073/pnas.0911331106.
Tripoliti E, Zrinzo L, Martinez-Torres I, Frost E, Pinto S, Foltynie T, Holl E, Petersen E, Roughton M, Hariz MI, Limousin P (2011) Effects of subthalamic stimulation on speech of consecutive patients with Parkinson disease. Neurology 76:80–86.
Twelves D, Perkins KSM, Counsell C (2003) Systematic review of incidence studies of Parkinson's disease. Mov Disord 18:19–31.
Tye KM, Deisseroth K (2012) Optogenetic investigation of neural circuits underlying brain disease in animal models. Nat Rev Neurosci 13:251–266 Available at: http://www.nature.com/doifinder/10.1038/nrn3171.
van Ede F, Quinn AJ, Woolrich MW, Nobre AC (2018) Neural Oscillations: Sustained Rhythms or Transient Burst-Events? Trends Neurosci xx:3–5 Available at:

https://doi.org/10.1016/j.tins.2018.04.004%0Ahttp://linkinghub.elsevier.com/retrieve/pii/S0166223618301036.
van Wijk BCM (2017) Is Broadband Gamma Activity Pathologically Synchronized to the Beta Rhythm in Parkinson's Disease? J Neurosci 37:9347–9349 Available at: http://www.jneurosci.org/lookup/doi/10.1523/JNEUROSCI.2023-17.2017.
van Wijk BCM, Beudel M, Jha A, Oswal A, Foltynie T, Hariz MI, Limousin P, Zrinzo L, Aziz TZ, Green AL, Brown P, Litvak V (2016) Subthalamic nucleus phase-amplitude coupling correlates with motor impairment in Parkinson's disease. Clin Neurophysiol 127:2010–2019 Available at: http://dx.doi.org/10.1016/j.clinph.2016.01.015.
van Wijk BCM, Jha A, Penny W, Litvak V (2015) Parametric estimation of cross-frequency coupling. J Neurosci Methods 243:94–102 Available at: http://dx.doi.org/10.1016/j.jneumeth.2015.01.032.
van Wijk BCM, Wijk BCM Van (2017) Is Broadband Gamma Activity Pathologically Synchronized to the Beta Rhythm in Parkinson's Disease? J Neurosci 37:9347–9349 Available at: http://www.jneurosci.org/lookup/doi/10.1523/JNEUROSCI.2023-17.2017.
Vidailhet M, Vercueil L, Houeto J-L, Krystkowiak P, Benabid A-L, Cornu P, Lagrange C, Tézenas du Montcel S, Dormont D, Grand S, Blond S, Detante O, Pillon B, Ardouin C, Agid Y, Destée A, Pollak P (2005) Bilateral deep-brain stimulation of the globus pallidus in primary generalized dystonia. N Engl J Med 352:459–467.
Volkmann J, Daniels C, Witt K (2010) Neuropsychiatric effects of subthalamic neurostimulation in Parkinson disease. Nat Rev Neurol 6:487–498 Available at: http://dx.doi.org/10.1038/nrneurol.2010.111.
Voytek B (2010) Shifts in gamma phase–amplitude coupling frequency from theta to alpha over posterior cortex during visual tasks. Front Hum Neurosci 4:1–9 Available at: http://journal.frontiersin.org/article/10.3389/fnhum.2010.00191/abstract.
Voytek B, Canolty RT, Shestyuk A, Crone NE, Parvizi J, Knight RT (2010) Shifts in gamma phase-amplitude coupling frequency from theta to alpha over posterior cortex during visual tasks. Front Hum Neurosci 4:1–9 Available at: http://journal.frontiersin.org/article/10.3389/fnhum.2010.00191/abstract.
Voytek B, Kayser AS, Badre D, Fegen D, Chang EF, Crone NE, Parvizi J, Knight RT, Esposito MD (2015) Oscillatory dynamics coordinating human frontal networks in support of goal maintenance. Nat Neurosci 18:1318–1324.
Wagle Shukla A, Okun MS (2014) Surgical Treatment of Parkinson's Disease: Patients, Targets, Devices, and Approaches. Neurotherapeutics 11:47–59.
Wang J, Hirschmann J, Elben S, Hartmann CJ, Vesper J, Wojtecki L, Schnitzler A (2014) High-Frequency Oscillations in Parkinson ' s Disease : Spatial Distribution and Clinical Relevance. 29:1265–1272.
Watrous AJ, Deuker L, Fell J, Axmacher N (2015) Phase-amplitude coupling supports phase coding in human ECoG. Elife 4:1–15.
Weinberger M, Mahant N, Hutchison WD, Lozano AM, Moro E, Hodaie M, Lang AE, Dostrovsky JO (2006) Beta Oscillatory Activity in the Subthalamic Nucleus and Its Relation to Dopaminergic Response in Parkinson's Disease. J Neurophysiol 96:3248–3256 Available at: http://jn.physiology.org/cgi/doi/10.1152/jn.00697.2006.
Wessel JR (2019) β-bursts reveal the trial-to-trial dynamics of movement initiation and cancellation. J Neurosci:1887–19 Available at: http://www.jneurosci.org/lookup/doi/10.1523/JNEUROSCI.1887-19.2019.

West TO, Berthouze L, Halliday DM, Litvak V, Sharott A, Magill PJ, Farmer SF (2018) Propagation of Beta/Gamma Rhythms in the Cortico-Basal Ganglia Circuits of the Parkinsonian Rat. J Neurophysiol:jn.00629.2017 Available at: http://www.physiology.org/doi/10.1152/jn.00629.2017%0Ahttp://www.ncbi.nlm.nih.gov/pubmed/29357448.

Whittington JCR, Bogacz R (2019) Theories of Error Back-Propagation in the Brain. Trends Cogn Sci 23:235–250 Available at: https://doi.org/10.1016/j.tics.2018.12.005.

Wichmann T, Bergman H, DeLong MR (1994) The primate subthalamic nucleus. I. Functional properties in intact animals. J Neurophysiol 72:494–506 Available at: https://www.physiology.org/doi/10.1152/jn.1994.72.2.494.

Wijk BCM Van, Pogosyan A, Hariz MI, Akram H, Foltynie T, Limousin P (2017) NeuroImage : Clinical Localization of beta and high-frequency oscillations within the subthalamic nucleus region. NeuroImage Clin 16:175–183 Available at: http://dx.doi.org/10.1016/j.nicl.2017.07.018.

Williams JC, Hippensteel JA, Dilgen J, Shain W, Kipke DR (2007) Complex impedance spectroscopy for monitoring tissue responses to inserted neural implants. J Neural Eng 4:410–423 Available at: http://iopscience.iop.org/1741-2552/4/4/007.

Wilson CJ (2015) Oscillators and Oscillations in the Basal Ganglia. Neuroscientist 21:530–539.

Wulff P, Ponomarenko AA, Bartos M, Korotkova TM, Fuchs EC, Bähner F, Both M, Tort ABL, Kopell NJ, Wisden W, Monyer H (2009) Hippocampal theta rhythm and its coupling with gamma oscillations require fast inhibition onto parvalbumin-positive interneurons. Proc Natl Acad Sci U S A 106:3561–3566.

Yamamoto T, Katayama Y, Ushiba J, Yoshino H, Obuchi T, Kobayashi K, Oshima H, Fukaya C (2013) On-demand control system for deep brain stimulation for treatment of intention tremor. Neuromodulation 16:230–235.

Yang AI, Vanegas N, Lungu C, Zaghloul KA (2014) Beta-Coupled High-Frequency Activity and Beta-Locked Neuronal Spiking in the Subthalamic Nucleus of Parkinson's Disease. J Neurosci 34:12816–12827 Available at: http://www.jneurosci.org/cgi/doi/10.1523/JNEUROSCI.1895-14.2014.

Yelnik J, Percheron G (1979) Subthalamic neurons in primates: A quantitative and comparative analysis. Neuroscience 4.

Zauber SE, Watson N, Comella CL, Bakay R a E, Metman LV (2009) Stimulation-induced parkinsonism after posteroventral deep brain stimulation of the globus pallidus internus for craniocervical dystonia. J Neurosurg 110:229–233 Available at: http://www.ncbi.nlm.nih.gov/pubmed/18976055.

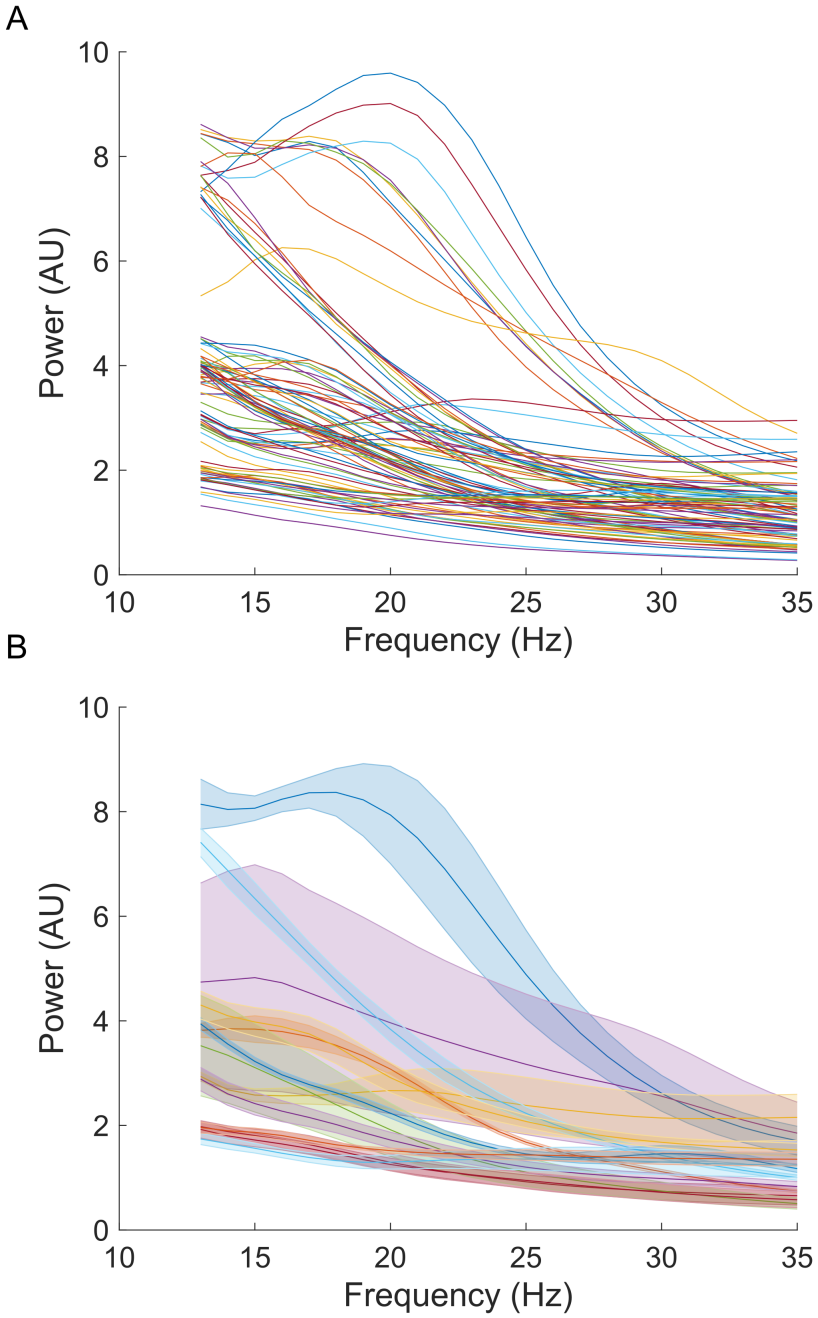
Zhang H, Watrous AJ, Patel A, Jacobs J (2018) Theta and Alpha Oscillations Are Traveling Waves in the Human Neocortex. Neuron 98:1269-1280.e5 Available at: https://doi.org/10.1016/j.neuron.2018.05.019.

Zhang W, Ge W, Wang Z (2007) A toolbox for light control of Drosophila behaviors through Channelrhodopsin 2-mediated photoactivation of targeted neurons. Eur J Neurosci 26:2405–2416 Available at: http://doi.wiley.com/10.1111/j.1460-9568.2007.05862.x.

Zrinzo L, Foltynie T, Limousin P, Hariz MI (2012) Reducing hemorrhagic complications in functional neurosurgery: a large case series and systematic literature review. J Neurosurg 116:84–94 Available at: http://www.ncbi.nlm.nih.gov/pubmed/21905798.

Appendix

Supplemental figures



Supplemental figure 1 Beta power spectra densities from ECoG recordings in the frequency range 10-35 Hz. A) All recordings (n = 96). B) Averaged per hemisphere ± 3 Hz (n = 13) for all recordings.